Process-understanding of the impact of dust deposition on marine primary production

Dissertation
zur Erlangung des akademischen Grades eines
Doktors der Naturwissenschaften
— Dr. rer. Nat. —
am Fachbereich 2 (Biologie/Chemie) der Universität Bremen

Gutachter
Prof. Dr. Dieter A. Wolf-Gladrow
Prof. Dr. Agostino Merico

vorgelegt von
Ying Ye
Bremen, Nov. 2010

Name: ..... Ort, Datum.....

Anschrift:.....

ERKLÄRUNG

Hiermit erkläre ich, das ich die Arbeit mit dem Titel:

selbstständig verfasst und geschrieben habe und außer den angegebenen Quellen keine weiteren Hilfsmittel verwendet habe.

Ebenfalls erkläre ich hiermit eidesstattlich, das es sich bei den von mir abgegebenen Arbeiten um 3 identische Exemplare handelt.

.....
(Unterschrift)

Acknowledgements

Ich war sehr glücklich während meiner Doktorarbeit. In der ersten Linie muss ich meinem Betreuer, Christoph Völker, bedanken. Deine Leidenschaft für Wissenschaft hat mich immer wieder begeistert und motiviert. Ohne dich wäre ich wahrscheinlich längst in einem für mich komplett neuen Gebiet — Modellierung — entmutigt worden. Sehr wichtig ist es auch, dass du mir gezeigt hast: ein Wissenschafter kann auch ein vielfältiges Leben genießen. ◡̈ Ich danke dir auch ganz herzlich für deine Ratschläge und Hilfsbereitschaft, als ich Schwierigkeiten bei der Arbeit oder im privaten Leben hatte.

Ich bedanke mich besonders bei Dieter A. Wolf-Gladrow. Du hast es mich ermöglicht, in dieser wunderbaren Gruppe zu arbeiten. Deine schnelle Feedbacks zu meinen Manuskripten und Ratschläge in den Komiteemeetings haben mir sehr geholfen.

Ich freue mich sehr, daß ich Thibaut Wagener kennengelernt habe. Du hast mir nicht nur ein spannendes Thema zur Modellierung angeboten. Ich möchte mich bei dir auch bedanken, dass du mir bei der Feldarbeit in Cape Verde viel beigebracht hast.

Bei Björn Rost und Sven Kranz bedanke ich mich für die interessanten und hilfreichen Diskussionen über *Trichodesmium*. Ich danke Dir Björn auch für deine Teilnahme an meinen Komiteemeetings und Dir Sven für das Informieren über die neuesten Veröffentlichungen.

Ich bedanke mich bei Astrid Bracher für die Breitstellung der Satellietendaten und das schnelle Korrekturlesen.

I am deeply grateful to Prof. Dr. Agostino Merico and Prof. Dr. Kai Bischof who are willing to review my PhD thesis as well as the disputation.

Weiterhin bedanke ich mich bei Dörte Burhop für das Korrekturlesen und ihre Hilfsbereitschaft bei jeder kleinen Frage.

Elizabeth Sweet, thank you for bringing so much fun in our office, for the proof-reading and for your readiness to help as I was suffering from finding the correct English words.

Ich danke euch auch ganz herzlich — meine Kochgruppe: Nike Fuchs, Judith Hauck, Clara Hoppe, Isabelle Schulz and Nina Keul. Die wunderschönen und köstlichen Mittagspausen haben mich so gut entspannt und wieder zur Arbeit motiviert.

Ich bin dankbar, dass Beate Müller meine erste Bürokollegin war und auch dass sie mich in die kleine nette Laufgruppe gebracht hat, so dass ich am Anfang meiner Doktorarbeit eine familinäre Atmophäre in Bremerhaven genießen konnte.

And thank all of you, the Biogeos, who provide such a family-like atmosphere.

最后，让我用母语衷心感谢支持、帮助过我的家人和朋友。离开家已经有十个年头，每个周末看到视频中爸爸妈妈的笑脸，仍然是对我最大的安慰和鼓励。我的十年寒窗也是你们十年的寂寞，是我永远无法弥补的、未能在你们身边尽孝的十年。幸运的是，我们不仅是家人，也是朋友，可以分享一切我的经历和喜怒哀乐，分享我们远隔大洋、却各自丰富的生活。

姜南，陪伴了我的硕士又迎来了博士毕业的煎熬。我不会忘记那些我们夜深人静时执着的专业讨论，还有你对我论文敬业的修改。当然也会想起你在家务中不寻常的贡献。☺“火车头”在你的维修和保养下才终于进站了。

所有在德国关心过我、帮助过我的中国朋友以及他们的德国家属，不用我说，你们都知道在这里，朋友意味着什么。谢谢你们，让我在潮湿阴冷的北德仍然感受到了家乡的温暖。

Twenty-five years ago
at a lecture at the Woods Hole Oceanographic Institution,
oceanographer John Martin stood up
and said in his best Dr. Strangelove accent:

Give me a half tanker of iron,
and I will give you an ice age.[1]

[1] modified from http://earthobservatory.nasa.gov/Features/Martin/martin.php written by John Weier.

Contents

Chapter 1

Introduction

1.1 The ultimate question: what controls the marine biological carbon pump?

The biological carbon pump, transporting carbon from the euphotic zone to the ocean interior, is fundamental for the earth's climate. The primary engine of the pump is photosynthetic carbon fixation. Marine biological carbon fixation has a much higher efficiency than terrestrial, thanks to the short turnover time of phytoplankton. This becomes apparent when considering that the global net primary production (NPP) is $\sim$100 Pg C y^{-1} with roughly equal contributions by land and ocean (Field et al., 1998). The contribution of the ocean is driven by $\sim$1 Pg phytoplankton biomass corresponding to one thousandth of global primary producer biomass (Field et al., 1998; Falkowski, 2005). Only a small fraction of the marine NPP is exported to the ocean interior where it is sequestered from the atmosphere for centuries to millennia (Eppley and Peterson, 1979). Without the contemporary biological pump, atmospheric CO_2 concentration would increase by more than 200 ppm (Maier-Reimer et al., 1996; Gruber and Sarmiento, 2002). Consuming all the available surface nutrients completely, this biological pump would reduce atmospheric CO_2 concentration by more than 100 ppm (Gruber and Sarmiento, 2002). Therefore, it is not surprising that variations in the strength of the biological pump have been proposed to contribute to the large oscillations of atmospheric pCO_2 during the glacial-interglacial cycles (Sarmiento and Toggweiler, 1984; Martin, 1990).

Biological carbon fixation in the ocean is constrained by grazing, reducing the biomass (Frost, 1991), and by the requirement for nutrients and light to grow. Studies seeking the limiting factors of marine primary production began with the determination of the elemental composition of particulate organic material and of the dissolved pool of inorganic nutrients. Redfield (1958) observed an average molar stoichiometry of C : N : P in marine phytoplankton of 106 : 16 : 1, referred to now as the "Redfield ratio". The N : P ratio of dissolved inorganic nutrients is close to that of phytoplankton. The Atlantic in particular, seems to become depleted in nitrate before phosphate is depleted (Fig. 1.1). Redfield attributed this to denitrification, a biological process which converts nitrate to N_2, resulting in a more than 10-fold shorter residence time of N compared to P in the ocean (Delaney, 1998). N_2 fixation com-

pensates the P excess over the Redfield ratio by converting N_2 to organic nitrogen which is further transformed to the dissolved pool by respiration and remineralisation. A theory of P control on primary production has therefore proposed that N_2 fixation and denitrification keep the balance of the marine N inventory in which N_2 fixation is simply regulated by P excess over Redfield ratio. This viewpoint has been applied further in the concept of P^* — P variation relative to Redfield ratio (P^*=$PO_4^{3-} - NO_3^-$ / Redfield N : P ratio). Deutsch et al. (2007) underlined the tight geographical and temporal association between N_2 fixation and denitrification and used P^* to determine the distribution of N_2 fixation.

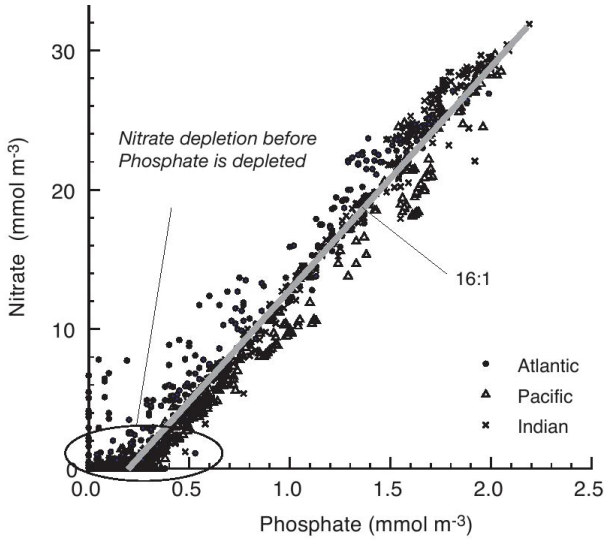

Figure 1.1: Plot of nitrate vs. phosphate in different oceans modified from Gruber and Sarmiento (2002).

A different viewpoint has also been developed from the analysis of nutrient elemental composition. Michaels et al. (1996), Gruber and Sarmiento (1997) defined a parameter N^* — N variation relative to Redfield ratio (N^*=NO_3^- − Redfield N : P ratio × PO_4^{3-}). Assuming that elevated N^* is caused by degradation of N-rich diazotroph biomass, they determined the distribution of N_2 fixation. High values of N^* in the North Atlantic were proposed to be a result of high growth rates of diazotrophs, stimulated by the large atmospheric iron input in that region. If N_2 fixation is limited by Fe or co-limited by Fe and P (Mills et al., 2004), the N : P ratio is not the only feedback mechanism controlling the balance between N_2 fixation and denitrification. This decoupling of the two central processes in the N cycle (Sect. 1.3.1) forms the basis of the N control theory (Falkowski, 1997; Falkowski et al., 1998).

The role of iron in limiting marine primary production has been recognised over the last decades. Iron may limit marine productivity on the one hand, by limiting primary production in the HNLC (high-nutrient, low-chlorophyll) regions (Martin, 1990), and on the other hand by limiting N_2 fixation in regions with low nitrate concentrations (Falkowski, 1997).

Waters in the HNLC regions represent one third of the world ocean surface waters. The

largest source of iron for surface waters is the deep water supply (Watson, 2001). Due to the depletion of Fe relative to NO_3^- in upwelling waters, only a small fraction of nitrate in the euphotic zone is utilized in these regions. Evidence for Fe limitation of phytoplankton growth has been found in shipboard incubation experiments in the HNLC waters (Martin and Fitzwater, 1988; Martin, 1990; Martin et al., 1991; Price et al., 1991; Fitzwater et al., 1996; Martin et al., 1993; Hutchins and Bruland, 1998). A number of *in situ* Fe fertilization experiments were carried out over the HNLC waters to study the impact of iron addition on pelagic ecosystem and biogeochemistry under natural conditions (de Baar et al., 2005; Boyd et al., 2007). All these experiments have confirmed that Fe supply limits primary production and has an impact on phytoplankton species composition. Growth of both small and large phytoplankton was stimulated by Fe addition. Blooms of large diatoms transformed some systems from Fe-limited into Si-limited, whereas small-size phytoplankton were strongly grazed and did not bloom (Price et al., 1994) [1]. The *in situ* Fe fertilization experiments still have certain temporal and spatial limitations (Boyd et al., 2007; Breitbarth et al., 2010) and the role of iron in reducing atmospheric CO_2 cannot yet be judged conclusively by means of the current understanding of Fe biogeochemistry and ecosystem responses.

The importance of iron for N_2 fixation is based on the higher requirement for iron by diazotrophs than non-diazotrophic phytoplankton (Sañudo Wilhelmy et al., 2001). In 75 % of the world oceans, N_2 fixation is estimated to be Fe-limited (Berman-Frank et al., 2001), although Fe is probably not the only limiting factor for N_2 fixation (Mills et al., 2004). Varying Fe supply in these regions changes the strength of interactions between diazotrophs and non-diazotrophic phytoplankton and thus the consumption of other nutrients such as P and Si.

Dust deposition is the major source of iron in the open ocean (Duce and Tindale, 1991; Fung et al., 2000). This PhD study is a contribution to the understanding of processes affecting the link between iron supplied by dust deposition and marine productivity, in particular via N_2 fixation. Background information on the marine iron and nitrogen cycle are given in Sect. 1.2 and 1.3. The focuses and motivation of this thesis are introduced in Sect. 1.4.

1.2 Iron cycle and bioavailability

1.2.1 Iron research

The physiological importance of Fe in the ocean has been recognised at least since the 1920s (e.g. Hart, 1934). Yet the first reliable vertical profiles of dissolved iron (DFe) were not published until 1980s (Gordon et al., 1982; Landing and Bruland, 1987; Martin and Gordon, 1988; Martin et al., 1989), after overcoming the contamination problems in collection and analytical procedures of iron measurements (Martin, 1990). The iron hypothesis of John Martin, based on the Fe concentrations in the Southern Ocean, in the subpolar North Pacific

[1] Besides N, P and Fe, other elements such as Si and Co can also limit growth of some phytoplankton species, depending on species-specific requirements and the ability to access these elements (Dugdale and Wilkerson, 1998; Saito et al., 2002).

and in ice cores, stimulated research on Fe variability over large timescales and biological responses to Fe limitation. During the 1990s, Fe profiles from different ocean basins were published and the near constancy of deepwater DFe concentrations led to a debate on what controls the distribution of dissolved iron in the ocean (Johnson et al., 1997). In recent years, thanks to further measurements of Fe profiles, considerable inter- and intra-basin variabilities in deepwater DFe concentrations have been revealed, reflecting multiple Fe-supply mechanisms in each basin, the influence of ocean circulation and Fe residence time. Moreover, advances in determining Fe redox speciation, organic complexation, precipitation and many other kinetic processes have improved the understanding of Fe speciation and biogeochemical cycling (Boyd and Ellwood, 2010).

1.2.2 Role of iron in marine life

The redox pair of Fe(II)/Fe(III) provides a classic electron transfer system. Fe(II) was abundant in the early anoxic ocean with a concentration up to $25\,\mathrm{mol\,m^{-3}}$ (Holland, 1984). Therefore, Fe has been already involved in the physiological processes of early life forms in the Archaean ocean, e.g. in the enzyme systems of cyanobacteria.

Iron containing proteins are essential components in various metabolic pathways. They are involved in photosynthetic and respiratory electron transport systems as cytochromes and Fe-S proteins; in oxygen cycling as a component of catalase, peroxidase and superoxide dismutase; in the tricarboxylic acid cycle as a component of enzymes like aconitase; in enzymes catalysing reduction of nitrate, nitrite and N_2; and in some other biosynthetic and degradative reactions (Geider and La Roche, 1994). The primary function of iron is in electron transport and redox catalysis rather than in structural components of cells, it is therefore more important in controlling rates of metabolism and growth than cell yields (Sunda and Huntsman, 1997). Decrease of the rates of metabolic processes such as photosynthesis, nitrate assimilation and N_2 fixation has been observed by phytoplankton under Fe starvation (e.g. Price et al., 1994; Rueter et al., 1990; Berman-Frank et al., 2001).

1.2.3 Iron cycle

Iron is transported into the ocean by rivers, hydrothermal fluids and atmospheric deposition (Fig. 1.2). Rivers transport significant quantities of iron into coastal regions, however, a major fraction of iron in river water exists as colloids, which are readily removed by flocculation in estuaries (Hunter and Boyd, 2007). Only a small fraction can escape the estuarine mixing zone and contribute to the pool of DFe (de Baar and de Jong, 2001).

A high amount of iron is reductively dissolved from the Mid Ocean Ridge Basalts (MORB) by hydrothermal circulation. This reduced Fe is rapidly reoxidised and mostly precipitates with cooling of the hydrothermal fluid (de Baar and de Jong, 2001). The net input of DFe might be thus negligible, although regionally it may contribute significantly to the DFe pool (Mackey et al., 2002; Tagliabue et al., 2010).

The melting of sea-ice, or icebergs is an additional iron source. Aeolian dust deposited by snow accumulates on ice, resulting in a high Fe concentration in icebergs (Lannuzel et al.,

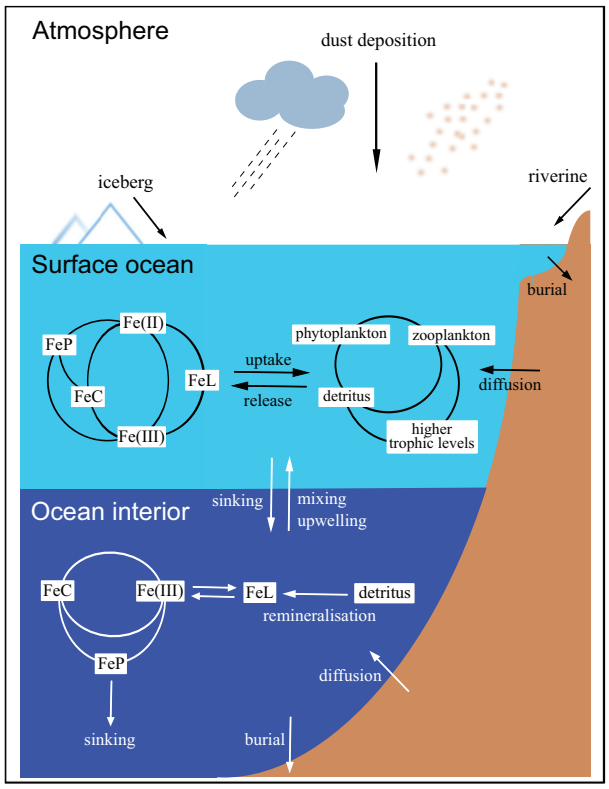

Figure 1.2: Schematic presentation of the main sources and the marine cycle of iron. Processes affecting Fe speciation and the biological cycle of iron are simplified mainly based on the model design in this thesis (Chap. 2).

2007, 2008; Raiswell et al., 2008). DFe concentration of ocean surface waters is elevated locally by ice melting up to $9\,\mathrm{nmol\,L^{-1}}$ (Löscher et al., 1997).

Estimates of atmospheric dust input are in the range of $400\text{–}1000\times10^{12}\,\mathrm{g\,y^{-1}}$ with 30 % delivered by wet deposition (Jickells and Spokes, 2001). Assuming an average mass percentage of iron in dust of 3.5 %, $0.25\text{–}0.63\times10^{12}\,\mathrm{mol\,Fe\,y^{-1}}$ enters the ocean via this pathway (Jickells and Spokes, 2001). This is likely the dominant external source of iron in open oceans (Duce and Tindale, 1991). It is notable that production, transport and deposition of dust are all episodic processes. About half of the annual transport of dust from North Africa over the North Atlantic Ocean is estimated to occur within 20 % of the year (Swap et al., 1996). On average, one third of the global annual dust is supplied to the North Atlantic Ocean and about half to the North Pacific Ocean (Duce and Tindale, 1991; Jickells and Spokes, 2001) (Fig. 1.3).

Within the ocean interior, the cycling of iron is mainly controlled by biological activities. Like other nutrients, iron is taken up by phytoplankton and bacteria within the euphotic zone and passed on through food chains. Sinking organic matters, e.g. settling plankton, detritus, fecal pellets or faeces of vertebrates (Lavery et al., 2010) transport iron downward,

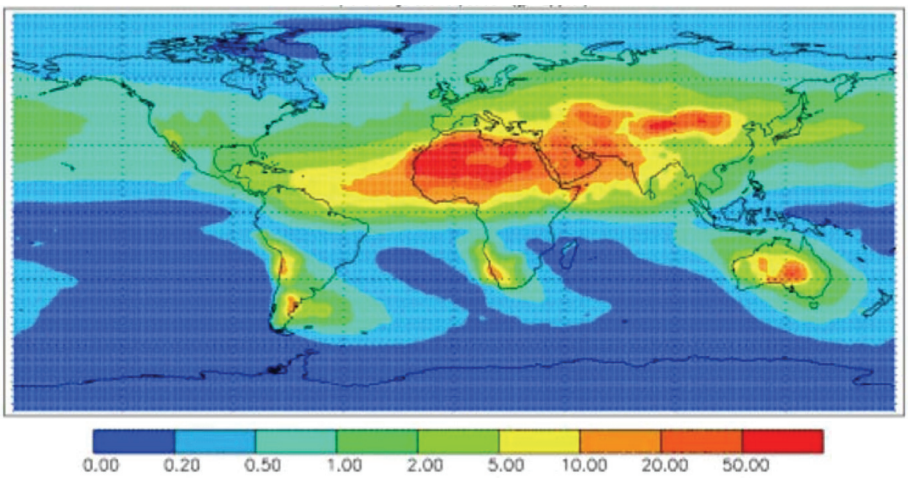

Figure 1.3: Annual average dust deposition ($g\,m^{-2}\,y^{-1}$) as estimated by Mahowald et al. (2005) using an atmospheric dust transport model.

while a part of this iron is released as DFe by microbial remineralisation. Upwelling and turbulent mixing bring the released iron back to the euphotic zone where it is available again for biological uptake. Other biological processes also return iron from organic matter into solution, e.g. grazing, excretion and viral lysis (Hutchins et al., 1993).

The dominant loss process of DFe deeper in the water column is likely the transport into the sediment by adsorption on surfaces of sinking particles, whereas biological uptake basically explains lower Fe concentrations in surface waters. Two pathways are known for the adsorptive removal of iron: the direct adsorption of soluble iron ("scavenging") (Balistieri et al., 1981) and the adsorption of colloidal iron (Honeyman et al., 1988). The adsorptive removal is related to particle dynamics. Sinking fluxes in the interior of the ocean are often dominated by larger aggregates, e.g. 'marine snow', and fecal pellets (e.g. Ratmeyer et al., 1999). Particle aggregation transforms small suspended particles into larger and more rapidly sinking particles (McCave, 1984; Jackson and Burd, 1998) where organic material such as TEP (transparent exopolymer particles) acts as glue for forming aggregates (Passow, 2004). Hence, DFe loss by particle adsorption not only depends on the concentration of lithogenic particles but also on the production of biogenic particles.

Iron, in settling particles or adsorbed on surfaces of particles, is transported down to the seafloor and buried in marine sediments. About half of this particulate iron is in the form of oxide and organic coating and can be mobilised by reductive dissolution (de Baar and de Jong, 2001). Although a substantial part of the mobilised iron is oxidised again and converted back into particulate form, the remaining minor portion escaping from reoxidation could increase DFe concentration significantly in waters in close contact with reducing sediments (Bucciarelli et al., 2001; Johnson et al., 1999).

1.2.4 Bioavailability of iron

1.2.4.1 Fe speciation

99 % of DFe in seawater is bound to organic ligands (Gledhill and van den Berg, 1994; Wu and Luther III, 1995; Rue and Bruland, 1995), molecules with low molecular weight and high iron affinity. Organic complexation of iron can be determined with competitive ligand equilibration/cathodic stripping voltammetry (CLE/CSV). Natural ligands may cover a whole spectrum of stability constants and only a part of them can be recognised due to the limitation of the detection window (Town and Filella, 2000). Two classes of natural organic ligands have been commonly distinguished by binding stability. The strong ligand predominates in surface waters and has a typical conditional stability constant ($K^{cond}_{L/Fe^{3+}}$) of $10^{12}\,\mathrm{L\,mol^{-1}}$-$10^{13}\,\mathrm{L\,mol^{-1}}$. The weak ligand is more abundant deeper in the water column and its conditional stability constant is about $10^{11}\,\mathrm{L\,mol^{-1}}$ (Rue and Bruland, 1995; Hunter and Boyd, 2007). The conditional stability constants of siderophores, Fe-binding ligands produced by a few marine microbes, are similar to those of the naturally occurring strong ligands in seawater (Rue and Bruland, 1995; Lewis et al., 1995; Macrellis et al., 2001), indicating that strong ligands are produced actively by marine microorganisms under iron limitation (Sect. 1.2.5.2). The weak ligands have similar conditional stability constants to those of the porphyrin-type ligands which are supposed to be released as degradation products of cytochrome system (Boye et al., 2001). The incubation study by Boyd et al. (2010) provided the first evidence of the concurrent release of weak ligands from sinking particles. Due to the strong binding strength, organic complexation decreases the concentration of reactive Fe(III)' and thus the formation of sparingly soluble hydroxides and oxides, and also the adsorption on particle surfaces. This results in a higher DFe concentration and the fraction of bioavailable iron, depending on different uptake strategies (Sect. 1.2.5.2).

In the oxic modern ocean, ferric iron is thermodynamically more stable than ferrous iron. The reactive Fe(III)' in seawater readily forms hydrolysed species as $Fe(OH)_2^+$, $Fe(OH)_3^0$ and $Fe(OH)_4^-$ (Byrne and Kester, 1976) which are sparingly soluble. After progressive dehydration and crystallization, more stable iron oxides as goethite and hematite are generated from the hydroxides and the solubility drops by orders of magnitudes (Kuma et al., 1996).

Hydrolysed iron forms polymers which grow to colloidal sized hydroxides. Colloidal iron could be in the form of inorganic hydroxides (Rich and Morel, 1990; Rose and Waite, 2003) or organic complexes (Wu et al., 2001; Cullen et al., 2006). Fe removal is increased by colloidal iron through aggregating to larger particles which sink faster into the sediment (Honeyman et al., 1988).

Ferrous iron is more soluble and can be taken up by marine organisms directly (e.g. Anderson and Morel, 1980; Maldonado and Price, 2001), however, this form of iron is labile and readily oxidised to ferric iron by O_2, O_2^- and H_2O_2 (Millero and Sotolongo, 1989). Hydrolysed species of iron, ferric organic complexes, colloidal hydroxides and iron oxides can be reduced to ferrous iron by direct photoreduction and indirect photoreduction by superoxide. Bioreduction at cell surfaces and in reducing environments as anoxic sediments also generate Fe(II) (Sunda, 2001). Fe(II) organic complexes mostly have a much weaker binding strength than Fe(III) complexes and are often products of the photoreduction of

organic complexes (Barbeau et al., 2001; Powell and Wilson-Finelli, 2003). Furthermore, the solubility of ferrous oxyhydroxides is much higher than that of ferric oxyhydroxides. Therefore, photoreduction generally increases the Fe solubility and bioavailability.

In measurements, Fe species are commonly operatively distinguished by filter cutoff: soluble iron is defined by a filter cutoff of $0.02\,\mu$m and is the sum of Fe(II)', Fe(III)' and the soluble fraction of organically complexed iron; colloidal iron has a size between 0.02–$0.4\,\mu$m and particulate iron is $>0.4\,\mu$m. Dissolved iron (DFe) consists of soluble and colloidal iron and is the form of iron most often measured.

1.2.4.2 DFe concentration and distribution

Iron is the fourth most abundant element in the Earth's crust (averaged 5.63% by weight) (Taylor, 1964). Nevertheless, its concentration in the surface ocean is very low, at the picomolar and nanomolar levels (Turner et al., 2001). This is due to the fact that in the oxygenated surface ocean, iron is present predominantly as Fe(III) which has a low solubility (see above).

While DFe concentration in surface waters show a large spatio-temporal variability ranging over 4–5 orders of magnitudes, deep water DFe varies little with depth and between ocean basins, with $\sim 0.7\,\mu\mathrm{mol\,m^{-3}}$ in the Pacific, up to $1.6\,\mu\mathrm{mol\,m^{-3}}$ in the Atlantic and lower values in the south Indian Ocean (Johnson et al., 1997; Boye et al., 2001; Bergquist and Boyle, 2006). DFe is enriched in coastal waters, with a maximum of $100\,\mu\mathrm{mol\,m^{-3}}$ (de Baar and de Jong, 2001). DFe higher than $1\,\mathrm{mmol\,m^{-3}}$ has been reported for the suboxic and anoxic waters in some semi-enclosed marine basins. The highest abundance of DFe is found in pore waters of marine sediments and hydrothermal vent fluids, up to $300\,\mathrm{mmol\,m^{-3}}$ and $3000\,\mathrm{mmol\,m^{-3}}$, respectively (de Baar and de Jong, 2001).

Very low DFe concentrations have been measured in surface waters in the HNLC regions (Coale et al., 1996; Johnson et al., 1997; de Baar et al., 1999; Sohrin et al., 2000). These regions, enclosing the subarctic North Pacific, the equatorial Pacific and the Southern Ocean, have high surface concentrations of macronutrients as NO_3^- and PO_4^{3-} enriched by large scale upwelling (Watson, 2001) but low aeolian dust flux (Duce and Tindale, 1991). Thus, the primary productivity in the HNLC regions could be limited by iron (Martin, 1990).

Iron is not only a limiting factor for primary productivity in the HNLC regions but also a controlling factor on phytoplankton growth, community composition and availability of other nutrients as N and P in other ocean regions. Strong Fe limitation at the end of spring blooms of diatoms (Moore et al., 2006) and co-limitation of Fe and P on N_2 fixation (Mills et al., 2004) have been reported outside the HNLC regions (Sect. 1.3.2.4).

1.2.5 Adaptation of marine organisms to limited iron supply

1.2.5.1 Iron requirement

Unlike the relatively constant C : N : P ratios in particulate organic matter (Redfield, 1958), measured C : Fe ratios in marine phytoplankton vary over a large range from 10^4–10^6 for different ambient Fe concentrations and phytoplankton species (Morel and Hudson, 1985;

Sunda and Huntsman, 1995; Sarthou et al., 2005; Twining et al., 2004). Coastal species often have lower C : Fe ratios than open ocean species (Sunda and Huntsman, 1995; Strzepek and Harrison, 2004).

Iron is involved in photosynthetic catalysts such as the photosystem I (PS I) and II (PS II) (Sect. 1.2.2), where PS I has a higher iron content. In general, cyanobacteria have higher PS I : P S II ratios than eukaryotic algae (Raven, 1990) and therefore a higher iron requirement. Moreover, nitrogenase, the enzyme responsible for reduction of N_2, contains Fe and Mo in its subunits to facilitate electron transfer (Falkowski, 1997). The iron use efficiency of this enzyme is one of the lowest of any Fe-containing enzyme known (Raven, 1988). Therefore, *Trichodesmium* spp. needs ∼5-fold more iron to support diazotrophic growth than growth on ammonium (Kustka et al., 2003).

1.2.5.2 Iron uptake

Two main iron uptake systems have been found in marine organisms: 1) the transport of ferric and ferrous ion by membrane transporters and 2) the siderophore-mediated iron uptake.

Direct transport of iron ions by membrane transporters is widespread in eukaryotic marine phytoplankton. A direct relationship between the concentration of labile inorganic iron species and iron uptake has been found in some diatoms and coccolithophores (Anderson and Morel, 1982; Hudson and Morel, 1990; Sunda and Huntsman, 1995). Morel et al. (1991) hypothesised that the uptake rates of these diatoms and coccolithophores are controlled by the rate of ligand exchange between Fe(III)' hydrolysis species and receptor ligand sites on membrane-bound iron transporters. In recent studies, some eukaryotic phytoplankton are found to be able to reduce Fe(III)-ligand chelates by excretion of superoxide (Kustka et al., 2005; Shaked et al., 2005) or to reduce them by reductases at the cell surface (Maldonado and Price, 1999, 2001; Maldonado et al., 2005).

Siderophores, 'iron carrier' in Greek, are low-weight molecules with a high affinity to ferric iron. Most siderophores can be classified into catecholates and hydroxamates according to their binding sites (Sunda, 2001). Siderophores were first found in terrestrial bacteria and several hundred structures are known (Sandy and Butler, 2009). During the last two decades, siderophore production has also been found in marine heterotrophic bacteria and cyanobacteria (Vraspir and Butler, 2009). The production of siderophores is thought to be a strategy, developed during the Proterozoic, to overcome the Fe(III) solubility problem in oxygenated surface waters (Hunter and Boyd, 2007). Siderophores are produced under iron limitation (Reid et al., 1993; Wilhelm and Trick, 1994; Wilhelm et al., 1996; Macrellis et al., 2001) and the production is regulated on the level of gene transcription by Fe cellular concentration (Sandy and Butler, 2009).

In the siderophore-mediated uptake system, there are two principle ways to access the siderophore-bound iron: either the whole complex is transported across the cell membrane and reduced inside the cell, or it is reduced by reductases at the cell surface and the single iron ion is then transported into cells by specific transporter proteins (Guerinot, 1994; Granger and Price, 1999; Maldonado and Price, 1999, 2001; Maldonado et al., 2005). The former way is the main uptake routine of bacteria and the latter found more in eukaryotes.

Although siderophore production is mostly species-specific, many marine bacteria possess multiple siderophore uptake systems and can also take up Fe bound to siderophores produced by other microorganisms, e.g. by fungi (Granger and Price, 1999; Hutchins et al., 1999). The advantage of siderophore production in iron uptake has been doubted because of the rapid diffusion of released siderophores into seawater (Hutchins et al., 1991). A model study on the efficiency of a siderophore-mediated uptake system shows that a siderophore-specific uptake system is a costly strategy in terms of cellular nutrient and energy budgets and only collective effort of a dense cell population can make this strategy effective (Völker and Wolf-Gladrow, 1999). Therefore, the siderophore-mediated uptake of iron may alleviate iron limitation of dense prokaryotic populations rather than of an individual organism or large diatoms which reach only small number densities.

1.2.5.3 Other adaptations to low iron supply

Other strategies have been developed besides the various uptake systems. For instance, Fe-containing proteins are substituted by non-Fe-containing proteins in some marine diatoms, e.g. the replacement of ferredoxin by flavodoxin (La Roche et al., 1995; McKay et al., 1999). Diatoms under Fe limitation reduce cell size (Martin et al., 1991; Price et al., 1991; Fitzwater et al., 1996), to enlarge cell surface per volume for more efficient Fe uptake. Oceanic diatoms live in an Fe-impoverished environment compared to the coastal species. They reduce the cellular iron requirement by changing their photosynthetic architecture and sacrificing their rapid regulation of light harvesting (Strzepek and Harrison, 2004). One adaption to episodic high Fe supply by e.g. dust deposition is the luxury uptake, observed for many oceanic and coastal eukaryotic algae under high Fe supply (Sunda and Huntsman, 1995, 1997). Production of Fe storage proteins is found in some bloom-forming marine pennate diatoms (Marchetti and Cassar, 2009).

1.2.5.4 Biological feedback to Fe chemistry

While Fe bioavailability is primarily determined by Fe chemistry and uptake strategies, biological activities also change the Fe chemistry in seawater.

Marine microorganisms can release Fe-binding ligands, thereby changing Fe speciation directly. Complexation of iron on the one hand reduces the formation of iron hydroxides and oxides and the loss by particle adsorption, on the other hand it increases photoreduction in surface waters, leading to a higher Fe solubility and bioavailability (Barbeau et al., 2003). Phytoplankton can also play a role in generating Fe(II) by bioreduction at cell surface or by excretion of superoxide into seawater (see above).

Organic particles play a significant role in transporting iron into the deep ocean. Phytoplankton blooms cause strong sinking fluxes of large biogenic particles which form the major export route for DFe from surface waters (de Baar and de Jong, 2001). Abundance and composition of organic sinking particles also influence aggregate formation (Passow, 2004), sweeping most of the iron out of the dissolved pool by fast sinking.

Less directly, and on longer temporal scales, biological CO_2 sequestration changes the concentration of CO_2 in the atmosphere and subsequently climate conditions. This affects

aerosol deposition and Fe solubility in the atmosphere (Jickells and Spokes, 2001) which change the bioavailable fraction of iron in seawater, forming a feedback loop between biology and Fe chemistry.

1.3 N cycle and N_2 fixation

Nitrogen is an essential element for life. As a structural component, N is widely involved in proteins, nucleic acids, photosynthetic pigments like chlorophyll, vitamins, bacterial cell walls and some storage products. N is also contained in nucleotides e.g. ATP, as energy transfer (Karl et al., 2002). Its necessity for life and relatively high cellular requirement makes N one of the most important factors controlling marine primary productivity and the biological carbon pump.

1.3.1 N cycle

N has five relatively stable oxidation states and exists in seawater in five different inorganic forms: nitrate (NO_3^-), nitrite (NO_2^-), nitrous oxide (N_2O), molecular nitrogen (N_2) and ammonia (NH_4^+). Most of these chemical forms, except N_2O and N_2, are bioavailable for marine organisms and called fixed or reactive nitrogen. NH_4^+ is preferred by phytoplankton, because no reduction step is needed for its assimilation (Zehr and Ward, 2002). Dissolved nitrogen gas N_2 can be fixed by many N_2 fixing microorganisms — diazotrophs.

Dissolved nitrogen gas, N_2, accounts for the largest marine N pool (∼94 % of total marine N) (Gruber, 2008). NO_3^- makes up ∼88 % of the remaining marine N and dissolved organic nitrogen almost the remaining 12 %. The other forms represent only 0.3 % of the total fixed pool (Gruber, 2008).

The marine N cycle is primarily driven by the photosynthetic fixation of carbon into organic matter in the euphotic zone. Inorganic N is transformed into organic N by biological assimilation converting fixed nitrogen into organic forms or by N_2 fixation (Fig. 1.4). Most of this organic N is respired or remineralised to NH_4^+ by ammonification and to NO_3^- by nitrification within the euphotic zone, whereas a smaller fraction sinks down to the aphotic ocean interior. A part of this fraction is remineralised further back to inorganic N and transported upwards to the euphotic zone by ocean circulation and vertical mixing. Some anaerobic bacteria can use NO_3^- as an electron acceptor to gain energy for growth and convert NO_3^- via NO_2^- and N_2O to N_2. This process is called denitrification. Another way to convert fixed nitrogen to N_2 is Anammox in which NO_2^- and NH_4^+ are converted to N_2.

Surface concentration of fixed nitrogen is often in the nanomolar range (Gruber, 2008) due to biological uptake. In surface waters, high nitrate concentration are mostly found in upwelling regions e.g. in some coastal regions and in the HNLC regions (Sect. 1.2.4.2). The dominant loss process of N is denitrification and Anammox, occurring mostly at depths of 200–700 m in the oxygen minimum zones (OMZs) of the ocean — in the tropical Eastern North Pacific, the tropical Eastern South Pacific, the Arabian Sea and in marine sediments (Capone and Knapp, 2007). The depletion of the marine N budget caused by denitrification is assumed to be balanced by N_2 fixation (Deutsch et al., 2004). Estimates of global N_2 fixation

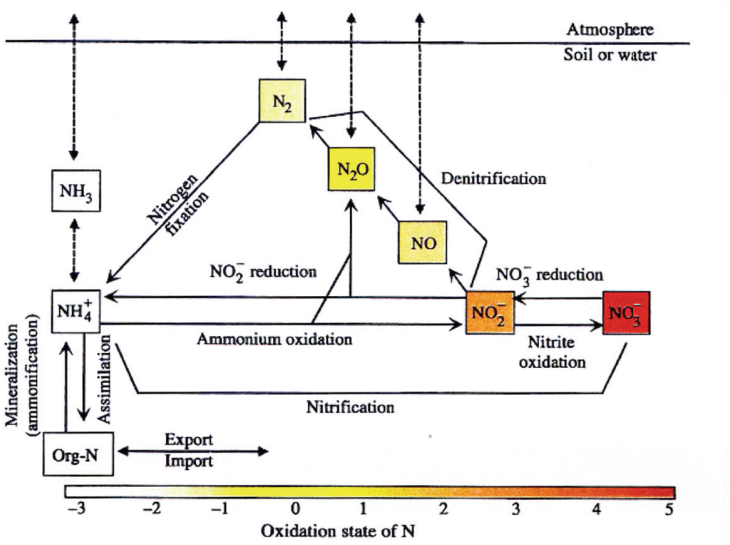

Figure 1.4: The marine nitrogen cycle following Galloway (2005). The different forms of N in seawater are grouped according to the oxidation states of N ion.

in recent studies are between 100–150 $\mathrm{Tg\,N\,y^{-1}}$ (Gruber and Sarmiento, 1997; Capone and Carpenter, 1999; Codispoti et al., 2001; Gruber, 2004; Galloway et al., 2004; Deutsch et al., 2007). This flux accounts for the largest source of fixed nitrogen to the ocean: ∼50 % of the total N source. Compared to the current estimates of denitrification, e.g. 350 $\mathrm{Tg\,N\,y^{-1}}$ by Brandes and Devol (2002), the marine N budget is still far from balanced, although the uncertainties of these estimates remain large (Gruber, 2008).

1.3.2 N_2 fixation

1.3.2.1 N_2 fixing reaction

Biological N_2 fixation converts N_2 to NH_4^+, where 8 mol ATP is required to fix 1 mol N (Eq. 1.1).

$$N_2 + 8H^+ + 8e^- + 16ATP \longrightarrow 2NH_3 + H_2 + 16ADP + 16P_i \tag{1.1}$$

Pi represents inorganic phosphorus. This reaction is catalysed by an enzyme system — nitrogenase, a complex of highly conserved proteins among various terrestrial and aquatic N_2 fixing prokaryotes (Karl et al., 2002). Nitrogenase has two components: N_2 reductase, an Fe protein coded in *nifH* genes, and dinitrogenase, an Fe-Mo protein (Postgate, 1982). The synthesis and activity of nitrogenase is inhibited by the presence of O_2 (Gallon, 1992). Therefore, N_2 fixation is a strictly anaerobic process. Oxygenic photosynthetic N_2 fixers have evolved various strategies to shield N_2 fixation from O_2 such as a spatial segregation of N_2 fixation in specialised cells — heterocysts and diazocytes, in which PS II activity is strongly

reduced or even lacking, or a temporal separation, where N_2 fixation takes place in the dark (Carpenter and Capone, 2008).

1.3.2.2 Diazotrophs

Only a limited number of prokaryotes perform biological N_2 fixation. The most conspicuous and best studied diazotroph in the open ocean is the filamentous, non-heterocystous cyanobacteria species *Trichodesmium*. *Trichodesmium* has a cosmopolitan distribution throughout the majority of the oligotrophic tropical and subtropical oceans. Habitats of *Trichodesmium* are characterised by low nutrient concentrations, clear and warm waters and deep light penetration (Capone et al., 1997). *Trichodesmium* grows mainly in the upper water column with high concentrations above 50 m (Capone et al., 1997). Its growth rate is lower than that of most eukaryotic phytoplankton (LaRoche and Breitbarth, 2005) due to the high energy demand of diazotrophy.

Besides *Trichodesmium*, cyanobacterial endosymbionts of marine diatoms are supposed to contribute significantly in basin-scale N budgets (Carpenter et al., 1999; Villareal, 1991; Zehr et al., 2001). Some recent studies found that some unicellular coccoid cyanobacteria and heterotrophic proteobacteria are able to express *nifH* genes (Zehr et al., 2001; Falcon et al., 2004; Langlois et al., 2005). Their physiology is still largely unknown, therefore their contribution to the total N input can not yet be quantified.

1.3.2.3 Distribution of pelagic N_2 fixation

Over the last decades, various methods have been applied to determine the distribution and activity of marine diazotrophs. An accurate global distribution map of N_2 fixation or diazotrophs does not exist due to the difficulty of sampling (LaRoche and Breitbarth, 2005) and discrepancies between estimates of N_2 fixation made by different methods (Mahaffey et al., 2005).

Net N_2 incorporation rate can be determined by direct $^{15}N_2$ uptake method, while gross fixation activity is measured by the classical C_2H_2 reduction method (Mahaffey et al., 2005). Recently, diazotrophs have been identified and visualized by a molecular ecological method — detection of *nifH* genes (Zehr et al., 2001, 2003; Church et al., 2005; Langlois et al., 2008), allowing the discovery of new habitats and community composition of diazotrophs.

These measurements can reflect variability over short timescales such as daily, seasonal or interannual. N_2 fixation over larger temporal and spatial scales can be estimated using global or basin-scale geochemical methods based on anomalies from the N : P ratio (N^* or P^*) and methods based on mass balance of stable N isotopes (Michaels et al., 1996; Gruber and Sarmiento, 1997; Karl et al., 1997; Montoya et al., 2002; Hansell et al., 2004; Deutsch et al., 2007; Reynolds et al., 2007). These geochemical estimates exhibit discrepancies in the distribution pattern of N_2 fixation caused by different assumptions on the limitation of N_2 fixation. For instance, Gruber and Sarmiento (1997) found highest fixation rates in the tropical and subtropical North Atlantic and in the Mediterranean Sea with the concept of the geochemical tracer N^*, where the atmospheric Fe supply is relatively high (Fig. 1.5). Whereas Deutsch et al. (2007) inferred highest N_2 fixation rates downstream from OMZs in

the Pacific Ocean, using the tracer P* (Fig. 1.6). They attributed the surplus of P relative to N in some surface waters to the denitrification in the OMZs typically below the euphotic zone down to 500 m. Upwelling brings this N depleted water to surface and provides habitats for diazotrophs: high P and low fixed nitrogen. This result implies a P control of N_2 fixation rather than Fe control.

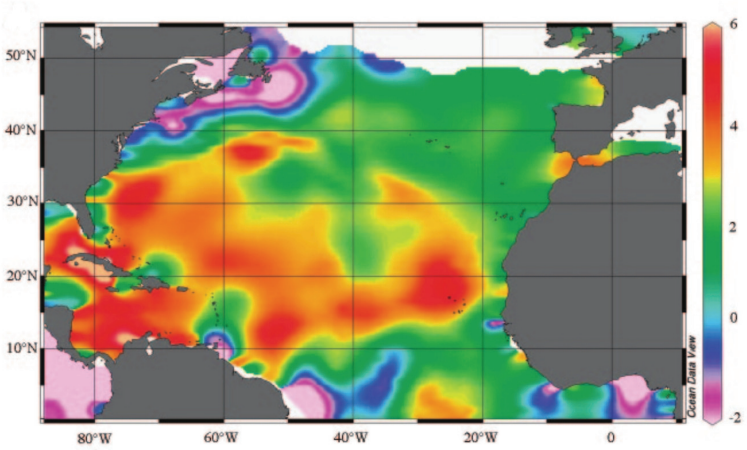

Figure 1.5: Distribution of N* ($\mathrm{mmol\,m^{-3}}$) on the isopycnal surface ($\sigma_\Theta = 26.5\,\mathrm{kg\,m^{-3}}$) in the tropical and subtropical North Atlantic according to Gruber and Sarmiento (1997) (Fig. 4 in Mahaffey et al. (2005)).

Another modern tool to study marine diazotrophs at broad spatial and temporal scales is ocean color remote sensing which can detect specific optical signals during *Trichodesmium* blooms (Subramaniam et al., 2001; Westberry et al., 2005). Bracher et al. (2009) more recently demonstrated the detection of cyanobacterial chlorophyll a at non-blooming concentration, using the PhytoDOAS (Differential Optical Absorption Spectroscopy including phytoplankton optical signatures) method.

1.3.2.4 Controlling factors of N_2 fixation

The mentioned advances in methodology not only improve the knowledge of the activity and distribution of N_2 fixation but also help in understanding their controlling factors.

Diazotrophic growth is often high during periods of high temperature, low winds and calm seas (e.g. Carpenter and Capone, 1992). Physical mixing has been taken as an important controlling factor of N_2 fixation, particularly for non-heterocystous diazotrophs such as *Trichodesmium*. Models based on mixed layer depth and light reproduced the distribution of *Trichodesmium* in the Atlantic (Hood et al., 2004), although relatively dense populations of *Trichodesmium* are also found in the trade wind belts with strong turbulence (Carpenter et al., 2004).

Temperature may control the distribution of tropical diazotrophs. *Trichodesmium* has been mostly observed in a temperature range from 20 to 34 °C (LaRoche and Breitbarth,

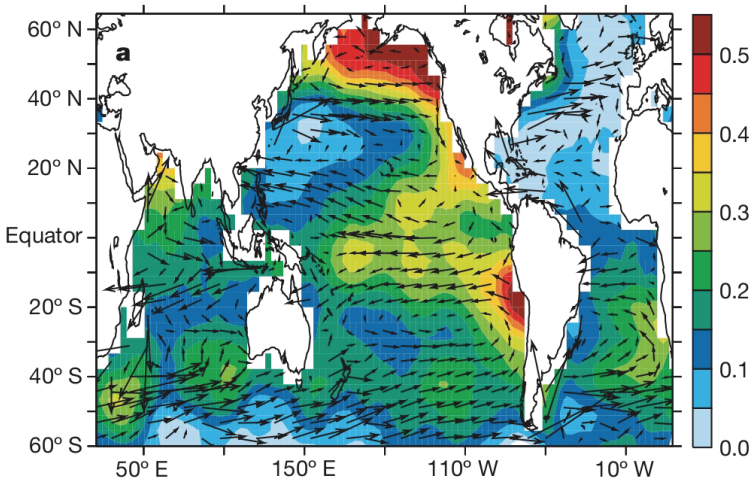

Figure 1.6: Distribution of P^* ($\mathrm{mmol\,m^{-3}}$) (Deutsch et al., 2007).

2005) with a maximum growth rate at ∼27°C (Breitbarth et al., 2007). Other diazotrophs have also been detected in waters colder than 20 °C (Holl et al., 2007; Needoba et al., 2007).

The different geochemical estimates of N_2 fixation distribution (see above) reveal the dependence of N_2 fixation on Fe and P. Iron is crucial for N_2 fixation based on the high Fe requirement of diazotrophy (Sañudo Wilhelmy et al., 2001; Kustka et al., 2003). N_2 fixation rates in Fe limited cultures of *Trichodesmium* were much lower than in Fe replete cultures (Berman-Frank et al., 2001).

While N_2 fixation is mainly limited by Fe in the Pacific Ocean (Moore and Doney, 2007), P-limitation (Sañudo Wilhelmy et al., 2001) or Fe-P-colimitation of N_2 fixation (Mills et al., 2004) was reported for the Atlantic. To overcome P limitation, different P pools are utilized by diazotrophs. A recent study found that *Trichodesmium* can exploit organic phosphorus besides PO_4^{3-} (Dyhrman et al., 2006). The contribution of this organic P to the total P availability still needs to be quantified.

After discussing the main factors controlling the marine N cycle (this section) and the biological carbon pump (Sect. 1.1), the interplay of P and Fe limitation can be summarised:

1. If Fe is replete, N_2 fixation and denitrification are coupled via the N : P ratio in the dissolved nutrient pool. This makes P the ultimate controlling factor for the marine N cycle and the biological carbon pump.

2. Under Fe limitation, N_2 fixation could be decoupled from denitrification (Lenton and Watson, 2000), leading to lower fixed N compared to that expected from given P concentrations. Besides influencing the primary production via the N inventory, Fe

is a direct trigger of the productivity in the HNLC regions. This complicates the whole picture and argues that both Fe and P should be taken into account for estimating the global primary production in the ocean.

1.4 PhD thesis in a complex picture of the marine system

Dust deposition fluxes, the dominant iron source for phytoplankton, might be considerably altered by climate change (Mahowald et al., 1999; Maher et al., 2010). Processes influencing the cycling of iron supplied by dust deposition and ecosystem feedbacks therefore become crucial for understanding the interactions between climate and marine productivity in the past, as well as for predicting them in the future. These processes link the cycling of different elements together. Studying them therefore requires a complex picture of the marine system. This thesis focuses on two key questions in this picture:

1. How does dust deposition impact Fe speciation and bioavailability? (Sect. 1.4.1)
2. How does dust deposition influence N_2 fixation and subsequently marine productivity? (Sect. 1.4.2)

1.4.1 Impact of dust deposition on Fe speciation and bioavailability

This thesis tries to answer this question from 3 aspects:

1. One vital topic in studies of iron speciation and bioavailability is its organic complexation. New insight into sources and the fate of organic Fe-binding ligands has been gained over the last decade. But existing models of Fe biogeochemistry do not describe these sources and fate explicitly. In this thesis, the cycle of organic ligands and its impact on DFe concentration is investigated in a model study for the Tropical Eastern North Atlantic Time-series Observatory (TENATSO). TENATSO is located between an oligotrophic and a mesotrophic region, with high but episodic dust deposition. Fe limitation may still occur during seasons of phytoplankton blooms and/or of low dust deposition.
2. Dust particles play a double role in changing DFe concentration: DFe is generated by dissolution from particles and at the same time removed by adsorption on particle surfaces and sinking. In the Fe model for TENATSO, the dynamics of sinking particles are taken into account by describing different size classes and particle aggregation. Processes controlling DFe loss are studied, including particle adsorption of soluble and colloidal iron as well as redissolution of iron from particles. Details of the model study of the iron biogeochemistry at TENATSO are introduced in Chapter 2.2.
3. Another opportunity to study the impact of dust particles on DFe concentration is by simulating a dust addition experiment in which particle dynamics and DFe change after the dust addition are monitored in a high temporal and spatial resolution. A model focusing on iron dissolution from and adsorption on dust particles has been developed

to simulate a mesocosm dust addition experiment. The experiment was carried out in typical LNLC (low-nutrient, low-chlorophyll) waters where phytoplankton productivity is supposed to be limited by the availability of macronutrients. Iron is not likely a growth limiting factor here because of the relatively high atmospheric input and the low phytoplankton biomass. Therefore, the physico-chemical processes controlling the change of DFe induced by dust addition dominate here, while the biological processes play a minor role in the Fe cycle. This model study is presented in Chapter 2.3.

1.4.2 Impact of dust deposition on N_2 fixation

At the TENATSO site, surface nitrate is low and the atmospheric iron input is high. According to the Fe control hypothesis (Sect. 1.1), TENATSO has a potentially high activity of N_2 fixation. Fe- and P-colimitation of N_2 fixation was observed in the tropical Eastern North Atlantic (Mills et al., 2004). It is however unclear if this limitation pattern can be generalised for this ocean region. Therefore, it is interesting to study, in a model, these limiting factors of N_2 fixation and the interactions between diazotrophic and non-diazotrophic phytoplankton. A NPZD (Nutrient-Phytoplankton-Zooplankton-Detritus) -type ecosystem model which describes the N, P and Fe content of biomass, is coupled with the complex Fe model for TENATSO (see above). N_2 fixation is described according to the physiology of *Trichodesmium*. Chapter 2.4 discusses the modelled impact of dust deposition on N_2 fixation by *Trichodesmium* and on the total primary productivity in this region.

In the general discussion following the chapters of publications, the main results from the studies are summarized and subjects and perspectives for future work are suggested.

Bibliography

M.A. Anderson and F.M.M. Morel. Uptake of Fe(II) by a diatom in oxic culture medium. *Mar. Biol. Lett.*, 1:263–268, 1980.

M.A. Anderson and F.M.M. Morel. The influence of aqueous iron chemistry on the uptake of iron by the coastal diatom *thalassiosira weissflogii*. *Limnology and Oceanography*, 27:789–831, 1982.

L. Balistieri, P.G. Brewer, and J.W. Murray. Scavenging residence times of trace metals and surface chemistry of sinking particles in the deep ocean. *Deep Sea Research*, 28A:101–121, 1981.

K. Barbeau, E.L. Rue, K.W. Bruland, and A. Butler. Photochemical cycling of iron in the surface ocean mediated by microbial iron(III)-binding ligands. *Nature*, 413:409–413, 2001.

K. Barbeau, E.L. Rue, C.G. Trick, K.W. Bruland, and A. Butler. Photochemical reactivity of siderophores produced by marine heterotrophic bacteria and cyanobacteria based on characteristic Fe(III) binding groups. *Limnology and Oceanography*, 48(3):1069–1078, 2003.

B.A. Bergquist and E.A. Boyle. Dissolved iron in the tropical and subtropical Atlantic Ocean. *Global Biogeochemical Cycles*, 20(1):GB1015, 2006. doi: 10.1029/2005GB002505.

Ilana Berman-Frank, Jay T. Cullen, Yeala Shaked, Robert M. Sherrell, and Paul G. Falkowski. Iron availability, cellular iron quotas, and nitrogen fixation in trichodesmium. *Limnology and Oceanography*, 46(6): 1249–1260, 2001.

P. W. Boyd and M. J. Ellwood. The biogeochemical cycle of iron in the ocean. *Nature Geosci*, 3(10):675–682, October 2010.

P. W. Boyd, T. Jickells, C. S. Law, S. Blain, E. A. Boyle, K. O. Buesseler, K. H. Coale, J. J. Cullen, H. J. W. de Baar, M. Follows, M. Harvey, C. Lancelot, M. Levasseur, N. P. J. Owens, R. Pollard, R. B. Rivkin, J. Sarmiento, V. Schoemann, V. Smetacek, S. Takeda, A. Tsuda, S. Turner, and A. J. Watson. Mesoscale iron enrichment experiments 1993-2005: Synthesis and future directions. *Science*, 315(5812): 612–617, February 2007.

P.W. Boyd, D.S. Mackie, and K.A. Hunter. Aerosol iron deposition to the surface ocean—modes of iron supply and biological responses. *Marine Chemistry*, 120(1-4):128–143, 2010. doi: 10.1016/j.marchem.2009.01.008.

M. Boye, C.M.G. van den Berg, J.T.M. de Jong, H. Leach, P. Croot, and H.J.W. de Baar. Organic complexation of iron in the Southern Ocean. *Deep-Sea Research Part I: Oceanographic Research Papers*, 48 (6):1477–1497, 2001.

A. Bracher, M. Vountas, T. Dinter, J. P. Burrows, R. Röttgers, and I. Peeken. Quantitative observation of cyanobacteria and diatoms from space using PhytoDOAS on SCIAMACHY data. *Biogeosciences*, 6(5): 751–764, 2009. doi: 10.5194/bg-6-751-2009.

Jay A. Brandes and Allan H. Devol. A global marine-fixed nitrogen isotopic budget: Implications for Holocene nitrogen cycling. *Global Biogeochem. Cycles*, 16(4):1120, December 2002. doi: 10.1029/2001GB001856.

E. Breitbarth, A. Oschlies, and J. LaRoche. Physiological constraints on the global distribution of Trichodesmium — effect of temperature on diazotrophy. *Biogeosciences*, 4(1):53–61, 2007. doi: 10.5194/bg-4-53-2007.

E. Breitbarth, E. P. Achterberg, M. V. Ardelan, A. R. Baker, E. Bucciarelli, F. Chever, P. L. Croot, S. Duggen, M. Gledhill, M. Hassellöv, C. Hassler, L. J. Hoffmann, K. A. Hunter, D. A. Hutchins, J. Ingri, T. Jickells, M. C. Lohan, M. C. Nielsdóttir, G. Sarthou, V. Schoemann, J. M. Trapp, D. R. Turner, and Y. Ye. Iron biogeochemistry across marine systems — progress from the past decade. *Biogeosciences*, 7 (3):1075–1097, 2010. doi: 10.5194/bg-7-1075-2010.

E. Bucciarelli, S. Blain, and P. Tréguer. Iron and manganese in the wake of the Kerguelen Islands (Southern Ocean). *Marine Chemistry*, 73(1):21–36, 2001.

R.H. Byrne and D.J. Kester. Solubility of hydrous ferric oxide and iron speciation in seawater. *Marine Chemistry*, 4:255–274, 1976.

D. G. Capone and E. J. Carpenter. Nitrogen fixation by marine cyanobacteria : historical and global perspectives. *Bulletin de l'Institut océanographique*, pages 235–256, 1999.

Douglas G. Capone and Angela N. Knapp. Oceanography: A marine nitrogen cycle fix? *Nature*, 445(7124): 159–160, January 2007.

Douglas G. Capone, Jonathan P. Zehr, HansW. Paerl, Birgitta Bergman, and Edward J. Carpenter. Trichodesmium, a globally significant marine cyanobacterium. *Science*, 276(5316):1221–1229, 1997. doi: 10.1126/science.276.5316.1221.

E. J. Carpenter, J. P. Montoya, J. Burns, M. R. Mulholland, A. Subramaniam, and D. G. Capone. Extensive bloom of a N_2-fixing diatom/cyanobacterial association in the tropical Atlantic Ocean. *Marine ecology. Progress series*, 185:273–283, 1999.

Edward J. Carpenter and Douglas G. Capone. Nitrogen fixation in the marine environment. In *Nitrogen in the Marine Environment (2nd Edition)*, pages 141–198. Academic Press, San Diego, 2008.

Edward J. Carpenter, Ajit Subramaniam, and Douglas G. Capone. Biomass and primary productivity of the cyanobacterium Trichodesmium spp. in the tropical N Atlantic ocean. *Deep Sea Research Part I: Oceanographic Research Papers*, 51(2):173–203, February 2004.

EJ. Carpenter and DG. Capone. Nitrogen fixation in Trichodesmium blooms. In EJ. Carpenter, DG. Capone, and J. Rueter, editors, *Marine pelagic cyanobacteria: Trichodesmium and other diazotrophs*, pages 211–217. Kluwer Academic Publishers, The Netherlands, 1992.

Matthew J. Church, Cindy M. Short, Bethany D. Jenkins, David M. Karl, and Jonathan P. Zehr. Temporal Patterns of Nitrogenase Gene *nifH* Expression in the Oligotrophic North Pacific Ocean. *Appl. Environ. Microbiol.*, 71(9):5362–5370, 2005. doi: 10.1128/AEM.71.9.5362-5370.2005.

Kenneth H. Coale, Kenneth S. Johnson, Steve E. Fitzwater, R. Michael Gordon, Sara Tanner, Francisco P. Chavez, Laurie Ferioli, Carole Sakamoto, Paul Rogers, Frank Millero, Paul Steinberg, Phil Nightingale, David Cooper, William P. Cochlan, Michael R. Landry, John Constantinou, Gretchen Rollwagen, Armando Trasvina, and Raphael Kudela. A massive phytoplankton bloom induced by an ecosystem-scale iron fertilization experiment in the equatorial Pacific Ocean. *Nature*, 383(6600):495–501, October 1996.

L. A. Codispoti, Jay A. Brandes, J. P. Christensen, S.W. A. Devol, A. H.and Naqvi, Hans W. Paerl, and T. Yoshinari. The oceanic fixed nitrogen and nitrous oxide budgets: Moving targets as we enter the anthropocene? *Scientia Marina*, 65(S2), 2001. doi: 10.3989/scimar.2001.65s285.

J.T. Cullen, B.A. Bergquist, and J.W. Moffett. Thermodynamic characterization of the partitioning of iron between soluble and colloidal species in the Atlantic Ocean. *Marine Chemistry*, 98(2-4):295–303, 2006.

H.J.W. de Baar and J.T.M. de Jong. Distributions, sources and sinks of iron in seawater. In D. Turner and K.A. Hunter, editors, *Biogeochemistry of Iron in Seawater*, volume 7 of *IUPAC Book Series on Analytical and Physical Chemistry of Environmental Systems*, pages 123–254. Wiley, 2001.

H.J.W. de Baar, J.T.M. de Jong, R.F. Nolting, K.R. Timmermans, M.A. van Leeuwe, U. Bathmann, M. Rutgers van der Loeff, and J. Sildam. Low dissolved Fe and the absence of diatom blooms in remote Pacific waters of the Southern Ocean. *Marine Chemistry*, 66(1-2):1–34, 1999.

H.J.W. de Baar, P.W. Boyd, K.H. Coale, M.R. Landry, A. Tsuda, P. Assmy, D.C.E. Bakker, Y. Bozec, R.T. Barber, M.A. Brzezinski, K.O. Buesseler, M. Boye, P.L. Croot, F. Gervais, M.Y. Gorbunov, P.J. Harrison, W.T. Hiscock, P. Laan, C. Lancelot, C.S. Law, M. Levasseur, A. Marchetti, F.J. Millero, J. Nishioka, Y. Nojiri, T. van Oijen, U. Riebesell, M.J.A. Rijkenberg, H. Saito, S. Takeda, K.R. Timmermans, M.J.W. Veldhuis, A.M. Waite, and C.-S. Wong. Synthesis of iron fertilization experiments: From the iron age in the age of enlightenment. *Journal of Geophysical Research C: Oceans*, 110(9):1–24, 2005.

M. L. Delaney. Phosphorus accumulation in marine sediments and the oceanic phosphorus cycle. *Global Biogeochem. Cycles*, 12(4):563–572, 1998.

Curtis Deutsch, Daniel M. Sigman, Robert C. Thunell, Anna Nele Meckler, and Gerald H. Haug. Isotopic constraints on glacial/interglacial changes in the oceanic nitrogen budget. *Global Biogeochem. Cycles*, 18 (4):GB4012, October 2004. doi: 10.1029/2003GB002189.

Curtis Deutsch, Jorge L. Sarmiento, Daniel M. Sigman, Nicolas Gruber, and John P. Dunne. Spatial coupling of nitrogen inputs and losses in the ocean. *Nature*, 445(7124):163–167, January 2007.

R.A. Duce and N.W. Tindale. Atmospheric transport of iron and its deposition in the ocean. *Limnology and Oceanography*, 36:1715–1726, 1991.

Richard C. Dugdale and Frances P. Wilkerson. Silicate regulation of new production in the equatorial Pacific upwelling. *Nature*, 391(6664):270–273, January 1998.

S. T. Dyhrman, P. D. Chappell, S. T. Haley, J. W. Moffett, E. D. Orchard, J. B. Waterbury, and E. A. Webb. Phosphonate utilization by the globally important marine diazotroph Trichodesmium. *Nature*, 439 (7072):68–71, January 2006.

Richard W. Eppley and Bruce J. Peterson. Particulate organic matter flux and planktonic new production in the deep ocean. *Nature*, 282(5740):677–680, December 1979.

Luisa I. Falcon, Edward J. Carpenter, Frank Cipriano, Birgitta Bergman, and Douglas G. Capone. N_2 fixation by unicellular bacterioplankton from the Atlantic and Pacific Oceans: Phylogeny and *in situ* rates. *Appl. Environ. Microbiol.*, 70(2):765–770, 2004. doi: 10.1128/AEM.70.2.765-770.2004.

P. G. Falkowski. Biogeochemistry of primary production in the sea. In William H. Schlesinger, editor, *Biogeochemistry*, volume 8 of *Treatise on geochemistry*, pages 185–213. Elsevier, 2005.

Paul G. Falkowski, Richard T. Barber, and Victor Smetacek. Biogeochemical controls and feedbacks on ocean primary production. *Science*, 281(5374):200–206, 1998. doi: 10.1126/science.281.5374.200.

P.G. Falkowski. Evolution of the nitrogen cycle and its influence on the biological sequestration of CO_2 in the ocean. *Nature*, 387:272–275, 1997.

Christopher B. Field, Michael J. Behrenfeld, James T. Randerson, and Paul Falkowski. Primary production of the biosphere: Integrating terrestrial and oceanic components. *Science*, 281(5374):237–240, 1998. doi: 10.1126/science.281.5374.237.

S.E. Fitzwater, K.H. Coale, R.M. Gordon, K.S. Johnson, and M.E. Ondrusek. Iron deficiency and phytoplankton growth in the equatorial Pacific. *Deep Sea Research*, 43 II:995–1015, 1996.

B. W. Frost. The role of grazing in nutrient-rich areas of the open sea. *Limnology and Oceanography*, 36(8): 1616–1630, 1991.

I. Fung, S.K. Meyn, I. Tegen, S.C. Doney, J. John, and J. Bishop. Iron supply and demand in the upper ocean. *Global Biogeochemical Cycles*, 14:281–301, 2000.

J. R. Gallon. Reconciling the incompatible: N2 fixation And O_2. *New Phytologist*, 122(4):571–609, 1992.

J. N. Galloway, F. J. Dentener, D. G. Capone, E. W. Boyer, R. W. Howarth, S. P. Seitzinger, G. P. Asner, C. C. Cleveland, P. A. Green, E. A. Holland, D. M. Karl, A. F. Michaels, J. H. Porter, A. R. Townsend, and C. J. Vosmarty. Nitrogen cycles: Past, present, and future. *Biogeochemistry*, 70:153–226, 2004. doi: 10.1007/s10533-004-0370-0.

James N. Galloway. The global nitrogen cycle: Past, present and future. *Science in China, Ser. C Life Sciences*, 48:669–677, 2005.

R.J. Geider and J. La Roche. The role of iron in phytoplankton photosynthesis and the potential for iron-limitation of primary productivity in the sea. *Photosynthesis Research*, 39:275–301, 1994.

M. Gledhill and C.M.G. van den Berg. Determination of complexation of iron(III) with natural organic complexing ligands in seawater using cathodic stripping voltammetry. *Marine Chemistry*, 47:41–54, 1994.

R.M. Gordon, J.H. Martin, and G.A. Knauer. Iron in north-east pacific waters. *Nature*, 299(5884):611–612, 1982.

J. Granger and N. M. Price. The importance of siderophores in iron nutrition of heterotrophic marine bacteria. *Limnology and Oceanography*, 44(3):541–555, 1999.

N. Gruber. The dynamics of the marine nitrogen cycle and its influence on atmospheric co_2 variations. In Mick Follows and Temel Oguz, editors, *The ocean carbon cycle and climate*, NATO ASI series, pages 97–148. Dordrecht, Kluwer Academic, 2004.

N. Gruber and J. L. Sarmiento. Large-scale biogeochemical/physical interactions in elemental cycles. In A. R. Robinson, J. J. McCarthy, and B. J. Rothschild, editors, *The sea: Biological-Physical interactions in the Ocean*, volume 12, pages 337–399. Wiley, 2002.

Nicolas Gruber. The marine nitrogen cycle: Overview and challenges. In *Nitrogen in the Marine Environment (2nd Edition)*, pages 1 – 50. Academic Press, San Diego, 2008. doi: 10.1016/B978-0-12-372522-6.00001-3.

Nicolas Gruber and Jorge L. Sarmiento. Global patterns of marine nitrogen fixation and denitrification. *Global Biogeochem. Cycles*, 11(2):235–266, 1997.

M.L. Guerinot. Microbial iron transport. *Annual Review of Microbiology*, 48:743–772, 1994.

Dennis A. Hansell, Nicholas R. Bates, and Donald B. Olson. Excess nitrate and nitrogen fixation in the North Atlantic Ocean. *Marine Chemistry*, 84(3-4):243–265, January 2004.

T.J. Hart. *On the phytoplankton of the south-west Atlantic and the Bellingshausen Sea, 1929-31*, volume 8 of *Discovery reports*. Cambridge: University Press, 1934.

Carolyn M. Holl, Anya M. Waite, Stephane Pesant, Peter A. Thompson, and Joseph P. Montoya. Unicellular diazotrophy as a source of nitrogen to Leeuwin Current coastal eddies. *Deep Sea Research Part II: Topical Studies in Oceanography*, 54(8-10):1045 – 1054, 2007. doi: 10.1016/j.dsr2.2007.02.002. The Leeuwin Current and its Eddies.

H. D. Holland. *The Chemical Evolution of the Atmosphere and Oceans*. Princeton Univ. Press, Princeton, NJ, 1984.

Bruce D. Honeyman, Laurie S. Balistrieri, and James W. Murray. Oceanic trace metal scavenging: the importance of particle concentration. *Deep Sea Research Part A. Oceanographic Research Papers*, 35(2): 227–246, 1988. doi: 10.1016/0198-0149(88)90038-6.

Raleigh R. Hood, Victoria J. Coles, and Douglas G. Capone. Modeling the distribution of Trichodesmium and nitrogen fixation in the Atlantic Ocean. *J. Geophys. Res.*, 109(C6):C06006–, June 2004.

R.J.M. Hudson and F.M.M. Morel. Iron transport in marine phytoplankton: Kinetics of cellular and medium coordination reactions. *Limnology and Oceanography*, 35:1002–1020, 1990.

K. A. Hunter and P. W. Boyd. Iron-binding ligands and their role in the ocean biogeochemistry of iron. *Environ. Chem.*, 4(4):221–232, August 2007.

D.A. Hutchins, J.G. Rueter, and W. Fish. Siderophore production and nitrogen fixation are mutually exclusive strategies in *Anabaena* 7120. *Limnology and Oceanography*, 36:1–12, 1991.

D.A. Hutchins, G.R. DiTullio, and K.W. Bruland. Iron and regenerated production — evidence for biological iron recycling in two marine environments. *Limnology and Oceanography*, 38:1242–1255, 1993.

D.A. Hutchins, A.E. Witter, A. Butler, and G.W. Luther III. Competition among marine phytoplankton for different chelated iron species. *Nature*, 400:858–861, 1999.

David A. Hutchins and Kenneth W. Bruland. Iron-limited diatom growth and Si:N uptake ratios in a coastal upwelling regime. *Nature*, 393(6685):561–564, June 1998.

George A. Jackson and Adrian B. Burd. Aggregation in the marine environment. *Environmental Science and Technology*, 32(19):2805–2814, 1998. doi: 10.1021/es980251w.

T.D. Jickells and L.J. Spokes. Atmospheric iron inputs to the oceans. In D.R. Turner and K. Hunter, editors, *The Biogeochemistry of Iron in Seawater*, volume 7 of *IUPAC Book Series on Analytical and Physical Chemistry of Environmental Systems*, pages 85–121. J. Wiley, 2001.

K. S. Johnson, F. P. Chavez, and G. E. Friederich. Continental-shelf sediment as a primary source of iron for coastal phytoplankton. *Nature*, 398(6729):697–700, 1999.

K.S. Johnson, R.M. Gordon, and K.H. Coale. What controls dissolved iron concentrations in the world ocean? *Marine Chemistry*, 57:137–161, 1997.

D. Karl, R. Letelier, L. Tupas, J. Dore, J. Christian, and D. Hebel. The role of nitrogen fixation in biogeochemical cycling in the subtropical North Pacific Ocean. *Nature*, 388(6642):533–538, August 1997.

D. Karl, A. Michaels, B. Bergman, D. Capone, E. Carpenter, R. Letelier, F. Lipschultz, H. Paerl, D. Sigman, and L. Stal. Dinitrogen fixation in the world's oceans. *Biogeochemistry*, 57-58:47–98, 2002.

K. Kuma, J. Nishioka, and K. Matsunaga. Controls on iron(III) hydroxide solubility in seawater: the influence of pH and natural organic chelators. *Limnology and Oceanography*, 41:396–407, 1996.

Adam B. Kustka, Sergio A. Sañudo Wilhelmy, Edward J. Carpenter, Douglas Capone, James Burns, and William G. Sunda. Iron requirements for dinitrogen- and ammonium-supported growth in cultures of Trichodesmium (IMS 101): Comparison with nitrogen fixation rates and iron: Carbon ratios of field populations. *Limnology and Oceanography*, 48:1869–1884, 2003.

Adam B. Kustka, Yeala Shaked, Allen J. Milligan, D. Whitney King, and François M. M. Morel. Extracellular production of superoxide by marine diatoms: Contrasting effects on iron redox chemistry and bioavailability. *Limnol. Oceanogr.*, 50(4):1172–1180, 2005. doi: 10.4319/lo.2005.50.4.1172.

J. La Roche, H. Murray, M. Orellana, and J. Newton. Flavodoxin expression as an indicator of iron limitation in marine diatoms1. *Journal of Phycology*, 31(4):520–530, 1995.

W.M. Landing and K.W. Bruland. The contrasting biochemistry of iron and manganese in the Pacific Ocean. *Geochimica et Cosmochimica Acta*, 51:29–43, 1987.

Rebecca J. Langlois, Julie LaRoche, and Philipp A. Raab. Diazotrophic Diversity and Distribution in the Tropical and Subtropical Atlantic Ocean. *Appl. Environ. Microbiol.*, 71(12):7910–7919, 2005. doi: 10.1128/AEM.71.12.7910-7919.2005.

Rebecca J. Langlois, Diana Hummer, and Julie LaRoche. Abundances and distributions of the dominant *nifH* phylotypes in the Northern Atlantic Ocean. *Appl. Environ. Microbiol.*, 74(6):1922–1931, 2008. doi: 10.1128/AEM.01720-07.

Delphine Lannuzel, Véronique Schoemann, Jeroen de Jong, Jean-Louis Tison, and Lei Chou. Distribution and biogeochemical behaviour of iron in the East Antarctic sea ice. *Marine Chemistry*, 106(1-2):18 – 32, 2007. doi: 10.1016/j.marchem.2006.06.010. Special issue: Dedicated to the memory of Professor Roland Wollast.

Delphine Lannuzel, Véronique Schoemann, Jeroen de Jong, Lei Chou, Bruno Delille, Sylvie Becquevort, and Jean-Louis Tison. Iron study during a time series in the western Weddell pack ice. *Marine Chemistry*, 108(1-2):85 – 95, 2008. doi: 10.1016/j.marchem.2007.10.006.

Julie LaRoche and Eike Breitbarth. Importance of the diazotrophs as a source of new nitrogen in the ocean. *Journal of Sea Research*, 53(1-2):67–91, January 2005.

Trish J. Lavery, Ben Roudnew, Peter Gill, Justin Seymour, Laurent Seuront, Genevieve Johnson, James G. Mitchell, and Victor Smetacek. Iron defecation by sperm whales stimulates carbon export in the Southern Ocean. *Proceedings of the Royal Society B: Biological Sciences*, 277(1699):3527–3531, November 2010.

Timothy M. Lenton and Andrew J. Watson. Redfield revisited: 1. regulation of nitrate, phosphate, and oxygen in the ocean. *Global Biogeochem. Cycles*, 14(1):225–248, 2000.

BL Lewis, GW III Luther, H Lane, and TM Church. Determination of metal-organic complexation in natural waters by SWASV with pseudopolarograms. *Electroanalysis*, 7(2):166–177, 1995.

B.M. Löscher, H.J.W. De Baar, J.T.M. de Jong, C. Veth, and F. Dehairs. The distribution of Fe in the Antarctic Circumpolar Current. *Deep-Sea Research II*, 44:143–187, 1997.

D. J. Mackey, J. E. O'Sullivan, and R. J. Watson. Iron in the western Pacific: a riverine or hydrothermal source for iron in the Equatorial Undercurrent? *Deep-Sea Research Part I-Oceanographic Research Papers*, 49(5):877–893, 2002.

H.M. Macrellis, C.G. Trick, E.L. Rue, G. Smith, and K.W. Bruland. Collection and detection of natural iron-binding ligands from seawater. *Marine Chemistry*, 76:175–187, 2001.

Claire Mahaffey, Anthony F. Michaels, and Douglas G. Capone. The conundrum of marine N_2 fixation. *Am. J. Sci.*, 305(6–8):546–595, 2005. doi: 10.2475/ajs.305.6-8.546.

B.A. Maher, J.M. Prospero, D. Mackie, D. Gaiero, P.P. Hesse, and Y. Balkanski. Global connections between aeolian dust, climate and ocean biogeochemistry at the present day and at the last glacial maximum. *Earth-Science Reviews*, 99(1-2):61 – 97, 2010. doi: 10.1016/j.earscirev.2009.12.001.

N. Mahowald, K. Kohfeld, M. Hansson, Y. Balkanski, S.P. Harrison, I.C. Prentice, M. Schulz, and H. Rodhe. Dust sources and deposition during the last glacial maximum and current climate: A comparison of model results with paleodata from ice cores and marine sediments. *Journal of Geophysical Research. D. Atmospheres*, 104:15895–15916, 1999.

Natalie M. Mahowald, Alex R. Baker, Gilles Bergametti, Nick Brooks, Robert A. Duce, Timothy D. Jickells, Nilgun Kubilay, Joseph M. Prospero, and Ina Tegen. Atmospheric global dust cycle and iron inputs to the ocean. *Global Biogeochem. Cycles*, 19(4):GB4025, December 2005.

Ernst Maier-Reimer, Uwe Mikolajewicz, and Arne Winguth. Future ocean uptake of CO_2: interaction between ocean circulation and biology. *Climate Dynamics*, 12(10):711–722, 1996.

Maria T Maldonado, Robert F Strzepek, Sylvia Sander, and Philip W Boyd. Acquisition of iron bound to strong organic complexes, with different Fe binding groups and photochemical reactivities, by plankton communities in Fe-limited subantarctic waters. *Global Biogeochemical Cycles*, 19(4):GB4S23, October 2005. doi: 10.1029/2005GB002481.

M.T. Maldonado and N.M. Price. Utilization of iron bound to strong organic ligands by plankton communities in the subarctic North Pacific. *Deep Sea Research*, II 46:2447–2473, 1999.

M.T. Maldonado and N.M. Price. Reduction and transport of organically bound iron by *Thalassiosira oceanica* (Bacillariophyceae). *Journal of Phycology*, 37:298–309, 2001.

A. Marchetti and N. Cassar. Diatom elemental and morphological changes in response to iron limitation: a brief review with potential paleoceanographic applications. *Geobiology*, 7(4):419–431, 2009.

J.H. Martin. Glacial-interglacial CO_2 change: The iron hypothesis. *Paleoceanography*, 5:1–13, 1990.

J.H. Martin and S.E. Fitzwater. Iron deficiency limits phytoplankton growth in the northeast Pacific subarctic. *Nature*, 331:341–343, 1988.

J.H. Martin and R.M. Gordon. Northeast Pacific iron distributions in relation to phytoplankton productivity. *Deep-Sea Research*, 35:177–196, 1988.

J.H. Martin, R.M. Gordon, S.E. Fitzwater, and W.W. Broenkow. VERTEX: phytoplankton/iron studies in the Gulf of Alaska. *Deep-Sea Research*, 36:649–680, 1989.

J.H. Martin, R.M. Gordon, and S.E. Fitzwater. The case for iron. *Limnology and Oceanography*, 36(8): 1793–1802, 1991.

J.H. Martin, S.E. Fitzwater, R.M. Gordon, C.N. Hunter, and S.J. Tanner. Iron, primary production and carbon-nitrogen flux studies during the JGOFS North Atlantic Bloom Experiment. *Deep-Sea Research, Part II*, 40(1-2):115–134, 1993.

I.N. McCave. Size spectra and aggregation of suspended particles in the deep ocean. *Deep-Sea Research A*, 31(4):329–352, 1984.

R. M. L. McKay, J. La Roche, A. F. Yakunin, D. G. Durnford, and R. J. Geider. Accumulation of ferredoxin and flavodoxin in a marine diatom in response to Fe. *Journal of Phycology*, 35(3):510–519, 1999.

A. Michaels, D. Olson, J. Sarmiento, J. Ammerman, K. Fanning, R. Jahnke, A. Knap, F. Lipschultz, and J. Prospero. Inputs, losses and transformations of nitrogen and phosphorus in the pelagic North Atlantic Ocean. *Biogeochemistry*, 35:181–226, 1996.

F.J. Millero and S. Sotolongo. The oxidation of Fe(II) with H_2O_2 in seawater. *Geochimica et Cosmochimica Acta*, 53:1867–1873, 1989.

M.M. Mills, C. Ridame, M. Davey, J. La Roche, and R. Geider. Iron and phosphorus co-limit nitrogen fixation in the eastern tropical North Atlantic. *Nature*, 429:292–294, 2004.

Joseph P. Montoya, Edward J. Carpenter, and Douglas G. Capone. Nitrogen fixation and nitrogen isotope abundances in zooplankton of the oligotrophic North Atlantic. *Limnology and Oceanography*, 47:1617–1628, 2002.

C. M. Moore, M. M. Mills, A. Milne, R. Langlois, E. P. Achterberg, K. Lochte, R. J. Geider, and J. La Roche. Iron limits primary productivity during spring bloom development in the central North Atlantic. *Global Change Biology*, 12(4):626–634, 2006.

J. Keith Moore and Scott C. Doney. Iron availability limits the ocean nitrogen inventory stabilizing feedbacks between marine denitrification and nitrogen fixation. *Global Biogeochem. Cycles*, 21(2):GB2001, April 2007.

F. M. M. Morel and R. J. M. Hudson. Geobiological cycle of trace elements in aquatic systems: Redfield revisited. In *Chemical Processes in Lakes*, pages 251–281. John Wiley and Sons, New York, 1985.

F.M.M. Morel, R.J.M. Hudson, and N.M. Price. Limitation of productivity by trace metals in the sea. *Limnology and Oceanography*, 36:1742–1755, 1991.

Rachel A. Needoba, Joseph A.and Foster, Carole Sakamoto, Jonathan P. Zehr, and Kenneth S. Johnson. Nitrogen fixation by unicellular diazotrophic cyanobacteria in the temperate oligotrophic North Pacific Ocean. *Limnology and Oceanography*, 52(4):1317–1327, 2007.

U Passow. Switching perspectives: Do mineral fluxes determine particulate organic carbon fluxes or vice versa? *Geochemistry Geophysics Geosystems*, 5:Q04002, 2004. doi: 10.1029/2003GC000670.

John Raymond Postgate. *The fundamentals of nitrogen fixation*. Cambridge University Press, 1982.

R.T. Powell and A. Wilson-Finelli. Photochemical degradation of organic iron complexing ligands in seawater. *Aquatic Sciences*, 65(4):367–374, 2003.

N. M. Price, B. A. Ahner, and F. M. M. Morel. The equatorial Pacific Ocean—grazer-controlled phytoplankton populations in an iron-limited ecosystem. *Limnology and Oceanography*, 39:520–534, 1994.

N.M. Price, L.F. Andersen, and F.M.M. Morel. Iron and nitrogen nutrition of equatorial Pacific plankton. *Deep-Sea Research*, 38:1361–1378, 1991.

Rob Raiswell, Liane Benning, Martyn Tranter, and Slawek Tulaczyk. Bioavailable iron in the Southern Ocean: the significance of the iceberg conveyor belt. *Geochemical Transactions*, 9(1):7, 2008. doi: 10.1186/1467-4866-9-7.

V. Ratmeyer, G. Fischer, and G. Wefer. Lithogenic particle fluxes and grain size distributions in the deep ocean off Northwest Africa: Implications for seasonal changes of aeolian dust input and downward transport. *Deep-Sea Research (Part I, Oceanographic Research Papers)*, 46(8):1289–1337, August 1999. doi: 10.1016/S0967-0637(99)00008-4.

J.A. Raven. The iron and molybdenum use efficiencies of plant growth with different energy, carbon, and nitrogen sources. *New Phytologist*, 109:279–287, 1988.

J.A. Raven. Predictions of Mn and Fe use efficiencies of phototrophic growth as a function of light availability for growth and C assimilation pathway. *New Phytologist*, 116:1–18, 1990.

A. C. Redfield. The biological control of chemical factors in the environment. *Am. Sci.*, 46:205–221, 1958.

RT Reid, DH Live, DJ Faulkner, and A. Butler. A siderophore from a marine bacterium with an exceptional ferric ion affinity constant. *Nature*, 366(6454):455–458, 1993.

Sarah E. Reynolds, Rhiannon L. Mather, George A. Wolff, Richard G. Williams, Angela Landolfi, Richard Sanders, and E. Malcolm S. Woodward. How widespread and important is N_2 fixation in the North Atlantic Ocean? *Global Biogeochem. Cycles*, 21(4):GB4015–, November 2007.

H.W. Rich and F.M.M. Morel. Availability of well-defined iron colloids to the marine diatom *Thalassiosira Weissdlogii*. *Limnology and Oceanography*, 35:652–662, 1990.

A.L. Rose and T.D. Waite. Kinetics of hydrolysis and precipitation of ferric iron in seawater. *Environmental Science & Technology*, 37:3897–3903, 2003.

E.L. Rue and K.W. Bruland. Complexation of iron(III) by natural organic ligands in the Central North Pacific as determined by a new competitive ligand equilibration / adsorptive cathodic stripping voltammetric method. *Marine Chemistry*, 50:117–138, 1995.

J. G. Rueter, K. Ohki, and Y. Fujita. The effect of iron nutrition on photosynthesis and nitrogen fixation in cultures of Trichodesmium (Cyanophyceae). *Journal of Phycology*, 26(1):30–35, 1990.

Sergio A. Sañudo Wilhelmy, Adam B. Kustka, Christopher J. Gobler, David A. Hutchins, Min Yang, Kamazima Lwiza, James Burns, Douglas G. Capone, John A. Raven, and Edward J. Carpenter. Phosphorus limitation of nitrogen fixation by Trichodesmium in the central Atlantic Ocean. *Nature*, 411(6833):66–69, May 2001.

Mak A. Saito, James W. Moffett, Sallie W. Chisholm, and John B. Waterbury. Cobalt limitation and uptake in Prochlorococcus. *Limnology and Oceanography*, 47(6):1629–1636, 2002.

Moriah Sandy and Alison Butler. Microbial iron acquisition: Marine and terrestrial siderophores. *Chemical Reviews*, 109(10):4580–4595, October 2009. doi: 10.1021/cr9002787.

J. L. Sarmiento and J. R. Toggweiler. A new model for the role of the oceans in determining atmospheric pCO_2. *Nature*, 308(5960):621–624, April 1984.

Geraldine Sarthou, Klaas R. Timmermans, Stephane Blain, and Paul Treguer. Growth physiology and fate of diatoms in the ocean: a review. *Journal of Sea Research*, 53(1-2):25–42, January 2005.

Y. Shaked, A. B. Kustka, and F. M. M. Morel. A general kinetic model for iron acquisition by eukaryotic phytoplankton. *Limnology and Oceanography*, 50(3):872–882, 2005.

Y. Sohrin, S. Iwamoto, M. Matsui, H. Obata, E. Nakayama, K. Suzuki, N. Handa, and M. Ishii. The distribution of Fe in the Australian sector of the Southern Ocean. *Deep-Sea Research Part I-Oceanographic Research Papers*, 47(1):55–84, 2000.

Robert F. Strzepek and Paul J. Harrison. Photosynthetic architecture differs in coastal and oceanic diatoms. *Nature*, 431(7009):689–692, October 2004.

Ajit Subramaniam, Christopher W. Brown, Raleigh R. Hood, Edward J. Carpenter, and Douglas G. Capone. Detecting Trichodesmium blooms in SeaWiFS imagery. *Deep Sea Research Part II: Topical Studies in Oceanography*, 49(1-3):107 – 121, 2001. doi: 10.1016/S0967-0645(01)00096-0. The US JGOFS Synthesis and Modeling Project: Phase 1.

W.G. Sunda. Bioavailability and bioaccumulation of iron in the sea. In *Biogeochemistry of Iron in Seawater*, volume 7 of *IUPAC Book Series on Analytical and Physical Chemistry of Environmental Systems*. Wiley, 2001.

W.G. Sunda and S.A. Huntsman. Iron uptake and growth limitation in oceanic and coastal phytoplankton. *Marine Chemistry*, 50:189–206, 1995.

W.G. Sunda and S.A. Huntsman. Interrelated influence of iron, light and cell size on marine phytoplankton growth. *Nature*, 390:389– 392, 1997.

Robert Swap, Stanley Ulanski, Matthew Cobbett, and Michael Garstang. Temporal and spatial characteristics of Saharan dust outbreaks. *J. Geophys. Res.*, 101(D2):4205–4220, 1996.

Alessandro Tagliabue, Laurent Bopp, Jean-Claude Dutay, Andrew R. Bowie, Fanny Chever, Philippe Jean-Baptiste, Eva Bucciarelli, Delphine Lannuzel, Tomas Remenyi, Geraldine Sarthou, Olivier Aumont, Marion Gehlen, and Catherine Jeandel. Hydrothermal contribution to the oceanic dissolved iron inventory. *Nature Geosci*, 3(4):252–256, April 2010.

S.R. Taylor. Abundance of chemical elements in the continental crust: a new table. *Geochimica et Cosmochimica Acta*, 28(8):1273 – 1285, 1964. doi: 10.1016/0016-7037(64)90129-2.

Raewyn M. Town and Montserrat Filella. Dispelling the myths: Is the existence of L1 and L2 ligands necessary to explain metal ion speciation in natural waters? *Limnology and Oceanography*, 45(6):1341–1357, 2000.

D. R. Turner, K. A. Hunter, and H. J. W. de Baar. Introduction. In D. Turner and K.A. Hunter, editors, *Biogeochemistry of Iron in Seawater*, volume 7 of *IUPAC Book Series on Analytical and Physical Chemistry of Environmental Systems*. Wiley, 2001.

Benjamin S. Twining, Stephen B. Baines, Nicholas S. Fisher, and Michael R. Landry. Cellular iron contents of plankton during the Southern Ocean Iron Experiment (SOFeX). *Deep Sea Research Part I: Oceanographic Research Papers*, 51(12):1827–1850, December 2004.

Tracy A. Villareal. Nitrogen-fixation by the cyanobacterial symbiont of the diatom genus Hemiaulus. *Mar. Ecol. Prog. Ser.*, 76:201–204, 1991.

Christoph Völker and Dieter A. Wolf-Gladrow. Physical limits on iron uptake mediated by siderophores or surface reductases. *Marine Chemistry*, 65(3-4):227 – 244, 1999. doi: 10.1016/S0304-4203(99)00004-3.

Julia M. Vraspir and Alison Butler. Chemistry of marine ligands and siderophores. *Annual Review of Marine Science*, 1(1):43–63, 2009. doi: 10.1146/annurev.marine.010908.163712.

A.J. Watson. Iron limitation in the ocean. In *The biogeochemistry of iron in seawater*, volume 7 of *IUPAC Book Series on Analytical and Physical Chemistry of Environmental Systems*, pages 9–39. Wiley, 2001.

T. K. Westberry, D. A. Siegel, and A. Subramaniam. An improved bio-optical model for the remote sensing of Trichodesmium spp. blooms. *J. Geophys. Res.*, 110(C6):C06012–, June 2005.

S.W. Wilhelm and C.G. Trick. Iron-limited growth of cyanobacteria: Multiple siderophore production is a common response. *Limnology and Oceanography*, 39:1979–1984, 1994.

S.W. Wilhelm, D.P. Maxwell, and C.G. Trick. Growth, iron requirements, and siderophore production in iron-limited *Synechococcus* PCC 7002. *Limnology and Oceanography*, 41:89–97, 1996.

J. Wu and G.W. Luther III. Complexation of Fe(III) by natural organic ligands in the Northwest Atlantic Ocean by a competitive ligand equilibration method and a kinetic approach. *Marine Chemistry*, 50: 159–177, 1995.

J. Wu, E. Boyle, W. Sunda, and L.-S. Wen. Soluble and colloidal iron in the oligotrophic North Atlantic and North Pacific. *Science*, 293:847–849, 2001.

J. P. Zehr, B. D. Jenkins, S. M. Short, and G. F. Steward. Nitrogenase gene diversity and microbial community structure: a cross-system comparison. *Environmental Microbiology*, 5(7):539–554, 2003.

Jonathan P. Zehr and Bess B. Ward. Nitrogen Cycling in the Ocean: New Perspectives on Processes and Paradigms. *Appl. Environ. Microbiol.*, 68(3):1015–1024, 2002. doi: 10.1128/AEM.68.3.1015-1024.2002.

Jonathan P. Zehr, John B. Waterbury, Patricia J. Turner, Joseph P. Montoya, Enoma Omoregie, Grieg F. Steward, Andrew Hansen, and David M. Karl. Unicellular cyanobacteria fix N_2 in the subtropical North Pacific Ocean. *Nature*, 412(6847):635–638, August 2001.

Chapter 2

Publications

2.1 Publication list and declaration of the own contribution to each publication

Publication I:

Y. Ye, C. Völker, and D. A. Wolf-Gladrow. A model of Fe speciation and biogeochemistry at the Tropical Eastern North Atlantic Time-Series Observatory site. Biogeosciences, 6(10): 2041-2061, 2009.

Die Entwicklung des Modells habe ich in Zusammenarbeit mit C. Völker geplant und durchgeführt. Das Manuskript wurde in Zusammenarbeit mit den Koautoren verfasst.

Publication II:

Y. Ye, T. Wagener, C. Völker, C. Guieu and D. A. Wolf-Gladrow. Dust deposition: iron source or sink? A case study. Biogeosciences Discuss., 7, 92199272, 2010.

Das *in situ* Experiment wurde von T. Wagener und seinen Kollegen durchgeführt. Die Entwicklung des Modells habe ich geplant und durchgeführt. Die Ergebnisse habe ich mit T. Wagener and C. Völker diskutiert. Das ManusKript wurde in Zusammenarbeit mit den Koautoren verfasst.

Publication III:

Y. Ye, C. Völker, A. Bracher, B. Schmitt and D. A. Wolf-Gladrow. Environmental controls on N_2 fixation by *Trichodesmium* in the tropical Eastern North Atlantic. (in prep.)

Die Entwicklung des Modells habe ich in Zusammenarbeit mit C. Völker geplant. Die Modellierung habe ich durchgeführt. Die Satellitendaten haben A. Bracher und ihre Kollegen erhoben. Das Manuskript wurde in Zusammenarbeit mit den Koautoren verfasst.

Publication IV (in the appendix):

E. Breitbarth, E. P. Achterberg, M. V. Ardelan, A. R. Baker, E. Bucciarelli, F. Chever, P. L. Croot, S. Duggen, M. Gledhill, M. Hassellöv, C. Hassler, L. J. Hoffmann, K. A. Hunter, D. A. Hutchins, J. Ingri, T. Jickells, M. C. Lohan, M. C. Nielsdóttir, G. Sarthou, V. Schoemann, J. M. Trapp, D. R. Turner, and Y. Ye. Iron biogeochemistry across marine systems — progress from the past decade. Biogeosciences, 7, 1075–1097, 2010.

Ich habe an der Diskussion während der Konferenz und der Verfassung des Manuskripts teilgenommen.

2.2 Publication I

A model of Fe speciation and biogeochemistry
at the Tropical Eastern North Atlantic
Time-Series Observatory site

Biogeosciences, 6, 2041–2061, 2009
www.biogeosciences.net/6/2041/2009/

Biogeosciences

A model of Fe speciation and biogeochemistry at the Tropical Eastern North Atlantic Time-Series Observatory site

Y. Ye, C. Völker, and D. A. Wolf-Gladrow

Alfred Wegener Institute for Polar and Marine Research, Bremerhaven, Germany

Received: 27 February 2009 – Published in Biogeosciences Discuss.: 17 April 2009
Revised: 2 September 2009 – Accepted: 16 September 2009 – Published: 7 October 2009

Abstract. A one-dimensional model of Fe speciation and biogeochemistry, coupled with the General Ocean Turbulence Model (GOTM) and a NPZD-type ecosystem model, is applied for the Tropical Eastern North Atlantic Time-Series Observatory (TENATSO) site. Among diverse processes affecting Fe speciation, this study is focusing on investigating the role of dust particles in removing dissolved iron (DFe) by a more complex description of particle aggregation and sinking, and explaining the abundance of organic Fe-binding ligands by modelling their origin and fate.

The vertical distribution of different particle classes in the model shows high sensitivity to changing aggregation rates. Using the aggregation rates from the sensitivity study in this work, modelled particle fluxes are close to observations, with dust particles dominating near the surface and aggregates deeper in the water column. POC export at 1000 m is a little higher than regional sediment trap measurements, suggesting further improvement of modelling particle aggregation, sinking or remineralisation.

Modelled strong ligands have a high abundance near the surface and decline rapidly below the deep chlorophyll maximum, showing qualitative similarity to observations. Without production of strong ligands, phytoplankton concentration falls to 0 within the first 2 years in the model integration, caused by strong Fe-limitation. A nudging of total weak ligands towards a constant value is required for reproducing the observed nutrient-like profiles, assuming a decay time of 7 years for weak ligands. This indicates that weak ligands have a longer decay time and therefore cannot be modelled adequately in a one-dimensional model.

The modelled DFe profile is strongly influenced by particle concentration and vertical distribution, because the most important removal of DFe in deeper waters is colloid formation and aggregation. Redissolution of particulate iron is required to reproduce an observed DFe profile at TENATSO site. Assuming colloidal iron is mainly composed of inorganic colloids, the modelled colloidal to soluble iron ratio is lower that observations, indicating the importance of organic colloids.

Correspondence to: Y. Ye
(ying.ye@awi.de)

1 Introduction

Iron is an essential micro-nutrient for marine phytoplankton. Its low availability in the upper ocean has been made responsible for the high-nitrate low-chlorophyll (HNLC) conditions in the Southern Ocean, the equatorial Pacific and the subpolar North Pacific (Boyd et al., 2007). It has been hypothesised that iron could also indirectly affect primary production in oligotrophic regions by limiting nitrogen-fixation (Mills et al., 2004.; Falkowski, 1997).

The solubility of iron is low under oxic conditions. Iron exists in seawater in different physical and chemical forms, e.g. inorganic soluble ferric and ferrous iron, organically complexed iron, colloidal and particulate iron. Some of these forms can be utilised by phytoplankton (Maldonado and Price, 1999; Hutchins et al., 1999) and transformed into organic particulate iron. Dissolved iron can be transported into the particulate pool also by scavenging onto particles (Balistieri et al., 1981), binding on cell surfaces (Hutchins et al., 2002; Tovar-Sanchez et al., 2003) and colloidal aggregation (Wells and Goldberg, 1993; Johnson et al., 1994; Wen et al., 1997), thereby becoming unavailable for biological uptake. Thus, iron bioavailability and residence time are controlled by its speciation and removal from the upper water layers.

Dust deposition, an important natural iron source for marine systems away from the continental shelf, is spatially and temporally variable and affected by climate change (Mahowald et al., 2003; Jickells et al., 2005). How it affects

Published by Copernicus Publications on behalf of the European Geosciences Union.

marine productivity and thus the carbon cycle depends on the processes influencing Fe speciation and bioavailability. Recent studies enhanced our knowledge on many reactions in Fe speciation and factors influencing them. To provide a better understanding of the interaction of individual processes and the response of ecosystems to varying iron speciation, several numerical models focusing on different questions or regions have been developed: global models of iron cycling primarily aimed at reproducing the removal of iron by scavenging in the deep ocean (Parekh et al., 2004) or the characteristics of regional features under iron limitation (Aumont et al., 2003); process-based models have been refined for coastal waters by Rose and Waite (2003a), for the upper ocean at the Bermuda Atlantic Time-series Study (BATS) site by Weber et al. (2005, 2007) and for understanding the influence of light and temperature on the marine iron cycle (Tagliabue et al., 2009).

Weber et al. (2007) coupled a one-dimensional model of iron speciation and biogeochemistry with the General Ocean Turbulence Model (GOTM) and a NPZD-type (Nitrogen, Phytoplankton, Zooplankton and Detritus) ecosystem model. Our model is based on the model by Weber et al. (2007) and has been adapted and extended for the specific questions in this study:

1. High dust deposition brings not only considerable input of iron into surface waters but also fine inorganic particles for particle aggregation and Fe scavenging. What are the characteristics of the particle distribution in seawater? And how do they influence DFe removal and thus its bioavailability?

2. Fe speciation and concentration is largely regulated by the abundance of organic Fe-binding ligands. 99% of dissolved Fe is organically complexed (Gledhill and van den Berg, 1994; van den Berg, 1995; Rue and Bruland, 1995). Studies in the last two decades have identified a number of different marine Fe-binding ligands and their vertical distribution are also measured in some regions (van den Berg, 1995; Rue and Bruland, 1995; Witter and Luther III, 1998; Witter et al., 2000; Boye et al., 2001, 2006; Cullen et al., 2006; Gerringa et al., 2006, 2008.). Sources and fate of these organic ligands are still largely unknown, although siderophore-like compounds are found to be produced by various marine bacteria and cyanobacteria and have similar conditional stability constants as the strong Fe-binding ligands occurring in natural seawater (Hunter and Boyd, 2007). Can the existing hypotheses on the origin and fate of organic ligands explain the observed ligand vertical distribution and organic complexation of iron?

Focusing on these two questions, we extended the model by Weber et al. (2007) by a more complex description of particle aggregation and sinking and by including organic ligand dynamics with sources and sinks (instead of prescribing ligands concentrations). We applied the model to simulate the cycling of iron at the Tropical Eastern North Atlantic Time-Series Observatory (TENATSO) site (17.4° N, 24.5° W), a new time-series station north of the Cape Verde Islands. The TENATSO site provides ideal conditions for investigation of dust deposition on Fe speciation and bioavailability in the upper ocean, because it is strongly influenced by Saharan dust events and its mixed layer depth has very low seasonal variability. Given that observations on Fe biogeochemistry are still sparse and that regular sampling at TENATSO has only recently begun, the main aim of this study is not the quantitative reproduction of the reality at TENATSO but the qualitative understanding of processes.

2 Model description

Our model consists of a physical, biological, and chemical model coupled in a one-dimensional vertical water column representing the upper 1000 m water depth. Horizontal gradients are assumed to be small and are thus neglected. The water column is divided into 100 layers. Layer spacing is given by $h_n = H \cdot (\tanh(2n/N) - \tanh(2(n-1)/N))/\tanh(2)$ where H is the depth of the water column, N is the number of layers, and $n=1$ is the lowermost layer, while $n=N$ is the surface layer. This results in a surface layer thickness of 1.5 m and 33 layers within the upper 100 m.

The model is integrated forward in time until deep-ocean concentration profiles become cyclostationary, using a repeated atmospheric forcing from the 1 January 1990 to 31 December 1993. Due to the slow equilibration of deep dissolved iron and ligand profiles, the total integration time is 30 years. After this spin-up period the model is integrated over five more years for analysis, using forcing from 1 January 1990 to 31 December 1994. The time-step of the model is 1200 s and the biochemical variables are integrated forward in time using a modified Patankar scheme (Burchard et al., 2005) which is positive, conservative, and able to solve accurately systems that contain reactions with time-scales much shorter than the model time-step, such as photochemical reactions (see Sect. 2.4 Chemical model).

2.1 Physical model

The physical model is the General Ocean Turbulence Model (GOTM, Umlauf and Burchard, 2005, http://www.gotm.net/), which provides the vertical mixing and advection for given forcing by wind, heat and freshwater fluxes at the surface. The model configuration is based on the configuration by Weber et al. (2007), and has been adapted for the TENATSO site by forcing the model with daily fluxes derived from the ERA40 atmospheric reanalysis (Uppala et al., 2005) for the TENATSO site, and using a $k-\epsilon$ turbulence closure, with a minimum turbulent kinetic energy (TKE) value of $10^{-5}\,\mathrm{m^2\,s^{-2}}$ to account for double diffusion. A

third-order scheme with flux limiter (Burchard and Umlauf, 2005) is used for vertical advection and sinking of biogeochemical variables.

2.2 Biological model

The biological part of our model is a nitrogen-based ecosystem model developed originally by Schartau and Oschlies (2003a,b). Its four compartments are nitrogen (N), phytoplankton (P), zooplankton (Z), and detritus (D). The processes and fluxes between them are mostly described in the same way as in Weber et al. (2007). We use the parameter values optimised for the North Atlantic by Schartau and Oschlies (2003a,b) (Table 1) which are also used successfully in the model for the European Station for Time-Series in the Ocean Canary Islands (ESTOC) station by Zielinski et al. (2002). A large set of sensitivity studies have been conducted to examine the effect of varying parameter values on primary and export production and the results are shown in the appendix (Appendix B, Table B1).

In Weber et al. (2007), the coupling between the ecosystem model and the chemical model is mediated by: 1) iron uptake by phytoplankton, 2) iron release during remineralisation, 3) scavenging of iron by detritus, and 4) the influence of phytoplankton on photochemical reactions through its influence on the attenuation of light. Our model contains additional interactions between biology and iron chemistry: 1) the bioavailability of iron controls the active production of ligands (Eq. A12 and Eq. A14), and 2) the organic complexation of iron is further affected by the release of ligands during remineralisation, and the biological and photochemical degradation of ligands (Eqs. A12, A13, A18 and Eq. A19); 3) furthermore, the formation of aggregates, and by that the vertical flux of adsorbed iron, is influenced by the amount of particulate organic matter (Eqs. A9–A11, Eqs. A22–A24).

Phytoplankton growth rate in our model depends on light, temperature, and nutrient supply. As in Weber et al. (2007), the uptake of iron by phytoplankton follows a Michaelis-Menten dependency on the concentration of organically complexed dissolved iron, assuming that the latter is bioavailable (Maldonado and Price, 1999). The growth limitation of phytoplankton by iron is then calculated from its internal Fe:N-quota Q_{Fe} according to

$$f_{\mathrm{Fe}}=\frac{Q_{\mathrm{Fe}}-Q_{\mathrm{Fe}}^{\mathrm{min}}}{Q_{\mathrm{Fe}}} \quad (1)$$

where $Q_{\mathrm{Fe}}^{\mathrm{min}}$ is a minimal cellular Fe quota. The actual growth rate is then calculated as the product of a light and temperature dependent maximal growth rate with the smaller of f_{Fe} and f_{N}, a Michaelis-Menten term in dissolved inorganic nitrogen:

$$f_{\mathrm{N}}=\frac{N}{N+K_{\mathrm{N}}} \quad (2)$$

where K_{N} is a half-saturation constant for dissolved inorganic nitrogen.

2.3 Particle classes and aggregation

The most important loss of DFe in deep waters is adsorption onto sinking particles (Balistieri et al., 1981; Honjo et al., 1982; Wen et al., 1997). Therefore, the vertical particle distribution and flux play a key role in determining the vertical profile of Fe and its deep-ocean residence time.

Sinking fluxes in the interior of the ocean are often dominated by larger aggregates (called "marine snow", if visible with the naked eye) and fecal pellets (e.g. Ratmeyer et al., 1999). These aggregates may contain dust (lithogenic) particles. On the other hand, fine particles dominate in Saharan dust deposition (Guieu et al., 2002; Heinold et al., 2007; Chiapello et al., 1997). Chiapello et al. (1997) reported a median size of 1.8 μm for dust particles collected on Sal Island.

In the model we consider three size categories:

1. fine terrigenous material deposited by Saharan dust events with a mean size of around 2 μm (B) and a sinking velocity of 1 m d^{-1};
2. small detritus and small aggregates with a typical size of 10 μm and a sinking velocity of 5 m d^{-1};
3. large detritus and large aggregates with a typical size of 50 μm and a sinking velocity of 50 m d^{-1}.

Both small and large aggregates contain a biogenic and a lithogenic part. In the model equations (Appendix A), we use the symbols D_S and D_L for their organic part, and A_S and A_L for their inorganic part. The sinking velocity for fine dust particles and for small aggregates has been estimated from Stokes' law; for the larger aggregates it is close to estimates by Smayda (1970); Asper et al. (1992); Asper and Smith (2003); Kriest (2002). We neglect the impact of minerals on the sinking of organic particles (Armstrong et al., 2002; Francois et al., 2002; Hamm, 2002; Klaas and Archer, 2002) or vice versa (Passow, 2004) through fragmentation, influences on sinking velocity or on degradation rates.

Besides sinking, small suspended particles are removed by aggregation which transforms them into larger and more rapidly sinking particles (McCave, 1984; Jackson and Burd, 1998). Analytical expressions exist for so-called coagulation kernels which describe the probability of encounter between differently-sized particles through the mechanisms of Brownian motion, turbulent shear, and differential settling (e.g. Burd and Jackson, 2009). We used these analytical expressions to estimate aggregation rates for our three particle classes, and the relative role that the three mechanisms of encounter play in aggregation dynamics (Table 2). Small particles coagulate mainly by turbulent shear, whereas differential sedimentation dominates the coagulation between small and large particles. Brownian motion plays only a negligible role.

The different stickiness of particles was ignored in the calculation of coagulation kernels, assuming it to be one. This is certainly an overestimate, especially for dust particles. Furthermore, the coagulation kernels are strictly valid only if one

Table 1. Parameters in the biological model. Source of parameter values are shown as footnotes; other parameters are optimised for the North Atlantic by Schartau and Oschlies (2003a,b).

Parameters	Symbol	Unit	Value
maximum growth rate of phytoplankton	$\mu_{\max}$	d^{-1}	0.27
phytoplankton mortality	γ_p	d^{-1}	0.04
initial slope P-I curve	α	$m^2\,W^{-1}\,d^{-1}$	0.256
nitrate half-saturation constant	K_N	$\mu mol\,L^{-1}$	0.7
iron half-saturation constant	K_{Fe}	$nmol\,L^{-1}$	0.2
phytoplankton aggregation rate	γ_{p^2}	$(\mu mol\,L^{-1})^{-1}\,d^{-1}$	0.025
maximum grazing rate	$g_{\max}$	d^{-1}	1.575
prey capture rate	ϵ	$(\mu mol\,L^{-1})^{-1}\,d^{-1}$	1.6
assimilation efficiency	γ_{za}	–	0.925
excretion	γ_{zb}	d^{-1}	0.01
quadratic mortality of zooplankton	γ_{z^2}	$(\mu mol\,L^{-1})^{-1}\,d^{-1}$	0.34
detritus remineralisation	γ_d	d^{-1}	0.048
sinking velocity of dust particles	w_d	$m\,d^{-1}$	1[a]
sinking velocity of small particles	w_s	$m\,d^{-1}$	5[a]
sinking velocity of aggregates	w_l	$m\,d^{-1}$	50[b]
coeff. for temp. func.	C_{ref}	–	1.066
PAR:short-wave irradiance ratio	f_{PAR}	–	0.43
attenuation due to chlorophyll	κ	$m^2\,(mmol\,N)^{-1}$	0.03
maximum Fe:N ratio in organic matter	Q_{Fe}^{max}	$nmol\,L^{-1}\,(\mu mol\,L^{-1})^{-1}$	0.033[c]
minimum Fe:N ratio in organic matter	Q_{Fe}^{min}	$nmol\,L^{-1}\,(\mu mol\,L^{-1})^{-1}$	6.6×10^{-3}[a]
mass:N ratio in organic matter	$r_{m:N}$	$g\,mol^{-1}$	159[d]

[a] Estimated from Stokes' Law, see Sect. 2.3.
[b] Estimates by Smayda (1970); Asper et al. (1992); Asper and Smith (2003); Kriest (2002).
[c] Sunda and Huntsman (1995).
[d] Calculated with Redfield C:N ratio and the assumption that 1 g C corresponds 2 g mass.

Table 2. Aggregation rates ($kg^{-1}\,L\,s^{-1}$) estimated from coagulation kernels in Burd and Jackson (2009) for different combinations of particle classes. Conversion from coagulation rates (in $L\,s^{-1}$) was done by dividing through the weight of the larger particle, resulting in a aggregation loss rate for the smaller particle concentration per concentration of the larger particle.

Particles	Brownian motion	Turbulent shear	Differential settling
dust& small particles*	0.8	4×10^3	1.0×10^4
between small particles*	0.3	2.6×10^4	0
small& large particles*	2.1×10^{-2}	8.8×10^3	3.3×10^4
dust& large particles*	0.1	3.6×10^3	2.8×10^4

* small particles include both small detritus and small aggregates, large particles include both large detritus and large aggregates.

represents the size distribution by a sufficiently fine resolved size distribution. Empirical estimates of aggregation rates for models with low size resolution, such as ours, are lower, sometimes orders of magnitude, than those determined from aggregation kernels (Ruiz et al., 2002). Ruiz et al. (2002) used mesocosms data to estimate an aggregation rate between two size classes approximately corresponding to our small and large aggregates of $15.8\,kg^{-1}\,L\,s^{-1}$, while e.g. Gruber et al. (2006) used a value of $3.6\times10^{-5}\,kg^{-1}\,L\,s^{-1}$ for the formation of large aggregates through aggregation between small-sized particles.

We therefore ran the model with a range of different aggregation rates (Table 3) and compared the resulting particle distribution and flux with observations (Ratmeyer et al., 1999; Emery and Honjo, 1979; Bory et al., 2001). Based on this sensitivity study, we choose the constant from Ruiz et al. (2002) for the aggregation between small and large aggregates (k_{coag3}) and calculated constants for other aggregation processes using the ratios between the different rates from Table 2.

Table 3. List of sensitivity model runs with respect to aggregation rates. Shown in the table is only the aggregation rate between small and large aggregates k_{coag3}; the other aggregation rates were varied in parallel, keeping the ratio between the different aggregation rates at the ratios from Table 2. Other columns show some integral characteristics of the runs, averaged over the last 5 years of the run: F_{org} is the sinking flux of organic carbon at 100 m and 1000 m depth (in brackets). C_B, C_{AS} and C_{AL} are the fractions of inorganic particulates that are contained in dust particles, small and large aggregates, respectively, at the surface and at 1000 m (in brackets). Run R corresponds to the aggregation rate estimated by Ruiz et al. (2002), run A4 to the values from Table 2.

Name	k_{coag3} ($\mathrm{kg^{-1}\,L\,s^{-1}}$)	F_{org} ($\mathrm{mg\,C\,m^{-2}\,d^{-1}}$)	C_B (%)	C_{AS} (%)	C_{AL} (%)
A0	0.0	91.8 (17.0)	100 (100)	0 (0)	0 (0)
A1	1.5	92.0 (17.0)	100 (99.1)	0 (0.4)	0 (0.4)
R	15	81.7 (15.1)	99.7 (74.3)	0.3 (14.6)	0 (11.1)
A2	150	93.1 (18.2)	96.2 (0)	3.5 (1)	0.3 (99)
A3	1500	91.7 (18.7)	87.8 (0)	9.1 (0)	3.1 (100)
A4	33000	92.5 (18.9)	63.8 (0)	5.8 (0)	30.3 (100)

2.4 Chemical model

2.4.1 Fe speciation

Five iron species are distinguished in the chemical part of the model: 1) soluble (truly dissolved) inorganic ferric iron Fe(III)', which includes all hydrolysed species in the form of $\mathrm{Fe(OH)_n^{3-n}}$; 2) soluble inorganic ferrous iron Fe(II)'; 3) organically complexed iron $\mathrm{Fe_{lig}}$ which is further subdivided into complexes with strong ($\mathrm{FeL_{str}}$) and weak ligands ($\mathrm{FeL_{we}}$); 4) colloidal iron $\mathrm{Fe_{col}}$; and 5) iron bound to the surface of sinking particles $\mathrm{Fe_p}$. In field work, soluble iron ($\mathrm{Fe_{sol}}$) is often defined by a filter cutoff of 0.02 μm which corresponds to the sum of Fe(III)', Fe(II)' and $\mathrm{Fe_{lig}}$ in our model; colloidal iron has the size between 0.02–0.4 μm and particulate iron is >0.4 μm. Dissolved iron (DFe) consists of soluble and colloidal iron and is the form of iron most often measured. To represent the kinetics of photochemical reactions, we also model the concentrations of $\mathrm{H_2O_2}$ and $\mathrm{O_2^-}$.

The following processes converting iron between different species are included in our model (Fig. 1): 1) photoreduction of different ferric forms: the direct photo-reduction of Fe(III)', organically complexed iron, colloidal and particulate iron; and the indirect photo-reduction of Fe(III)' by photoreduced superoxide; 2) oxidation of Fe(II)' by oxygen, superoxide and hydrogen peroxide; 3) complex formation and dissociation; 4) direct scavenging of Fe(III)' onto sinking particles; 5) colloid formation and redissolution; 6) colloidal aggregation and redissolution of particulate iron. Most of the rate laws and constants are adopted from Weber et al. (2005) and the results of sensitivity studies in Weber et al. (2007). Parameter values and references are shown in Table 4.

Model results by Parekh et al. (2004) and Weber et al. (2007) show that it is necessary to introduce a pathway from particulate to dissolved iron in order to reproduce the relatively constant concentration of DFe in deep-water. The vertical distributions of another particle-reactive element, Th, also seem to require a desorptive pathway to explain continuous increases in depth of both particulate and dissolved fractions (Bacon and Anderson, 1982). The rates of this pathway for iron are still not well known. Here we choose the rate for colloid redissolution from Rose and Waite (2003b) (k_{cd}=0.41 $\mathrm{d^{-1}}$) and conducted a sensitivity study with respect to the rate of redissolution of particulate iron (see Sect. 3.4.2 Modelled DFe concentration).

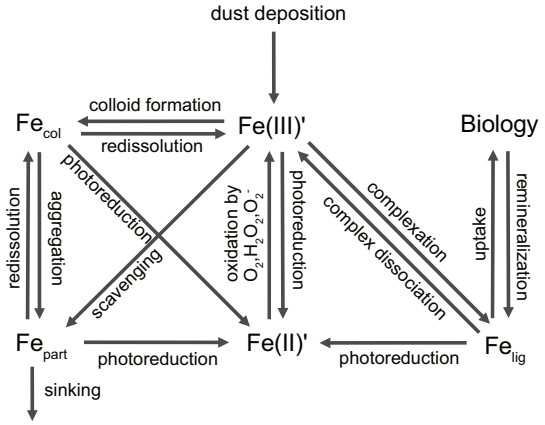

Fig. 1. Schematic representation of processes involved in the iron cycle in the model.

Dust deposition fluxes simulated by Mahowald et al. (2003) are used for prescribing the surface flux of dust particles. The surface flux of iron is calculated with a constant content of iron and 1% solubility which is close to the mean value reported for the Saharan dust close to the source region (Spokes and Jickells, 1996; Baker et al., 2006a,b; Baker and Jickells, 2006). Fe content in dust varies from 3 to 7.6% (Wedepohl, 1995; Duce and Tindale, 1991; Spokes and Jickells, 1996; Desboeufs et al., 2001). A sensitivity study with

Table 4. Parameters in the chemical model. By some parameters, the unit conversion results in a larger number of digits, e.g. k_{ox1}, giving a false sense of accuracy.

Parameters	Symbol	Unit	Value
Fe(II)' oxidation rate by O_2	k_{ox1}	$(\mu mol\,L^{-1})^{-1}\,d^{-1}$	0.864[a]
oxygen concentration	$[O_2]$	$\mu mol\,L^{-1}$	214[b]
Fe(II)' oxidation rate by O_2^-	k_{ox2}	$(nmol\,L^{-1})^{-1}\,d^{-1}$	864[a]
Fe(II)' oxidation rate by H_2O_2	k_{ox3}	$(nmol\,L^{-1})^{-1}\,d^{-1}$	6.24[c]
reference irradiance	ir_{ref}	$\mu Em^{-3}\,s^{-1}$	1978
Fe(III)' photoreduction rate	k_{ph3}	d^{-1}	1.32[d]
Fe_{col} photoreduction rate	k_{ph1}	d^{-1}	1.32[e]
Fe_p photoreduction rate	k_{ph4}	d^{-1}	20.2[d]
FeL_{str} photoreduction rate	k_{phls}	d^{-1}	0.38[f]
FeL_{we} photoreduction rate	k_{phlw}	d^{-1}	7.6[g]
Fe(III)' reduction rate by O_2^-	k_{red}	$(nmol\,L^{-1})^{-1}\,d^{-1}$	1.3×10^{4}[a]
Fe_{col} formation rate	k_{col}	d^{-1}	2.4[d]
Fe_{lig} formation rate	k_{fel}	$(nmol\,L^{-1})^{-1}\,d^{-1}$	172.8[h]
FeL_{str} conditional stability constant	k_{lsd}	$(mol\,L^{-1})^{-1}$	10^{12}[i]
FeL_{we} conditional stability constant	k_{lwd}	$(mol\,L^{-1})^{-1}$	$10^{10.3}$[i]
Fe(III)' scavenging rate	k_{sca}	$kg^{-1}\,L\,d^{-1}$	2500[j]
Fe_{col} aggregation rate	k_{ag}	$kg^{-1}\,L\,d^{-1}$	1.224×10^{6}[k]
Fe_{col} redissolution rate	k_{cd}	d^{-1}	0.41[l]
Fe_p redissolution rate	k_{pd}	d^{-1}	0.015[m]
O_2^- dismutation rate	k_{dm}	$(nmol\,L^{-1})^{-1}\,d^{-1}$	2.64[a]
O_2^- production rate	$S_{O_2^-}$	$(nmol\,L^{-1})^{-1}\,d^{-1}$	1037[n]
H_2O_2 decay rate	k_{dis}	d^{-1}	0.24[a]
solubility of atmospheric iron	k_{sol}	%	1[o]
Total Cu concentration	$[Cu_T]$	$nmol\,L^{-1}$	1[p]
Cu(I) oxidation rate by O_2^-	k_{cuox}	$(nmol\,L^{-1})^{-1}\,d^{-1}$	8.1×10^{5}[a]
Cu(II) reduction rate by O_2^-	k_{cured}	$(nmol\,L^{-1})^{-1}\,d^{-1}$	182
ligand production rate by phytoplankton	γ_{lp}	$nmol\,L^{-1}\,(\mu mol\,L^{-1})^{-1}\,d^{-1}$	0.5[q]
ligand release rate from detritus	γ_{ld}	$nmol\,L^{-1}\,(\mu mol\,L^{-1})^{-1}\,d^{-1}$	0.04[r]
ligand remineralisation	γ_{ls}	d^{-1}	0.038[s]
ligand remineralisation	γ_{lw}	d^{-1}	0.00038[m]
coagulation rate	k_{coag1}	$(kg\,L^{-1})^{-1}\,s^{-1}$	4.5[t]
coagulation rate	k_{coag2}	$(kg\,L^{-1})^{-1}\,s^{-1}$	11[t]
coagulation rate	k_{coag3}	$(kg\,L^{-1})^{-1}\,s^{-1}$	15[u]
coagulation rate	k_{coag4}	$(kg\,L^{-1})^{-1}\,s^{-1}$	13[t]

[a] Voelker and Sedlak (1995); [b] estimated from the solubility of oxygen at 25°C; [c] Millero and Sotolongo (1989); [d] Johnson et al. (1994); [e] Barbeau and Moffett (2000); [f] estimated from Powell and Wilson-Finelli (2003); [g] calculated from k_{phls} according to their ratio in Rose and Waite (2003c); [h] Hudson et al. (1992), found in the range of Witter and Luther III (1998); [i] Rue and Bruland (1995); [j] Sensitivity study of Weber et al. (2007); [k] Wen et al. (1997); [l] Rose and Waite (2003b); [m] sensitivity study in this work; [n] in the range of 2 and 100 $pM\,s^{-1}$ (Micinski et al., 1993), cited in Voelker and Sedlak (1995); [o] see Appendix B, Table B2; [p] van der Loeff et al. (1997); [q] estimated in this work; [r] estimated from Schlosser and Croot (2009); [s] Amon and Benner (1994); [t] calculated according to their ratio to k_{coag3} (Table 2); [u] Ruiz et al. (2002).

respect to the product of iron content and solubility (see Appendix B, Table B2) resulted in choosing 3.5% for the calculation of surface iron flux.

2.4.2 Organic ligands and complexation

Some marine microorganisms, mostly heterotrophic bacteria and cyanobacteria, are reported to produce siderophores to facilitate Fe uptake (Trick, 1989; Reid et al., 1993; Wilhelm and Trick, 1994; Wilhelm et al., 1996; Granger and Price,

1999; Martinez et al., 2000; Martinez and Haygood, 2001; Martinez et al., 2003; Barbeau et al., 2001; Macrellis et al., 2001). This production is widely supposed to be regulated by iron level (Reid et al., 1993; Wilhelm and Trick, 1994; Wilhelm et al., 1996; Macrellis et al., 2001). The conditional stability constant of siderophores is similar to that of the naturally occurring strong Fe-binding ligands in seawater (Rue and Bruland, 1995; Lewis et al., 1995; Macrellis et al., 2001) which predominate in the upper water column (Rue and Bruland, 1995, 1997). Weak ligands are more abundant deeper in the water column and have similar conditional stability constant as the porphyrin-type ligands which are supposed to be released as degradation products of cytochrome system (Boye et al., 2001).

To the best of our knowledge, this is the first model considering the sources and fate of organic Fe-binding ligands explicitly. Weber et al. (2007) assumed a fixed concentration of free Fe-binding organic ligands, in excess of DFe concentration. In our model, two types of ligands are introduced with different conditional stability constants: free strong ligands (L_{str}) and weak ligands (L_{we}), as well as two types of complexes, respectively: FeL_{str} and FeL_{we} (Fig. 2).

We assume a production of strong ligands by phytoplankton under Fe-limitation. The rate of siderophore production is not yet well known. We tested the sensitivity of phytoplankton growth to the rate of ligand production and found that phytoplankton growth decreases without the active production of ligands, because of strong Fe-limitation in surface waters. We estimated the maximal production rate (γ_{lp}) by keeping the phytoplankton concentration close to the observations (see Sect. 3.2 Biological conditions). The ligand production rate is regulated by the internal Fe:N-quota of phytoplankton (Eq. A14). Weak ligands are released by decomposition of detritus. Schlosser and Croot (2009) used data from the Mauritanian upwelling zone to estimate a PO_4^{3-}:ligand ratio in the decomposition of organic matter. We use this estimate together with a Redfield P:N ratio to calculate the release rate (γ_{ld}) of weak ligands in our model.

Another source of weak ligands in the model is photoreaction of the strong Fe-ligand complex (FeL_{str}). Organic ligands are often photochemically reactive and the product of photolysis of strong ligands is reported to retain a lower ability to complex Fe(III)' (Barbeau et al., 2001, 2003; Powell and Wilson-Finelli, 2003). In our model, organic complexes with both strong and weak ligands are degraded by photolysis. We assume that ligands released by photolysis of FeL_{str} have the same ability to form organic complexes as weak ligands, and ligands oxidised by photolysis of FeL_{we} lose their binding ability completely. Photoreduction rate of FeL_{str} (k_{phls}) is estimated from the experimental data by Powell and Wilson-Finelli (2003) and that of FeL_{we} is calculated according to Rose and Waite (2003c) in proportion to k_{phls}. Both of them are made proportional to light intensity in our model.

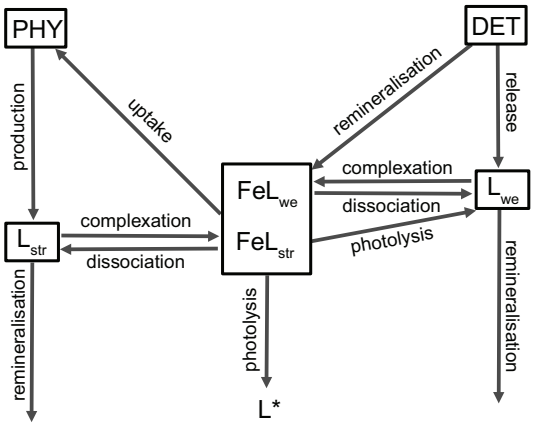

Fig. 2. Schematic representation of sources and fate of organic ligands in the model. L* is the product of photolysis of FeL_{we} which loses the ability to bind iron.

Measured ligand concentrations in the deep ocean show small variation with depth, indicating that ligands have a long decay time or a fraction of them is refractory (Hunter and Boyd, 2007). A major part of these ligands might be humic substances (Laglera and van den Berg, 2009), which are degraded very slowly compared to other DOM. We use the decay time of DOM from Amon and Benner (1994) (26 days) for remineralisation of strong ligands because of their relatively small molecular weight compared to weak ligands and their predominance in upper water column. A sensitivity study is conducted to estimate the decay time of weak ligands (see Sect. 3.4.1 Organic complexation).

Other processes controlling concentration of organic ligands are: organic complexation with Fe(III)' and complex dissociation (Witter and Luther III, 1998) as well as uptake by phytoplankton (Hutchins et al., 1999; Maldonado and Price, 1999; Wang and Dei, 2001). In our model, phytoplankton take up all the forms of complexed iron with the same rate coefficient.

3 Results and discussion

3.1 Physical conditions

The annual cycle of the mixed layer depth in the model is primarily driven by seasonal changes in surface heat flux and wind stress. Averaged daily high temperatures in the subtropical climate at the TENATSO site range only from 25°C to 29°C. The modelled thermal stratification is strong during the whole year and the mixed layer depth shows relatively low seasonal variability. The annual pattern of mixed layer depth is similar to the climatological estimate by De Boyer Montegut et al. (2004) (Fig. 3).

A characteristic feature observed at the TENATSO site is the existence of a shallow layer of high-salinity water underneath the winter maximum mixed layer depth which originates from near the centre of the subtropical gyre at 30° N and spreads along isopycnals. Maintaining the effect of this lateral source of high-salinity water on density stratification in a one-dimensional model requires an additional unphysical forcing for salinity and temperature towards observations. We have used a weak uniform forcing proportional to model-data difference with a time-scale of three months. Not surprisingly therefore, modelled temperature and salinity are in good agreement with observations. This unphysical forcing is weak enough to allow for a realistic high-frequency variability in mixed-layer depth.

3.2 Biological conditions

The modelled chlorophyll a concentration in surface waters is between 0.25 to 0.45 μg L^{-1} which is within the range of the observations at the TENATSO site or during cruises past the Cape Verde Islands. Between March and November, a deep chlorophyll maximum with values around 0.45 μg L^{-1} develops at the depth of the nutricline near 70 m. However, the observed chlorophyll surface concentrations vary somewhat more strongly from 0.06 to 0.7 μg L^{-1} (Cruise data of POS 320/1, POS 332, Meteor 68/3, POS 348/2, Merian 20 April 2008, L. Cotrim da Cunha, personal communication, 2008 and I. Peeken, personal communication, 2009). One explanation for the lower than observed Chl variability in the model could be a fixed Chl:C ratio (0.01 mg Chl (mg C)$^{-1}$) used for calculation of Chl concentration. Alternatively, we calculated Chl concentrations using the empirical Chl:C-ratio from Cloern et al. (1995) and obtained lower surface concentrations (0.05–0.33 μg L^{-1}) and higher subsurface maximum (mean 0.9 μg L^{-1}). Figure 4 shows that the calculated Chl reproduces well the observed surface Chl, whereas the subsurface maximum is higher than the observations. For better estimation of the Chl:C ratio at TENATSO, phytoplankton community composition and different physiology need to be considered, resulting in a more complex ecosystem model. This is, however, out of the scope of our study.

Primary production in the model varies seasonally from 450 mg C m^{-2} day^{-1} in winter to 700 mg C m^{-2} day^{-1} during spring blooms. The annual average is approximately 620 mg C m^{-2} day^{-1}. Morel et al. (1996) reported primary productivity for typical eutrophic, mesotrophic and oligotrophic regimes in the tropical northeast Atlantic (EUMELI program). Primary production at the mesotrophic station (18.5° N, 21° W), the nearest station to TENATSO, is ca. 700 mg C m^{-2} day^{-1}. This value is a little higher than our modelled mean primary production which can be explained by the more remote location of TENATSO from the Northwest African coast. Primary production estimated from MODIS data, using the algorithm by Behrenfeld and

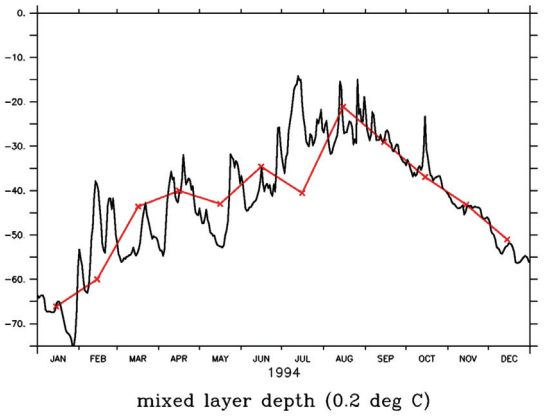

Fig. 3. Comparison of mixed layer depth (m) calculated with a 0.2°C criterion. Black: modelled mixed layer depth, red: climatological estimate by De Boyer Montegut et al. (2004).

Falkowski (1997) averages to 470 mg C m^{-2} day^{-1} for the 1° × 1° square around the TENATSO station and the period from July 2002 to December 2007. Due to the relatively large variation between reported values, we are pleased with our value being within the variation.

Modelled export of POC at 100 m ranges from 40 to 120 mg C m^{-2} day^{-1} which is 6–20% of integrated primary production. This export to primary production ratio is in agreement with the typical open ocean values which range from 5 to 25% (De La Rocha and Passow, 2007). The POC concentration at 100 m varies from 30 to 80 mg m^{-3} in the model, consistent with the observed 35–74 mg m^{-3} (Meteor 68/3, Atalánte cruise February 2008, I. Peeken, personal communication, 2009).

Phytoplankton growth in the model is limited by nitrogen rather than iron which is consistent with observations in North Atlantic (Graziano et al., 1996). The lowest value of the nitrogen limiting factor f_N (Eq. 2) is around 0.3 found in surface waters in summer and autumn when nitrogen is largely depleted after spring blooms. The iron limiting factor f_{Fe} (Eq. 1) varies between 0.65 and 0.80. The strongest Fe limitation occurs immediately below the depth of the deep chlorophyll maximum where it is also stronger than N limitation. A feedback of phytoplankton to Fe limitation is provided by the production of strong organic ligands, primarily at the depth of the deep chlorophyll maximum. It is interesting to note that without production of strong organic ligands and restoring of weak ligands in the model, Fe limitation develops so fast that phytoplankton concentration falls to 0 within the first 2 years in the model integration. N limitation at TENATSO might be overestimated in our model, because we do not consider diazotrophs which are temporally abundant in this region (Tyrrell et al., 2003; Carpenter

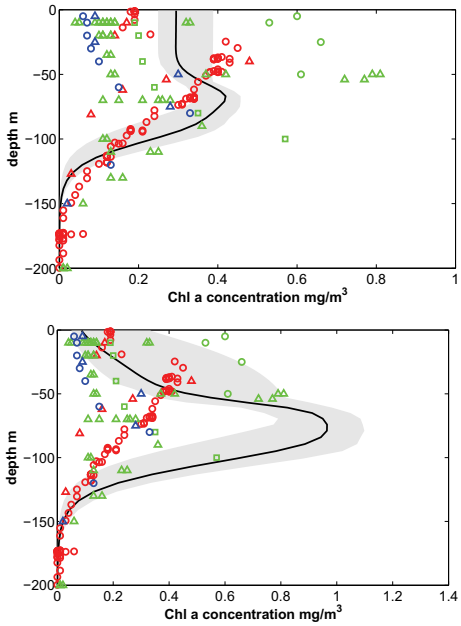

Fig. 4. Comparison of modelled Chl concentration with a fixed Chl:C ratio (upper panel) and with the empirical ratio from Cloern et al. (1995) (lower panel) to observations at TENATSO from: POS 332 cruise (red circle), POS 348 (red triangle), POS 320/1 (green circle), MERIAN 2008 (green triangle), Meteor 68/3 (blue circle), MSM 08/2 (green square). The gray area shows the variability of modelled Chl.

et al., 2004). On the other hand, diazotrophs have higher Fe requirement and might also influence Fe availability significantly.

3.3 Aggregation and particle distribution and fluxes

Aggregation rates have an influence on the vertical distribution of organic and inorganic particles, and by that also on the removal of dissolved iron from the water column, yet there exists very little information on their values. We therefore conducted a series of sensitivity experiments (Table 3) varying all four different aggregation rates in our model setup in parallel.

The aggregation rates strongly influence the distribution of lithogenic material over the three model size classes, especially at depth. This becomes evident from the distribution of lithogenic material over all three particle size classes at 1000 m depth (last three columns in Table 3): while in runs A0 and A1, all lithogenic material remains in the smallest size class, in runs A2, A3 and A4, virtually all lithogenic material is found within the larger aggregates. Neither of the two extremes is compatible with the sediment trap size distributions by Ratmeyer et al. (1999), who found that the average size of lithogenic material-bearing particles varies between 12 and 19 μm. At their sediment trap location, somewhat south of the Cape Verde islands, the lithogenic flux at 1000 m depth in the size range from 6 to 11 μm varies between 5 and 70 mg m^{-2} d^{-1}, and between 3 and 30 mg m^{-2} d^{-1} in the size range from 20 to 63 μm. The only model run that is qualitatively compatible to this flux size distribution is model run R, in which the lithogenic flux in the smaller two size classes together varies between 5 and 10 mg m^{-2} d^{-1}, and in the larger size class between 8 and 52 mg m^{-2} d^{-1}. Without sediment flux directly from the TENATSO site we are not able to infer whether the somewhat larger fraction of the flux carried by large particles in model run R, compared to Ratmeyer et al. (1999), points to a slight overestimate of aggregation or is simply an effect of local conditions.

The time-averaged vertical flux of lithogenic material must be independent of depth due to conservation of mass. As the flux is dominated by the sinking flux, a shift from smaller, slowly sinking particles to larger, faster particles, is accompanied by a decrease in the total concentration of suspended lithogenic material (Fig. 5a): with low or no aggregation (runs A0 and A1), the vertical profile is almost constant, the small decrease with depth being caused by diffusive fluxes in addition to sinking. With the aggregation rate from Ruiz et al. (2002) we obtain a continuous decrease of the concentration with depth to about 14% of the surface values, caused by a slow shift to a larger average particle size. With higher aggregation rates (A2, A3, A4), the profile becomes constant below a certain depth, indicating that all material has been transferred to the largest particle class. In runs A3 and A4, even the surface concentration of lithogenic material decreases, although the smallest particles still dominate the concentration.

The third column of Table 3 also shows that the choice of the aggregation rate has a comparatively small influence on the sinking flux of organic material both directly under the mixed layer and at 1000 m depth. Fluxes at 1000 m depth are between 18% and 20% of the flux in 100 m depth. From the empirical depth dependency by Martin et al. (1987) we would have expected a ratio between the fluxes at 1000 and 100 m of about 15%. Absolute values of the fluxes are also somewhat higher than measured values in sediment traps from the region, the best agreement being shown by model run R with 15.1 mg C m^{-2} day^{-1}. Organic carbon flux at a mooring to the south of Cape Verde is between 2.0 and 12.7 mg C m^{-2} day^{-1} (Fischer and Wefer, 2000), for the Northwest African upwelling it varies between 3.5 and 9.3 mg C m^{-2} day^{-1} (Lutz et al., 2002) and for the mesotrophic site of the EUMELI program it is about 10 mg C m^{-2} day^{-1} (Bory et al., 2001).

Based on these results we conclude that an aggregation rate that corresponds to the data-based estimate by Ruiz et al. (2002) is best compatible with the available sediment trap information from regional sediment traps. We acknowledge, however, that, given the available data, we are probably not

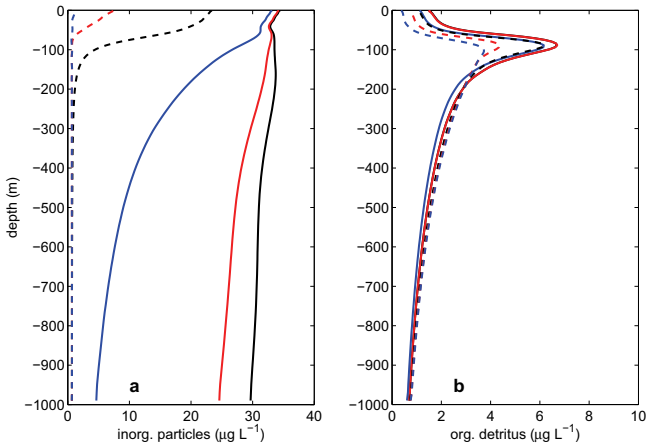

Fig. 5. Vertical distribution of modelled inorganic (left) and organic (right) particles of the sensitivity model runs with respect to aggregation rates, $\mu g\,L^{-1}$. The aggregations rates and the numbers of the runs are shown in Table 3. Solid black line: A0, solid red line: A1, solid blue line: R, dashed black line: A2, dashed red line: A3 and dashed blue line: A4.

able to constrain the aggregation rate more than by about an order of magnitude from our sensitivity analysis.

In model run R, the ratio between organic and inorganic matter at the surface varies between 0.5 and 6.5, with a mean of 2.5, much lower than the average of 45 from the open-ocean measurements of Emery and Honjo (1979). This indicates that, although open ocean, TENATSO is still in a high-dust deposition region. Near the surface, however, the detritus fraction of biogenic matter is, however, much smaller than the total biogenic matter. If one focuses on sinking material alone the removal of dissolved Fe by adsorption onto sinking particles is dominated by lithogenic particles (Fig. 5). Deeper in the water column, the ratio of organic:inorganic fraction in aggregates is shifted towards lower values with depth due to remineralisation. In small aggregates, the organic fraction falls below a few percent at about 400 m depth, at which limit the aggregates might become unstable (Passow, 2004). In large aggregates, this limit is not reached within the upper 1000 m.

The percentage of small particles in the organic fraction of aggregates within the mixed layer varies between 50% and 90% annually and remains almost uninfluenced by the aggregation rate for the runs A0, A1, R, A2; only at aggregation rates that are larger by a factor of hundred or more than the value in R (runs A3 and A4), aggregation begins to deplete small aggregates within the mixed layer. This points to a strong role of zooplankton excretion rather than aggregation for the genesis of the larger organic particles in our model.

There are certainly a number of shortcomings in our parameterisation of vertical sinking: minerals add density to aggregates (Armstrong et al., 2002; Francois et al., 2002; Klaas and Archer, 2002) but also decrease their size and fragment them into smaller particles if reaching a certain concentration (Hamm, 2002; Passow and De la Rocha, 2006). The model resolves only three particle size classes, and does not take into account disaggregation of particles and the variation of sinking speed with the mineral load. As sediment trap data directly from the TENATSO site becomes available a validation of this aspect of the model and a better judgment of model deficiencies will become possible.

3.4 Results from the chemical model

3.4.1 Organic complexation

Weak ligands are typically more abundant than strong ligands and predominate deeper in the water column (Rue and Bruland, 1995, 1997). They are therefore important in controlling the structure of Fe profile below annual mixed layer. In our model, the abundance of weak ligands in deeper waters is mainly determined by release during remineralisation of organic matter and by the rate of microbial degradation, while their photoreactivity and uptake by phytoplankton are also significant loss processes in surface waters.

In a sensitivity study with respect to the decay rate of weak ligands, we ran the model assuming four different degradation rates for weak ligands, γ_{lw}. In the first study, we used a typical degradation rate for marine DOM of 1/(26 days) (Amon and Benner, 1994), the same as for strong ligands, while in the other three, we used one tenth and one hundredth of that value, and completely excluded L_{we} degradation. In an additional run, we changed the temperature dependency of all remineralisation rates, including that of sinking organic particles.

In the first sensitivity run, the concentration of total ligands ranges from 0.1 to 1 nmol L^{-1} with a subsurface maximum at 100 m (data not shown). Below this maximum, ligand concentration decreases dramatically with depth. This could be an indication of a too high degradation rate or a too low temperature dependence of microbial activities. This was tested in the remaining sensitivity studies.

In the run with γ_{lw} set to 1/(260 days), ligand concentration still decreases strongly with depth below its subsurface maximum (Fig. 6). At the end of the 30-year integration, the deep concentration falls to 0.1 nmol L^{-1} and approaches a steady state. The ligand concentration of the run with γ_{lw} set to 1/(2600 days) is higher and closer to the observations, showing a subsurface maximum at 80 m due to the production of strong ligands and a maximum of 2 nmol L^{-1} between 150 and 200 m due to remineralisation. However, it still decreases with depth and the values at 1000 m depth are 60% lower than the maximum. Depth-integrated concentration decreases with time. Although the decrease slows down with time, a steady state is not yet obtained at the end of the 30-year integration. Without degradation, finally, ligand concentrations are unrealistically high with a maximum of 190 nmol L^{-1} between 300 and 400 m at the end of the 30-year integration, indicating that microbial degradation can not be neglected for simulating a reasonable concentration of weak ligands.

To test the effect of temperature dependence, we changed the factor by which remineralisation decreases with a 10 degree temperature decrease (Q10) from 2 to 3 in a further run with a degradation rate γ_{lw} of 1/(2600 days), keeping the remineralisation rate at 20°C constant (Eq. A8). Above the isothermal curve of 20°C between 75 and 85 m, the stronger remineralisation leads to a lower ligand concentration (Fig. 6). From its subsurface maximum at 100 m to 1000 m depth, ligand concentrations become nearly constant with depth, which is comparable to the profile from Boye et al. (2006). However, another effect of the stronger temperature dependence is the increase of POC export at depth because of the slower remineralisation of detritus. The export at 1000 m rises from 15 to 38 mgC m^{-2} d^{-1}, exceeding observations (see Sect.3.3 Aggregation and particle distribution and fluxes). We therefore reject this model setup as a plausible hypothesis.

In summary, the model sensitivity runs show that weak ligands probably contain a fraction of more refractory material with decay times longer than 2600 days (approximately 7 years). This is consistent with hypotheses from other researchers (Hunter and Boyd, 2007; Kondo et al., 2008). In consequence, the model would have to be run for a longer integration period than 30 years for the concentration of weak ligands to reach a steady state. Over such long timeperiods, however, lateral advection becomes non-negligible and could also affect the the local concentration of weak ligands (Kondo et al., 2008). These processes can not be represented within our one-dimensional model and we thus refrained from extending our model integration period for even longer. This clearly is a question that can only be modelled successfully in three dimensions.

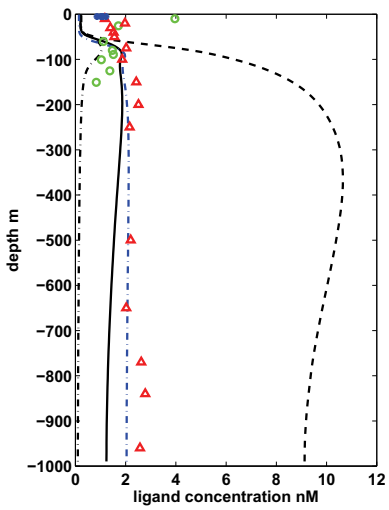

Fig. 6. Annual mean profiles of total ligands in the sensitivity study with different remineralisation rates for weak ligands and Q10, nmol L^{-1}. Black dash-dot line: Q10=2, γ_{lw}=1/(260 days); black solid line: Q10=2, γ_{lw}=1/(2600 days); black dashed line: Q10=2, γ_{lw}=0; blue dash-dot line: Q10=3, γ_{lw}=1/(2600 days). Colour symbols show the observations from: Boye et al. (2006) (red triangle), Gerringa et al. (2006) (green circle) and Rijkenberg et al. (2008) (blue dot, only surface data).

However, a realistic profile of ligands, especially in the deep ocean, is a prerequisite for further modelling iron speciation at depth and its influence on the removal of dissolved iron through particles. As we are not able to obtain a weak ligand profile that is both realistic and stable within the integration time of our model, we introduced a restoring of the concentration of total weak ligands towards a constant value for all further model runs, so that iron speciation and losses will not be affected by too little complexation. Weak ligands are restored throughout the water column with a rate of 0.1 d^{-1} towards 2.5 nmol L^{-1}, a typical ligand concentration in the deep Atlantic Ocean (Boye et al., 2006; Gledhill and van den Berg, 1994; Witter and Luther III, 1998). This restoring is weak enough so that loss processes near the surface (biological uptake and photochemical decay) still lead to the observed vertical gradient of total weak ligand concentration there.

Our modelled total strong ligands (Fig. 7) have a high abundance from 40 to 100 m and decline rapidly with depth below the subsurface maximum, which is consistent with their production by phytoplankton and degradation by microbes. Some observations show a qualitatively similar vertical distribution of strong ligands (Rue and Bruland, 1995,

1997; Gerringa et al., 2006), although in other oceanic regions. The subsurface maximum is at and a little below the depth of the chlorophyll maximum in the model which is also observed by Gerringa et al. (2006).

Modelled concentrations of total ligands increase with depth in surface waters and reach their maximum around 3 nmol L^{-1} at 80 m. They range in the same magnitude as the observations (Fig. 7). However, some observed high values can not be included in the range of modelled variability which might be caused by an overestimation of photolysis of organic complexes. Below the maximum, the modelled mean concentration decreases to 2.5 nmol L^{-1} at 150 m and keeps constant from there to 1000 m depth due to the restoring of weak ligands. This profile reproduces the measured profile by Boye et al. (2006) quite well.

In summary, our model results agree with the qualitative picture put forward by Hunter and Boyd (2007) that the low vertical gradients of ligand concentrations within the deep ocean indicate that the ligand pool contains a fraction that is not decomposed very quickly by bacteria (our model results indicate a degradation time-scale of longer than a decade, from the value of γ_{lw} in the most realistic model run and a temperature dependency with Q10=2), and that is produced from the remineralisation of sinking particles. Strong ligands on the other hand, which are probably directly produced by procaryotes in response to iron deficiency, could well be degraded like most non-refractory dissolved organic matter (Amon and Benner, 1994).

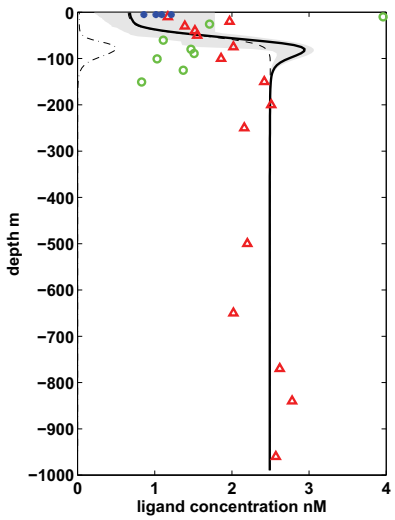

Fig. 7. Modelled annual mean profile of total ligands (solid), strong (dash-dot) and weak ligands (dashed), nmol L^{-1}. The gray area shows the variability of modelled total ligand. Colour symbols show the observations from: Boye et al. (2006) (red triangle), Gerringa et al. (2006) (green circle) and Rijkenberg et al. (2008) (blue dot, only surface data).

3.4.2 Modelled DFe concentration

Measured profiles of dissolved iron (DFe) often show a nutrient-like distribution: the minimal concentration is in surface waters and averages globally 0.07 nmol L^{-1}; like for other remineralised nutrients (Broecker and Peng, 1982), DFe concentrations increase with depth. However, unlike other nutrients, deep-water DFe show no obvious inter-ocean fractionation (Johnson et al., 1997). Concentrations in the deep ocean are rather constant near 0.6 nmol L^{-1} away from the influence of continental shelves, with lower values in the Southern Ocean and higher values in the tropical Atlantic (Johnson et al., 1997; Wu and Boyle, 2002; Boye et al., 2006; Sarthou et al., 2007). This has been ascribed to removal of DFe through particles.

Deeper in the water column, DFe concentration in our model is mainly determined by iron release by detritus remineralisation and removal by sinking particles, whereas in surface waters, other processes like dust input, photochemical reactions and biological uptake play a more important role. Iron release from remineralisation of organic matter decreases with depth due to its dependence on detritus abundance and temperature. We would therefore expect a continuous decrease of DFe in deeper waters, if there was no redissolution of iron from its particle-adsorbed forms. The removal of DFe at depth is dominated by the formation and adsorption of colloids to sinking particles. Fluxes of these processes are 2 orders of magnitude larger than the fluxes due to direct scavenging of Fe(III)'.

We conducted a sensitivity study with respect to the rate of redissolution or desorption of particulate iron (k_{pd}). In the sensitivity model runs, the redissolution rate of particulate iron is set to be 0, 0.015 and 0.15 d^{-1}. Without redissolution, DFe is in steady state after 20 modelling years. DFe concentration decreases continuously with depth as expected and reaches a value of 0.07 nmol L^{-1} at 1000 m (Fig. 8, left), in contrast to observations. In the other two runs, increasing k_{pd} leads to an increase of DFe concentration below ca. 80 m, the depth of the subsurface chlorophyll maximum and the highest particle concentration (see Sect. 3.3 Aggregation and particle distribution and fluxes). With k_{pd}=0.015 d^{-1}, modelled DFe shows a nearly constant concentration in deeper waters which is very close to the so far only DFe profile measured at TENATSO site (Fig. 8 left, deep DFe profile data courtesy of Micha Rijkenberg, unpublished data). We also compared model results to the deep DFe concentrations by Boye et al. (2006) from a more northerly region near the Canary Islands (Fig. 8). With k_{pd}=0.15 d^{-1}, the vertical DFe profile increases more strongly with depth, exceeding the values by Rijkenberg, and coming closer to the profile by Boye et al. (2006). It has to be noted, though, that in both cases with $k_{pd}>0$ the DFe profiles are not completely stable at the end of the 30-year integration period, with deep

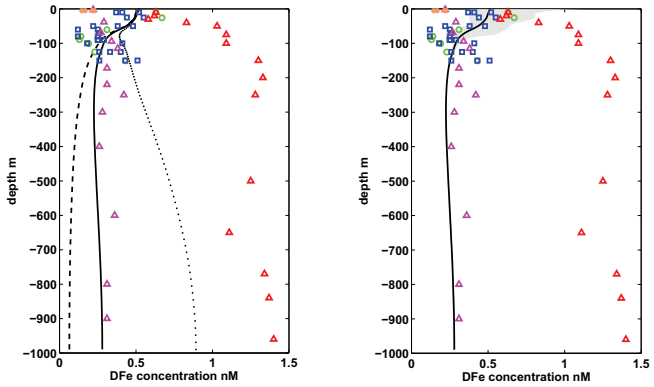

Fig. 8. Modelled annual mean profiles of DFe concentration in the sensitivity study with different redissolution rates (k_{pd}) of Fe_p (left) and compared to measured profiles (right), nmol L^{-1}. Dashed line: k_{pd}=0; solid line: k_{pd}=0.015, dotted line: k_{pd}=0.15. Modelled DFe variability is shown with gray area. Colour symbols show the observations from: Rijkenberg et al. (2008) (orange dot) and Rijkenberg (unpublished data from the POS 332 cruise, magenta triangle), Sarthou et al. (2007) (blue square), Gerringa et al. (2006) (green circle), and Boye et al. (2006) (red triangle).

concentrations still slightly increasing with time. In the case with k_{pd}=0.015 d^{-1} this increase is about 5% over the last 5 model years. Without more observations, it is impossible to estimate the value of k_{pd} more exactly, but we would argue from the comparison to the data by Rijkenberg that k_{pd}=0.015 d^{-1} is not a bad choice. We introduced the redissolution of Fe_p with 0.015 d^{-1} for further analysis of Fe speciation in the model.

Modelled DFe profile (Fig. 8 right) shows high concentration in surface waters which decreases rapidly between 50 and 80 m, caused by high biological uptake. Below the deep chlorophyll maximum at 80 m, DFe decreases moderately till 200 m and reaches a minimum of 0.25 nmol L^{-1}. Below that, the concentration increases slightly with depth and varies around 0.3 nmol L^{-1} at 1000 m depth.

The modelled DFe surface concentration shows a clear seasonal pattern with higher concentration in winter (from December to March) and in late summer and autumn (from August to September). The high concentration in winter is mainly caused by high dust deposition and in summer additionally by the shallower mixed layer depth. The surface concentration varies from 0.4 to 0.9 nmol L^{-1} and its annual average is ca. 0.5 nmol L^{-1}. Overlaid on this seasonal variability there is considerable interannual and also short-term variability due to the episodic nature of dust deposition. There are a few measurements of surface DFe near TENATSO: Sarthou et al. (2003): 0.28 nmol L^{-1}, Sarthou et al. (2007): 0.37–0.52 nmol L^{-1} and Rijkenberg et al. (2008): 0.1–0.4 nmol L^{-1}). The modelled variability covers most observations except for the low concentrations from Rijkenberg et al. (2008). The interannual variability of dust deposition might play a role, since the surface flux in our model is based on the data for 1990–1995. The fixed solubility and Fe content in the model also might impact the variability of DFe concentration. Another reason could be the simplification of the ecosystem model which only considers one average phytoplankton with the average Fe requirement. It is known that diazotrophs have higher Fe requirement and occur in high abundance in tropical North Atlantic (Tyrrell et al., 2003; Carpenter et al., 2004). This might lead to an underestimation of biological iron uptake in our model.

Fe_{col} in the model represents the inorganic colloidal iron which is formed by Fe(III)' and removed from the dissolved pool by colloidal aggregation. The modelled Fe_{col}:Fe_{sol} ratio is nearly constant below 150 m and reaches 1:40 at 1000 m. Some recent studies found that about half of DFe in the deep ocean is colloidal (Wu et al., 2001; Cullen et al., 2006; Bergquist et al., 2007). This indicates that a fraction of colloidal iron must be prevented from removing processes (Wu et al., 2001; Cullen et al., 2006; Bergquist et al., 2007). One possible explanation of the discrepancy between our model and the observations could be the co-existence of organic colloids. Organic complexes of iron are found in both soluble and colloidal form (Wu et al., 2001; Cullen et al., 2006). It is reported that remineralisation releases Fe_{lig} preferentially in colloidal form (Bergquist et al., 2007). We suggest that organic colloids could be kept longer in the dissolved pool and be more biologically available than the inorganic colloids by transformation into soluble organic complexes via ligand exchange reactions. Hence, introducing organic colloidal iron in further modelling works may be helpful for understanding the observed Fe_{col}:Fe_{sol} ratio in deep waters, which of course must be supported by more studies on the colloidal nature of iron and Fe-binding ligands (Hunter and Boyd, 2007).

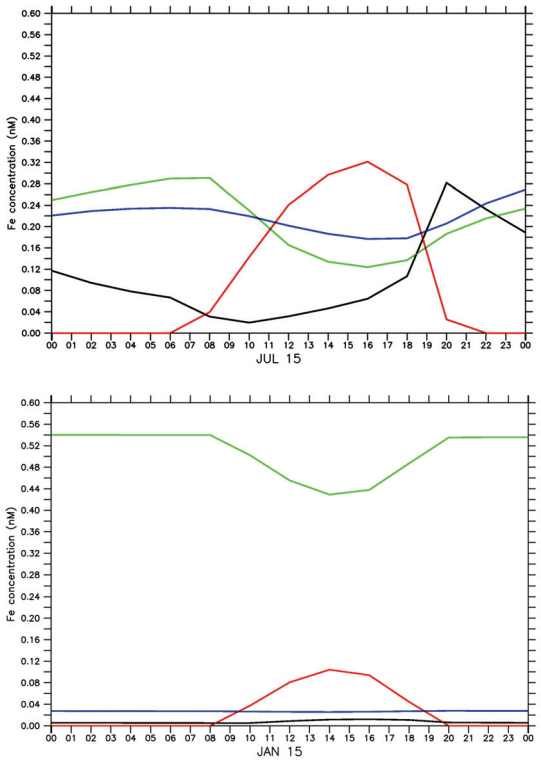

Fig. 9. Modelled diurnal variability of Fe species in summer (upper panel) and winter (lower panel). Fe(III)': black, Fe(II)': red, Fe_{col}: blue, Fe_{lig}: green.

3.4.3 Diurnal variation of Fe speciation

Because of the influence of O_2^- and H_2O_2 on the redox state of Fe, the modelled Fe speciation near the surface shows a strong diurnal variability. O_2^- is mainly produced by the photo-oxidation of coloured dissolved organic matter (CDOM). We assumed a production rate in the range of the rates estimated for open ocean by Micinski et al. (1993) and made it proportional to light intensity in our model. Thus the concentration of O_2^- increases after sunrise, reaches its maximum at noon and then falls to zero after sunset. H_2O_2 has a longer lifetime than O_2^-, especially in the absence of Fe(II)', and does not vanish during the night. Its rate of production which is proportional to [Fe(II)'][O_2^-] has a strong maximum at noon and rapidly decreases afterwards. Its rate of consumption, which is proportional to [Fe(II)'][H_2O_2] has a lower but broader maximum. In consequence, the concentration of H_2O_2 reaches its maximum 3–4 h after noon, when the loss becomes larger than the production.

Reduction of Fe(III)' mediated by O_2^- is the most important source of Fe(II)' in the model and its rate is more than 100 times the rate of all the direct photo-reductions together. The concentration of Fe(II)' is mainly controlled by photo-reduction mediated by O_2^- and oxidation by H_2O_2 and O_2^-. With the sunrise, Fe(II)' increases quickly with increasing light intensity and O_2^- concentration (Fig. 9). Photo-reduction of ferric iron outweighs the oxidation till shortly after noon. In the afternoon, H_2O_2 reaches its maximum and light intensity becomes lower. The balance between photo-reduction and oxidation is shifted, leading to a rapid decrease of Fe(II)'. During the night, the concentration of Fe(II)' is close to 0 because of its extremely short lifetime.

Concentration of Fe(III)' is mainly controlled by Fe(II)' oxidation and organic complexation. During the day in summer, Fe(III)' has a low concentration and shows a rapid increase after sunset. However, organic complexation leads to a decrease of Fe(III)' after 08:00 p.m. again, such that Fe_{lig} (both FeL_{str} and FeL_{we}) are the dominant forms during the night in summer and throughout the daily cycle in winter.

Fe_{col} shows a lower sensibility to changes in light than Fe_{lig}, since colloid formation is a much slower process than oxidation and organic complexation (Rose and Waite, 2003a).

The pattern of the daily cycle in winter (Fig. 9) is similar to that in summer, but shows a smaller amplitude caused by the weaker irradiance and deeper mixed layers in winter. Fe_{lig} has a much higher concentration than in summer. Besides the decrease of photoredox reaction rate, higher biological uptake in summer also plays a role.

Copper redox reactions compete for superoxide with iron (Voelker and Sedlak, 1995) and thus influence the amplitude of the daily cycle of superoxide concentration and Fe speciation. We estimated total copper concentration from the measurements of van der Loeff et al. (1997) and assumed that Cu(II) is strongly complexed (Moffett, 1995). Redox reactions of copper are considered in our model in the same way as Weber et al. (2005). Increasing Cu concentration from 1 nmol L^{-1} to 5 nmol L^{-1} in our model reduces the daily amplitude of Fe(II)' to a third of its value.

Because Fe redox speciation has not yet been measured at the TENATSO site, we compared the modelled H_2O_2 with observations which is a measure for photochemical reactions of iron. The modelled H_2O_2 integrated for 0–200 m ranges from 3 to 7 mmol m^{-2} and is comparable with a H_2O_2 inventory of about 3.7 mmol m^{-2} for the same depth interval measured in the vicinity (Steigenberger and Croot, 2008).

4 Summary and conclusions

A one-dimensional model of iron biogeochemistry developed for the BATS site (Weber et al., 2007) has been extended for the TENATSO site with a more complex description of particle aggregation and sinking and origin and fate of organic Fe-binding ligands.

Despite the simplicity of the NPZD-type ecosystem model, simulated chlorophyll a concentration and seasonality of primary production at the TENATSO site are in agreement with observations. Time-averaged primary production ranges between the observations at the oligotrophic and mesotrophic stations in the tropical Eastern North Atlantic. Export production varies seasonally between 6 and 20% which is consistent with published values. These provide good boundary conditions for modelling Fe uptake and release as well as the biological origin and decay of organic ligands.

Modelled particles are classified due to size and composition. Particle aggregation and sinking are described based on the calculation of coagulation kernels and data-based estimation of aggregation rates. Modelled fluxes of inorganic particles and their size distribution at 1000 m are qualitatively compatible with the measurements from Ratmeyer et al. (1999), whereas the POC export is somewhat higher than measured values from regional sediment traps, which might be caused by the simplified classification and constant sinking rates of particles.

Sources and decay of organic ligands are connected to biological activities. The profile of dissolved iron is strongly influenced by the abundance of organic ligands. Modelled strong ligands have a high abundance near the surface and decline rapidly below the deep chlorophyll maximum, in qualitative agreement with observations. However, a restoring of total weak ligands towards a constant value is required for reproducing the observed nutrient-like profile of weak ligands. This possibly indicates that weak ligands contain a fraction of more refractory material whose decay time is longer than the assumed 7 years in the model, and that the dynamics of this refractory material cannot be described well with a one-dimensional model which takes only local processes into account.

We investigated a number of hypotheses on processes affecting Fe speciation with sensitivity studies. Our best model runs come close to observed DFe concentrations at the surface and at depth near the TENATSO station. The reproduction of the DFe profile by Rijkenberg requires a redissolution of DFe from particle-adsorbed iron with a timescale around 60 days. The low Fe_{col}:Fe_{lig} ratio in the model suggests introducing organic colloids into the model in future work.

The model extension on particle dynamics and ligand source and fate provide a better understanding of Fe speciation and biogeochemical cycle. This process-based understanding can be applied for explaining and reproducing the reality, when more observations on particle and ligand distribution as well as Fe speciation directly at TENATSO site become available.

Appendix A

Model equations

The rate of change of biogeochemical variables can be separated into a biogeochemical and a physical part:

$$\frac{\partial}{\partial t}X = \mathrm{BIO} + M(X, z) \tag{A1}$$

where advection and mixing are taken into account in the physical part *M(X,z)*. Here M stands for the advection and mixing operator and X is the mixed compound. The biogeochemical rate of change is described by corresponding sources minus sinks.

The change of the biological variables N, P, Z and D (in μmol L^{-1}) is described by:

$$\frac{\partial}{\partial t}N = \gamma_d\, f_T\, (D + A_{\mathrm{or}}) + \gamma_{zb}\, f_T\, Z + \gamma_p\, f_T\, P + \gamma_l\, f_T\, (L_{\mathrm{str}} + L_{\mathrm{we}}) - \mu\, P + M(N, z) \tag{A2}$$

$$\frac{\partial}{\partial t}P = \left(\mu - \gamma_p\, f_T\right)\, P - f_G\, Z - \gamma_{p^2}\, P^2 - r_L\, \gamma_{lp}\, f_Q\, P + M(P, z) \tag{A3}$$

$$\frac{\partial}{\partial t}Z = \gamma_{za}\, f_G\, Z - \gamma_{zb}\, f_T\, Z - \gamma_{z^2}\, Z^2 + M(Z, z) \tag{A4}$$

Detritus is subdivided into two size classes: D_s for small and D_l for large detritus. We use the same symbols for organic part of small aggregates and large aggregates, respectively, because we treat them same as the detritus in particle aggregation, sinking and remineralisation.

$$\frac{\partial}{\partial t}D_S = \gamma_{p^2}\, P^2 + (1 - \gamma_{za})\, f_G\, Z - (\gamma_d + r_L\, \gamma_{ld})\, f_T\, D_S - k_{\mathrm{coag2}}\, D_S\, (D_S\, r_{\mathrm{m:N}} + A_S) - k_{\mathrm{coag3}}\, D_S\, (D_L\, r_{\mathrm{m:N}} + A_L) - w_s\, \frac{\partial D_S}{\partial z} + M(D_S, z) \tag{A5}$$

$$\frac{\partial}{\partial t}D_L = \gamma_{z^2}\, Z^2 - (\gamma_d + r_L\, \gamma_{ld})\, f_T\, D_L + k_{\mathrm{coag2}}\, D_S\, (D_S\, r_{\mathrm{m:N}} + A_S) + k_{\mathrm{coag3}}\, D_S\, (D_L\, r_{\mathrm{m:N}} + A_L) - w_l\, \frac{\partial D_L}{\partial z} + M(D_L, z) \tag{A6}$$

where μ is the growth rate of phytoplankton regarding light, temperature and nutrient limitation. $\gamma_{lp}\, f_Q\, P$ describes the loss of nitrogen due to the excretion of Fe-binding ligands and r_L is a factor converting ligand nitrogen (nmol L^{-1}) into phytoplankton and detritus nitrogen (μmol L^{-1}). The loss of zooplankton by its mortality $\gamma_{z^2}\, Z^2$ is considered as a source of organic aggregates. The grazing function f_G depends on

the maximal grazing rate g, the prey capture rate ϵ and phytoplankton concentration:

$$f_G = \frac{g\,\epsilon\,P^2}{g + \epsilon\,P^2} \tag{A7}$$

The growth and remineralisation rate are related to temperature by:

$$f_T = 0.9\,C_2^{T(z)} \tag{A8}$$

which represents a temperature dependence for Q10=2.

Further sinking particles are dust particles B, the inorganic fraction of small aggregates A_S and of large aggregates A_L (all in $\mathrm{kg\,L^{-1}}$). Coagulation is described by a coagulation constant k_{coag} times the product of concentration of the two particle classes participating in the coagulation.

$$\frac{\partial}{\partial t}B = F_{\mathrm{dust}} - k_{coag1}\,B\,(D_S\,r_{\mathrm{m:N}} + A_S) - k_{\mathrm{coag4}}\,B\,(D_L\,r_{\mathrm{m:N}} + A_L) - w_d\,\frac{\partial B}{\partial z} + M(B,z) \tag{A9}$$

$$\frac{\partial}{\partial t}A_S = k_{\mathrm{coag1}}\,B\,(D_S\,r_{\mathrm{m:N}} + A_S) - k_{\mathrm{coag3}}\,A_S\,(D_L\,r_{\mathrm{m:N}} + A_L) - k_{\mathrm{coag2}}\,A_S\,(D_S\,r_{\mathrm{m:N}} + A_S) - w_s\,\frac{\partial A_S}{\partial z} + M(A_S,z) \tag{A10}$$

$$\frac{\partial}{\partial t}A_L = k_{\mathrm{coag4}}\,B\,(D_L\,r_{\mathrm{m:N}} + A_L) + k_{\mathrm{coag3}}\,A_S\,(D_L\,r_{\mathrm{m:N}} + A_L) + k_{\mathrm{coag2}}\,A_S\,(D_S\,r_{\mathrm{m:N}} + A_S) - w_l\,\frac{\partial A_L}{\partial z} + M(A_L,z) \tag{A11}$$

where F_{dust} is the deposition of dust at the ocean surface.

Processes controlling ligand concentration are described as ligand production by phytoplankton or release during remineralisation + release of free ligands by complex dissociation − ligands complexed with Fe(III)' – biological decomposition of free ligands + the physical term. An additional source of weak ligands is photolysis of strong complexes $k_{\mathrm{phls}}\,f_I\,\mathrm{FeL_{str}}$.

$$\frac{\partial}{\partial t}\mathrm{L_{str}} = \gamma_{lp}\,f_Q\,P + k_{\mathrm{flsd}}\,\mathrm{FeL_{str}} - k_{\mathrm{fel}}\,\mathrm{Fe(III)'}\,\mathrm{L_{str}} - \gamma_l\,f_T\,\mathrm{L_{str}} + M(\mathrm{L_{str}},z) \tag{A12}$$

$$\frac{\partial}{\partial t}\mathrm{L_{we}} = \gamma_{ld}\,f_T\,D + k_{\mathrm{flwd}}\,\mathrm{FeL_{we}} + k_{\mathrm{phls}}\,f_I\,\mathrm{FeL_{str}} - k_{\mathrm{fel}}\,\mathrm{Fe(III)'}\,\mathrm{L_{we}} - \gamma_l\,f_T\,\mathrm{L_{we}} + M(\mathrm{L_{we}},z) \tag{A13}$$

where the production rate of strong ligands is regulated by the internal Fe:N-quota of phytoplankton:

$$f_Q = \frac{Q_{\mathrm{Fe}}^{\mathrm{max}} - Q_{\mathrm{Fe}}}{Q_{\mathrm{Fe}}^{\mathrm{max}}} \tag{A14}$$

and a function of light intensity f_I is introduced in all photochemical reactions:

$$f_I = \frac{I(z)}{I_{\mathrm{ref}}} \tag{A15}$$

where $I(z)$ is the photosynthetically active radiation in the given vertical layer z.

The description of the concentration change of different Fe forms is more complex than in Weber et al. (2007) due to our introduction of more than one type of particles and ligands. The equations are:

$$\frac{\partial}{\partial t}\mathrm{Fe(III)'} = F_{\mathrm{Fe(III)',surf}} + \left(k_{\mathrm{ox1}}\,\mathrm{O_2} + k_{\mathrm{ox2}}\,\mathrm{O_2^-} + k_{\mathrm{ox3}}\,\mathrm{H_2O_2}\right)\mathrm{Fe(II)'} + k_{cd}\,\mathrm{Fe_{col}} + k_{\mathrm{flwd}}\,\mathrm{FeL_{we}} + k_{\mathrm{flsd}}\,\mathrm{FeL_{str}} - \left(k_{\mathrm{fel}}\,(\mathrm{L_{str}} + \mathrm{L_{we}}) + k_{\mathrm{ph3}}\,f_I + k_{\mathrm{red}}\,\mathrm{O_2^-} + k_{\mathrm{col}} + k_{\mathrm{sca}}\,(B + A_S + A_L + r_{\mathrm{m:N}}\,D_S + r_{\mathrm{m:N}}\,D_L)\right)\mathrm{Fe(III)'} + M(\mathrm{Fe(III)'},z) \tag{A16}$$

where the flux of Fe(III)' at the surface $F_{\mathrm{Fe(III)',surf}}$ is calculated from modelled dust deposition by Mahowald et al. (2003) F_{dust} with 3.5% Fe content in dust and 1% solubility.

$$\frac{\partial}{\partial t}\mathrm{Fe(II)'} = k_{\mathrm{red}}\,\mathrm{O_2^-}\,\mathrm{Fe(III)'} + f_I\left(k_{\mathrm{ph3}}\,\mathrm{Fe(III)'} + k_{\mathrm{phls}}\,\mathrm{FeL_{str}} + k_{\mathrm{phlw}}\,\mathrm{FeL_{we}} + k_{\mathrm{ph1}}\,\mathrm{Fe_{col}}\right) + k_{\mathrm{ph4}}\left(\mathrm{Fe_{dust}} + \mathrm{Fe_{parts}} + \mathrm{Fe_{partl}}\right) - \left(k_{\mathrm{ox1}}\,\mathrm{O_2} + k_{\mathrm{ox2}}\,\mathrm{O_2^-} + k_{\mathrm{ox3}}\,\mathrm{H_2O_2}\right)\mathrm{Fe(II)'} + M(\mathrm{Fe(II)'},z) \tag{A17}$$

where $\mathrm{Fe_{dust}}$, $\mathrm{Fe_{parts}}$, and $\mathrm{Fe_{partl}}$ are Fe adsorbed on surface of dust particles, small detritus and aggregates, and large detritus and aggregates, respectively.

$$\frac{\partial}{\partial t}\mathrm{FeL_{str}} = k_{\mathrm{fel}}\,\mathrm{Fe(III)'}\,\mathrm{L_{str}} - k_{\mathrm{flsd}}\,\mathrm{FeL_{str}} - f_I\,k_{\mathrm{phls}}\,\mathrm{FeL_{str}} - k_{\mathrm{upt}}\,\frac{\mathrm{FeL_{str}}}{\mathrm{FeL_{str}} + \mathrm{FeL_{we}}} + M(\mathrm{FeL_{str}},z) \tag{A18}$$

$$\frac{\partial}{\partial t}\mathrm{FeL_{we}} = \gamma_d\,f_T\,D_{\mathrm{Fe}} + \gamma_p\,f_T\,P_{\mathrm{Fe}} + \gamma_{zb}\,f_T\,Z_{\mathrm{Fe}} + k_{\mathrm{fel}}\,\mathrm{Fe(III)'}\,\mathrm{L_{we}} - k_{\mathrm{flwd}}\,\mathrm{FeL_{we}} - f_I\,k_{\mathrm{phlw}}\,\mathrm{FeL_{we}} - k_{\mathrm{upt}}\,\frac{\mathrm{FeL_{we}}}{\mathrm{FeL_{str}} + \mathrm{FeL_{we}}} + M(\mathrm{FeL_{we}},z) \tag{A19}$$

The uptake rate k_{upt} of $\mathrm{FeL_{str}}$ and $\mathrm{FeL_{we}}$ by phytoplankton is determined by:

$$k_{\mathrm{upt}} = \min\left(\mu_{\mathrm{max}}\,\frac{\mathrm{FeL_{str}} + \mathrm{FeL_{we}}}{(\mathrm{FeL_{str}} + \mathrm{FeL_{we}} + K_{\mathrm{Fe}})}\,P,\ \mu\,Q_{\mathrm{Fe}}^{\mathrm{ave}}\,P\right) \tag{A20}$$

Choosing the smaller one of the terms ensures a dependence of uptake on $\mathrm{Fe_{lig}}$ availability and a storage uptake is not considered.

$$\frac{\partial}{\partial t}\mathrm{Fe_{col}} = k_{\mathrm{col}}\,\mathrm{Fe(III)}' + k_{pd}\,\left(\mathrm{Fe_{dust}}+\mathrm{Fe_{parts}}+\mathrm{Fe_{partl}}\right) - k_{ag}\,\left(B+A_S+A_L+r_{\mathrm{m:N}}\,D_S+r_{\mathrm{m:N}}\,D_L\right)\,\mathrm{Fe_{col}} - k_{cd}\mathrm{Fe_{col}} - f_I\,k_{\mathrm{ph1}}\,\mathrm{Fe_{col}} + M(\mathrm{Fe_{col}}, z) \quad \text{(A21)}$$

$$\frac{\partial}{\partial t}\mathrm{Fe_{dust}} = \left(k_{\mathrm{sca}}\,\mathrm{Fe(III)}' + k_{ag}\,\mathrm{Fe_{col}}\right)\,B - \left(f_I\,k_{\mathrm{ph4}}+k_{pd}\right)\,\mathrm{Fe_{dust}} - k_{\mathrm{coag1}}\,\mathrm{Fe_{dust}}\,\left(D_S\,r_{\mathrm{m:N}}+A_S\right) - k_{\mathrm{coag4}}\,\mathrm{Fe_{dust}}\,\left(D_L\,r_{\mathrm{m:N}}+A_L\right) - w_d\,\frac{\partial \mathrm{Fe_{dust}}}{\partial z} + M(\mathrm{Fe_{dust}}, z) \quad \text{(A22)}$$

$$\frac{\partial}{\partial t}\mathrm{Fe_{parts}} = \left(k_{\mathrm{sca}}\,\mathrm{Fe(III)}' + k_{ag}\,\mathrm{Fe_{col}}\right)\,\left(r_{\mathrm{m:N}}\,D_s+A_S\right) + k_{\mathrm{coag1}}\,\mathrm{Fe_{dust}}\,\left(D_S\,r_{\mathrm{m:N}}+A_S\right) - k_{\mathrm{coag3}}\,\mathrm{Fe_{parts}},\,\left(D_L\,r_{\mathrm{m:N}}+A_L\right) - k_{\mathrm{coag2}}\,\mathrm{Fe_{parts}}\,\left(D_S\,r_{\mathrm{m:N}}+A_S\right) - \left(f_I\,k_{\mathrm{ph4}}+k_{pd}\right)\,\mathrm{Fe_{parts}} - w_s\,\frac{\partial \mathrm{Fe_{parts}}}{\partial z} + M(\mathrm{Fe_{parts}}, z) \quad \text{(A23)}$$

$$\frac{\partial}{\partial t}\mathrm{Fe_{partl}} = \left(k_{\mathrm{sca}}\,\mathrm{Fe(III)}' + k_{ag}\,\mathrm{Fe_{col}}\right)\,\left(r_{\mathrm{m:N}}\,D_L+A_L\right) - k_{\mathrm{coag4}}\,\mathrm{Fe_{dust}}\,\left(D_L\,r_{\mathrm{m:N}}+A_L\right) + k_{\mathrm{coag2}}\,\mathrm{Fe_{parts}}\,\left(D_S\,r_{\mathrm{m:N}}+A_S\right) + k_{\mathrm{coag3}}\,\mathrm{Fe_{parts}},\,\left(D_L\,r_{\mathrm{m:N}}+A_L\right) - \left(f_I\,k_{\mathrm{ph4}}+k_{pd}\right)\,\mathrm{Fe_{partl}} - w_l\,\frac{\partial \mathrm{Fe_{partl}}}{\partial z} + M(\mathrm{Fe_{partl}}, z) \quad \text{(A24)}$$

Finally, a variable Fe:N-quota is introduced in P, Z, and D and evolution of the respective Fe concentrations P_{Fe}, Z_{Fe} and D_{Fe} is described by:

$$\frac{\partial}{\partial t}P_{\mathrm{Fe}} = k_{\mathrm{upt}}\,\left(\mathrm{FeL_{str}}+\mathrm{FeL_{we}}\right) - Q_{\mathrm{Fe}}\left(f_G\,Z+\gamma_{p^2}\,P^2\right) - \gamma_p\,f_T\,P_{\mathrm{Fe}} + M(P_{\mathrm{Fe}}, z) \quad \text{(A25)}$$

$$\frac{\partial}{\partial t}Z_{\mathrm{Fe}} = Q_{\mathrm{Fe}}\,\gamma_{za}\,f_G\,Z - \gamma_{zb}\,f_T\,Z_{\mathrm{Fe}} - Q_{\mathrm{ZFe}}\,\gamma_{z^2}\,Z^2 + M(Z_{\mathrm{Fe}}, z) \quad \text{(A26)}$$

$$\frac{\partial}{\partial t}D_{\mathrm{SFe}} = Q_{\mathrm{Fe}}\,\gamma_{p^2}\,P^2 + Q_{\mathrm{Fe}}\,\left(1-\gamma_{za}\right)\,f_G\,Z - k_{\mathrm{coag2}}\,D_{\mathrm{SFe}}\,\left(D_S\,r_{\mathrm{m:N}}+A_S\right) - k_{\mathrm{coag3}}\,D_{\mathrm{SFe}}\,\left(D_L\,r_{\mathrm{m:N}}+A_L\right) - \gamma_d\,f_T\,D_{\mathrm{Fe}} + M(D_{\mathrm{Fe}}, z) \quad \text{(A27)}$$

$$\frac{\partial}{\partial t}D_{\mathrm{LFe}} = Q_{\mathrm{ZFe}}\,\gamma_{z^2}\,Z^2 - \gamma_d\,f_T\,D_{\mathrm{LFe}} + k_{\mathrm{coag2}}\,D_{\mathrm{SFe}}\,\left(D_S\,r_{\mathrm{m:N}}+A_S\right) + k_{\mathrm{coag3}}\,D_{\mathrm{SFe}}\,\left(D_L\,r_{\mathrm{m:N}}+A_L\right) - \gamma_d\,f_T\,D_{\mathrm{LFe}} + M(D_{\mathrm{LFe}}, z) \quad \text{(A28)}$$

Table B1. Sensitivity studies with respect to ecosystem parameters. Relative change is calculated as the ratio of the parameter value in the sensitivity study to the one in the standard model run.

parameter symbol	relative change of parameter value	relative change of primary production	relative change of export (100 m)
$\mu_{\max}$	0.8	0.99	0.89
	1.2	0.99	1.03
K_{N}	0.5	0.98	1.0
	2.0	0.99	0.95
α	0.6	0.96	0.92
	0.8	0.98	0.96
γ_p	0.5	0.74	1.40
	2.0	1.25	0.38
$g_{\max}$	0.5	1.00	0.98
	1.5	0.98	0.98
γ_{p^2}	0.5	0.99	0.98
	2.0	0.99	0.98
γ_{z^2}	0.5	0.94	1.0
	2.0	0.94	1.09
γ_{za}	0.54	1.21	0.82
	1.07	0.97	1.0
γ_d	0.5	0.93	1.02
	2.0	1.09	0.91

Table B2. Sensitivity studies with respect to iron solubility and content in dust particles

study number	iron content (%)	surface DFe (nM)
1	3	0.15–0.49
2	6	0.17–0.72
3	12	0.23–1.33
4	24	0.32–2.6

Appendix B

Sensitivity studies

Primary and export production are not very sensitive to most parameters, except to the exudation rate of phytoplankton (γ_p) (Table B1). This exudation rate determines the flux of the shortcut from phytoplankton to nutrients. Decreasing γ_p to half of the standard value leads to a decrease of primary production to 74%, because less nutrients are available for phytoplankton growth. This result is closer to the estimated primary production from MODIS data. However, the ratio of export/primary production rises to 27% which is higher than most typical values estimated for open-ocean (De La Rocha and Passow, 2007), indicating too slow transformation of biomass into nutrient in surface waters. Therefore, we kept applying the parameter values from Schartau and Oschlies (2003a,b) optimised for the North Atlantic.

Measured Fe content in dust varies from 3 to 7.6% (Wedepohl, 1995; Duce and Tindale, 1991; Spokes and Jickells, 1996; Desboeufs et al., 2001). We only varied iron content in the sensitivity study (Table B2) and multiplied it with 1% iron solubility which is close to the most reported mean iron solubility of Saharan dust (Baker et al., 2006a,b; Baker and Jickells, 2006; Spokes and Jickells, 1996). DFe surface concentration increases in the sensitivity study exponentially with increasing iron content. The modelled DFe surface concentration from the sensitivity studies No. 3 and 4 is much too high compared to the observations near Cape Verde Islands, which ranges between 0.15 to 0.52 nmol L^{-1} (see Sect. 3.4.2 Modelled DFe concentration). In the other two studies (No. 1 and 2), surface DFe is in the similar range as the observations and biology is quite insensitive to different Fe input: the averaged primary production is changed only about 1%. This result supports our choice of 1% solubility and 3.5% iron content which is between the parameter values in the sensitivity studies No. 1 and 2. TENATSO is close to the dust source region and dry deposition is predominant which also makes it reasonable to take a smaller solubility or a smaller product of solubility and iron content for our model calculation.

Acknowledgements. This work is a contribution to the project SOPRAN (Surface Ocean Processes in the ANtropocene), which is funded by the German Federal Ministry of Education and Research (BMBF project 03F0462C). We sincerely thank M. Rijkenberg and I. Peeken for kindly providing unpublished data, L. Cotrim da Cunha, I. Hense, and J. Wu for providing data, and H. Burchard and K. Bolding for technical support.

Edited by: K. Hunter

References

Amon, R. and Benner, R.: Rapid cycling of high-molecular-weight dissolved organic matter in the ocean, Nature, 369, 549–552, 1994.

Armstrong, R., Lee, C., Hedges, J., Honjo, S., and Wakeham, S.: A new, mechanistic model for organic carbon fluxes in the ocean based on the quantitative association of POC with ballast minerals, Deep-Sea Res. II, 49, 219–236, 2002.

Asper, V. and Smith, W. J.: Abundance, distribution and sinking rates of aggregates in the Ross Sea, Antarctica, Deep-Sea Res. I, 50, 131–150, doi:10.1016/S0967-0637(02)00146-2, 2003.

Asper, V., Deuser, W., Knauer, G., and Lohrenz, S.: Rapid coupling of sinking particle fluxes between surface and deep ocean waters, Nature, 357, 670–672, 1992.

Aumont, O., Maier-Reimer, E., Blain, S., and Monfray, P.: An ecosystem model of the global ocean including Fe, Si, P colimitations, Global Biogeochem. Cy., 17, 1060, doi:10.1029/2001GB001745, 2003.

Bacon, M. P. and Anderson, R. F.: Distribution of thorium isotopes between dissolved and particulate forms in the deep sea, J. Geophys. Res., 87(C3), 2045–2056, doi:10.1029/JC087iC03p02045, 1982.

Baker, A., Jickells, T., Biswas, K., Weston, K., and French, M.: Nutrients in atmospheric aerosol particles along the Atlantic Meridional Transect, Deep Sea Res. II, 53, 1706–1719, doi:10.1016/j.dsr2.2006.05.012, 2006a.

Baker, A., Jickells, T., Witt, M., and Linge, K.: Trends in the solubility of iron, aluminium, manganese and phosphorus in aerosol collected over the Atlantic Ocean, Mar. Chem., 98, 43–58, 2006b.

Baker, A. R. and Jickells, T. D.: Mineral particle size as a control on aerosol iron solubility, Geophys. Res. Lett., 33, L17608, doi:10.1029/2006GL026557, 2006.

Balistieri, L., Brewer, P., and Murray, J.: Scavenging residence times of trace metals and surface chemistry of sinking particles in the deep ocean, Deep Sea Res., 28A, 101–121, 1981.

Barbeau, K. and Moffett, J.: Laboratory and field studies of colloidal iron oxide dissolution as mediated by phagotrophy and photolysis, Limnol. Oceanogr., 45(4), 827–835, 2000.

Barbeau, K., Rue, E., Bruland, K., and Butler, A.: Photochemical cycling of iron in the surface ocean mediated by microbial iron(III)-binding ligands, Nature, 413, 409–413, 2001.

Barbeau, K., Rue, E., Trick, C., Bruland, K., and Butler, A.: Photochemical reactivity of siderophores produced by marine heterotrophic bacteria and cyanobacteria based on characteristic Fe(III) binding groups, Limnol. Oceanogr., 48, 1069–1078, 2003.

Behrenfeld, M. and Falkowski, P.: Photosynthetic rates derived from satellite-based chlorophyll concentration, Limnol. Oceanogr., 42, 1–20, 1997.

Bergquist, B., Wu, J., and Boyle, E.: Variability in oceanic dissolved iron is dominated by the colloidal fraction, Geochim. Cosmochim. Ac., 71, 2960–2974, doi:10.1016/j.gca.2007.03.013, 2007.

Bory, A., Jeandel, C., Leblond, N., Vangriesheim, A., Khripounoff, A., Beaufort, L., Rabouille, C., Nicolas, E., Tachikawa, K., Etcheber, H., and Buat-Ménard, P.: Downward particle fluxes within different productivity regimes off the Mauritanian upwelling zone (EUMELI program), Deep Sea Res. I, 48, 2251–2282, 2001.

Boyd, P. W., Jickells, T., Law, C. S., Blain, S., Boyle, E. A., Buesseler, K. O., Coale, K. H., Cullen, J. J., de Baar, H. J. W., Follows, M., Harvey, M., Lancelot, C., Levasseur, M., Owens, N. P. J., Pollard, R., Rivkin, R. B., Sarmiento, J., Schoemann, V., Smetacek, V., Takeda, S., Tsuda, A., Turner, S., and Watson, A. J.: Mesoscale Iron Enrichment Experiments 1993–2005: Synthesis and Future Directions, Science, 315, 612–617, 2007.

Boye, M., Van den Berg, C., De Jong, J., Leach, H., Croot, P., and De Baar, H.: Organic complexation of iron in the Southern Ocean, Deep-Sea Res. I, 48, 1477–1497, 2001.

Boye, M., Aldrich, A., van den Berg, C., de Jong, J., Nirmaier, H., Veldhuis, M., Timmermans, K., and de Baar, H.: The chemical speciation of iron in the north-east Atlantic Ocean, Deep-Sea Res. I, 53, 667–683, 2006.

Broecker, W. S. and Peng, T.-H.: Tracers in the sea, in: Tracers in the sea, Eldigio Press Lamont Doherty Geological Observatory, 2–5, 1982.

Burchard, H. and Umlauf, L.: Observations and numerical modelling of mixed-layer turbulence: Do they represent the same statistical quantities?, Deep Sea Res. II, 52, 1069–1074, doi:10.1016/j.dsr2.2005.03.002, 2005.

Burchard, H., Delersnijder, E., and Meister, A.: Application of modified Patankar schemes to stiff biogeochemical models for the water column, Ocean Dynam., 55, 326–337, 2005.

Burd, A. and Jackson, G.: Particle Aggregation, Annu. Rev. Mar. Sci., 1, 65–90, doi:10.1146/annurev.marine.010908.163904, 2009.

Carpenter, E. J., Subramaniam, A., and Capone, D. G.: Biomass and primary productivity of the cyanobacterium Trichodesmium spp. in the tropical N Atlantic ocean, Deep Sea Res. I, 51, 173–203, 2004.

Chiapello, I., Bergametti, G., Chatenet, B., Bousquet, P., Dulac, F., and Soares, E. S.: Origins of African dust transported over the northeastern tropical Atlantic, J. Geophys. Res., 102(D12), 13701–13709, 1997.

Cloern, J. E., Grenz, C., and Vidergar-Lucas, L.: An empirical model of the phytoplankton chlorophyll : carbon ratio-the conversion factor between productivity and growth rate, Limnol. Oceanogr., 40(7), 1313–1321, 1995.

Cullen, J., Bergquist, B., and Moffett, J.: Thermodynamic characterization of the partitioning of iron between soluble and colloidal species in the Atlantic Ocean, Mar. Chem., 98, 295–303, 2006.

De Boyer Montegut, C. Madec, G., Fischer, A., Lazar, A., and Iudicone, D.: Mixed layer depth over the global ocean: An examination of profile data and a profile-based climatology, J. Geophys. Res. C. Oceans, 109, C12003, doi:10.1029/2004JC002378, 2004.

De La Rocha, C. and Passow, U.: Factors influencing the sinking of POC and the efficiency of the biological carbon pump, Deep Sea Res. II, 54, 639–658, doi:10.1016/j.dsr2.2007.01.004, 2007.

Desboeufs, K. V., Losno, R., and Colin, J. L.: Factors influencing aerosol solubility during cloud processes, Atmos. Environ., 35, 3529–3537, 2001.

Duce, R. and Tindale, N.: Atmospheric transport of iron and its deposition in the ocean, Limnol. Oceanogr., 36, 1715–1726, 1991.

Emery, K. and Honjo, S.: Surface suspended matter off western Africa: relations of organic matter, skeletal debris and detrital minerals, Sedimentology, 26, 775–794, 1979.

Falkowski, P.: Evolution of the nitrogen cycle and its influence on the biological sequestration of CO_2 in the ocean, Nature, 387, 272–275, 1997.

Fischer, G; Ratmeyer, V. and Wefer, G.: Organic carbon fluxes in the Atlantic and the Southern Ocean: relationship to primary production compiled from satellite radiometer data, Deep-Sea Res. II, 47, 1961–1997, doi:10.1016/S0967-0645(00)00013-8, 2000.

Francois, R., Honjo, S., Krishfield, R., and Manganini, S.: Factors controlling the flux of organic carbon to the bathypelagic zone of the ocean, Global Biogeochem. Cy., 16, 1087, doi:10.1029/2001GB001722, 2002.

Gerringa, L., Veldhuis, M., Timmermans, K., Sarthou, G., and de Baar, H.: Co-variance of dissolved Fe-binding ligands with phytoplankton characteristics in the Canary Basin, Mar. Chem., 102, 276–290, 2006.

Gerringa, L., Blain, S., Laan, P., Sarthou, G., Veldhuis, M., Brussaard, C., Viollier, E., and Timmermans, K.: Fe-binding dissolved organic ligands near the Kerguelen Archipelago in the Southern Ocean (Indian sector), Deep Sea Res. II, 55, 606–621, 2008.

Gledhill, M. and van den Berg, C.: Determination of complexation of iron(III) with natural organic complexing ligands in seawater using cathodic stripping voltammetry, Mar. Chem., 47, 41–54, 1994.

Granger, J. and Price, N. M.: The importance of siderophores in iron nutrition of heterotrophic marine bacteria, Limnol. Oceanogr., 44, 541–555, 1999.

Graziano, L., Geider, R., Li, W., and Olaizola, M.: Nitrogen limitation of North Atlantic phytoplankton: analysis of physiological condition in nutrient enrichment experiments, Aquat. Microb. Ecol., 11, 53–64, 1996.

Gruber, N., Frenzel, H., Doney, S., Marchesiello, P., McWilliams, J., Moisan, J., Oram, J., Plattner, G.-K., and Stolzenbach, K.: Eddy-resolving simulation of plankton ecosystem dynamics in the California Current System, Deep Sea Res. I, 53, 1483–1516, doi:10.1016/j.dsr.2006.06.005, 2006.

Guieu, C., Bozec, Y., Blain, S., Ridame, C., Sarthou, G., and Leblond, N.: Impact of high Saharan dust inputs on dissolved iron concentrations in the Mediterranean Sea, Geophys. Res. Lett., 29, 17-1–17-4, doi:10.1029/2001GL014454, 2002.

Hamm, C.: Interactive aggregation and sedimentation of diatoms and clay-sized lithogenic material, Limnol. Oceanogr., 47, 1790–1795, 2002.

Heinold, B., Helmert, J., Hellmuth, O., Wolke, R., Ansmann, A., Marticorena, B., Laurent, B., and Tegen, I.: Regional modeling of Saharan dust events using LM-MUSCAT: Model description and case studies, J. Geophys. Res., 112, D11204, doi:10.1029/2006JD007443, 2007.

Honjo, S., Manganini, S., and Poppe, L.: Sedimentation of lithogenic particles in the deep ocean, Mar. Geol., 50, 199–220, 1982.

Hudson, R., Covault, D., and Morel, F.: Investigations of iron coordination and redox reactions in seawater using ^{59}Fe radiometry and ion-pair solvent extraction of amphiphilic iron complexes, Mar. Chem., 38, 209–235, 1992.

Hunter, K. A. and Boyd, P. W.: Iron-binding ligands and their role in the ocean biogeochemistry of iron, Environ. Chem., 4, 221–232, 2007.

Hutchins, D., Witter, A., Butler, A., and Luther III, G.: Competition among marine phytoplankton for different chelated iron species, Nature, 400, 858–861, 1999.

Hutchins, D., Hare, C., Weaver, R., Zhang, Y., Firme, G., DiTullio, G., Alm, M., Riseman, S., Maucher, J., Geesey, M., Trick, C., Smith, G., Rue, E., Conn, J., and Bruland, K.: Phytoplankton iron limitation in the Humboldt Current and Peru Upwelling, Limnol. Oceanogr., 47, 997–1011, 2002.

Jackson, G. A. and Burd, A. B.: Aggregation in the Marine Environment, Environ. Sci. Technol., 32, 2805–2814, doi:10.1021/es980251w, 1998.

Jickells, T. D., An, Z. S., Andersen, K. K., Baker, A. R., Bergametti, G., Brooks, N., Cao, J. J., Boyd, P. W., Duce, R. A., Hunter, K. A., Kawahata, H., Kubilay, N., laRoche, J., Liss, P. S., Mahowald, N., Prospero, J. M., Ridgwell, A. J., Tegen, I., and Torres, R.: Global Iron Connections Between Desert Dust, Ocean Biogeochemistry, and Climate, Science, 308, 67–71, 2005.

Johnson, K., Coale, K., Elrod, V., and Tindale, N.: Iron photochemistry in seawater from the equatorial Pacific, Mar. Chem., 46, 319–334, 1994.

Johnson, K., Gordon, R., and Coale, K.: What controls dissolved iron concentrations in the world ocean?, Mar. Chem., 57, 137–

161, 1997.

Klaas, C. and Archer, D.: Association of sinking organic matter with various types of mineral ballast in the deep sea: Implications for the rain ratio, Global Biogeochem. Cy., 16, 1116, doi: 10.1029/2001GB001765, 2002.

Kondo, Y., Takeda, S., Nishioka, J., Obata, H., Furuya, K., Johnson, W. K., and Wong, C. S.: Organic iron (III) complexing ligands during an iron enrichment experiment in the western subarctic North Pacific, Geophys. Res. Lett., 35, L12601, doi: 10.1029/2008GL033354, 2008.

Kriest, I.: Different parameterizations of marine snow in a 1D-model and their influence on representation of marine snow, nitrogen budget and sedimentation, Deep-Sea Res. I, 49, 2133–2162, doi:10.1016/S0967-0637(02)00127-9, 2002.

Laglera, L. M. and van den Berg, C. M. G.: Evidence for geochemical control of iron by humic substances in seawater, Limnol. Oceanogr., 54(2), 610–619, 2009.

Lewis, B., Luther, G. I., Lane, H., and Church, T.: Determination of metal-organic complexation in natural waters by SWASV with pseudopolarograms, Electroanalysis, 7, 166–177, 1995.

Lutz, M., Dunbar, R., and Caldeira, K.: Regional variability in the vertical flux of particulate organic carbon in the ocean interior, Global Biogeochem. Cy., 16, 1037, doi:10.1029/2000GB001383, 2002.

Macrellis, H., Trick, C., Rue, E., Smith, G., and Bruland, K.: Collection and detection of natural iron-binding ligands from seawater, Mar. Chem., 76, 175–187, 2001.

Mahowald, N., Luo, C., Del Corral, J., and Zender, C.: Interannual variability in atmospheric mineral aerosols from a 22-year model simulation and observational data, J. Geophys. Res.-Atmos., 108, 4352, doi:10.1029/2002JD002821, 2003.

Maldonado, M. and Price, N.: Utilization of iron bound to strong organic ligands by plankton communities in the subarctic North Pacific, Deep Sea Res. II, 46, 2447–2473, 1999.

Martin, J., Knauer, G., Karl, D., and Broenkow, W.: VERTEX: Carbon cycling in the Northeast Pacific, Deep-Sea Res. A, 34, 267–285, 1987.

Martinez, J. and Haygood, M.: Identification of a natural desferrioxamine siderophore produced by a marine bacterium, Limnol. Oceanogr. Suppl., 420–424, 2001.

Martinez, J., Carter-Franklin, J., Mann, E., Martin, J., Haygood, M., and Butler, A.: Structure and membrane affinity of a suite of amphiphilic siderophores produced by a marine bacterium, P. Natl. Acad. Sci. USA, 100, 3754–3759, doi:10.1073/pnas.0637444100, 2003.

Martinez, J. S., Zhang, G. P., Holt, P. D., Jung, H.-T., Carrano, C. J., Haygood, M. G., and Butler, A.: Self-assembling amphiphilic siderophores from marine bacteria, Science, 287, 1245–1247, doi:10.1126/science.287.5456.1245, 2000.

McCave, I.: Size spectra and aggregation of suspended particles in the deep ocean, Deep-Sea Res. A, 31, 329–352, 1984.

Micinski, E., Ball, L. A., and Zafiriou, O. C.: Photochemical Oxygen Activation: Superoxide Radical Detection and Production Rates in the Eastern Caribbean, J. Geophys. Res., 98(C2), 2299–2306, doi:10.1029/92JC02766, 1993.

Millero, F. and Sotolongo, S.: The oxidation of Fe(II) with H_2O_2 in seawater, Geochim. Cosmochim. Ac., 53, 1867–1873, 1989.

Mills, M., Ridame, C., Davey, M., La Roche, J., and Geider, R.: Iron and phosphorus co-limit nitrogen fixation in the eastern tropical North Atlantic, Nature, 429, 292–294, 2004.

Moffett, J. W.: Temporal and spatial variability of copper complexation by strong chelators in the Sargasso Sea, Deep Sea Res. I, 42, 1273–1295, 1995.

Morel, A., Antoine, D., Babin, M., and Dandonneau, Y.: Measured and modeled primary production in the northeast Atlantic (EUMELI JGOFS program): the impact of natural variations in photosynthetic parameters on model predictive skill, Deep Sea Res. I, 43, 1273–1304, 1996.

Parekh, P., Follows, M., and Boyle, E.: Modelling the global ocean iron cycle, Global Biogeochem. Cy., 18, GB1002, doi: 1029/2003GB002061, 2004.

Passow, U.: Switching perspectives: Do mineral fluxes determine particulate organic carbon fluxes or vice versa?, Geochem. Geophy. Geosy., 5, Q04002, doi:10.1029/2003GC000670, 2004.

Passow, U. and De la Rocha, C.: Accumulation of mineral ballast on organic aggregates, Global Biogeochem. Cy., 20, GB4S23, doi:10.1029/2005GB002579, 2006.

Powell, R. and Wilson-Finelli, A.: Photochemical degradation of organic iron complexing ligands in seawater, Aquat. Sci., 65, 367–374, 2003.

Ratmeyer, V., Fischer, G., and Wefer, G.: Lithogenic particle fluxes and grain size distributions in the deep ocean off Northwest Africa: Implications for seasonal changes of aeolian dust input and downward transport, Deep-Sea Res. I, 46, 1289–1337, doi: 10.1016/S0967-0637(99)00008-4, 1999.

Reid, R., Live, D., Faulkner, D., and Butler, A.: A siderophore from a marine bacterium with an exceptional ferric ion affinity constant, Nature, 366, 455–458, 1993.

Rijkenberg, M., Powell, C., Dall'Osto, M., Nielsdottir, M., Patey, M., Hill, P., Baker, A., Jickells, T., Harrison, R., and Achterberg, E.: Changes in iron speciation following a Saharan dust event in the tropical North Atlantic Ocean, Mar. Chem., 110, 56–67, doi:10.1016/j.marchem.2008.02.006, 2008.

Rose, A. and Waite, T.: Predicting iron speciation in coastal waters from the kinetics of sunlight-mediated iron redox cycling, Aquat. Sci., 65, 375–383, 2003a.

Rose, A. and Waite, T.: Kinetics of hydrolysis and precipitation of ferric iron in seawater, Environ. Sci. Technol., 37, 3897–3903, 2003b.

Rose, A. and Waite, T.: Kinetics of iron complexation by dissolved natural organic matter in coastal waters, Mar. Chem., 84, 85–103, 2003c.

Rue, E. and Bruland, K.: Complexation of iron(III) by natural organic ligands in the Central North Pacific as determined by a new competitive ligand equilibration/adsorptive cathodic stripping voltammetric method, Mar. Chem., 50, 117–138, 1995.

Rue, E. and Bruland, K.: The role of organic complexation on ambient iron chemistry in the equatorial Pacific Ocean and the response of a mesoscale iron addition experiment, Limnol. Oceanogr., 42, 901–910, 1997.

Ruiz, J., Prieto, L., and Ortegón, F.: Diatom aggregate formation and fluxes: a modeling analysis under different size-resolution schemes and with empirically determined aggregation kernels, Deep Sea Res. I, 49, 495–515, 2002.

Sarthou, G., Baker, A., Blain, S., Achterberg, E., Boye, M., Bowie, A., Croot, P., Laan, P., De Baar, H., Jickells, T., and Worsfold, P.: Atmospheric iron deposition and sea-surface dissolved iron concentrations in the eastern Atlantic Ocean, Deep-Sea Res. I,

50, 1339–1352, 2003.

Sarthou, G., Baker, A. R., Kramer, J., Laan, P., Laës, A., Ussher, S., Achterberg, E. P., de Baar, H. J., Timmermans, K. R., and Blain, S.: Influence of atmospheric inputs on the iron distribution in the subtropical North-East Atlantic Ocean, Mar. Chem., 104, 186–202, doi:10.1016/j.marchem.2006.11.004, 2007.

Schartau, M. and Oschlies, A.: Simultaneous data-based optimization of a 1D-ecosystem model at three locations in the North Atlantic: Part I. Method and parameter estimates, J. Mar. Res., 61, 765–793, 2003a.

Schartau, M. and Oschlies, A.: Simultaneous data-based optimization of a 1D-ecosystem model at three locations in the North Atlantic: Part II. Standing stocks and nitrogen fluxes, J. Mar. Res., 61, 795–821, 2003b.

Schlosser, C. and Croot, P. L.: Controls on seawater Fe(III) solubility in the Mauritanian upwelling zone, Geophys. Res. Lett., 36, L18606, doi:10.1029/2009GL038963, 2009.

Smayda, T.: The suspension and sinking of phytoplankton in the sea (RV), Ocean. Mar. Biol., 8, 353–414, 1970.

Spokes, L. and Jickells, T.: Factors controlling the solubility of aerosol trace metals in the atmosphere and on mixing into seawater, Aquat. Geochem., 1, 355–374, 1996.

Steigenberger, S. and Croot, P.: Identifying the processes controlling the distribution of H_2O_2 in surface waters along a meridional transect in the eastern Atlantic, Geophys. Res. Lett., 35, L03616, doi:10.1029/2007GL032555, 2008.

Sunda, W. and Huntsman, S.: Iron uptake and growth limitation in oceanic and coastal phytoplankton, Mar. Chem., 50, 189–206, 1995.

Tagliabue, A., Bopp, L., Aumont, O., and Arrigo, K. R.: Influence of light and temperature on the marine iron cycle: From theoretical to global modeling, Global Biogeochem. Cy., 23, GB2017, doi:10.1029/2008GB003214, 2009.

Tovar-Sanchez, A., Sañudo-Wilhelmy, S. A., Garcia-Vargas, M., Weaver, R. S., Popels, L. C., and Hutchins, D. A.: A trace metal clean reagent to remove surface-bound iron from marine phytoplankton, Mar. Chem., 82, 91–99, doi:10.1016/S0304-4203(03)00054-9, 2003.

Trick, C.: Hydroxamate-siderophore production and utilization by marine eubacteria, Current Microbiology, 18, 375–378, 1989.

Tyrrell, T., Maranon, E., Poulton, A. J., Bowie, A. R., Harbour, D. S., and Woodward, E. M. S.: Large-scale latitudinal distribution of Trichodesmium spp. in the Atlantic Ocean, J. Plankton Res., 25, 405–416, 2003.

Umlauf, L. and Burchard, H.: Second-order turbulence closure models for geophysical boundary layers. A review of recent work, Cont. Shelf Res., 25, 795–827, 2005.

Uppala, S., Kå llberg, P., Simmons, A., Andrae, U., da Costa Bechtold, V., Fiorino, M., Gibson, J., Haseler, J., Hernandez, A., Kelly, G., Li, X., Onogi, K., Saarinen, S., Sokka, N., Allan, R., Andersson, E., Arpe, K., Balmaseda, M., Beljaars, A., van de Berg, L., Bidlot, J., Bormann, N., Caires, S., Chevallier, F., Dethof, A., Dragosavac, M., Fisher, M., Fuentes, M., Hagemann, S., Hólm, E., Hoskins, B., Isaksen, L., Janssen, P., Jenne, R., McNally, A., Mahfouf, J.-F., Morcrette, J.-J., Rayner, N., Saunders, R., Simon, P., Sterl, A., Trenberth, K., Untch, A., Vasiljevic, D., Viterbo, P., and Woollen, J.: The ERA-40 re-analysis, Q. J. Roy. Meteorol. Soc., 131, 2961–3012, doi:10.1256/qj.04.176, 2005.

van den Berg, C.: Evidence for organic complexation of iron in seawater, Mar. Chem., 50, 139–157, 1995.

van der Loeff, M. R., Helmers, E., and Kattner, G.: Continuous transects of cadmium, copper, and aluminium in surface waters of the Atlantic Ocean, 50° N to 50° S: correspondence and contrast with nutrient-like behaviour, Geochim. Cosmochim. Ac., 61, 47–61, 1997.

Voelker, B. and Sedlak, D.: Iron reduction by photoproduced superoxide in seawater, Mar. Chem., 50, 93–102, 1995.

Wang, W.-X. and Dei, R.: Biological uptake and assimilation of iron by marine plankton: Influences of macronutrients, Mar. Chem., 74, 213–226, 2001.

Weber, L., Völker, C., Schartau, M., and Wolf-Gladrow, D.: Modeling the speciation and biogeochemistry of iron at the Bermuda Atlantic Time-series Study site, Global Biogeochem. Cy., 19, GB1019, doi:10.1029/2004GB002340, 2005.

Weber, L., Völker, C., Oschlies, A., and Burchard, H.: Iron profiles and speciation of the upper water column at the Bermuda Atlantic Time-series Study site: a model based sensitivity study, Biogeosciences, 4, 689–706, 2007, http://www.biogeosciences.net/4/689/2007/.

Wedepohl, K. H.: The composition of the continental crust, Geochim. Cosmochim. Ac., 59, 1217–1232, doi:10.1016/0016-7037(95)00038-2, 1995.

Wells, M. and Goldberg, E.: Colloid aggregation in seawater, Mar. Chem., 41, 353–358, 1993.

Wen, L.-S., Santschi, P., and Tang, D.: Interactions between radioactively labeled colloids and natural particles: Evidence for colloidal pumping, Geochim. Cosmochim. Ac., 61, 2867–2878, 1997.

Wilhelm, S. and Trick, C.: Iron-limited growth of cyanobacteria: Multiple siderophore production is a common response, Limnol. Oceanogr., 39, 1979–1984, 1994.

Wilhelm, S., Maxwell, D., and Trick, C.: Growth, iron requirements, and siderophore production in iron-limited *Synechococcus* PCC 7002, Limnol. Oceanogr., 41, 89–97, 1996.

Witter, A. and Luther III, G.: Variation in Fe-organic complexation with depth in the northwestern Atlantic Ocean as determined using a kinetic approach, Mar. Chem., 62, 241–258, 1998.

Witter, A., Lewis, B., and Luther, G. I.: Iron speciation in the Arabian Sea, Deep-Sea Res. II, 47, 1517–1539, doi:10.1016/S0967-0645(99)00152-6, 2000.

Wu, J. and Boyle, E.: Iron in the Sargasso Sea: Implications for the processes controlling dissolved Fe distribution in the ocean, Global Biogeochem. Cy., 16, 1086, doi:10.1029/2001GB001453, 2002.

Wu, J., Boyle, E., Sunda, W., and Wen, L.-S.: Soluble and colloidal iron in the oligotrophic North Atlantic and North Pacific, Science, 293, 847–849, 2001.

Zielinski, O., Llinás, O., Oschlies, A., and Reuter, R.: Underwater light field and its effect on a one-dimensional ecosystem model at station ESTOC, north of the Canary Islands, Deep Sea Res. II, 49, 3529–3542, 2002.

2.3 Publication II

Dust deposition: iron source or sink? A case study

Biogeosciences Discuss., 7, 9219–9272, 2010
www.biogeosciences-discuss.net/7/9219/2010/
doi:10.5194/bgd-7-9219-2010

Biogeosciences Discussions

This discussion paper is/has been under review for the journal Biogeosciences (BG).
Please refer to the corresponding final paper in BG if available.

Dust deposition: iron source or sink? A case study

Y. Ye[1], T. Wagener[2,*], C. Völker[1], C. Guieu[3], and D. A. Wolf-Gladrow[1]

[1]Alfred Wegener Institute for Polar and Marine Research, Bremerhaven, Germany
[2]IFM-GEOMAR, Leibniz-Institut für Meereswissenschaften, Kiel, Germany
[3]INSU-CNRS UMR7093, Laboratoire d'Océanographie de Villefranche/Mer (LOV), Université Paris 06, Observatoire Océanologique de Villefranche-sur-mer, France, Villefranche-sur-mer, France
[*]now at: LOPB, UMR6535, CNRS Université de la Méditerranee, Marseille, France

Received: 3 November 2010 – Accepted: 1 December 2010 – Published: 21 December 2010

Correspondence to: Y. Ye (ying.ye@awi.de)

Published by Copernicus Publications on behalf of the European Geosciences Union.

Abstract

A significant decrease of dissolved iron (DFe) concentration has been observed after dust addition into mesocosms during the DUst experiment in a low Nutrient low chlorophyll Ecosystem (DUNE), carried out in the summer of 2008. To understand the processes regulating the observed DFe variation, we simulated the experiment by a one-dimensional model of the Fe biogeochemical cycle, coupled with a simple ecosystem model. Different size classes of particles and particle aggregation are taken into account to describe the particle dynamics. DFe concentration is regulated in the model by dissolution from dust particles and adsorption onto particle surfaces, biological uptake, and photochemical mobilisation of particulate iron. The model reproduces the observed DFe decrease after dust addition well, choosing particle adsorption rates of 30, 150 and 750 $m^3\,kg^{-1}\,d^{-1}$ for particles of different size classes. These adsorption rates range between the measured adsorption rates of soluble iron and those of colloidal iron, indicating both processes controlling the DFe removal during the experiment. Sensitivity studies reveal that initial DFe concentration before dust addition was crucial for the net impact of dust addition on DFe during the DUNE experiment. From the balance between sinks and sources of DFe, a critical DFe concentration, above which dust deposition acts as a net sink of DFe, rather than a source, has been estimated for the DUNE experiment. Taking into account the role of excess iron binding ligands, this concept of a critical DFe concentration might be applied to explain the short-term variability of DFe after natural dust deposition.

1 Introduction

Iron is an essential micronutrient for marine life. Due to its low solubility under oxic conditions, the bioavailability of iron in the ocean is often limited. The important role of iron in controlling marine primary production has been widely confirmed in bottle incubation and in situ iron fertilisation experiments over the last decades (Martin et al.,

1990; Hutchins and Bruland, 1998; Mills et al., 2004; de Baar et al., 2005; Boyd et al., 2007). One of the major sources of iron in open ocean regions is the atmospheric input of dust (Duce and Tindale, 1991; Jickells et al., 2005). Only a few studies have investigated the impact of dust addition on biological activity. Mills et al. (2004) found in a shipboard experiment that dust addition stimulated a significant growth of chlorophyll. Some field studies in the HNLC (high-nutrient-low-chlorophyll) and oligotrophic waters also reported enhancement of biomass following natural dust deposition, in particular by nitrogen fixers; whereas others found no evidence of a response or low biological responses to dust supply (Boyd et al., 2010). The difference between these observations is attributed to limiting factors other than iron, e.g. phosphorus and light (Sedwick et al., 2005; Boyd et al., 2004), but also to complex processes controlling the bioavailability of iron supplied by dust events.

The bioavailable fraction of iron input by atmospheric deposition strongly depends on dissolution and removal processes in seawater. Elevated concentrations of dissolved iron (DFe) in surface waters following dust events have been widely observed (Vink and Measures, 2001; Bishop et al., 2002; Sarthou et al., 2003; Johnson et al., 2003; Rijkenberg et al., 2008), although the reported Fe solubility shows a large range from 0.01–80% (Mahowald et al., 2009). Interactions with organic Fe binding ligands are supposed to alter the solubility of deposited iron (Boyd et al., 2010).

Since the studies on loss processes of iron in the 1980's (e.g., Balistieri et al., 1981; Honjo et al., 1982), it is well known that iron has the metallic property to adsorb onto surface of sinking particles and is removed out of the dissolved pool. The measured sorption time varies from hours to days (Nyffeler et al., 1984; Honeyman et al., 1988), indicating that several different processes regulate the adsorption kinetics. Importance has been attached to a pathway called "colloidal pumping" by Honeyman and Santschi (1989). "Colloidal pumping" describes the removal of DFe via colloid formation and aggregation. The kinetics of these reactions has been further investigated in a few studies (Wells and Goldberg, 1993; Johnson et al., 1994; Wen et al., 1997; Rose and Waite, 2003b). Measurements on colloidal and particulate iron are however very limited and

the chemical properties of particulate iron in the ocean are largely unknown (Bruland and Rue, 2001; Moffet, 2001). One of the most important issues in the study on the marine Fe cycle is still how adsorptive scavenging and solubilisation of particulate iron influence the steady state concentration of DFe.

Dust deposition plays a double role in regulating iron concentration in seawater. Besides the dissolution of iron from dust particles, dust particles provide surfaces for adsorption. They are also involved in particle aggregation and act as ballast for sinking organic material (e.g., Armstrong et al., 2002; Ternon et al., 2010), changing the settling velocity of iron adsorbed on particle surfaces. The net effect of dust deposition on DFe in surface waters is therefore influenced by various factors: while the input flux of iron is mainly determined by the Fe solubility and content in dust particles, the loss flux depends on the size and composition of sinking particles, rates of particle aggregation as well as of the Fe adsorption and desorption at particle surfaces. Dust deposition does not only supply Fe but also other nutrients like P (Baker et al., 2003; Ridame and Guieu, 2002). Phytoplankton growth induced by this nutrient supply changes the strength of biological Fe cycling and thus DFe concentration in surface waters.

To better understand ecosystem responses to dust addition, a DUst experiment in a low Nutrient low chlorophyll Ecosystem (DUNE) was carried out in the preservation area of Scandola (Corsica Island) in the summer of 2008 (Guieu et al., 2010a). One of the focuses of this project is to investigate the role of dust particles in Fe cycling in a high temporal and spatial resolution. Processed dust particles were added into mesocosms. Within first hours after the dust addition, a rapid decrease of DFe concentration inside the mesocosms was observed and this lower concentration remained until the end of the experiment (8 days after the dust addition). This indicates a predominant effect of adsorptive scavenging compared to Fe dissolution from dust particles (Wagener et al., 2010).

In this study, we simulate the DUNE experiment by a one-dimensional model of the Fe cycle. Fe speciation and particle dynamics are described based on prior model studies by Weber et al. (2007) and Ye et al. (2009), and adapted for the DUNE experiment.

We aim to explain mechanisms controlling the observed decrease of DFe following dust addition by:

1. discussing how the dissolution of iron from dust particles regulates the iron input;
2. estimating the adsorption rate constant needed for reproducing the observed DFe concentrations;
3. testing hypotheses on why the dust addition in the DUNE experiment was a net sink of DFe.

2 Experiment description

In June 2008, six mesocosms were deployed in the preservation area of Scandola near Corsica (42.37° N, 8.55° E). The mesocosms were cylindrical with a diameter of 2.3 m and a volume of 52 m^3, enclosing a upper water layer of 15 m. Details of the mesocosm construction have been described in Guieu et al. (2010a). After deployment and closing of the mesocosms, the initial conditions of the experiment were measured. Dust particles were collected in a dust source area in southern Tunisia and processed by physico-chemical treatment in laboratory to mimic the aging of dust particles by cloud cycling. These particles contain 4.12 ± 0.39% Al and 2.31 ± 0.04% Fe by weight (Guieu et al., 2010a). Three of the mesocosms (DUST-meso) each had 41.5 g of the processed dust particles added with a trace metal clean water spray to simulate a wet dust deposition of 10 g m^{-2}. The addition lasted for 60 min. No dust was added to the other three mesocosms used as control (CONTROL-meso). Sampling was performed daily for 3 depths (0, 5 and 10 m) during 8 days to determine particulate aluminium (PAl), dissolved (DFe) and particulate iron (PFe), and chlorophyll concentration (Chl). Every 48 h, sediment traps at the bottom of the mesocosms were recovered and replaced to determine the fluxes of total mass, inorganic and organic carbon, nitrogen, total iron and aluminium.

The DUNE experiment site is representative of typical oligotrophic conditions of the open ocean (Guieu et al., 2010a). Concentrations of dissolved inorganic phosphorus (DIP) are in the range of observations in the summer mixed layer in the open Mediterranean Sea (Pulido-Villena et al., 2010) where P-limitation of biological activity has been extensively reported (e.g., Thingstad et al., 1998). A macronutrient-depleted but Fe-replete site is optimal for investigating the physico-chemical processes controlling Fe speciation and removal, because the biological uptake and remineralisation of iron only play a minor role in the Fe cycling. Thanks to the original design of the clean mesocosms deployed during the experiment, this experiment represented a unique opportunity to study and quantify the abiotic processes of dissolution and adsorption of DFe occurring from/at mineral particle surfaces.

3 Model description

The DUNE experiment is simulated in a one-dimensional model representing the upper 15 m of the water column. The water column is divided into 30 layers with a uniform water layer thickness of 0.5 m. The model consists of an ecosystem model coupled to a physical model (Sects. 3.1–3.4). Data measured in the mesocosms before dust addition are used to initialise the model. The temporal evolution of state variables is calculated at a time step of 10 min. The model is spun up for 48 h and further integrated for the entire experiment period from 11 to 19 June 2008. Dust particles are added in the beginning of the integration as a surface flux of 1.4×10^{-6} kg m^{-2} s^{-1} lasting for 60 min, corresponding to a total addition of 41.5 g dust particles.

3.1 Physical model

The physical part of the model is the General Ocean Turbulence Model (GOTM, Umlauf and Burchard, 2005, www.gotm.net) which provides the vertical mixing and advection for a given forcing by wind, heat and freshwater fluxes at the surface. Forcing data

for the DUNE site are 6-hourly fluxes derived from the Japan Meteorological Agency Climate Data Assimilation System (JCDAS) (Onogi et al., 2007). A k-ϵ turbulence closure is used to calculate turbulence kinetic energy. Vertical advection and sinking of biogeochemical quantities are calculated using a third-order scheme with flux limiter (Burchard and Umlauf, 2005).

3.2 Ecosystem model

The focus of this study are the processes controlling DFe change during the dust addition experiment, not the impact of the additional iron on diverse biological activities. Therefore, the ecosystem responses to dust addition are described in a very simple NPZD-type model. There are two nutrient pools – dissolved inorganic phosphorus (DIP) and dissolved iron (DFe), a phytoplankton (PHY), a zooplankton (ZOO) and detritus (DET) which is divided into two size classes (Fig. 1, for the classification of detritus see Table 3). The model is based on P, because the low surface DIP concentration at the DUNE site (Pulido-Villena et al., 2010) suggests that primary production there is P-limited rather than N-limited. We introduced a variable Fe:P ratio for each component, so that the effect of P and Fe added with dust particles on the ecosystem can be simulated separately. The flux description of the model and the parameter values are mostly taken from Ye et al. (2009), and the half saturation constant of P uptake (K_p) is modified from Sohm and Capone (2006), reproducing the observed temporal evolution of DIP and Chl at the DUNE site. The surface input of P by dust addition is calculated with a P content in dust particles of 0.05% (Guieu et al., 2010a) and a solubility of 35% (Pulido-Villena et al., 2010).

3.3 Particle dynamics

The size distribution of dust particles used in the experiment can be described with three log-normal modes of roughly the same total volume (~33%). Particles having the median volume of each mode are about 1.6, 6.2 and 12 µm, respectively (Guieu et al.,

2010a). In order to keep a certain model simplicity and at the same time consider the different behavior of particle size classes in surface adsorption and sinking, we modelled two size classes of dust particles with a mean size of 2 and 10 µm (P_d and P_s), representing the smallest mode and the two larger modes together. 33% of the dust particles is added as surface flux into P_d during the dust addition, and 67% into P_s.

The mean settling velocity of dust particles, calculated from the temporal variations of measured PAI in the upper 5 m, is much higher than that estimated from Stoke's law using the size distribution of the added dust particles (Guieu et al., 2010b). This strongly suggests the importance of particle aggregation. We therefore took into account particle aggregation in our model and introduced another particle class (P_l) for large aggregates which have a mean size of 50 µm.

Sinking organic matter in the model has two classes with comparable size to P_s and P_l, respectively: D_s representing small detritus and the organic part of small aggregates and D_l representing large detritus and the organic part of large aggregates. Table 3 gives an overview of modelled particle classes, their size and settling velocities estimated from Stoke's law.

3.4 Chemical model

Concentration of DFe and PFe were measured in the water column of the mesocosms and PFe flux was determined in the sediment traps (Wagener et al., 2010). We simplified the Fe speciation model by Ye et al. (2009) based on these two measured forms of Fe to avoid unnecessary speculation on the various Fe species which can not be compared to observations. There are four main Fe species in this model: the dissolvable fraction of iron in dust particles (Fe_{dust}), iron inside the organic matter Fe_{org}, dissolved iron (DFe), including soluble and colloidal iron, and iron adsorbed on sinking particles (PFe_{sorp}) (Fig. 2). PFe_{sorp} differs from the measured PFe which includes not only iron adsorbed on particles but also iron inside sinking particles. Three subclasses of PFe_{sorp} (PFe_d, PFe_s and PFe_l) are considered in the model due to adsorption on

particles of different size classes. Iron adsorbed on the surface of organic sinking particles (D_s and D_l) is also involved in PFe_s and PFe_l. Four processes supply DFe (Fig. 2): (1) dissolution from added dust particles, (2) iron release by remineralisation of organic matter, (3) desorption and (4) photoreduction of PFe_{sorp}. Biological uptake and adsorption onto sinking particles remove iron from the dissolved pool. Parameter values are listed in Table 1.

We calculated the input of iron by dust addition with an Fe content in the added dust particles of 2.31% (Guieu et al., 2010a) and a solubility of 0.1% (Wagener et al., 2010). In lab studies, increasing leaching time results in increases in percent Fe dissolution (Bonnet and Guieu, 2004) indicating that Fe dissolution is a multi-timescale process. Wagener et al. (2008) studied the dissolution kinetics of Fe from dust particles and supposed one fast and one slowly dissolvable iron fraction. We introduced a dissolution timescale of 3 days into our model which represents the fast dissolution of iron. Surface iron flux by dust addition is divided into two dissolvable iron pools which are proportional to the two size-fractions of dust particles (P_d and P_s). From these two pools, iron is released to the DFe pool with a time constant of 3 days. The difference to a run with instantaneous dissolution of iron is discussed in Sect. 4.3.3.

The adsorption rate of iron onto particles is proportional to particle surface. Since in lab studies, the adsorption rate of iron is often determined in relationship to particle mass, we scaled the mass-related adsorption rate constants with the surface:volume ratios of the modelled particle size classes, assuming that all the particles are spherical.

The observed DFe decrease of $\sim 1\,\mu mol\,m^{-3}$ immediately following the dust addition indicates strong removal processes of DFe by sinking particles. The adsorption of DFe onto particles is described in the model as a function of DFe and particle concentration. Because DFe in the model is the sum of colloidal and soluble iron, both adsorption of colloidal and soluble iron are taken into account in this way. Different adsorption rate constants were tested in a sensitivity study for reproducing the observed DFe concentrations (Sect. 4.3.4).

4 Results

To provide realistic physical conditions for biological and chemical processes, we compared at first modelled temperature and mixing to measurements during DUNE. Model runs without and with dust surface flux simulate the average situation in CONTROL-meso and DUST-meso, respectively.

4.1 Physical conditions

During the DUNE experiment, seawater temperatures ranged from 18–21.5 °C. The vertical temperature gradient was highest on the day before the dust addition. The diurnal variability of temperature was relatively weak and the water was well mixed during the night. Towards the end of the experiment, a stronger temperature gradient was built up again (Fig. 3). Using the meteorological forcing data from JCDAS (Sect. 3.1), the modelled temperature ranges from 18.5–22.5 °C (Fig. 3). A similar temporal evolution of temperature to the observation is found in the model: in the beginning of the experiment, high surface temperature and larger vertical gradient cause stronger stratification. The gradient declines with cooling of surface waters within the first 3 days. From 14 June on, water is mixed completely in the upper 15 m. Surface temperature increases during the last 2 days of the experiment and a clear vertical gradient is built up again. Yet, the modelled vertical temperature gradient is clearly higher than that observed, particularly during the first days of the experiment. This produces a stronger stratification. One possible explanation could be that the wind forcing is too weak, because the reanalysis data lacks small-scale effects. The experimental site is relatively close to land and one would expect a strong daily cycle of winds driven by the different heat capacities of land and sea surface. Increasing the wind speed in the forcing data with a factor of two in a test run (not shown), modelled stratification becomes closer to the observations. Comparing the forcing data to local observations of wind strength could be very helpful for improving the model-data agreement.

4.2 Simulation of CONTROL-meso

4.2.1 Chlorophyll

Measured Chl in CONTROL-meso varied between 0.08–0.15 mg m^{-3}. We calculated Chl from modelled phytoplankton phosphorus by using a mean Chl:C weight ratio of 1:60 for typical phytoplankton and the molar Redfield C:P ratio of 106:1. The calculated Chl varies from 0.09–0.13 mg m^{-3} (Fig. 4), in the range of the observations.

4.2.2 Inorganic particles

Particulate aluminium (PAl) has been measured at 5 m depth in CONTROL-meso. We calculated concentrations of inorganic particles using an average Al content of 7.7% for continental crust (Wedepohl, 1995), assuming that inorganic particles in CONTROL-meso were from lithogenic sources. Concentrations of inorganic particles are in the order of 10^{-8} kg m^{-3}, decreasing slowly with time. Similarly, we calculated exported particle mass from exported PAl which was measured every 2 days in the sediment traps at the bottom of the mesocosms. Fluxes of particle export (mg m^{-2} d^{-1}) through the area of the mesocosms (4.15 m^2) are averaged for every 2 days. The particle export shows a relatively high variability both within and between the mesocosms (from 2–25 mg m^{-2} d^{-1}) and different temporal patterns in the three mesocosms (Table 4). The mean export of CONTROL-meso varies with time from 4–14 mg m^{-2} d^{-1}.

The observed particle concentrations decreased slowly with time, indicating that the main part of sinking particles in CONTROL-meso is very small. We thus used the observed concentration at 5 m as the initial concentration of the smallest particle class (P_d) throughout the water column. With the assumption of a settling velocity of 0.2 m d^{-1} for P_d (Table 3), the model-produced concentration of total inorganic particles at 5 m is in the same order as the measured data. Particle export flux averaged over 2 days varies between 7–12 mg m^{-2} d^{-1} (Table 4), in good agreement with the observed mean.

4.2.3 Iron

Observed DFe was relatively constant around 2.5 µmol m^{-3} with a decrease to 2 µmol m^{-3} in the upper 5 m and increase to 3.5 µmol m^{-3} at 10 m depth (Fig. 5). The iron adsorption rate constants are estimated in a sensitivity study (Sect. 4.3.4), mainly based on the change of DFe concentrations in DUST-meso. In CONTROL-meso, the different adsorption rate constants tested in the sensitivity study do not influence DFe concentration to a significant extent, because the concentration of sinking particles is low. DFe in the model decreases with time from 2.5 to 2.3 µmol m^{-3} caused by adsorptive removal. Although DFe shows a smaller variability than in the observations, its concentrations represent well the average condition in CONTROL–meso. Modelled export of total PFe which includes iron inside sinking particles and iron adsorbed on particles, varies between 0.2–0.3 mg m^{-2} d^{-1} which is close to the mean of the three mesocosms (Table 5).

4.3 Simulation of DUST-meso

4.3.1 Phosphorus and chlorophyll evolution

Six hours after the dust addition, surface DIP in all three DUST-meso increased from 4 ± 1 to 17 ± 4 µmol m^{-3}. No increase was observed at 5 and 10 m depth (Pulido-Villena et al., 2010). The modelled DIP concentration is about 3–5 µmol m^{-3} before dust addition and is elevated to ~50 µmol m^{-3} at surface immediately after DUST addition (Fig. 6). After that, DIP falls back to the initial concentration within 72 h caused by strong phytoplankton uptake. The modelled surface DIP at 6 h after dust addition is about 42 µmol m^{-3}, more than twice as high as the observations. This is caused by the modelled stronger stratification in the first days of the experiment, preventing mixing down of DIP supplied by dust addition (Sect. 4.1). The decline of DIP after its maximum is therefore also a little slower in the model than observed.

Before the dust addition at 10:00 on 11 June, modelled Chl varies from 0.12 at the surface to 0.09 mg m^{-3} at 15 m depth with a clear diurnal pattern (Fig. 7). Immediately after the dust addition, Chl concentration starts to increase and reaches a maximum of 0.2 mg m^{-3} on the last day of the experiment. The growth limitation by P in the model is described with a Michaelis-Menten term (Eq. A7). This term increases from 0.2 before to 0.9 shortly after the dust addition and drops back below 0.6 within 24 h. The limitation by Fe is described with the internal Fe:P ratio (Eq. A6). In contrast to the P-limitation term, the Fe-limitation term falls with the dust addition from 0.93 to 0.88 and remains at this level until the end of the experiment. As the actual growth rate is determined by the smaller of these two terms and the P-limitation term is almost always smaller than that of Fe, the Chl increase in the model is stimulated by DIP input, as suggested by Pulido-Villena et al. (2010).

The temporal evolution of Chl is also consistent with the observation of a doubling at the end of the experiment (Guieu et al., 2010b; Guieu, 2009). However, the observed Chl concentrations reached 0.2 mg m^{-3} already 48 h after the addition and remained at this level until the end of the experiment. This suggests that a faster growth was induced by DIP addition and that some loss factors, e.g. grazing, balanced the growth of phytoplankton during the last days of the experiment. The modelled stronger stratification in the beginning of the experiment might delay the DIP supply for the entire water column and thus delay the increase of phytoplankton. A better reproduction of the observed Chl could be obtained by changing biological parameters in the model, if direct observations of phytoplankton community composition, grazers or phytoplankton mortality are available. For the focus of this study – the Fe cycling, this biological model is sufficient. Iron in organic matter is only a negligible fraction of the entire budget. Before the dust addition, the organic Fe fraction in the water column is about 0.1% (the insoluble part of iron inside the dust particles is not considered). Immediately after the addition, it falls to 0.05% and increases to the end of the experiment to 0.2%. Moreover, the main removal process of DFe is particle adsorption and biological uptake is 2–4 orders of magnitudes lower than the adsorptive loss.

4.3.2 Particle dynamics

In DUST-meso, particle concentration has been measured at 0, 5 and 10 m depth. The model reproduces the particle concentration at 0 m well with a sharp increase to a maximum immediately after addition and a quick decrease within the first 6 h (Fig. 8). The decrease slows down with time, because sinking particles become more and more dominated by the fine dust particles (P_d).

At 5 m depth, modelled particle concentration shows two peaks around 10^{-3} kg m^{-3}: a first one at 3 h after addition and a second one after 24 h. The first peak is a result of P_s aggregation in surface water and the subsequent sinking of large aggregates. The second peak is due to sinking of P_s itself which takes one day from the surface to 5 m depth. Particle concentration decreases slowly after that, because P_d also dominates at this depth after P_s sinks out. The first peak is in good agreement with the observations, while the second one is not found in the measurements. This might be due to the limited time resolution in the data.

At 10 m depth, a first peak occurs later than the one at 5 m because of longer sinking. After that, particle concentration increases slowly for about one day which is mainly caused by sinking of P_s from surface waters. In the last days of the experiment, the particle concentration is low and decreases slowly with time, because fine dust particles dominate and sink slowly. Particle concentration at 10 m depth is basically in the same magnitude as measured. However, like at the other depths above, modelled particle concentration from the 3rd day to the end of the experiment is 2–3 fold as high as the average of the triplicate mesocosms. Two reasons could explain the difference between model and measurement: (1) water layer with high particle concentration could be missed due to the limitation of spatial resolution by sampling (Wagener et al., 2010); and (2) particles might have adhered to mesocosms (see below).

Like in the comparison with control conditions, we also calculated the mean export of inorganic particles for every 2 days (Table 6). The modelled export in the first 24 h after the dust addition is obviously higher than the measured mean, whereas the later

export fluxes are close to the observations. The high export within the first 24 h in the model is caused by the aggregation of P_s which comes into surface water by addition in a very high concentration. This must have happened, since otherwise, particles could not be exported out of the upper 10 m within the first 48 h as observed by Wagener et al. (2010).

Several factors could lead to the lower particle export in the measurement. Guieu et al. (2010a) mentioned that a fraction of particles could have been lost during exchange of the traps or adhered to the conical bottom of mesocosms. The sticking of particles on the mesocosm walls and in the conical part of the mesocosms could play a role for both reduced concentration in the water column and lower sedimentation. The shape of the mesocosm bottom with reducing diameter may have enlarged the sticking effect. Because of the small surface:volume ratio of the mesocosms, the adsorption on mesocosm walls could be negligible (Wagener et al., 2010). A similar difference between model and observation is also found in concentration and export of PFe (Sect. 4.3.5). Only about half of the added iron has been recovered by measuring iron concentration in the water column and exported iron in sediment traps (Table 8). The missing part in the mass balance indicates a higher concentration in the water column and/or larger sedimentation. Therefore, we did not change model parameters to fit the data.

4.3.3 Sensitivity study with respect to iron dissolution timescale

A dissolution timescale of 3 days is used in our standard model setup, corresponding to the stage of fast dissolution in Wagener et al. (2008). Surface DFe drops rapidly in the first hours, adsorbing onto large particles in high abundance (Fig. 9). After that, it increases slightly and remains at $\sim 2\,\mu mol\,m^{-3}$ for about 2 days. This indicates a balance between iron dissolution and slower removal by small particles. The mixing event on early 14 June leads to a higher concentration of DFe in the surface water. Later on, DFe decreases linearly due to further removal by small particles, while no more iron is dissolved from dust particles. Comparing this to a run with instantaneous

dissolution of iron from dust particles, we found a huge increase of surface DFe up to $\sim 7.5\,\mu mol\,m^{-3}$ in the first hours with instantaneous dissolution, which clearly disagrees with the observation.

4.3.4 Sensitivity study with respect to adsorption rate

Particle adsorption is described as a function of DFe concentration and total particle concentration. The measured rate constants for the adsorption of colloidal iron are hundreds of times higher than that of soluble ferric iron (Wen et al., 1997). In the sensitivity study with respect to the adsorption rate constant k_{sorp}, we started with the rate constant for direct scavenging of soluble ferric iron from Ye et al. (2009) ($2.5\,m^3\,kg^{-1}\,d^{-1}$) and then increased k_{sorp} 20-, 40-, 60- and 80-fold. The model run with the lowest k_{sorp} shows a slight increase of DFe after the dust addition (Fig. 10), indicating that a much stronger scavenging is needed to reduce DFe concentration to the observed level by the given particle concentration. Comparing all the model runs, we found that higher adsorption rates lead to faster decrease of DFe after dust addition and lower DFe concentration at the end of the experiment. The observed DFe decrease of $\sim 1\,\mu mol\,m^{-3}$ can be reproduced best by an enlargement of k_{sorp} of 60 times over the adsorption of soluble iron from (Ye et al., 2009).

The estimated adsorption rate constants in this sensitivity study (30, 150 and $750\,m^3\,kg^{-1}\,d^{-1}$ for different particle classes) are higher than the estimate for adsorption of soluble iron by Nyffeler et al. (1984) ($25\,m^3\,kg^{-1}\,d^{-1}$) using sediment particles. Although different surface properties of particles can influence metal adsorption, we do not think that it can explain the high rate constant needed in our model. Compared to the rate of colloidal aggregation reported by Wen et al. (1997) ($1.2-51\times10^{-2}\,h^{-1}$ with a particle concentration of $10\,mg\,L^{-1}$ resulting in $240–1220\,m^3\,kg^{-1}\,d^{-1}$), our estimates for the 2 smaller particle classes are lower and the one for large aggregates is in the range of Wen's estimates. This indicates strongly that the model description of particle adsorption represents a combined effect of direct scavenging and colloidal aggregation

and thus the rate estimate should be regarded as a gross constant of these two processes together. The significant role of colloidal iron in the Fe cycle is in agreement with recent findings that atmospheric iron mainly increases the colloidal pool of iron in seawater (Wu et al., 2001) and that the colloidal fraction accounts for a substantial portion of DFe throughout the water column (Cullen et al., 2006; Bergquist et al., 2007). This fraction of DFe should be considered explicitly in modelling iron removal, if direct observations of colloidal iron during dust fertilisation experiments are available.

4.3.5 Iron budget

The model reproduces the rapid decrease of DFe after the dust addition (Fig. 11). DFe in surface water is elevated on 14 June because the lower water layer with higher DFe concentration is mixed up with surface water. The pattern of PFe_{sorp} shows a different trend: it increases rapidly after the dust addition and remains relatively high until the end of the experiment (Fig. 12). Linked to the change of particle concentrations with time (Fig. 8), this results in a low iron loading per particle immediately after dust addition (down to 10^{-6} mg Fe per mg particle) and a high iron loading per particle at the end of the experiment (up to 10^{-3} mg Fe per mg particle).

To compare with the iron budget estimated from measured data, we calculated total DFe and total particulate iron within the upper 15 m as well as the export of total particulate iron at 15 m from 0 to 24, 120 and 168 h after the dust addition. Table 8 compares the measured distribution of Fe species in two mesocosms to the modelled one. Modelled DFe stock agrees well with the measurements, whereas PFe stock and export are both higher than the data (see also Table 7).

PFe stock is 2–5 times higher in the model from 24 h after dust addition to the end of the experiment. Modelled PFe export is particularly high in the first 24 h after the dust addition, whereas measured PFe is mainly exported between 24 and 120 h (Table 7). The same reasons for the discrepancy between model and data of inorganic particles should be responsible for that of PFe (see Sect. 4.3.2). The delayed high values in the measurement are also found in the export of particles (Table 6). This could be

caused by the conical shape of mesocosm bottom which may have slowed up the sedimentation.

The sediment trap design and the uncertainties by sampling might explain why the recovery of added iron in the two mesocosms is only 59 and 53%, respectively (Guieu et al., 2010a). It would be helpful for further adjustment of our model to have measurements in a better spatial resolution and estimates of PFe loss through exchanging traps or adhering to mesocosms.

4.3.6 Role of dust deposition in iron replete waters

The significant decrease of DFe induced by dust addition is contradicting the positive correlation between dust deposition and DFe concentration which is widely established in direct observations and model studies. How is it possible to interpret the observed phenomenon in DUNE and observations of elevated DFe concentration by episodic dust events in an integrative way?

Wagener et al. (2010) pointed out that the initial iron concentration before the dust addition was at the higher end of former measurements in that region. A Saharan dust deposition two weeks before the DUNE experiment and the rain events days before are supposed to be responsible for the high DFe initial concentration. Since particle surface adsorption not only depends on the amount of added particles but also on the ambient DFe in the medium before deposition, we hypothesise that the net impact of dust deposition on DFe ambient concentration depends in part on initial DFe concentration in seawater.

To test this hypothesis, several model runs were conducted with DFe initial concentrations varying from 0–2 µmol m^{-3}. The difference of surface DFe between a run with dust addition and a run without is illustrated in Fig. 13 for each initial DFe concentration, representing the net influence of dust addition on DFe concentration. A transition is found between 0.25 and 0.5 µmol m^{-3}: dust addition increases DFe concentration in seawater in the runs with initial DFe concentrations up to 0.25 µmol m^{-3}, whereas in the runs with higher initial DFe concentrations, dust addition lowers DFe concentration.

In the case of DUNE experiment, we assume that no excess ligands existed at the beginning of the experiment based on the batch dissolution experiments performed in parallel to the mesocosm experiments (Wagener et al., 2010). Therefore, one may understand the effect of dust addition by only considering the balance between Fe release and adsorption in the first moment after the addition.

The dissolution is given by Eq. (1):

$$F_{\mathrm{diss}} = \frac{P_{\mathrm{tot}}\, r_{\mathrm{Fe}}\, r_{\mathrm{sol}}\, k_{\mathrm{rel}}}{M_{\mathrm{W}}} \tag{1}$$

where P_{tot} ($\mathrm{kg\,m^{-3}}$) is the concentration of total dust particles, r_{Fe} (−) the Fe fraction in dust, r_{sol} (−) the Fe solubility, k_{rel} ($\mathrm{d^{-1}}$) the rate of Fe release from dust particles (the reciprocal of the dissolution timescale), and M_{W} ($\mathrm{g\,mol^{-1}}$) the molar weight of Fe.

The adsorption is calculated by Eq. (2):

$$F_{\mathrm{sorp}} = P_{\mathrm{tot}}\, k_{\mathrm{sorp}}\, R_{\mathrm{surf}}\, \mathrm{DFe}\, C \tag{2}$$

where k_{sorp} ($\mathrm{m^3\,kg^{-1}\,d^{-1}}$) is the mass-related adsorption rate and R_{surf} (−) is the surface:volume ratio of the given particle size class relative to that of the particles in the middle size (P_{s}). C ($\mathrm{nmol\,g\,mol^{-1}\,kg^{-1}}$) is a factor for unit conversion.

The critical concentration of initial DFe ($\mathrm{DFe^{crit}}$) can be defined, assuming a balance between Eqs. (1) and (2):

$$\mathrm{DFe^{crit}} = \frac{r_{\mathrm{Fe}}\, r_{\mathrm{sol}}\, k_{\mathrm{rel}}}{k_{\mathrm{sorp}}\, R_{\mathrm{surf}}\, M_{\mathrm{W}}\, C} \tag{3}$$

where $\mathrm{DFe^{crit}}$ depends on the types of dust particles and on environmental conditions.

For the DUNE experiment, we calculated R_{surf} from the surface:volume ratios and fractions of the two size classes of dust particles in the model and estimated a critical DFe concentration of 0.35 µmol $\mathrm{m^{-3}}$.

In Eq. (3), we do not consider organic complexation of Fe which prevents DFe from scavenging removal. Therefore, this estimate represents a critical concentration of the

reactive fraction of DFe – Fe′, rather than of the total DFe ($\mathrm{DFe_{tot}}$). In a region with excess ligands, added iron should be kept longer in the dissolved pool even for higher initial DFe concentration. Since organic complexation is much faster than particle adsorption (Rose and Waite, 2003a), the critical total DFe concentration ($\mathrm{DFe_{tot}^{crit}}$) can be calculated assuming an equilibrium between Fe′ and organic complexed iron (FeL). The conditional stability constant K^* with respect to Fe′ is described by Eq. (4):

$$K^* = \frac{\mathrm{FeL}}{L'\,\mathrm{Fe'}} \tag{4}$$

L' is excess ligand and can be calculated from total ligand (L_{tot}):

$$L' = L_{\mathrm{tot}} - \mathrm{FeL} \tag{5}$$

With an additional equation of $\mathrm{DFe_{tot}}$ (Eq. 6), the critical total DFe concentration ($\mathrm{DFe_{tot}^{crit}}$) is described as a function of Fe′ and L_{tot} (Eq. 7) where Fe′ can be calculated as $\mathrm{DFe^{crit}}$ by Eq. (3):

$$\mathrm{DFe_{tot}} = \mathrm{Fe'} + \mathrm{FeL} \tag{6}$$

$$\mathrm{DFe_{tot}^{crit}} = \mathrm{Fe'}\left(1 + \frac{K^* L_{\mathrm{tot}}}{1 + K^*\,\mathrm{Fe'}}\right) = \mathrm{DFe^{crit}}\left(1 + \frac{K^* L_{\mathrm{tot}}}{1 + K^*\,\mathrm{DFe^{crit}}}\right) \tag{7}$$

This equation results in a higher critical total DFe concentration in a system with excess ligands than without. The difference between these two depends on total ligands and Fe′ concentration. With this concept, the net impact of dust deposition on seawater DFe concentration at a short timescale could be predicted, helping assessing the impact of dust deposition on biogeochemical processes. To prove the applicability of this concept, more local observations of DFe change after dust deposition are needed and the role of excess ligands must be more carefully examined. Because of the complex feedback mechanisms of an ecosystem to dust deposition (Wagener et al., 2010), this

concept might be only applicable for explaining the short-term change of DFe and immediate biological responses to dust events. However, it clearly points out that natural dust deposition could have different effects on DFe surface concentration due to different initial conditions. This might be a possibility to explain the discrepancies between observed biological responses to natural dust deposition (Boyd et al., 2010).

5 Conclusions

A significant decrease of dissolved iron concentration has been observed after dust addition in a LNLC system. To simulate the experiment and study the mechanisms controlling DFe change, processes such as dissolution, scavenging, biological uptake, photoreduction and redissolution of particulate iron are described in a one-dimensional model of the Fe cycle coupled with a simple NPZD-type ecosystem model based on phosphorus. Different size classes of sinking particles and particle aggregation have been taken into account.

A good agreement of modelled and measured particle sedimentation is found under control condition. This provides evidence that the model description and parameter choice of particle aggregation and sinking are applicable for explaining particle dynamics during the DUNE experiment. In the mesocosms with dust addition, about 50% of the added iron was recovered in the measurements which might be caused by loss during exchange of sediment traps and/or by adhering to the conical part of mesocosms. Modelled concentration and export of particles and particulate iron are significantly higher than measured, covering the missing part in the mass balance of iron.

The DFe decrease is well reproduced with a dissolution timescale of 3 days and high adsorption rate constants of 30, 150 and 750 $m^3\,kg^{-1}\,d^{-1}$ for different particle size classes. These adsorption rate constants are generally higher than measured adsorption rate constants for soluble iron and lower than those for colloidal iron. This suggests that the removal pathway of dissolved iron via colloidal aggregation should be considered besides the direct scavenging of soluble iron to explain the rapid decrease

of DFe. Direct measurements on colloidal iron during future dust addition experiments would help to improve our understanding of iron loss kinetics.

The initial DFe concentration before dust deposition has been shown to be crucial for determining whether dust deposition is a net source or sink of dissolved iron. A critical DFe concentration, above which dust deposition acts as a net sink of iron, rather than a source, can be estimated from the balance between abiotic processes of iron release from and iron loss to particles. This critical DFe concentration, however, also depends on characteristics of the dust particles (e.g. iron solubility, surface:volume ratio) and seawater (e.g. iron binding ligand concentration). It remains to be seen whether the concept of a critical DFe concentration may help in explaining observed reactions of marine ecosystems to dust deposition.

Appendix A

Model equations

The rate of change of biogeochemical variables is described by a biogeochemical and a physical part:

$$\frac{\partial}{\partial t}X = \mathrm{BIO} + M(X,z) \tag{A1}$$

Advection and mixing are taken into account in the physical part $M(X,z)$. M stands for the advection and mixing operator and X is the mixed compound. The change rate of the biogeochemical part is described by corresponding sources minus sinks.

A1 Equations for the biological model

The change of the biological variables DIP, PHY, ZOO, D_s and D_l (in mmol m^{-3}) is described by:

$$\frac{\partial}{\partial t}\mathrm{DIP} = \gamma_d f_T (D_s + D_l) + \gamma_{zb} f_T \mathrm{ZOO} + \gamma_p f_T \mathrm{PHY} - \mu \mathrm{PHY} + M(\mathrm{DIP}, z) \quad (A2)$$

$$\frac{\partial}{\partial t}\mathrm{PHY} = \left(\mu - \gamma_p f_T\right)\mathrm{PHY} - f_G \mathrm{ZOO} - \gamma_{p^2} \mathrm{PHY}^2 + M(\mathrm{PHY}, z) \quad (A3)$$

μ is the growth rate of phytoplankton regarding light, temperature and nutrient limitation. The light limited growth rate is described by:

$$f_l = \frac{\mu_{max}\, \alpha\, I(z)}{\left(\mu_{max}{}^2 + (\alpha\, I(z))^2\right)^{0.5}} \quad (A4)$$

where $I(z)$ is the photosynthetically active radiation in the given vertical layer z. Both growth and remineralisation rate are related to temperature by:

$$f_T = 0.9\, C_{ref}{}^T \quad (A5)$$

which represents a temperature dependence for $Q10 = 2$. The growth limitation by iron depends on the internal Fe:P-quota Q_{Fe} according to:

$$f_{Fe} = \frac{Q_{Fe} - Q_{Fe}^{min}}{Q_{Fe}} \quad (A6)$$

where Q_{Fe}^{min} is a minimal cellular Fe quota. The actual growth rate is then the product of the light and temperature dependent maximal growth rate with the smaller of f_{Fe} and f_P, a Michaelis-Menten term in dissolved inorganic phosphorus:

$$f_P = \frac{\mathrm{DIP}}{\mathrm{DIP} + K_P} \quad (A7)$$

where K_P is a half-saturation constant for DIP uptake.

ZOO change rate is determined by the rate of grazing, excretion and mortality.

$$\frac{\partial}{\partial t}\mathrm{ZOO} = \gamma_{za} f_G \mathrm{ZOO} - \gamma_{zb} f_T \mathrm{ZOO} - \gamma_{z^2} \mathrm{ZOO}^2 + M(\mathrm{ZOO}, z) \quad (A8)$$

The grazing function f_G depends on the maximal grazing rate g, the prey capture rate ϵ and phytoplankton concentration:

$$f_G = \frac{g\, \epsilon\, \mathrm{PHY}^2}{g + \epsilon\, \mathrm{PHY}^2} \quad (A9)$$

The loss of zooplankton by its mortality ($\gamma_{z^2}\, \mathrm{ZOO}^2$) is considered as a source of organic aggregates.

Detritus is divided into two size classes: D_s for small and D_l for large detritus. We use the same symbols for organic part of small aggregates and large aggregates, respectively, because we treat them same as the detritus in particle aggregation, sinking and remineralisation.

$$\frac{\partial}{\partial t}D_s = \gamma_{p^2} \mathrm{PHY}^2 + (1 - \gamma_{za}) f_G \mathrm{ZOO} - \gamma_d f_T D_s - k_{coag2} D_s (D_s r_{m:P} + P_s) - k_{coag3} D_s (D_l r_{m:P} + P_l) - w_s \frac{\partial D_s}{\partial z} + M(D_s, z) \quad (A10)$$

$$\frac{\partial}{\partial t}D_l = \gamma_{z^2} \mathrm{ZOO}^2 - \gamma_d f_T D_l + k_{coag2} D_s (D_s r_{m:P} + P_s) + k_{coag3} D_s (D_l r_{m:P} + P_l) - w_l \frac{\partial D_l}{\partial z} + M(D_l, z) \quad (A11)$$

A2 Equations for inorganic sinking particles

Inorganic sinking particles are small dust particles P_d, large dust particles and the inorganic fraction of small aggregates P_s and the inorganic fraction of large aggregates P_l (all in kg m^{-3}). Coagulation is described by a coagulation constant k_{coag} times the product of concentration of the two particle classes involved in the coagulation.

$$\frac{\partial}{\partial t}P_d = F^d_{surf} - k_{coag1}\,P_d\,(D_s\,r_{m:P} + P_s) - k_{coag4}\,P_d\,(D_l\,r_{m:P} + P_l) - w_d\,\frac{\partial P_d}{\partial z} + M(P_d, z) \quad \text{(A12)}$$

$$\frac{\partial}{\partial t}P_s = F^s_{surf} + k_{coag1}\,P_d\,(D_s\,r_{m:P} + P_s) - k_{coag3}\,P_s\,(D_l\,r_{m:P} + P_l) - k_{coag2}\,P_s\,(D_s\,r_{m:P} + P_s) - w_s\,\frac{\partial P_s}{\partial z} + M(P_s, z) \quad \text{(A13)}$$

$$\frac{\partial}{\partial t}P_l = k_{coag4}\,P_d\,(D_l\,r_{m:P} + P_l) + k_{coag3}\,P_s\,(D_l\,r_{m:P} + P_l) + k_{coag2}\,P_s\,(D_s\,r_{m:P} + P_s) - w_l\,\frac{\partial P_l}{\partial z} + M(P_l, z) \quad \text{(A14)}$$

F^d_{surf} and F^s_{surf} are the surface fluxes of dust particles where 33% of the total flux is put into P_d and 67% into P_s. $r_{m:P}$ is a factor converting biomass from mmol P m^{-3} into kg m^{-3}.

A3 Equations for the iron cycle

DFe change is described by:

$$\frac{\partial}{\partial t}\mathrm{DFe} = k_{rel}\left(\mathrm{Fe}^d_{dust} + \mathrm{Fe}^s_{dust}\right) + \gamma_d\,f_T\,(\mathrm{DS_{Fe}} + \mathrm{DL_{Fe}}) + \gamma_p\,f_T\,\mathrm{PHY_{Fe}} + \gamma_{zb}\,f_T\,\mathrm{ZOO_{Fe}}$$

$$+\left(f^{ph}_l\,k_{ph} + k_{pd}\right)(\mathrm{PFe_d} + \mathrm{PFe_s} + \mathrm{PFe_l}) - k_{upt} - k_{sorp}\left(P_d\,R^d_{surf} + (P_s + D_s\,r_{m:P})\,R^s_{surf} + (P_l + D_l\,r_{m:P})\,R^l_{surf}\right)\mathrm{DFe} + M(\mathrm{DFe}, z) \quad \text{(A15)}$$

where Fe^d_{dust} and Fe^s_{dust} are the two dissolvable pools of iron in dust particles. Iron release from these pools is dependent on the dissolution rate k_{rel}. A function of light intensity f^{ph}_l is introduced in the photochemical reduction of PFe:

$$f^{ph}_l = \frac{I(z)}{I_{ref}} \quad \text{(A16)}$$

The DFe uptake k_{upt} by phytoplankton is determined by:

$$k_{upt} = \min\left(\mu_{max}\,\frac{\mathrm{DFe}}{(\mathrm{DFe} + K_{Fe})}\,\mathrm{PHY},\ \mu\,Q^{ave}_{Fe}\,\mathrm{PHY}\right) \quad \text{(A17)}$$

Q^{ave}_{Fe} is the mean Fe:P ratio of phytoplankton. Choosing the smaller one of the terms ensures a dependence of uptake on DFe availability and a storage uptake is not considered.

PFe is divided in three classes due to the adsorption on different particles: $\mathrm{PFe_d}$ adsorbs on P_d, $\mathrm{PFe_s}$ on P_s and D_s, $\mathrm{PFe_l}$ on P_l and D_l.

$$\frac{\partial}{\partial t}\mathrm{PFe_d} = k_{sorp}\,R^d_{surf}\,\mathrm{DFe}\,P_d - \left(f^{ph}_l\,k_{ph} + k_{pd}\right)\mathrm{PFe_d} - k_{coag1}\,\mathrm{PFe_d}\,(D_s\,r_{m:P} + P_s) - k_{coag4}\,\mathrm{PFe_d}\,(D_l\,r_{m:P} + P_l) - w_d\,\frac{\partial \mathrm{PFe_d}}{\partial z} + M(\mathrm{PFe_d}, z) \quad \text{(A18)}$$

$$\frac{\partial}{\partial t}\mathrm{PFe_s} = k_{sorp}\,R^s_{surf}\,\mathrm{DFe}\,(r_{m:P}\,D_s + P_s) + k_{coag1}\,\mathrm{PFe_d}\,(D_s\,r_{m:P} + P_s) - k_{coag3}\,\mathrm{PFe_s}\,(D_l\,r_{m:P} + P_l) - k_{coag2}\,\mathrm{PFe_s}\,(D_s\,r_{m:P} + P_s) - \left(f^{ph}_l\,k_{ph} + k_{pd}\right)\mathrm{PFe_s} - w_s\,\frac{\partial \mathrm{PFe_s}}{\partial z} + M(\mathrm{PFe_s}, z) \quad \text{(A19)}$$

$$\frac{\partial}{\partial t}\mathrm{PFe_l} = k_{\mathrm{sorp}} R^{\mathrm{l}}_{\mathrm{surf}} \mathrm{DFe}\,(r_{\mathrm{m:P}}\,\mathrm{D_l}+P_{\mathrm{l}}) + k_{\mathrm{coag4}}\,\mathrm{PFe_d}\,(\mathrm{D_l}\,r_{\mathrm{m:P}}+P_{\mathrm{l}}) + k_{\mathrm{coag2}}\,\mathrm{PFe_s}\,(\mathrm{D_s}\,r_{\mathrm{m:P}}+P_{\mathrm{s}}) + k_{\mathrm{coag3}}\,\mathrm{PFe_s},(\mathrm{D_l}\,r_{\mathrm{m:P}}+P_{\mathrm{l}}) - \left(f_{\mathrm{l}}^{\mathrm{ph}}\,k_{\mathrm{ph}}+k_{\mathrm{pd}}\right)\mathrm{PFe_l} - w_{\mathrm{l}}\,\frac{\partial \mathrm{PFe_l}}{\partial z} + M(\mathrm{PFe_l}, z) \quad \text{(A20)}$$

Finally, a variable Fe:P-quota is introduced in PHY, ZOO, and DET and evolution of the respective Fe concentrations $\mathrm{PHY_{Fe}}$, $\mathrm{ZOO_{Fe}}$, $\mathrm{DS_{Fe}}$ (for iron contained in small detritus) and $\mathrm{DL_{Fe}}$ (for iron contained in large detritus) is described by:

$$\frac{\partial}{\partial t}\mathrm{PHY_{Fe}} = k_{\mathrm{upt}} - Q_{\mathrm{Fe}}\left(f_{\mathrm{G}}\,\mathrm{ZOO}+\gamma_{\mathrm{p}^2}\,\mathrm{PHY}^2\right) - \gamma_{\mathrm{p}}\,f_T\,\mathrm{PHY_{Fe}} + M(\mathrm{PHY_{Fe}}, z) \quad \text{(A21)}$$

$$\frac{\partial}{\partial t}\mathrm{ZOO_{Fe}} = Q_{\mathrm{Fe}}\,\gamma_{\mathrm{za}}\,f_{\mathrm{G}}\,\mathrm{ZOO} - \gamma_{\mathrm{zb}}\,f_T\,\mathrm{ZOO_{Fe}} - Q_{Z\mathrm{Fe}}\,\gamma_{\mathrm{z}^2}\,\mathrm{ZOO}^2 + M(\mathrm{ZOO_{Fe}}, z) \quad \text{(A22)}$$

$$\frac{\partial}{\partial t}\mathrm{DS_{Fe}} = Q_{\mathrm{Fe}}\,\gamma_{\mathrm{p}^2}\,\mathrm{PHY}^2 + Q_{\mathrm{Fe}}\,(1-\gamma_{\mathrm{za}})\,f_{\mathrm{G}}\,\mathrm{ZOO} - k_{\mathrm{coag2}}\,\mathrm{DS_{Fe}}\,(\mathrm{D_s}\,r_{\mathrm{m:P}}+P_{\mathrm{s}}) - k_{\mathrm{coag3}}\,\mathrm{DS_{Fe}}\,(\mathrm{D_l}\,r_{\mathrm{m:P}}+P_{\mathrm{l}}) - \gamma_{\mathrm{d}}\,f_T\,\mathrm{DS_{Fe}} + M(\mathrm{DS_{Fe}}, z) \quad \text{(A23)}$$

$$\frac{\partial}{\partial t}\mathrm{DL_{Fe}} = Q_{Z\mathrm{Fe}}\,\gamma_{\mathrm{z}^2}\,\mathrm{ZOO}^2 + k_{\mathrm{coag2}}\,\mathrm{DS_{Fe}}\,(\mathrm{D_s}\,r_{\mathrm{m:P}}+P_{\mathrm{s}}) + k_{\mathrm{coag3}}\,\mathrm{DS_{Fe}}\,(\mathrm{D_l}\,r_{\mathrm{m:P}}+P_{\mathrm{l}}) - \gamma_{\mathrm{d}}\,f_T\,\mathrm{DL_{Fe}} + M(\mathrm{DL_{Fe}}, z) \quad \text{(A24)}$$

where $Q_{Z\mathrm{Fe}}$ is the internal Fe:P ratio in zooplankton.

Acknowledgements. This work is a contribution to the project SOPRAN (Surface Ocean Processes in the ANtropocene), which is funded by the German Federal Ministry of Education and Research (BMBF project 03F0462C). The mesocosm experimental study was funded by the ANR DUNE under the contract ANR-07-BLAN-0126-01. The work of T. Wagener was supported by a Marie Curie IEF, Grant agreement No.: PIEF-GA-2009-236694, DAPOP. We would like to thank the "Réserve naturelle de Scandola, Parc naturel régional de Corse", in particular J. M. Dominici and collaborators, for professionalism and cooperation in the implementation of the field work in the Elbo bay. F. Louis, J. M. Grisoni, D. Luquet, M. Deschatres, C. Ridame, E. Pulido-Villena, S. Blain, C. Brunet, L. Gilleta and C. Rouvières are greatly acknowledged for their involvement during the DUNE-1 experiment. Sincerely, we thank the Japan Meteorological Agency Climate Data Assimilation System (JCDAS) for the free access of data.

References

Armstrong, R., Lee, C., Hedges, J., Honjo, S., and Wakeham, S.: A new, mechanistic model for organic carbon fluxes in the ocean based on the quantitative association of POC with ballast minerals, Deep-Sea Res. Pt. II, 49, 219–236, 2002. 9222

Baker, A., Kelly, S., Biswas, K., Witt, M., and Jickells, T.: Atmospheric deposition of nutrients to the Atlantic Ocean, Geophys. Res. Lett., 30, OCE 11-1–4, 2003. 9222

Balistieri, L., Brewer, P., and Murray, J.: Scavenging residence times of trace metals and surface chemistry of sinking particles in the deep ocean, Deep-Sea Res., 28A, 101–121, 1981. 9221

Bergquist, B., Wu, J., and Boyle, E.: Variability in oceanic dissolved iron is dominated by the colloidal fraction, Geochim. Cosmochim. Ac., 71, 2960–2974, doi:10.1016/j.gca.2007.03.013, 2007. 9235

Bishop, J. K. B., Davis, R. E., and Sherman, J. T.: Robotic Observations of Dust Storm Enhancement of Carbon Biomass in the North Pacific, Science, 298, 817–821, 2002. 9221

Bonnet, S. and Guieu, C.: Dissolution of atmospheric iron in seawater, Geophys. Res. Lett., 31, 1–4, 2004. 9227

Boyd, P. W., McTainsh, G., Sherlock, V., Richardson, K., Nichol, S., Ellwood, M., and Frew, R.: Episodic enhancement of phytoplankton stocks in New Zealand subantarctic waters: Contribution of atmospheric and oceanic iron supply, Global Biogeochem. Cy., 18, 1–23, 2004. 9221

Boyd, P. W., Jickells, T., Law, C. S., Blain, S., Boyle, E. A., Buesseler, K. O., Coale, K. H., Cullen, J. J., de Baar, H. J. W., Follows, M., Harvey, M., Lancelot, C., Levasseur, M., Owens, N. P. J., Pollard, R., Rivkin, R. B., Sarmiento, J., Schoemann, V., Smetacek, V., Takeda, S., Tsuda, A., Turner, S., and Watson, A. J.: Mesoscale Iron Enrichment Experiments 1993–2005: Synthesis and Future Directions, Science, 315, 612–617, 2007. 9221

Boyd, P., Mackie, D., and Hunter, K.: Aerosol iron deposition to the surface ocean – Modes of iron supply and biological responses, Mar. Chem., 120, 128–143, doi:10.1016/j.marchem.2009.01.008, 2010. 9221, 9239

Bruland, K. W. and Rue, E. L.: Analytical methods for the determination of concentrations and speciation of iron, in: The Biogeochemistry of Iron in Seawater, edited by: Turner, D. and Hunter, K., SCOR/IUPAC Series, J. Wiley, 1–7, 2001. 9222

Burchard, H. and Umlauf, L.: Observations and numerical modelling of mixed-layer turbulence: Do they represent the same statistical quantities?, Deep-Sea Res. Pt. II, 52, 1069–1074, doi:10.1016/j.dsr2.2005.03.002, 2005. 9225

Cullen, J., Bergquist, B., and Moffett, J.: Thermodynamic characterization of the partitioning of iron between soluble and colloidal species in the Atlantic Ocean, Mar. Chem., 98, 295–303, 2006. 9235

de Baar, H., Boyd, P., Coale, K., Landry, M., Tsuda, A., Assmy, P., Bakker, D., Bozec, Y., Barber, R., Brzezinski, M., Buesseler, K., Boye, M., Croot, P., Gervais, F., Gorbunov, M., Harrison, P., Hiscock, W., Laan, P., Lancelot, C., Law, C., Levasseur, M., Marchetti, A., Millero, F., Nishioka, J., Nojiri, Y., van Oijen, T., Riebesell, U., Rijkenberg, M., Saito, H., Takeda, S., Timmermans, K., Veldhuis, M., Waite, A., and Wong, C.-S.: Synthesis of iron fertilization experiments: From the iron age in the age of enlightenment, J. Geophys. Res.-Oceans, 110, 1–24, 2005. 9221

Duce, R. and Tindale, N.: Atmospheric transport of iron and its deposition in the ocean, Limnol. Oceanogr., 36, 1715–1726, 1991. 9221

Guieu, C.: DUNE – a DUst experiment in a low Nutrient, low chlorophyll Ecosystem – Quantifying the role of atmospheric input on marine ecosystem using large clean mesocosms, SOLAS Newsl., 9, 36–37, 2009. 9231

Guieu, C., Dulac, F., Desboeufs, K., Wagener, T., Pulido-Villena, E., Grisoni, J.-M., Louis, F., Ridame, C., Blain, S., Brunet, C., Bon Nguyen, E., Tran, S., Labiadh, M., and Dominici, J.-M.: Large clean mesocosms and simulated dust deposition: a new methodology to investigate responses of marine oligotrophic ecosystems to atmospheric inputs, Biogeosciences,

7, 2765–2784, doi:10.5194/bg-7-2765-2010, 2010a. 9222, 9223, 9224, 9225, 9227, 9233, 9236

Guieu, C., Ridame, C., Pulido-Villena, E., Blain, S., Wagener, T., Dulac, F., Desboeufs, K., Pondaven, P., Leblond, N., Stemman, L., Obernesterer, I., and Dominici, J-M: Dust inputs and marine carbon cycle: new insights from mesocosms study, in preparation, 2010b. 9231

Honeyman, B. and Santschi, P.: A Brownian-pumping model for trace metal scavenging: evidence from Th isotopes, J. Mar. Res., 47, 951–992, 1989. 9221

Honeyman, B. D., Balistrieri, L. S., and Murray, J. W.: Oceanic trace metal scavenging: the importance of particle concentration, Deep-Sea Res., 35, 227–246, doi:10.1016/0198-0149(88)90038-6, 1988. 9221

Honjo, S., Manganini, S., and Poppe, L.: Sedimentation of lithogenic particles in the deep ocean., Mar. Geol., 50, 199–220, 1982. 9221

Hutchins, D. and Bruland, K.: Iron-limited diatom growth and Si:N uptake ratios in a coastal upwelling regime, Nature, 393, 561–564, 1998. 9221

Jickells, T. D., An, Z. S., Andersen, K. K., Baker, A. R., Bergametti, G., Brooks, N., Cao, J. J., Boyd, P. W., Duce, R. A., Hunter, K. A., Kawahata, H., Kubilay, N., laRoche, J., Liss, P. S., Mahowald, N., Prospero, J. M., Ridgwell, A. J., Tegen, I., and Torres, R.: Global Iron Connections Between Desert Dust, Ocean Biogeochemistry, and Climate, Science, 308, 67–71, 2005. 9221

Johnson, K., Coale, K., Elrod, V., and Tindale, N.: Iron photochemistry in seawater from the equatorial Pacific, Mar. Chem., 46, 319–334, 1994. 9221, 9252

Johnson, K. S., Elrod, V. A., Fitzwater, S. E., Plant, J. N., Chavez, F. P., Tanner, S. J., Gordon, R. M., Westphal, D. L., Perry, K. D., Wu, J., and Karl, D. M.: Surface ocean-lower atmosphere interactions in the Northeast Pacific Ocean Gyre: Aerosols, iron, and the ecosystem response, Global Biogeochem. Cy., 17, 32-1–14, 2003. 9221

Mahowald, N. M., Engelstaedter, S., Luo, C., Sealy, A., Artaxo, P., Benitez-Nelson, C., Bonnet, S., Chen, Y., Chuang, P. Y., Cohen, D. D., Dulac, F., Herut, B., Johansen, A. M., Kubilay, N., Losno, R., Maenhaut, W., Paytan, A., Prospero, J. M., Shank, L. M., and Siefert, R. L.: Atmospheric Iron Deposition: Global Distribution, Variability, and Human Perturbations, Annual Review of Marine Science, 1, 245–278, doi:10.1146/annurev.marine.010908.163727, 2009. 9221

Martin, J., Gordon, R., and Fitzwater, S.: Iron in Antarctic waters, Nature, 345, 156–158, 1990. 9220

Mills, M., Ridame, C., Davey, M., La Roche, J., and Geider, R.: Iron and phosphorus co-limit nitrogen fixation in the eastern tropical North Atlantic, Nature, 429, 292–294, 2004. 9221

Moffet, J.: Transformations among different forms of iron in the ocean, in: The Biogeochemistry of Iron in Seawater, edited by: Turner, D. and Hunter, K., SCOR/IUPAC Series, J. Wiley, 1–7, 2001. 9222

Nyffeler, U., Li, Y.-H., and Santschi, P.: A kinetic approach to describe trace-element distribution between particles and solution in natural aquatic systems, Geochim. Cosmochim. Ac., 48, 1513–1522, 1984. 9221, 9234

Onogi, K., Tsutsui, J., Koide, H., Sakamoto, M., Kobayashi, S., Hatshushika, H., Matshumoto, T., Yamazaki, N., Kamahort, H., Takahashi, K., Kadokura, S., Wada, K., Kato, K., Oyama, R., Ose, T., Mannoji, N., and Taira, R.: The JRA-25 Reanalysis, J. Meteorol. Soc. Jpn. Ser. II, 85, 369–432, 2007. 9225

Pulido-Villena, E., Rèrolle, V., and Guieu, C.: Transient fertilizing effect of dust in P-deficient LNLC surface ocean, Geophys. Res. Lett., 37, L01603, doi:10.1029/2009GL041415, 2010. 9224, 9225, 9230, 9231

Ridame, C. and Guieu, C.: Saharan input of phosphate to the oligotrophic water of the open western Mediterranean Sea, Limnol. Oceanogr., 47, 856–869, 2002. 9222

Rijkenberg, M., Powell, C., Dall'Osto, M., Nielsdottir, M., Patey, M., Hill, P., Baker, A., Jickells, T., Harrison, R., and Achterberg, E.: Changes in iron speciation following a Saharan dust event in the tropical North Atlantic Ocean, Mar. Chem., 110, 56–67, doi:10.1016/j.marchem.2008.02.006, 2008. 9221

Rose, A. and Waite, T.: Predicting iron speciation in coastal waters from the kinetics of sunlight-mediated iron redox cycling, Aquat. Sci., 65, 375–383, 2003a. 9238

Rose, A. and Waite, T.: Kinetics of hydrolysis and precipitation of ferric iron in seawater, Environ. Sci. Technol., 37, 3897–3903, 2003b. 9221

Sarthou, G., Baker, A., Blain, S., Achterberg, E., Boye, M., Bowie, A., Croot, P., Laan, P., De Baar, H., Jickells, T., and Worsfold, P.: Atmospheric iron deposition and sea-surface dissolved iron concentrations in the eastern Atlantic Ocean, Deep-Sea Res. Pt. I, 50, 1339–1352, 2003. 9221

Schartau, M. and Oschlies, A.: Simultaneous data-based optimization of a 1D-ecosystem model at three locations in the North Atlantic: Part I. Method and parameter estimates, J. Mar. Res., 61, 765–793, 2003a. 9253

Schartau, M. and Oschlies, A.: Simultaneous data-based optimization of a 1D-ecosystem

model at three locations in the North Atlantic: Part II. Standing stocks and nitrogen fluxes, J. Mar. Res., 61, 795–821, 2003b. 9253

Sedwick, P. N., Church, T. M., Bowie, A. R., Marsay, C. M., Ussher, S. J., Achilles, K. M., Lethaby, P. J., Johnson, R. J., Sarin, M. M., and McGillicuddy, D. J.: Iron in the Sargasso Sea (Bermuda Atlantic Time-series Study region) during summer: Eolian imprint, spatiotemporal variability, and ecological implications, Global Biogeochem. Cy., 19, GB4006, doi:10.1029/2004GB002445, 2005. 9221

Sohm, J. A. and Capone, D. G.: Phosphorus dynamics of the tropical and subtropical north Atlantic: Trichodesmium spp. versus bulk plankton, Mar. Ecol.-Prog. Ser., 317, 21–28, 2006. 9225, 9253

Sunda, W. and Huntsman, S.: Iron uptake and growth limitation in oceanic and coastal phytoplankton, Mar. Chem., 50, 189–206, 1995. 9253

Ternon, E., Guieu, C., Loÿe-Pilot, M.-D., Leblond, N., Bosc, E., Gasser, B., Miquel, J.-C., and Martín, J.: The impact of Saharan dust on the particulate export in the water column of the North Western Mediterranean Sea, Biogeosciences, 7, 809–826, doi:10.5194/bg-7-809-2010, 2010. 9222

Thingstad, T., Li Zweifel, U., and Rassoulzadegan, F.: P limitation of heterotrophic bacteria and phytoplankton in the northwest Mediterranean, Limnol. Oceanogr., 43, 88–94, 1998. 9224

Umlauf, L. and Burchard, H.: Second-order turbulence closure models for geophysical boundary layers. A review of recent work, Cont. Shelf Res., 25, 795–827, 2005. 9224

Vink, S. and Measures, C.: The role of dust deposition in determining surface water distributions of A1 and Fe in the South West Atlantic, Deep-Sea Res. Pt. II, 48, 2787–2809, 2001. 9221

Wagener, T., Pulido-Villena, E., and Guieu, C.: Dust iron dissolution in seawater: Results from a one-year time-series in the Mediterranean Sea, Geophys. Res. Lett., 35, L16601, doi:10.1029/2008GL034581, 2008. 9227, 9233, 9252

Wagener, T., Guieu, C., and Leblond, N.: Effects of dust deposition on iron cycle in the surface Mediterranean Sea: results from a mesocosm seeding experiment, Biogeosciences, 7, 3769–3781, doi:10.5194/bg-7-3769-2010, 2010. 9222, 9226, 9227, 9232, 9233, 9236, 9237, 9238, 9252, 9259

Weber, L., Völker, C., Oschlies, A., and Burchard, H.: Iron profiles and speciation of the upper water column at the Bermuda Atlantic Time-series Study site: a model based sensitivity study, Biogeosciences, 4, 689–706, doi:10.5194/bg-4-689-2007, 2007. 9222

Wedepohl, K. H.: The composition of the continental crust, Geochim. Cosmochim. Ac., 59,

1217–1232, doi:10.1016/0016-7037(95)00038-2, 1995. 9229
Wells, M. and Goldberg, E.: Colloid aggregation in seawater, Mar. Chem., 41, 353–358, 1993. 9221
Wen, L.-S., Santschi, P., and Tang, D.: Interactions between radioactively labeled colloids and natural particles: Evidence for colloidal pumping, Geochim. Cosmochim. Ac., 61, 2867–2878, 1997. 9221, 9234
Wu, J., Boyle, E., Sunda, W., and Wen, L.-S.: Soluble and colloidal iron in the oligotrophic North Atlantic and North Pacific, Science, 293, 847–849, 2001. 9235
Ye, Y., Völker, C., and Wolf-Gladrow, D. A.: A model of Fe speciation and biogeochemistry at the Tropical Eastern North Atlantic Time-Series Observatory site, Biogeosciences, 6, 2041–2061, doi:10.5194/bg-6-2041-2009, 2009. 9222, 9225, 9226, 9234, 9252

Table 1. Parameters in the chemical model.

Parameters	Symbol	Unit	Value
solubility of atmospheric iron	r_{sol}	%	0.1[1]
iron content of dust particles	r_{Fe}	%	2.3[1]
iron dissolution rate	k_{rel}	d^{-1}	3[2]
DFe adsorption rate	k_{sorp}	$kg^{-1}\,m^3\,d^{-1}$	150[3]
scaling factor of the surface-related adsorption rate for P_d	R^d_{surf}	–	5[4]
scaling factor of the surface-related adsorption rate for P_s	R^s_{surf}	–	1[4]
scaling factor of the surface-related adsorption rate for P_l	R^l_{surf}	–	0.2[4]
reference irradiance	I_{ref}	$\mu Em^{-3}\,s^{-1}$	1978
PFe photoreduction rate	k_{ph}	d^{-1}	20.2[5]
PFe redissolution rate	k_{pd}	d^{-1}	0.015[6]
coagulation rate	k_{coag1}	$(kg\,L^{-1})^{-1}\,s^{-1}$	4.5[7]
coagulation rate	k_{coag2}	$(kg\,L^{-1})^{-1}\,s^{-1}$	11[7]
coagulation rate	k_{coag3}	$(kg\,L^{-1})^{-1}\,s^{-1}$	15[7]
coagulation rate	k_{coag4}	$(kg\,L^{-1})^{-1}\,s^{-1}$	13[7]

[1] Wagener et al. (2010).
[2] Wagener et al. (2008).
[3] Estimated in the sensitivity study in Sect. 4.3.4.
[4] Calculated from the size of modelled particles assuming all the particles are spherical.
[5] Johnson et al. (1994).
[6] Sensitivity study in Ye et al. (2009).
[7] Adapted from Ye et al. (2009).

Table 2. Parameters in the biological model. Source of parameter values are shown as footnotes; other parameters are optimised for the North Atlantic by Schartau and Oschlies (2003a,b).

Parameters	Symbol	Unit	Value
maximum growth rate of phytoplankton	μ_{max}	d^{-1}	0.27
phytoplankton mortality	γ_p	d^{-1}	0.04
initial slope P-I curve	α	$m^2\,W^{-1}\,d^{-1}$	0.256
phosphate half-saturation constant	K_P	$mmol\,m^{-3}$	0.01[1]
iron half-saturation constant	K_{Fe}	$\mu mol\,m^{-3}$	0.2
phytoplankton aggregation rate	γ_{p^2}	$(mmol\,m^{-3})^{-1}\,d^{-1}$	0.025
maximum grazing rate	g_{max}	d^{-1}	1.575
prey capture rate	ε	$(mmol\,m^{-3})^{-1}\,d^{-1}$	1.6
assimilation efficiency	γ_{za}	–	0.925
excretion	γ_{zb}	d^{-1}	0.01
quadratic mortality of zooplankton	γ_{z^2}	$(mmol\,m^{-3})^{-1}\,d^{-1}$	0.34
detritus remineralisation	γ_d	d^{-1}	0.048
sinking velocity of small dust particles	w_d	$m\,d^{-1}$	0.2[2]
sinking velocity of large dust particles, small detritus and small aggregates	w_s	$m\,d^{-1}$	5[2]
sinking velocity of large detritus and large aggregates	w_l	$m\,d^{-1}$	50[2]
coefficient for temperature function	C_{ref}	–	1.066
PAR:short-wave irradiance ratio	f_{PAR}	–	0.43
attenuation due to chlorophyll	κ	$m^2\,(mmol\,N)^{-1}$	0.03
maximum Fe:P ratio in organic matter	Q_{Fe}^{max}	$\mu mol\,m^{-3}\,(mmol\,m^{-3})^{-1}$	0.53[3]
minimum Fe:P ratio in organic matter	Q_{Fe}^{min}	$\mu mol\,m^{-3}\,(mmol\,m^{-3})^{-1}$	0.11[3]
mass:P ratio in organic matter	$r_{m:P}$	$g\,mol^{-1}$	$2.5 \times 10^{+3}$ [4]

[1] Modified from Sohm and Capone (2006).
[2] Calculated from Stoke's Law.
[3] Calculated from the Fe:N ratio by Sunda and Huntsman (1995) and the Redfield N:P ratio.
[4] Calculated with the Redfield C:P ratio and the assumption that 1 g C corresponds 2 g mass.

Table 3. Particle classification in the model.

Particles	Symbol	Size (μm)	Settling velocity ($m\,d^{-1}$)
small dust particles	P_d	2	0.2
large dust particles and inorganic part of small aggregates	P_s	10	5
small detritus and organic part of small aggregates	D_s	10	5
inorganic part of large aggregates	P_l	50	50
large detritus and organic part of large aggregates	D_l	50	50

Table 4. Measured and modelled export flux of inorganic particles (mg m^{-2} d^{-1}) under control conditions, calculated assuming an Al content of 7.7%. C1–C3 stand for the triplicate CONTROL-meso, C_{ave} for the mean of C1–C3 and M for model results. Numbers are averaged fluxes in the time periods after dust addition in DUST-meso.

	24 h*	72 h	120 h	168 h
C1	9.7	6.3	1.9	5.5
C2	2.0	9.9	13.0	2.8
C3	5.9	24.6	1.9	NaN
C_{ave}	5.9	13.6	5.6	4.2
M	11.8	8.8	7.5	7.3

* Exported mass from 24 h before to 24 h after the addition.

Table 5. Measured and modelled export flux of Fe (mg m^{-2} d^{-1}) under control conditions. C1–C3 stand for the triplicate CONTROL-meso, C_{ave} for the mean of C1–C3 and M for model results. Numbers are averaged fluxes in the time periods after dust addition in DUST-meso.

	24 h*	72 h	120 h	168 h
C1	0.4	0.3	0.1	0.2
C2	0.1	0.4	0.5	0.1
C3	0.3	1.0	0.1	NaN
C_{ave}	0.3	0.6	0.2	0.2
M	0.3	0.3	0.2	0.2

* Exported mass from 24 h before to 24 h after the addition.

Table 6. Measured and modelled export flux of inorganic particles ($g\,m^{-2}\,d^{-1}$) under dust addition, calculated assuming an Al content of 4%. D1–D3 stand for the triplicate mesocosms with dust addition, D_{ave} for the mean of D1–D3 and M for model results. Numbers are averaged fluxes in the time periods after dust addition.

	24 h*	72 h	120 h	168 h
D1	0.6	1.7	0.3	0.1
D2	0.5	1.2	0.8	0.1
D3	0.9	0.9	0.5	0.1
D_{ave}	0.6	1.3	0.5	0.1
M	2.3	0.9	0.5	0.2

* Exported mass from 24 h before to 24 h after the addition.

Table 7. Measured and modelled export flux of Fe ($mg\,m^{-2}\,d^{-1}$) under dust addition. D1–D3 stand for the triplicate mesocosms with dust addition, D_{ave} for the mean of D1–D3 and M for model results. Numbers are averaged fluxes in the time periods after dust addition.

	24 h*	72 h	120 h	168 h
D1	14.8	41.0	6.6	2.5
D2	10.5	28 3	17.4	2.8
D3	20.2	20.3	10.5	1.5
D_{ave}	15.2	29.9	11.5	2.2
M	54.0	21.5	11.1	5.3

* Exported mass from 24 h before to 24 h after the addition.

Table 8. Iron budget estimated from measured data and model (mg) under dust addition. D1–D2 stand for the two mesocosms with dust addition showed in Wagener et al. (2010) and M for model results. Time (0–168) is in hours after dust addition. DFe and PFe stock are the total mass in the water column. PFe export is the total export from dust addition to the corresponding time points. "recovery" is calculated as the sum of iron stock and export divided by the iron input by dust addition.

		0	24	120	168	recovery (%)
D1	DFe stock	7	6	5	6	
	PFe stock	41	270	52	54	59
	PFe export	0	123	518	538	
D2	DFe stock	7	6	6	5	
	PFe stock	42	169	67	43	53
	PFe export	0	88	467	490	
M	DFe stock	8	7	6	5	
	PFe stock	57	602	278	229	100
	PFe export	0	429	713	759	

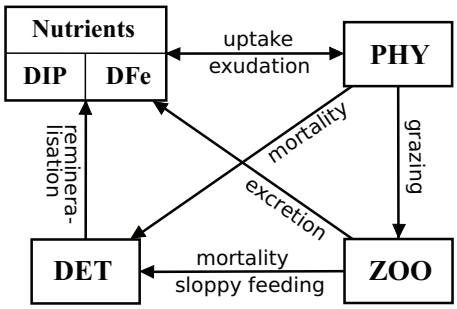

Fig. 1. Ecosystem model.

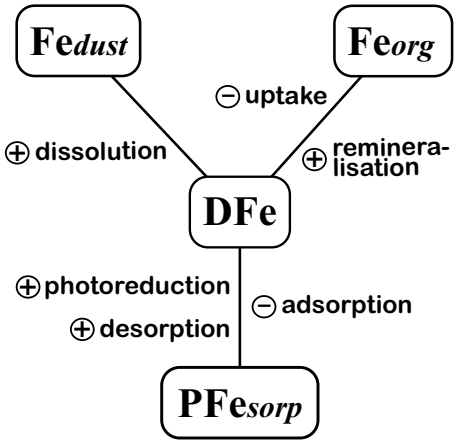

Fig. 2. Chemical model of iron. Processes supplying DFe haven a sign of + and those removing DFe a sign of −.

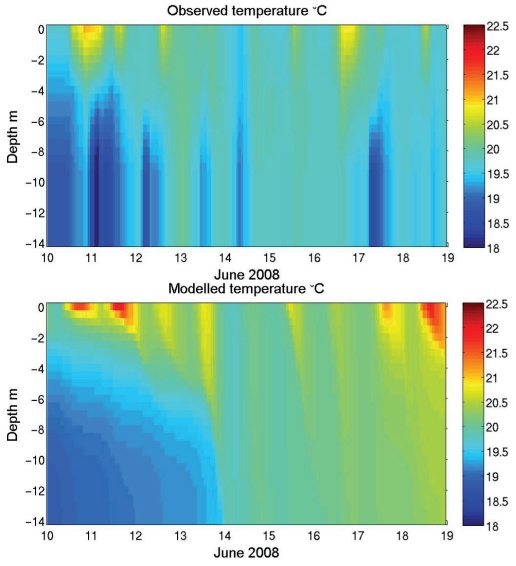

Fig. 3. Observed and modelled temperature during the DUNE experiment.

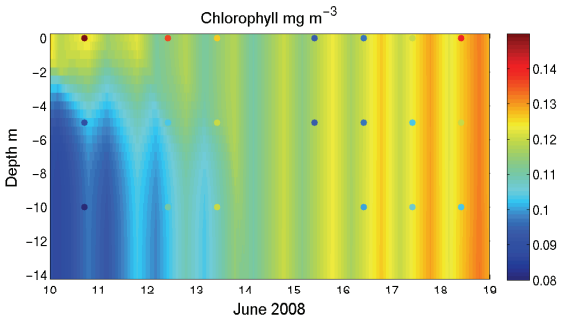

Fig. 4. Modelled chlorophyll concentration in CONTROL-meso. Colored dots are the measured chlorophyll concentrations.

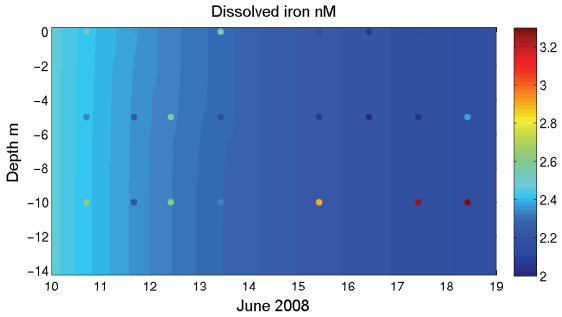

Fig. 5. Modelled DFe concentration in CONTROL-meso. Colored dots are the measured DFe concentrations.

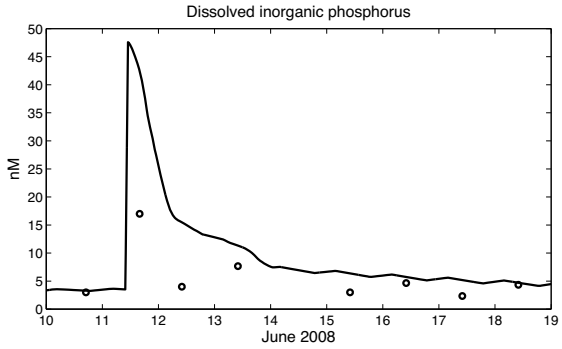

Fig. 6. Modelled surface DIP concentration in DUST-meso. Circles are the measured DIP concentration.

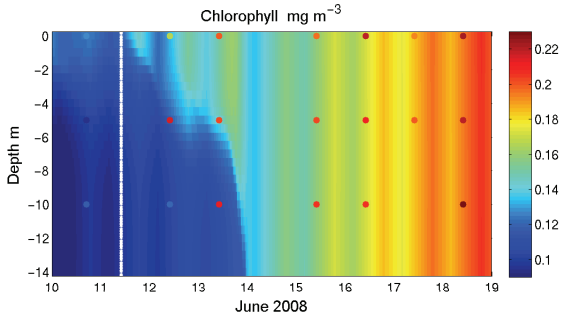

Fig. 7. Modelled chlorophyll concentration in DUST-meso. Colored dots are the measured chlorophyll concentrations. The white bar shows the time of dust addition.

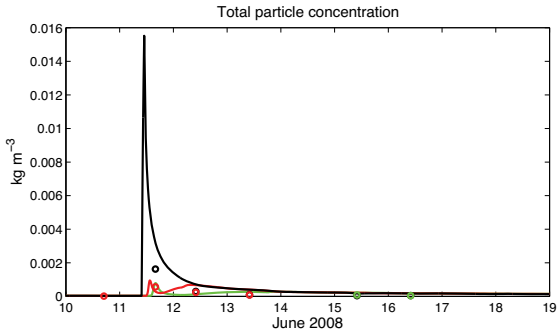

Fig. 8. Inorganic particle concentration in DUST-meso at different depths: 0 m (black), 5 m (red) and 10 m (green). Colored circles are the measured concentrations at the corresponding depths.

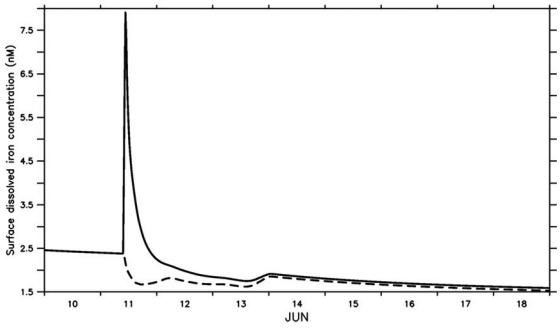

Fig. 9. Sensitivity study with respect to iron dissolution timescale. Solid: dissolvable iron in dust particles is input into dissolved iron pool instantaneously by dust addition; dashed: dissolvable iron is dissolved from dust particles with a timescale of 3 days.

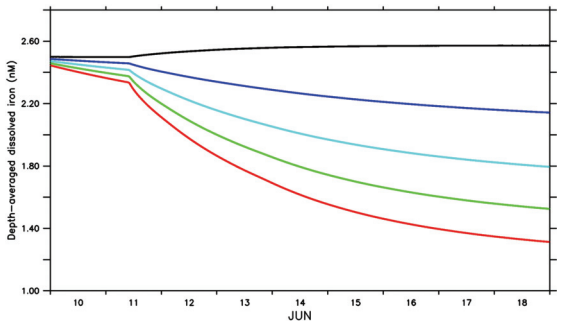

Fig. 10. Sensitivity study with respect to adsorption rate constant (k_{sorp}). Depth-averaged DFe is plotted with $k_{sorp} = 2.5$ (black), 2.5×20 (blue), 2.5×40 (light blue), 2.5×60 (green) and 2.5×80 (red) $m^3\,kg^{-1}\,d^{-1}$.

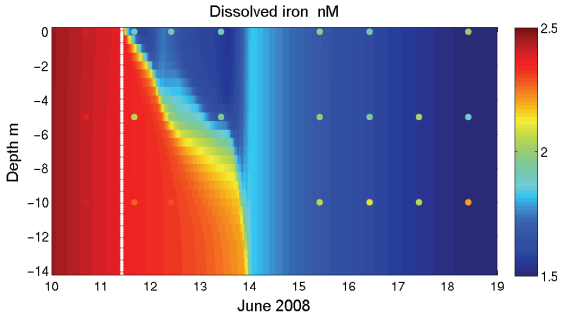

Fig. 11. DFe concentration in DUST-meso. Colored dots are the measured DFe concentrations. The white bar shows the time of dust addition.

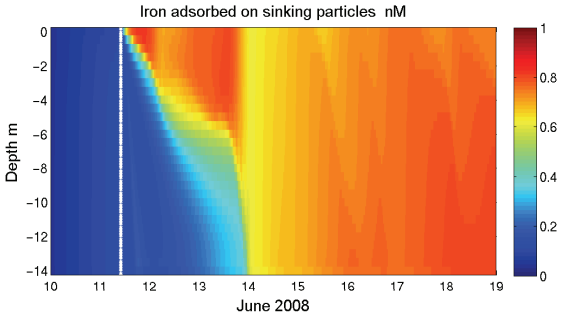

Fig. 12. Modelled PFe concentration in DUST-meso. The white bar shows the time of dust addition.

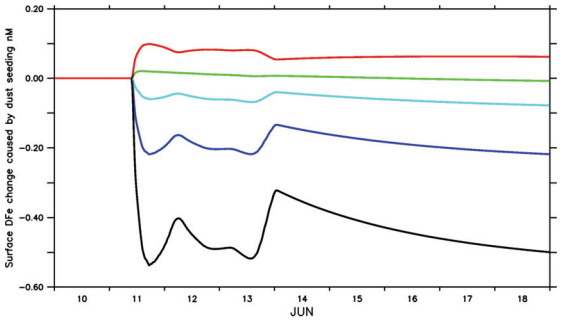

Fig. 13. Sensitivity study with respect to initial DFe concentration before dust addition. Surface DFe change caused by dust addition is calculated as the difference of surface DFe concentration with and without dust addition and plotted for different initial DFe concentrations: 2.0 (black), 1.0 (blue), 0.5 (light blue), 0.25 (green) and 0 µmol m^{-3} (red).

2.4 Publication III

Environmental controls on N_2 fixation by *Trichodesmium* in the tropical eastern North Atlantic

Environmental controls on N_2 fixation by *Trichodesmium* in the tropical eastern North Atlantic

Ying Ye, Christoph Völker, Astrid Bracher, Bettina Schmitt, Dieter A. Wolf-Gladrow

Alfred Wegener Institute for Polar and Marine Research, Bremerhaven, Germany

Abstract

The low surface nitrate concentration and high atmospheric iron input in the tropical eastern North Atlantic provide beneficial conditions for N_2 fixation. Different abundances of diazotrophs have been observed (e.g. Capone et al., 2005; Langlois et al., 2008) and an Fe- and P-colimitation of N_2 fixation was reported in this ocean region (Mills et al., 2004). It is however unclear how different limiting factors control the temporal variability of N_2 fixation and what the role of Fe-limitation is in a region with high fluxes of dust deposition.

To study the environmental controls on N_2 fixation, a one-dimensional ecosystem model is coupled with a physical model for the Tropical Eastern North Atlantic Times-series Station (TENATSO), north of the Cape Verde Islands. The model describes diazotrophy according to the physiology of *Trichodesmium*, taking into account a growth dependence on light, temperature, iron, dissolved inorganic and organic phosphorus. The modelled *Trichodesmium* abundance is constrained by satellite-derived cyanobacterial chlorophyll a concentrations.

Model results show a complex pattern of competitive as well as mutually beneficial interactions between diazotrophs and non-diazotrophic phytoplankton. Spring blooms of non-diazotrophic phytoplankton deplete dissolved inorganic phosphorus (DIP) in surface waters but enhance the concentration of dissolved organic phosphorus (DOP). This high DOP availability and the ability of *Trichodesmium* to take up DOP are crucial for their autumn blooms. The atmospheric iron input at the TENATSO site is required to enable the diazotrophic growth and to support the observed abundance of non-diazotrophic phytoplankton, however a simple relationship between dust fluxes and the magnitude of N_2 fixation is not found. Newly fixed nitrogen by diazotrophs increases the growth of non-diazotrophic phytoplankton significantly. The effect is mainly seasonal due to the periodically high abundance of *Trichodesmium* in autumn.

1 Introduction

Biological N_2 fixation is an essential N supply for primary production in nitrate-depleted oceans. Up to half of the primary production in the tropical and subtropical oceans is supposed to be supported by N_2 fixation (Capone et al., 1997). N_2 fixation and denitrification are the main processes holding the marine N cycling in balance (Deutsch et al., 2007). Variation in N_2 fixation affects the entire N budget and subsequently the coupled carbon sequestration. In the subtropical Pacific gyre and in the oligotrophic North Atlantic, N_2 fixation is responsible for up to 50 % of the organic carbon exported from the photic zone (Karl et al., 1997; Gruber and Sarmiento, 1997).

Organisms carrying out N_2 fixation, the so-called diazotrophs, have an advantage living in nitrate-depleted regions. However, their growth and distribution are often limited by the scarcity of other nutrients such as P and Fe (Wu et al., 2000; Berman-Frank et al., 2001; Mills et al., 2004). Factors as atmospheric dust deposition and the relative concentration of P to N are often used to explain the global distribution and the strength of N_2 fixation (Gruber and Sarmiento, 1997; Deutsch et al., 2007).

In the last decades, many studies have contributed to estimating the spatial extent and rates of N_2 fixation under different assumptions on regulating factors. Most of the studies found the highest N_2 fixation activity in surface waters at low latitudes, indicating a strong dependence of diazotrophic growth on light and temperature (Carpenter and Capone, 1992; Capone et al., 1997; Tyrrell et al., 2003; Mahaffey et al., 2005). With the concept of the geochemical tracer N^*, Gruber and Sarmiento (1997) found high fixation rates in the tropical and subtropical North Atlantic and in the Mediterranean, and attributed this to the high atmospheric iron supply in these regions. Reynolds et al. (2007) examined the distribution of N_2 fixation by determining the isotopic composition of N in suspended particulate organic matter and concluded that a smaller region from 15°N–30°N and 30°W–50°W is most likely the main region of N_2 fixation in the North Atlantic. These estimates for the North Atlantic are supported by historical and present observations of high *Trichodesmium* concentrations and high N_2 fixation rates in the Caribbean Sea and in the western tropical North Atlantic (Carpenter and Price, 1977; Carpenter and Romans, 1991; Carpenter et al., 2004; Capone et al., 2005; Davis and McGillicuddy, 2006). Deutsch et al. (2007) on the other hand attributed the surplus of P relative to N in some surface waters to subsurface denitrification and used the gradual loss of this P excess as a tracer for N_2 fixation. They presented that N_2 fixation rates are highest downstream from oxygen minimum zones in the Pacific Ocean, suggesting that P, instead of Fe, is the main regulating factor for N_2 fixation. These estimates reveal that using different tracers or weighing the regulating factors differently may result in inconsistence in the distribution patterns of N_2 fixation. Thus, the key to understand the distribution and variability of N_2 fixation is to find out at first what are the factors limiting diazotrophic growth and how these factors interplay.

In this study, we investigate different limiting factors of diazotrophic growth by simulating a marine ecosystem under the influence of periodically strong dust deposition at the Tropical Eastern North Atlantic Times-series Station (TENATSO), north of the Cape Verde Islands. Most of the geochemical studies on N_2 fixation in the Atlantic found weaker signals in the tropical eastern North Atlantic than in the western North Atlantic and the subtropical Atlantic gyre (Gruber and Sarmiento, 1997; Mahaffey et al., 2003; Hansell et al., 2004; Reynolds et al., 2007). However, direct observations of diazotrophs in this region show moderate abundances up to 200 trichomes L^{-1} and high N_2 fixation rates with large variations (integrated for the mixed layer up to $180\,\mu\mathrm{mol\,N\,m^{-2}\,d^{-1}}$) (Agusti et al., 2001; Tyrrell et al., 2003; Carpenter et al., 2004; Voss et al., 2004; Capone et al., 2005; Staal et al., 2007; Mark Moore et al., 2009; Fernández et al., 2010). Moreover, given the massive Fe input by Saharan dust events, the tropical eastern North Atlantic is potentially a region of high N_2 fixation. In a previous study (Ye et al., 2009), we investigated the processes controlling Fe biogeochemical cycle at TENATSO in a one-dimensional model. The knowledge from that study provides a good basis for studying the impact of dust deposition on N_2 fixation as well as total primary productivity.

The dominant role of *Trichodesmium* among diverse marine diazotrophs has been recognised decades ago (Capone et al., 1997). The contribution of N_2 fixed by *Trichodesmium* in the tropical

and subtropical Atlantic is in the same order of magnitude as the vertical flux of nitrate (Capone et al., 2005). At TENATSO, Langlois et al. (2008) showed that *Trichodesmium* and *Katagnymene* are dominant groups among diazotrophs and cover over 50 % of *nifH* gene copies detected in natural waters there. Both of them are non-heterocystous and fix N_2 only at daylight (Zehr et al., 2000). Physiology of *Trichodesmium* is well studied and its natural occurrence is widely observed. Therefore, we consider one photoautotrophic diazotrophic group in our ecosystem model and describe its physiology according to studies on *Trichodesmium*. Certainly, many other diazotrophs are missing in this model: high abundances of unicellular diazotrophic cyanobacterial have been recently reported (Zehr et al., 2001; Montoya et al., 2004); and symbiotic diazotrophs are supposed to contribute significantly in basin-scale N budgets (Carpenter et al., 1999; Villareal, 1991; Zehr et al., 2001). However, their physiology and contribution in the marine N cycle are still unclear, and thus introducing them into our model would result in higher complexity and uncertainty.

There are several previous studies modelling N_2 fixation or considering diazotrophs as a member of the ecosystem. Fennel et al. (2001) modelled N_2 fixation at the ALOHA station in the subtropical North Pacific Ocean and introduced the effect of light, temperature and phosphorus on diazotrophic growth, using different but fixed N:P ratios for each ecosystem functional group. The model for the Atlantic Ocean by Coles and Hood (2007) additionally took into account iron deposition and uptake of dissolved organic phosphorus, and used variable stoichiometric ratios, but the role of temperature is neglected. Moore et al. (2001) explored a wide variety of marine ecosystems, including N, P, and Fe-limited systems, in which diazotrophs, beside other phytoplankton, are also represented. In our model, *Trichodesmium* and its ecological function are in focus. The growth of *Trichodesmium* is determined by light, temperature, iron, dissolved inorganic and organic phosphorus. The complex model of Fe speciation and biogeochemistry by Ye et al. (2009) is coupled with a N_2 fixation model, allowing us to describe the interactions between Fe and N cycles more reasonably. Variable Fe : N and P : N ratios are used for each functional group in the ecosystem model. Satellite-derived cyanobacterial chlorophyll concentrations are used as the upper limit of modelled *Trichodesmium* concentrations to constrain the model. Based on this model design, we aim to reveal the factors controlling the seasonal and vertical distribution of *Trichodesmium* at TENATSO and estimate the contribution of N_2 fixation to the primary productivity and the N budget in the eastern tropical North Atlantic.

2 Methods

2.1 Model description

Our model consists of a physical, biological, and chemical model coupled in a one-dimensional vertical water column representing the upper 400 m water depth. The water column is divided into 67 layers and the thickness of water layer increases nonlinearly with depth. This results in a surface layer thickness of 1.5 m and 33 layers within the upper 100 m. This high vertical resolution allows us to describe in detail the role of mixing and light in segregating vertically the habitats of *Trichodesmium* and other ecosystem functional groups. We use the General Ocean Turbulence Model (GOTM, Umlauf and Burchard, 2005, `www.gotm.net`) as the physical model providing the vertical mixing and advection. The model configuration and choice of calculation schemes are described in Ye et al. (2009).

Derived from a N-based ecosystem model developed originally by Schartau and Oschlies (2003a,b),

our biological model consists of dissolved inorganic nitrogen (DIN) including nitrate and ammonium, dissolved inorganic phosphorus (DIP), dissolved organic phosphorus (DOP), *Trichodesmium* (Tri), non-diazotrophic phytoplankton (Phy), zooplankton (Z), and detritus (D) (Fig. 1). We use the parameters and flux descriptions in Ye et al. (2009) for processes not involving Tri and describe the fluxes from and to Tri more in detail in Sect. 2.1.1–2.1.4. Table 2 and 3 show values and sources of parameters used in this model. A complex model of Fe speciation and biogeochemistry is coupled with the biological model providing a reasonable description of bioavailable iron for phytoplankton growth (details of the Fe model see Ye et al. (2009)).

The model is integrated forward in time until deep-ocean concentration profiles become cyclostationary. After a spin-up period from 1 January 2000 to 31 December 2004, the model is integrated over four more years for analysis. We used, as forcing data for the entire model period, 6 hourly fluxes for the TENATSO site derived from the Japan Meteorological Agency Climate Data Assimilation System (JCDAS) (Onogi et al., 2007). The time-step of the model is 1200 s. The fast chemical reactions of iron (e.g. photoredox reactions and organic complexation) are assumed to be in an equilibrium and the concentrations of Fe species involved in these reactions are calculated as diagnostic variables from state variables which change slowly with time. The biochemical variables are integrated forward in time using a first order explicit Eulerian scheme (Völker *et al.*, in prep.).

2.1.1 Growth rate of Tri

The growth rate of *Trichodesmium* in the model is regulated by light, temperature, phosphorus and iron.

Trichodesmium colonies are found in high abundance in warm and sunlit surface waters in tropical and subtropical oceans (Carpenter and Capone, 1992; Capone et al., 1997; Tyrrell et al., 2003; Mahaffey et al., 2005), indicating a strong dependence of growth on temperature and light. In the model, this dependence is described using the empirical correlations between temperature and growth rate, and between light and growth rate from Breitbarth et al. (2007, 2008) (Eq. 15 and Eq. 16).

Trichodesmium can take up NO_3^- and NH_4^+, and fix N_2 simultaneously (Mulholland and Capone, 1999). Holl and Montoya (2005) found that in the presence of NO_3^-, N_2 fixation is reduced up to 70 %, indicating a preference for NO_3^- by *Thichodesmium*. In the model, we enabled Tri to take up DIN and meet its N requirement additionally by N_2 fixation. Thus, the growth rate of Tri is not limited by the DIN availability.

N_2 fixation in the eastern tropical North Atlantic is reported to be limited by Fe and P (Mills et al., 2004). We introduced a dependence of Tri growth on the availability of Fe and P into the model and described it with the internal Fe : N (Q_{Tri}^{Fe}) and P : N quota (Q_{Tri}^{PO}) (Eq. 18 and Eq. 17). The actual growth rate of Tri is then calculated as the product of the temperature dependent maximal growth rate with the smaller of f_{PAR}^t, f_{Fe}^t and f_{PO}^t (Eq. 19).

2.1.2 P uptake by Tri

Measured concentrations of DIP range from 0.01 to 0.25 mmol m^{-3} in surface waters near TENATSO (Cruise data of POS 320/1, POS 332, Meteor 68/3, POS 348/2, Merian 20 April 2008, L. Cotrim da Cunha and Ilka Peeken: personal communication). Growth rates supported by these nanomolar levels of DIP are about 2 orders of magnitudes below the reported growth rates of the natural populations in the North Atlantic (Fu et al., 2005). Studies on DIP uptake suggest that *Trichodesmium*

is a poor competitor for DIP relative to bulk phytoplankton and might meet a majority of its P demand by taking up DOP (Mulholland et al., 2002; Fu et al., 2005; Sohm and Capone, 2006; Orchard et al., 2010). Ambient concentrations of DOP are often 1-2 orders of magnitudes higher than those of DIP in the Atlantic (Karl et al., 2002), as well as at TENATSO (Torres-Valdès et al., 2009). To allow the observed growth rates, only a small fraction of DOP needs to be bioavailable (Orchard et al., 2010). In a recent study on P acquisition, Dyhrman et al. (2006) found evidence that *Trichodesmium* can exploit phosphonates and monophosphate esters, besides PO_4^{3-}.

Based on the ability of *Trichodesmium* to access DOP, we introduced two P pools into the model: DIP which is available for both *Trichodesmium* (Tri) and other phytoplankton (Phy), and DOP taken up only by Tri. Sources of DOP in the model include degradation of detritus, phytoplankton exudation and zooplankton excretion (Eq. 22). DOP is further remineralised to DIP by bacteria. We simulated this process, without explicitly involving bacteria. A time constant of about 200 days is used for direct transformation of DOP to DIP. P uptake in the model is regulated by the sum of DIP and DOP availability in a Michaelis-Menten term. DIP and DOP are taken up by Tri simultaneously. The half saturation constant of DIP uptake ($K_{\mathrm{DIP_t}}$) by Tri is assumed to be $0.4\,\mathrm{mmol\,m^{-3}}$, which is in the range of measured values in culture and field studies (0.2–$0.7\,\mathrm{mmol\,m^{-3}}$: Fu et al., 2005; Sohm and Capone, 2006; Sohm et al., 2008; Orchard et al., 2010). We used a K_{DIP} of $0.15\,\mathrm{mmol\,m^{-3}}$ (Sohm and Capone, 2006) for non-diazotrophic phytoplankton (Phy), thus representing the different competitiveness of Tri and Phy for DIP uptake. The half saturation constant for DOP uptake (K_{DOP}) by Tri is $0.18\,\mathrm{mmol\,m^{-3}}$, taken from Orchard et al. (2010). This differs from the model by Hood et al. (2001) in which the larger one of DIP and DOP is taken up by Tri and the same kinetics is used for the DIP and DOP uptake.

Measured P : N ratios in *Trichodesmium* vary from near the Redfield ratio of 1 : 16 to 1 : 125 (Karl et al., 1992; Letelier and Karl, 1996, 1998; Sañudo Wilhelmy et al., 2001; Fu et al., 2005; Hutchins et al., 2007). This argues for a flexible regulation of stoichiometry by *Trichodesmium* under different nutrient conditions. We introduced variable P : N ratios for each component in the ecosystem model. As a result, P uptake by Tri is a function of the sum of DIP and DOP in a Michaelis-Menten term and the actual internal P : N quota (Eq. 23 and 24).

2.1.3 Fe uptake

As in the model by Ye et al. (2009), organically complexed iron is assumed to be the only bioavailable iron. Fe-binding ligands are classified according to their binding strength. Their sources and decay are described as in Ye et al. (2009), except the production of strong ligands. Siderophore production has not been reported for *Trichodesmium* spp., but for other cyanobacterial such as *Synechococcus* (Wilhelm and Trick, 1994; Wilhelm et al., 1996). To represent a simple relationship between Fe limitation and ligand production, we assume, that both Tri and Phy produce strong ligands under Fe-depleted conditions. The production rate is regulated by their internal Fe : N ratios ($\mathrm{Q_{Fe}}$) (Eq. 20), respectively.

2.1.4 Loss term of Tri

To reproduce reasonable biomass and termination of phytoplankton blooms, loss processes need to be considered in models. These can be grazing and mortality. Hood et al. (2001) ignored the grazing on *Trichodesmium* and enhanced the mortality to lower modelled N_2 fixation rates.

Grazing on *Trichodesmium* has been rarely reported. Some *Trichodesmium* spp. are toxic to

calanoid and cyclopoid copepods, the major grazers in the oligotrophic ocean (Hawser et al., 1992). A specialised group of harpacticoid copepods is able to graze *Trichodesmium* (O'Neil and Roman, 1994), although their quantitative role in consumption of *Trichodesmium* is still unknown (Capone et al., 1997). However, Montoya et al. (2002) and McClelland et al. (2003) attributed the low δ^{15}N of zooplankton in the tropical North Atlantic to the consumption of newly fixed N by zooplankton.

In our model, loss of Tri is regulated by both mortality and grazing by zooplankton. We assume that Tri is less preferred by zooplankton than other phytoplankton (Phy) and introduce a grazing preference (β) to calculate different grazing rates for Phy and Tri (Eq. 7). The grazing preference of 0.1 for Tri results from a sensitivity study, in which the model is fitted to the observed magnitude of *Trichodesmium* concentrations by changing β (Sect. 2.2).

Trichodesmium in the model is not removed from surface waters by sinking. Instead of sinking, *Trichodesmium* is capable of ascending at several meters an hour (Walsby, 1978). We considered a positive buoyancy of $5\,\mathrm{m\ d^{-1}}$ which keeps Tri growing within the upper 50 m as mostly observed (Capone et al., 1997).

2.2 Sensitivity study with respect to the grazing preference factor β

We conducted the sensitivity study with 3 different values of the preference factor β (Tab. 1). Tri abundance is highly sensitive to the change of β and varies over four orders of magnitudes. Decreasing β from 0.1 to 0.05 results in an increase of Tri surface Chl concentration by a factor of 2–5. The highest Chl concentration, converted with a Chl : C ratio of 1 : 100 by weight, is 3-fold the concentrations of the satellite-derived cyanobacterial Chl a. Increasing β to 0.2 leads to a negligible Chl surface concentration of Tri, indicating a too strong grazing pressure. The Chl concentration of Tri in the study B presents a stable seasonal pattern (Fig. 3) and the surface values vary in the same range as the satellite data (Fig. 4).

Table 1: Sensitivity study with respect to the grazing preference factor β. The 4. column is surface Chl of Tri in each study relative to that in the study B.

study number	β	surface Tri Chl ($\mathrm{mg\,m^{-3}}$)	relative surface Tri Chl (-)
A	0.05	0–0.3	2–5
B	0.10	0–0.1	1
C	0.20	$0–5.7\times10^{-5}$	4×10^{-4}–2×10^{-3}

2.3 Satellite-derived Chl a and HPLC pigment data

We used satellite data of cyanobacterial chlorophyll a to constrain the modelled *Trichodesmium* biomass. One year data (from December 2007 to November 2008) of cyanobacterial Chl a concentration, including *Prochlorococcus*, was retrieved at $\pm\,5°$ latitude and longitude around the TENATSO station. To retrieve cyanobacterial chlorophyll a, satellite data of the sensor SCIAMACHY (Scanning Imaging Absorption Spectrometer for Atmospheric CHartographY) were analysed using the PhytoDOAS (Differential Optical Absorption Spectroscopy including phytoplankton optical signatures) method (Bracher et al., 2009). These cyanobacterial Chl a concentrations had been verified by comparisons to collocated cyanobacterial Chl a *in situ* data measured with HPLC technique and to data derived from the NASA Ocean Biogeochemical Model (NOBM, Gregg et al., 2003; Gregg

and Casey, 2007). These first comparisons of SCIAMACHY PhytoDOAS indicate that the range of SCIAMACHY different phytoplankton group's Chl a is in a comparable range with observations, although a thorough validation still needs to be completed (Bracher et al., 2009).

HPLC (High Performance Liquid Chromatography) can be used to differentiate cyanobacterial by detecting specific marker pigments. For instance, zeaxanthin is a marker pigment for all cyanobacterial, while divinyl-Chl-a is only typical for *Prochlorococcus*. By applying the Chemtax program (Mackey et al., 1996) and the input matrix typical for the tropical Atlantic (Veldhuis and Kraay, 2004) to the HPLC data, Chl a concentrations of cyanobacterial excluding *Prochlorococcus* were determined. Another difference between *Prochlorococcus* and other cyanobacterial is that *Prochlorococcus* has no phycobilins. Therefore, we use the term of phycobilin-containing cyanobacterial to refer to cyanobacterial excluding *Prochlorococcus*. The HPLC data measured close to TENATSO show a fraction of phycobilin-containing cyanobacterial in total cyanobacterial up to 90 % in November 2007 and less than 12 % in May 2008. We used this satellite-derived cyanobacterial Chl a as the upper limit for *Trichodesmium* Chl a in our model tuning. As *Trichodesmium* is contained in phycobilin-containing cyanobacterial, we adjusted this upper limit in May and November according to the fraction of phycobilin-containing cyanobacterial. The upper limit is reached in the phase of Tri blooms (September to November), while Tri Chl a is significantly lower than the satellite estimates during the rest of the year.

Total Chl a in the model, the sum of Phy and Tri Chl a, is compared to the satellite data of total Chl a. Daily values of marine phytoplankton Chl a concentrations were taken from the merged daily Full Product Set (FPS) of the GlobColour Archive (`hermes.acri.fr`). This data set is based on the merging of MERIS, SeaWiFS and MODIS level-2 data with the GSM model and algorithm, developed by Maritorena and Siegel (2005) over the whole globe. The best resolution of the data is 4.6 km. The GlobColour Chl a product has undergone an extensive validation based on a validation protocol (ACRI-STLOV, 2006) derived from the Sensor Intercomparison for Marine Biological and Interdisciplinary Ocean Studies (SIMBIOS) protocol (`oceancolor.gsfc.nasa.gov/MEETINGS/simbios_ref.html`). Results of this validation are published in Maritorena et al. (2010).

For comparing the model to these satellite data, we calculated surface chlorophyll concentration of Tri from its N content, assuming a mean Chl : C ratio by weight of 1 : 100 (Breitbarth et al., 2008; Kranz et al., 2010) and a C : N ratio of 6.3 : 1 (LaRoche and Breitbarth, 2005). Phy chlorophyll concentration is calculated using the empirical Chl : C ratio from Cloern et al. (1995) and the Redfield C : N ratio of 106 : 16.

3 Results and discussion

3.1 Modelled seasonal and vertical distribution of *Trichodesmium*

The modelled total phytoplankton blooms in spring and has a deep chlorophyll maximum (DCM) around 70 m. Its seasonality is similar to that described in Ye et al. (2009). The modelled surface total Chl a concentration varies within the range of the satellite data (Fig. 2) and of direct observations (Ye et al., 2009). In contrast, Tri displays a different seasonality with negligibly low concentrations in spring and summer and high concentrations in autumn and early winter (Fig. 3). The highest concentrations occur between September and November and range interannually from 0.02 to 0.35 mmol N m^{-3}. Tri grows mainly in the upper 40 m and its concentration gradually decreases with depth. This pattern is in agreement with the observed high abundance of *Tri-*

chodesmium from August to November and absence in spring in the upwelling region off Northwest Africa (Vallespinos, 1985).

There are few direct observations of *Trichodesmium* near TENATSO. Modelled Tri surface concentrations vary in the same magnitude as the observations (Capone et al., 1997; Carpenter et al., 2004; Davis and McGillicuddy, 2006; Fernández et al., 2010), considering the uncertainty by converting the measured abundance in trichomes L^{-1} or colonies L^{-1} into biomass L^{-1}.

The modelled surface Tri Chl a concentrations from December 2007 to December 2008 are compared to the satellite-derived cyanobacterial chlorophyll a concentrations (Fig. 4). The highest values in the satellite data near TENATSO were used as the upper limit of Tri Chl a to constrain the model. It is therefore not surprising, that the maximal concentrations of Tri Chl a vary within the range of the satellite data. However, both the satellite data and modelled surface Chl a demonstrate peaks in September/October and smaller values in spring and summer, presenting good model-data agreement of *Trichodesmium* seasonality.

3.2 Modelled N_2 fixation rates

The modelled surface N_2 fixation rates vary from near zero in spring and summer to around 10–100 μ mol N m^{-3} d^{-1} in October (Fig. 5). The rates integrated for the mixed layer have a similar seasonality and the maxima in October range from 150 to 600 μmol N m^{-2} d^{-1} (Fig. 5). N_2 fixation rates in the eastern tropical North Atlantic has been rarely measured and the values are in a range from 1–24 μmol N m^{-3} d^{-1} in October and November (Mills et al., 2004; Voss et al., 2004; Mark Moore et al., 2009). N_2 fixation rates integrated for the mixed layer are measured more often during spring and winter cruises and vary from a few to 180 μmol N m^{-2} d^{-1} (Mills et al., 2004; Voss et al., 2004; Mark Moore et al., 2009; Capone et al., 2005; Staal et al., 2007; Falcon et al., 2004; Agusti et al., 2001). Although these observations barely cover the modelled years or the months with highest fixation rates, the modelled fixation rates in spring and winter are in the same order of magnitude as the measurements. The modelled fixation activity can be compared more quantitatively, when direct observations of the seasonality of N_2 fixation at TENATSO become available.

3.3 Factors determining the seasonal and vertical distribution of Tri

The seasonal pattern of Tri biomass is predominantly determined by the seasonal variability of temperature, showing a maximum in August and September (Fig. 6), because of the strong growth dependence of Tri on temperature (Sect. 2.1.1).

DIP and DOP show completely different distribution patterns in the model (Figure 7), caused by their different sources. DIP in the upper ocean is depleted by algal growth and then restored mainly by winter mixing. The major source of DOP in the model is phytoplankton release. Therefore, DOP concentrations follow the pattern of Phy with higher values during spring and a subsurface maximum at the depth of deep chlorophyll maximum (DCM: between 70 and 80 m). In surface waters, DOP is up to 2 orders of magnitudes higher than DIP, consistent with the observation by Torres-Valdès et al. (2009). Based on the vertical distribution of DIP and DOP, Tri growth is essentially supported by DOP in surface waters, resulting a considerable depletion of DOP from September to November.

Modelled surface Fe concentrations compare well with the observations near TENATSO (Ye et al., 2009). Modelled bioavailable iron in surface waters shows higher concentration during win-

ter mixing (Fig. 8). Consumed by phytoplankton during spring blooms, its concentration decreases with time and reaches a minimum of $0.1\,\mu\mathrm{mol\,m^{-3}}$ in late summer and autumn, when *Trichodesmium* starts to bloom. Between 50 and 90 m, bioavailable iron has a subsurface maximum caused by Fe release by remineralisation of organic matter.

Comparing the limiting strength of light, P and Fe on Tri growth rate, the model presents an interesting pattern of the interplay of these factors in controlling the seasonal and vertical distribution of Tri (Fig. 9). In late summer, Tri blooms are initialized by the increase of temperature. After the spring blooms of Phy, phosphorus, particularly DOP availability, is relatively high, whereas Fe supply becomes short. The high Fe requirement of diazotrophic growth elevates further the depletion of Fe, leading to the dominance of Fe limitation in the upper 20 m in the beginning of Tri blooms. Massive Fe input is brought by Saharan dust events occurring often in winter/spring and autumn at TENATSO (Ye et al., 2009). This atmospheric Fe supply might alleviate Fe shortage for Tri growth and shifts the pattern of the effective limitation from Fe to P in September. The trend of Fe limitation is more apparent in the first 4–5 model years (2000–2004) which are used as spin-up. From 2005 to 2008, the Fe limitation is much weaker, because the modelled concentration of organic complexed iron in surface waters increases with time gradually. Below the upper 15–20 m, Tri growth is strongly light-limited during the whole year (see also Fig. 10). Tri bloom is terminated in December by a decrease of temperature to values lower than 22°C.

This pattern of the effective limitation indicates that growth of *Trichodesmium* is controlled in the upper water layer by Fe and P at similar strength, and in lower water layer uniformly by light. Dust deposition or interactions with other biota can shift the pattern of the effective limitation between Fe and P temporally. This model result is supported by field studies in the North Atlantic. Studies in the central (Sañudo Wilhelmy et al., 2001) and western North Atlantic (Wu et al., 2000) suggested P limitation of diazotrophy in spring during the period of highest dust depositions, whereas Mills et al. (2004) found that N_2 fixation in the eastern tropical North Atlantic was co-limited by Fe and P during their cruise during October and November 2002.

3.4 Role of dust deposition in supporting N_2 fixation and primary production

The global distribution pattern of N_2 fixation is often attributed to the spatial and temporal variability of dust deposition (Gruber and Sarmiento, 1997; Mark Moore et al., 2009). TENATSO is located in a region strongly influenced by Saharan dust events which are characterized by episodic depositions with high frequency in late winter and spring (January–April) as well as in autumn (September and October) (Fig. 11). The temporal variability of dust deposition plays an important role in impacting Fe bioavailability and thus regulating primary production. In the model, this impact is described in two pathways: on the one hand dust deposition supplies bioavailable Fe for Phy growth and on the other hand it meets the high Fe requirement of Tri growth which enhances subsequently the bioavailability of N for non-diazotrophic phytoplankton growth. In order to study the effects of dust deposition and N_2 fixation on primary productivity separately, we compared the standard (R_0) to a run without N_2 fixation (R_{nf}) and to a run without dust deposition (R_{nd}).

3.4.1 Impact of N_2 fixation

In R_{nf}, Tri dies off after the first model year, outcompeted by Phy in DIN uptake. In R_0 as well as in R_{nf}, the effective limitation of Phy growth is N limitation in the upper 70 m and light limitation below. From September to November, Phy concentrations in the upper 60 m are up to 25 % lower

in R_{nf} than in R_0 in autumn (Fig. 12), which can be well explained by the missing N supply by Tri N_2 fixation. Below that, higher N supply from deeper water relieves N limitation of Phy growth. Light limitation of Phy here is lower because of missing Tri and lower Phy concentrations in surface waters. This results in higher Phy concentrations below 60 m in R_{nf}.

The total primary production in R_0 is on average about 4 % higher than in R_{nf} (Fig. 13, the black and red curves). The difference between the two runs varies seasonally and interannually. It is negligible during spring and early summer and becomes larger rapidly in August. After reaching a maximum up to 25 % in October, the difference lessens again. The seasonal variation of the difference is mainly caused by Tri growth. However, because of the substantially lower abundance and shorter bloom period of Tri compared to Phy, its direct contribution to total primary productivity and to organic matter exported from the euphotic zone is generally small (annually averaged ∼4 %).

The comparison of R_0 and R_{nf} indicates that *Trichodesmium* needs diazotrophy to maintain its growth. The N input by N_2 fixation alleviates the N limitation of Phy during autumn and early winter significantly. Considering the main DOP source — Phy release, the model reveals an associated coexistence of Phy and Tri: on the one hand, Tri autumn bloom benefits from the DOP release during Phy spring bloom and the N input by N_2 fixation in autumn supports a moderate abundance of Phy, and on the other hand they also compete for light and Fe.

3.4.2 Impact of dust deposition

In the model run without dust deposition (R_{nd}), Tri also dies off after the first model year, caused by too strong Fe limitation. This indicates that the episodic dust events are necessary to support the observed occurrence of *Trichodesmium* at TENATSO. In R_{nd}, Phy abundance above the DCM is up to 40 % lower than in R_0 (Fig. 14). Phy growth is most limited by Fe in surface waters and by light below the DCM. The difference of the limitation pattern to R_0 indicates that higher Phy concentrations in R_0 are mainly caused by higher Fe availability. At the depth of DCM and below that, Phy in R_0 is up to 20 % lower caused by enhancing light limitation, particularly in November and December when Tri occurs in high concentrations.

Averaged over the whole year, total primary production in R_{nd} is ∼35 % lower than in R_0 (Fig. 13, the black and green curves). The difference during spring and summer (∼30 %) is mainly explained by Fe-supported Phy growth. Tri blooms and subsequently higher Phy abundance supported by newly fixed N enlarge the difference between the two runs in autumn and early winter to over 50 %. On average, ∼85 % of the exported organic matter from the euphotic zone (defined here as the sinking of organic N over the 100 m depth) is contributed to dust deposition and diazotrophy supported by it, with higher values in winter and lower values in summer.

3.4.3 Comparison with observations and other estimates

There have been only a few direct measurements or estimates of the role N_2 fixation at TENATSO. For the Azores Front region, Bourbonnais et al. (2009) estimated that ∼5 % of N required for primary production could be provided by N_2 fixation. Another study for the Caribbean Sea which is characterized by very high N_2 fixation activity suggested that diazotrophy accounts for ∼20 % of primary production in surface waters (Carpenter and Price, 1977). Our estimate of ∼4 % from the comparison of R_0 and R_{nf} is close to the former. However, we might underestimate the contribution of N_2 fixation, because firstly, we only estimated the contribution of *Trichodesmium*, not of the

entire diazotroph community at TENATSO; and secondly, the difference between R_0 and R_{nf} might be smaller than the real effect of N_2 fixation, because Phy in R_{nf} experiences better light condition without the competition with Tri.

Bourbonnais et al. (2009) suggested that 31–41 % of the export production in the Azores Front region could be explained by N_2 fixation. A fraction up to 50 % of export production is attributed to N_2 fixation in the subtropical Pacific gyre and in the oligotrophic North Atlantic (Karl et al., 1997; Deutsch et al., 2007; Gruber and Sarmiento, 1997). Our estimated annual average of N_2 fixation contribution to organic carbon export is much lower than these estimates. However, the modelled contribution of *Trichodesmium* blooms of 15–40 % is of a comparable size, indicating that the contribution of other diazotrophs which have different seasonality, should be taken into account for further comparisons.

3.4.4 Role of the unicellular cyanobacterial

Recently reported high abundances and estimated N_2 fixation rates by unicellular cyanobacterial in the North Pacific suggest an important contribution of unicellular cyanobacterial to the global N budget (Zehr et al., 2001; Montoya et al., 2004). In the North Atlantic, abundance and N_2 fixation activity of unicellular cyanobacterial are rarely measured. Detection of *nifH* gene copies shows that the unicellular cyanobacterial group A is the most dominant group by numbers during the spring cruises in a region northwest of the Cape Verde Islands and the distribution of filamentous and group A is well separated as a function of temperature (Langlois et al., 2008). Goebel et al. (2010) found, during a cruise across the tropical Atlantic in June 2006, that the unicellular cyanobacterial group A dominated the cooler waters in the eastern North Atlantic and *Trichodesmium* was more abundant in the warmer waters of the western Atlantic. A temporal variability of the diazotroph community composition is also found in the North Pacific subtropical gyre: in the late winter and early spring, unicellular diazotrophs showed high abundance within the diazotroph community, while filamentous diazotrophs occurred mostly in summer (Church et al., 2009). These observations support the modelled low concentration of Tri in spring and early summer controlled by temperature, however, they also indicate that our estimates of annually newly fixed N could miss a considerable fraction contributed by unicellular diazotrophs probably occurring from late winter to early summer. During spring cruises, the number of *nifH* gene copies of unicellular cyanobacterial was reported 1-2 orders of magnitudes higher than that of *Trichodesmium* near TENATSO (Langlois et al., 2008). We estimated the possible missing N_2 fixation in spring from the modelled N_2 fixation rates of *Trichodesmium*, assuming a linear relationship between *nifH* gene copies and N_2 fixation rate. Unicellular diazotrophs could contribute 20–130 μ mol m^{-2} d^{-1} from January to May at TENATSO.

4 Conclusions

This study investigates how different environmental factors control the abundance and seasonal as well as interannual variability of *Trichodesmium* at TENATSO. In a one-dimensional ecosystem model, the rate of N_2 fixation by *Trichodesmium* is made dependent on the availability of DIN and the growth rate of *Trichodesmium*. Light, temperature, phosphorus and iron are taken into account in controlling the growth rate. A grazing preference, much smaller than that for other phytoplankton, is introduced to describe the loss process of *Trichodesmium*. Modelled *Trichodesmium*

chlorophyll concentration is compared to the satellite-derived cyanobacterial Chl a concentration to constrain the model.

The modelled seasonality of *Trichodesmium* abundance is in agreement with the observation of the high abundance from August to November and absence in spring (Vallespinos, 1985) and with the satellite-derived seasonal trend of cyanobacterial Chl a concentrations. This seasonal variability is explained in the model primarily by temperature. The growth of *Trichodesmium* is controlled by P and Fe together, with more Fe-controlled at the beginning of its bloom and increasingly P-controlled during its bloom. The modelled limitation pattern underlines the interplay of mutual benefit and competition between *Trichodesmium* and other phytoplankton: the autumn bloom of *Trichodesmium* provides more fixed N supporting growth of other phytoplankton, and at the same time *Trichodesmium* meets its P demand by taking up DOP mainly released during phytoplankton spring bloom. Fe consumption by other phytoplankton earlier in a year accelerates Fe limitation of *Trichodesmium* in late summer, whereas *Trichodesmium* bloom in surface waters reduces phytoplankton abundance deeper in the water column by light limitation.

Running the model with and without dust deposition, we conclude that on the one hand, dust deposition provides a high amount of bioavailable Fe for all phytoplankton including *Trichodesmium* and enhances primary production significantly; on the other hand, the variability of dust deposition also limits their growth rates and accordingly primary productivity. In our study, the pathway in which atmospheric Fe supply enhances N_2 fixation which in turn provides new fixed N for further primary production, is only seasonally important. This is caused by the high abundance of *Trichodesmium* at TENATSO only during its autumn blooms and the absence of other diazotrophs in this model. For more realistic estimates of the contribution of N_2 fixation in the tropical eastern North Atlantic to the global N budget, the diazotrophic community composition needs to be studied more closely and the role of non-filamentous diazotrophs should be taken into account.

5 Acknowledgements

This work is a contribution to the project SOPRAN (Surface Ocean Processes in the ANtropocene), which is funded by the German Federal Ministry of Education and Research (BMBF project 03F0462C). Funding for A. Bracher and B. Taylor has been supplied by the Helmholtz Innovative Network Fund. We thank DLR, ESA and the SCIAMACHY Quality Working Group for SCIAMACHY level-1 data. We are grateful to NASA and ESA, particularly to the GlobColour project, for processing and supplying Satellite total Chl a concentrations. We also like to thank the crew, principal investigators and other scientists on board the RV Polarstern cruises ANTXXIV-1, ANTXXIV-4 and ANTXXV-1 for their support. Finally, we thank sincerely the Japan Meteorological Agency Climate Data Assimilation System (JCDAS) for the free access to data, and I. Peeken for kindly providing unpublished data.

Appendix — Model equations

The rate of change of biogeochemical variables can be separated into a biogeochemical and a physical part:

$$\frac{\partial}{\partial t}X = BIO + M(X,z) \tag{1}$$

where advection and mixing are taken into account in the physical part $M(X,z)$. Here M stands for the advection and mixing operator and X is the mixed compound. The biogeochemical rate of change is described by corresponding sources minus sinks.

Presentation of the equations is grouped into those effecting the N-, P- and Fe-cycle.

A N-cycle

The change of the biological variables DIN, Phy, Z and D (in $\mu\mathrm{mol\,N\,L^{-1}}$) is described as in Ye et al. (2009), except for additional terms due to the influence of Tri.

$$\begin{aligned}\frac{\partial}{\partial t}DIN &= \gamma_d\, f_T\, (D + A_{or}) + \gamma_{zb}\, f_T\, Z + \gamma_p\, f_T\, Phy + \gamma_t\, f_T\, Tri \\ &\quad + \gamma_l\, f_T\, (L_{str} + L_{we}) - \mu\, Phy - k^{DIN}_{\mathrm{upt\_t}}\, Tri + M(DIN,z)\end{aligned} \tag{2}$$

where the uptake of DIN by Tri ($k^{\mathrm{DIN}}_{\mathrm{upt\_t}}$) is the smaller of the actual growth rate μ_{t} and the temperature- and DIN-limited growth rate μ^{DIN}_{t}:

$$k^{DIN}_{upt\_t} = \min\left(\mu_{\mathrm{t}}, \mu^{DIN}_{\mathrm{t}}\right) \tag{3}$$

$$\mu^{DIN}_t = \frac{DIN}{DIN + K_{\mathrm{N_t}}}\, f^t_T\, \mu_{\mathrm{max_t}} \tag{4}$$

N_2 fixation is the difference between Tri growth in N units and N uptake:

$${N_2}^{fix} = \left(\mu_t - k^{DIN}_{upt\_t}\right)\, Tri \tag{5}$$

μ_t is described in Eq. 19.

The equation for phytoplankton is slightly changed because Tri affects the grazing by zooplankton.

$$\frac{\partial}{\partial t}Phy = (\mu - \gamma_p\, f_T)\; Phy - f_G\, Z\, \frac{Phy}{Phy + \beta\, Tri} - \gamma_{p^2}\, Phy^2 - r_L\, \gamma_{lp}\, f_Q\, Phy + M(Phy,z) \tag{6}$$

The grazing function f_G depends on the maximal grazing rate $g_{\max}$, the prey capture rate ϵ, the grazing preference β and the prey concentrations:

$$f_G = \frac{g_{\max}\, \epsilon\, (Phy + \beta\, Tri)^2}{g_{\max} + \epsilon\, (Phy + \beta\, Tri)^2} \tag{7}$$

The dependence of Phy growth on light, temperature, dissolved N and Fe are discussed in Ye et al. (2009). In this model, its growth rate is controlled additionally by the internal P : N ratio Q^P_{PO}:

$$f^p_{PO}=\frac{Q^P_{\mathrm{PO}}-Q^P_{\mathrm{PO\_min}}}{Q^P_{\mathrm{PO}}} \tag{8}$$

and the actual growth rate of Phy (μ) is determined by the smaller of the function of light (f^p_{PAR}), Fe (f^p_{Fe}) and P limitation (f^p_{PO}).

$$\mu=\min\left(f^p_{PAR}, f^p_{Fe}, f^p_{PO}\right)\ f^p_T\,\mu_{\max} \tag{9}$$

Zooplankton is also affected by grazing on Tri:

$$\frac{\partial}{\partial t}Z=\gamma_{za}\,f_G\,Z-\gamma_{zb}\,f_T\,Z-\gamma_{z^2}\,Z^2+M(Z,z) \tag{10}$$

Detritus is subdivided into two size classes: D_{S} for small and D_{L} for large detritus. Their different sources and aggregation behavior are described in detail in Ye et al. (2009).

$$\begin{aligned}\frac{\partial}{\partial t}D_{\mathrm{S}} &= \gamma_{p^2}\,Phy^2+\gamma_{t^2}\,Tri^2+(1-\gamma_{za})\ f_G\,Z- \\ &\quad (\gamma_d+r_L\,\gamma_{ld})\ f_T\,D_{\mathrm{S}}-k_{coag2}\,D_{\mathrm{S}}\ (D_{\mathrm{S}}\,r_{\mathrm{m:N}}+A_{\mathrm{S}}) \\ &\quad -k_{coag3}\,D_{\mathrm{S}}\ (D_{\mathrm{L}}\,r_{\mathrm{m:N}}+A_{\mathrm{L}})-w_s\,\frac{\partial D_{\mathrm{S}}}{\partial z}+M(D_{\mathrm{S}},z)\end{aligned} \tag{11}$$

$$\begin{aligned}\frac{\partial}{\partial t}D_{\mathrm{L}} &= \gamma_{z^2}\,Z^2-(\gamma_d+r_L\,\gamma_{ld})\ f_T\,D_{\mathrm{L}}+k_{coag2}\,D_{\mathrm{S}}\ (D_{\mathrm{S}}\,r_{\mathrm{m:N}}+A_{\mathrm{S}}) \\ &\quad +k_{coag3}\,D_{\mathrm{S}}\ (D_{\mathrm{L}}\,r_{\mathrm{m:N}}+A_{\mathrm{L}})-w_l\,\frac{\partial D_{\mathrm{L}}}{\partial z}+M(D_{\mathrm{L}},z)\end{aligned} \tag{12}$$

Temperature dependence of Phy growth and D remineralisation (f_T) differs from that of Tri growth (f^t_T, Eq. 15):

$$f_T=0.9\,C^{T(z)}_{ref} \tag{13}$$

where $T(z)$ is temperature in °C at given depth.

The change of Tri is described as growth - mortality - grazing - ligand production + positive buoyancy:

$$\begin{aligned}\frac{\partial}{\partial t}Tri &= (\mu_t-\gamma_t\,f_T)\ Tri-f_G\,Z\,\frac{\beta\,Tri}{P+\beta\,Tri}-\gamma_{t^2}\,Tri^2 \\ &\quad -r_L\,\gamma_{lp}\,f^t_Q\,Tri+w_t\,\frac{\partial Tri}{\partial z}+M(Tri,z)\end{aligned} \tag{14}$$

where w_t is the upward velocity of Tri due to the positive buoyancy. The growth rate of Tri (μ_t) is not limited by the concentration of dissolved N (DIN) but by temperature, light, Fe and P:

$$f^t_T=\frac{\left(2.32\,10^{-5}\,T\,(z)^4-2.52\,10^{-3}\,T\,(z)^3+9.75\,10^{-2}\,T\,(z)^2-1.58\,T\,(z)+9.12\right)}{0.25} \tag{15}$$

Here, we divide the function by Breitbarth et al. (2007) by $0.25\,\mathrm{d}^{-1}$ which is their measured maximal growth rate, to keep the maximum of f_T^t by 1. The function for light dependence stems from Breitbarth et al. (2008):

$$f_{PAR}^t = \tanh\left(\frac{\alpha_t\, PAR}{\mu_{\max_\mathrm{t}}}\right) \tag{16}$$

Dependence of growth rate on Fe and P is described by the actual and maintenance internal Fe : N and P : N ratios:

$$f_{Fe}^t = \frac{Q_\mathrm{Fe}^{Tri} - Q_\mathrm{Fe\_min}^{Tri}}{Q_\mathrm{Fe}^{Tri}} \tag{17}$$

$$f_{PO}^t = \frac{Q_\mathrm{PO}^{Tri} - Q_\mathrm{PO\_min}^{Tri}}{Q_\mathrm{PO}^{Tri}} \tag{18}$$

Finally, the actual growth rate of Tri is a product of the temperature function, the maximal growth rate and the minimum of the function for light, iron and phosphorus dependence:

$$\mu_t = \min\left(f_{PAR}^t, f_{PO}^t, f_{Fe}^t\right)\, f_T^t\, \mu_{\max_\mathrm{t}} \tag{19}$$

Fe-binding ligand production is regulated by the internal Fe : N ratio:

$$f_Q^t = \frac{Q_\mathrm{Fe\_max}^{Tri} - Q_\mathrm{Fe}^{Tri}}{Q_\mathrm{Fe\_max}^{Tri}} \tag{20}$$

where $Q_\mathrm{Fe\_max}^{Tri}$ is the maximal cellular Fe quota.

B P-cycle

Two types of dissolved P are considered as nutrient source–dissolved inorganic P DIN and dissolved organic P DOP:

$$\frac{\partial}{\partial t} DIP = \gamma_{dop}\, f_T\, DOP - k_\mathrm{upt\_p}^{DIN} - k_\mathrm{upt\_t}^{DIN} + M(DIP, z) \tag{21}$$

$$\begin{aligned} \frac{\partial}{\partial t} DOP &= \gamma_d\, f_T\, (D_\mathrm{SPO} + D_\mathrm{LPO}) + \gamma_{zb}\, f_T\, Z_\mathrm{PO} + \gamma_p\, f_T\, P_\mathrm{PO} \\ &\quad + \gamma_t\, f_T\, Tri_\mathrm{PO} - \gamma_{dop}\, f_T\, DOP - k_\mathrm{upt\_t}^{DOP} + M(DOP, z) \end{aligned} \tag{22}$$

The internal P : N ratio and availability of P source determine the uptake of DIN and DOP by Tri:

$$k_\mathrm{upt\_t}^{DIP} = \frac{DIP}{DIP + K_{\mathrm{DIP_t}}}\, \frac{\tanh\frac{\left(Q_\mathrm{PO\_max}^{Tri} - Q_\mathrm{PO}^{Tri}\right) 10}{Q_\mathrm{PO\_max}^{Tri} - Q_\mathrm{PO\_min}^{Tri}}}{\tanh(10)}\, \mu_{\max_\mathrm{t}}\, Tri \tag{23}$$

The term of hyperbolic tangent ensures that the uptake rate decreases rapidly while the actual P : N quota approaches the maximal P : N ratio. DIP uptake by Phy is described by the same function but the variables and parameters are changed correspondingly for Phy.

$$k^{DOP}_{\mathrm{upt\_t}}=\frac{DOP}{DOP+K_{\mathrm{DOP}}}\;\frac{\tanh\frac{\left(Q^{Tri}_{\mathrm{PO\_max}}-Q^{Tri}_{\mathrm{PO}}\right)10}{Q^{Tri}_{\mathrm{PO\_max}}-Q^{Tri}_{\mathrm{PO\_min}}}}{\tanh\left(10\right)}\,\mu_{\max_{\mathrm{t}}}\,Tri \tag{24}$$

The evolution of the respective P concentrations P_{PO}, Tri_{PO}, Z_{PO} and D_{PO} is described by the same processes for Phy, Tri, Z and D.

$$\frac{\partial}{\partial t}P_{\mathrm{PO}}=k^{DIP}_{\mathrm{upt\_p}}-\gamma_p\,f_T\,P_{\mathrm{PO}}-Q^{P}_{\mathrm{PO}}\,\left(f_G\,Z\,\frac{Phy}{Phy+\beta\,Tri}+\gamma_{p^2}\,Phy^2\right)+M(P_{\mathrm{PO}},z) \tag{25}$$

$$\begin{aligned}\frac{\partial}{\partial t}Tri_{\mathrm{PO}} &= k^{DIP}_{upt\_t}+k^{DOP}_{upt}-Q^{Tri}_{\mathrm{PO}}\left(f_G\,Z\,\frac{\beta\,Tri}{Phy+\beta\,Tri}+\gamma_{t^2}\,Tri^2\right)\\ &\quad -\gamma_t\,f_T\,Tri_{\mathrm{PO}}+w_t\,\frac{\partial Tri_{\mathrm{PO}}}{\partial z}+M(Tri_{\mathrm{PO}},z)\end{aligned} \tag{26}$$

$$\begin{aligned}\frac{\partial}{\partial t}Z_{\mathrm{PO}} &= \left(Q^{P}_{\mathrm{PO}}\,\frac{P}{P+\beta\,Tri}+Q^{Tri}_{\mathrm{PO}}\,\frac{Tri}{P+\beta\,Tri}\right)\,\gamma_{za}\,f_G\,Z\\ &\quad -\gamma_{zb}\,f_T\,Z_{\mathrm{PO}}-Q^{Z}_{\mathrm{PO}}\,\gamma_{z^2}\,Z^2+M(Z_{\mathrm{PO}},z)\end{aligned} \tag{27}$$

$$\begin{aligned}\frac{\partial}{\partial t}D_{\mathrm{SPO}} &= Q^{P}_{\mathrm{PO}}\,\left(\gamma_{p^2}\,Phy^2+(1-\gamma_{za})\;f_G\,\frac{Phy}{Phy+\beta\,Tri}\,Z\right)\\ &\quad +Q^{Tri}_{\mathrm{PO}}\,\left(\gamma_{t^2}\,Tri^2+(1-\gamma_{za})\;f_G\,\frac{Tri}{Phy+\beta\,Tri}\,Z\right)\\ &\quad -\gamma_d\,f_T\,D_{\mathrm{SPO}}-k_{coag2}\,D_{\mathrm{SPO}}\,\left(D_{\mathrm{S}}\,r_{\mathrm{m:N}}+A_{\mathrm{S}}\right)\\ &\quad -k_{coag3}\,D_{\mathrm{SPO}}\,\left(D_{\mathrm{L}}\,r_{\mathrm{m:N}}+A_{\mathrm{L}}\right)-w_s\,\frac{\partial D_{\mathrm{SPO}}}{\partial z}+M(D_{\mathrm{SPO}},z)\end{aligned} \tag{28}$$

$$\begin{aligned}\frac{\partial}{\partial t}D_{\mathrm{LPO}} &= Q^{Z}_{\mathrm{PO}}\gamma_{z^2}\,Z^2-\gamma_d\,f_T\,D_{\mathrm{LPO}}+k_{coag2}\,D_{\mathrm{SPO}}\,\left(D_{\mathrm{S}}\,r_{\mathrm{m:N}}+A_{\mathrm{S}}\right)\\ &\quad +k_{coag3}\,D_{\mathrm{SPO}}\,\left(D_{\mathrm{L}}\,r_{\mathrm{m:N}}+A_{\mathrm{L}}\right)-w_l\,\frac{\partial D_{\mathrm{LPO}}}{\partial z}+M(D_{\mathrm{LPO}},z)\end{aligned} \tag{29}$$

C Fe-cycle

The Fe cycle is based on the processes described in Ye et al. (2009). The interactions of Tri and other components in the ecosystem model are added correspondingly.

$$\frac{\partial}{\partial t}P_{\mathrm{Fe}}=k^{\mathrm{Fe}}_{\mathrm{upt\_p}}-Q^{P}_{\mathrm{Fe}}\left(f_G\,\frac{Phy}{Phy+\beta\,Tri}\,Z+\gamma_{p^2}\,Phy^2\right)-\gamma_p\,f_T\,P_{\mathrm{Fe}}+M(P_{\mathrm{Fe}},z) \tag{30}$$

$$\begin{aligned}\frac{\partial}{\partial t}Tri_{\mathrm{Fe}} &= k^{\mathrm{Fe}}_{\mathrm{upt\_t}}-Q^{Tri}_{\mathrm{Fe}}\left(f_G\,Z\,\frac{\beta\,Tri}{P+\beta\,Tri}+\gamma_{t^2}\,Tri^2\right)\\ &\quad -\gamma_t\,f_T\,Tri_{\mathrm{Fe}}+w_t\,\frac{\partial Tri_{\mathrm{Fe}}}{\partial z}+M(Tri_{\mathrm{Fe}},z)\end{aligned} \tag{31}$$

$$\frac{\partial}{\partial t} Z_{\mathrm{Fe}} = \left(Q_{\mathrm{Fe}}^{P} \frac{Phy}{Phy+\beta\, Tri} + Q_{\mathrm{Fe}}^{Tri} \frac{Tri}{Phy+\beta\, Tri} \right) \gamma_{za}\, f_G\, Z - \gamma_{zb}\, f_T\, Z_{\mathrm{Fe}} - Q_{\mathrm{Fe}}^{Z}\, \gamma_{z^2}\, Z^2 + M(Z_{\mathrm{Fe}}, z) \tag{32}$$

$$\begin{aligned} \frac{\partial}{\partial t} D_{\mathrm{SFe}} = {} & Q_{\mathrm{Fe}}^{P} \left(\gamma_{p^2}\, Phy^2 + (1-\gamma_{za})\; f_G\, \frac{Phy}{Phy+\beta\, Tri}\, Z \right) \\ & + Q_{\mathrm{Fe}}^{Tri} \left(\gamma_{t^2}\, Tri^2 + (1-\gamma_{za})\; f_G\, \frac{Tri}{Phy+\beta\, Tri}\, Z \right) \\ & - k_{coag2}\, D_{\mathrm{SFe}}\, (D_{\mathrm{S}}\, r_{\mathrm{m:N}} + A_{\mathrm{S}}) - k_{coag3}\, D_{\mathrm{SFe}}\, (D_{\mathrm{L}}\, r_{\mathrm{m:N}} + A_{\mathrm{L}}) \\ & - \gamma_d\, f_T\, D_{\mathrm{SFe}} - w_s\, \frac{\partial D_{\mathrm{SFe}}}{\partial z} + M(D_{\mathrm{SFe}}, z) \end{aligned} \tag{33}$$

$$\begin{aligned} \frac{\partial}{\partial t} D_{\mathrm{LFe}} = {} & Q_{\mathrm{Fe}}^{Z} \gamma_{z^2}\, Z^2 - \gamma_d\, f_T\, D_{\mathrm{LFe}} + k_{coag2}\, D_{\mathrm{SFe}}\, (D_{\mathrm{S}}\, r_{\mathrm{m:N}} + A_{\mathrm{S}}) \\ & + k_{coag3}\, D_{\mathrm{SFe}}\, (D_{\mathrm{L}}\, r_{\mathrm{m:N}} + A_{\mathrm{L}}) - w_l\, \frac{\partial D_{\mathrm{LFe}}}{\partial z} + M(D_{\mathrm{LFe}}, z) \end{aligned} \tag{34}$$

Fe uptake by Phy and Tri is described analogically but presenting different Fe requirement and uptake ability:

$$k_{\mathrm{upt\_p}}^{\mathrm{Fe}} = \frac{FeL}{FeL + K_{\mathrm{Fe}}}\, \frac{tanh \frac{\left(Q_{\mathrm{Fe\_max}}^{P} - Q_{\mathrm{Fe}}^{P}\right) 10}{Q_{\mathrm{Fe\_max}}^{P} - Q_{\mathrm{Fe\_min}}^{P}}}{tanh 10}\, \mu_{\max}\, Phy \tag{35}$$

$$k_{\mathrm{upt\_t}}^{\mathrm{Fe}} = \frac{FeL}{FeL + K_{\mathrm{Fe_t}}}\, \frac{tanh \frac{\left(Q_{\mathrm{Fe\_max}}^{Tri} - Q_{\mathrm{Fe}}^{Tri}\right) 10}{Q_{\mathrm{Fe\_max}}^{Tri} - Q_{\mathrm{Fe\_min}}^{Tri}}}{tanh 10}\, \mu_{\max_{\mathrm{t}}}\, Tri \tag{36}$$

The equations describing Fe speciation and removal by sinking particles as well as particle aggregation are taken from Ye et al. (2009). Here, they are not listed repeatedly.

References

ACRI-STLOV. Globcolour: An eo based service supporting global ocean carbon cycle research: validation protocol. Technical report, GC-PL-NIVA-VP-03, 2006.

Susana Agusti, Carlos M. Duarte, Dolors Vaqué, Mette Hein, Josep M. Gasol, and Montserrat Vidal. Food-web structure and elemental (C, N and P) fluxes in the eastern tropical North Atlantic. *Deep Sea Research Part II: Topical Studies in Oceanography*, 48(10):2295–2321, 2001.

V.L. Asper and W.O. Jr Smith. Abundance, distribution and sinking rates of aggregates in the Ross Sea, Antarctica. *Deep-Sea Research (Part I, Oceanographic Research Papers)*, 50(1):131–150, January 2003. doi: 10.1016/S0967-0637(02)00146-2.

V.L. Asper, W.G. Deuser, G.A. Knauer, and S.E. Lohrenz. Rapid coupling of sinking particle fluxes between surface and deep ocean waters. *Nature*, 357(6380):670–672, 1992. ISSN 0028-0836.

Ilana Berman-Frank, Jay T. Cullen, Yeala Shaked, Robert M. Sherrell, and Paul G. Falkowski. Iron Availability, Cellular Iron Quotas, and Nitrogen Fixation in Trichodesmium. *Limnology and Oceanography*, 46(6):1249–1260, 2001.

Annie Bourbonnais, Moritz F. Lehmann, Joanna J. Waniek, and Detlef E. Schulz-Bull. Nitrate isotope anomalies reflect N2 fixation in the Azores Front region (subtropical NE Atlantic). *J. Geophys. Res.*, 114(C3):C03003, March 2009.

A. Bracher, M. Vountas, T. Dinter, J. P. Burrows, R. Röttgers, and I. Peeken. Quantitative observation of cyanobacteria and diatoms from space using PhytoDOAS on SCIAMACHY data. *Biogeosciences*, 6(5):751–764, 2009. doi: 10.5194/bg-6-751-2009.

E. Breitbarth, A. Oschlies, and J. LaRoche. Physiological constraints on the global distribution of Trichodesmium — effect of temperature on diazotrophy. *Biogeosciences*, 4(1):53–61, 2007. doi: 10.5194/bg-4-53-2007.

E. Breitbarth, J. Wohlers, Kläs J., LaRoche J. J, and I. Peeken. Nitrogen fixation and growth rates of Trichodesmium IMS-101 as a function of light intensity. *Mar Ecol Prog Ser*, 359:25–36, 2008.

Douglas G. Capone, Jonathan P. Zehr, HansW. Paerl, Birgitta Bergman, and Edward J. Carpenter. Trichodesmium, a globally significant marine cyanobacterium. *Science*, 276(5316):1221–1229, 1997. doi: 10.1126/science.276.5316.1221.

Douglas G. Capone, James A. Burns, Joseph P. Montoya, Ajit Subramaniam, Claire Mahaffey, Troy Gunderson, Anthony F. Michaels, and Edward J. Carpenter. Nitrogen fixation by Trichodesmium spp.: An important source of new nitrogen to the tropical and subtropical North Atlantic Ocean. *Global Biogeochem. Cycles*, 19(2):GB2024, June 2005.

E. J. Carpenter, J. P. Montoya, J. Burns, M. R. Mulholland, A. Subramaniam, and D. G. Capone. Extensive bloom of a N_2-fixing diatom/cyanobacterial association in the tropical Atlantic Ocean. *Marine ecology Progress series*, 185:273–283, 1999.

Edward J. Carpenter and IV Charles C. Price. Nitrogen fixation, distribution, and production of Oscillatoria (Trichodesmium) spp. in the western Sargasso and Caribbean Seas. *Limnology and Oceanography*, 22(1):60–72, 1977.

Edward J. Carpenter and Kristen Romans. Major role of the cyanobacterium Trichodesmium in nutrient cycling in the North Atlantic Ocean. *Science*, 254(5036):1356–1358, 1991. doi: 10.1126/science.254.5036.1356.

Edward J. Carpenter, Ajit Subramaniam, and Douglas G. Capone. Biomass and primary productivity of the cyanobacterium Trichodesmium spp. in the tropical N Atlantic ocean. *Deep Sea Research Part I: Oceanographic Research Papers*, 51(2):173–203, February 2004.

EJ. Carpenter and DG. Capone. Nitrogen fixation in Trichodesmium blooms. In EJ. Carpenter, DG. Capone, and J. Rueter, editors, *Marine pelagic cyanobacteria: Trichodesmium and other diazotrophs*, pages 211–217. Kluwer Academic Publishers, The Netherlands, 1992.

Matthew J. Church, Claire Mahaffey, Ricardo M. Letelier, Roger Lukas, Jonathan P. Zehr, and David M. Karl. Physical forcing of nitrogen fixation and diazotroph community structure in the North Pacific subtropical gyre. *Global Biogeochem. Cycles*, 23(2):GB2020, June 2009. doi: doi:10.1029/2008GB003418.

James E. Cloern, Christian Grenz, and Lisa Vidergar-Lucas. An empirical model of the phytoplankton chlorophyll : carbon ratio-the conversion factor between productivity and growth rate. *Limnology and Oceanography*, 40(7):1313–1321, 1995.

V. J. Coles and R. R. Hood. Modeling the impact of iron and phosphorus limitations on nitrogen fixation in the Atlantic Ocean. *Biogeosciences*, 4(4):455–479, 2007. doi: 10.5194/bg-4-455-2007.

Cabell S. Davis and Jr. McGillicuddy, Dennis J. Transatlantic abundance of the N_2-fixing colonial cyanobacterium Trichodesmium. *Science*, 312(5779):1517–1520, 2006. doi: 10.1126/science.1123570.

Curtis Deutsch, Jorge L. Sarmiento, Daniel M. Sigman, Nicolas Gruber, and John P. Dunne. Spatial coupling of nitrogen inputs and losses in the ocean. *Nature*, 445(7124):163–167, January 2007.

S. T. Dyhrman, P. D. Chappell, S. T. Haley, J. W. Moffett, E. D. Orchard, J. B. Waterbury, and E. A. Webb. Phosphonate utilization by the globally important marine diazotroph Trichodesmium. *Nature*, 439(7072):68–71, January 2006.

Luisa I. Falcon, Edward J. Carpenter, Frank Cipriano, Birgitta Bergman, and Douglas G. Capone. N_2 fixation by unicellular bacterioplankton from the Atlantic and Pacific Oceans: Phylogeny and *in situ* rates. *Appl. Environ. Microbiol.*, 70(2):765–770, 2004. doi: 10.1128/AEM.70.2.765-770.2004.

Katja Fennel, Yvette H. Spitz, Ricardo M. Letelier, Mark R. Abbott, and David M. Karl. A deterministic model for N_2 fixation at stn. ALOHA in the subtropical North Pacific Ocean. *Deep Sea Research Part II: Topical Studies in Oceanography*, 49(1-3):149–174, 2001. doi: 10.1016/S0967-0645(01)00098-4.

A. Fernández, B. Mouriño Carballido, A. Bode, M. Varela, and E. Marañón. Latitudinal distribution of Trichodesmium spp. and N_2 fixation in the Atlantic Ocean. *Biogeosciences*, 7(10):3167–3176, 2010. doi: 10.5194/bg-7-3167-2010.

Fei-Xue Fu, Yaohong Zhang, Peter R. F. Bell, and David A. Hutchins. Phosphate uptake and growth kinetics of Trichodesmium (cyanobacteria) isolates from the North Atlantic Ocean and the Great Barrier Reef, Australia. *Journal of Phycology*, 41(1):62–73, 2005.

N. L. Goebel, K. A. Turk, K. M. Achilles, R. Paerl, I. Hewson, A. E. Morrison, J. P. Montoya, C. A. Edwards, and J. P. Zehr. Abundance and distribution of major groups of diazotrophic cyanobacteria and their potential contribution to N_2 fixation in the tropical Atlantic Ocean. *Environmental Microbiology*, 2010. doi: 10.1111/j.1462-2920.2010.02303.x.

Watson W. Gregg and Nancy W. Casey. Modeling coccolithophores in the global oceans. *Deep Sea Research Part II: Topical Studies in Oceanography*, 54(5-7):447–477, 2007. doi: 10.1016/j.dsr2.2006.12.007. The Role of Marine Organic Carbon and Calcite Fluxes in Driving Global Climate Change, Past and Future.

W.W. Gregg, P. Ginoux, P.S. Schopf, and N.W. Casey. Phytoplankton and iron: Validation of a global three-dimensional ocean biogeochemical model. *Deep-Sea Research Part II: Topical Studies in Oceanography*, 50(22-26):3143–3169, 2003.

Nicolas Gruber and Jorge L. Sarmiento. Global patterns of marine nitrogen fixation and denitrification. *Global Biogeochem. Cycles*, 11(2):235–266, 1997.

Dennis A. Hansell, Nicholas R. Bates, and Donald B. Olson. Excess nitrate and nitrogen fixation in the North Atlantic Ocean. *Marine Chemistry*, 84(3-4):243–265, January 2004.

S. Hawser, J. O'Neil, M. Roman, and G. Codd. Toxicity of blooms of the cyanobacterium Trichodesmium to zooplankton. *Journal of Applied Phycology*, 4(1):79–86, March 1992.

Carolyn M. Holl and Joseph P. Montoya. Interactions between nitrate uptake and nitrogen fixation in continuous cultures of the marine diazotroph Trichodesmium (cyanobacteria). *Journal of Phycology*, 41(6):1178–1183, 2005. doi: doi:10.1111/j.1529-8817.2005.00146.x.

Raleigh R. Hood, Nicholas R. Bates, Douglas G. Capone, and Donald B. Olson. Modeling the effect of nitrogen fixation on carbon and nitrogen fluxes at BATS. *Deep Sea Research Part II: Topical Studies in Oceanography*, 48(8-9):1609 – 1648, 2001. doi: DOI:10.1016/S0967-0645(00)00160-0.

DA Hutchins, FX Fu, Y Zhang, ME Warner, Y Feng, K Portune, PW Bernhardt, and MR Mulholland. CO_2 control of trichodesmium N_2 fixation, photosynthesis, growth rates, and elemental ratios: Implications for past, present, and future ocean biogeochemistry. *Limnology and Oceanography*, 52:1293–1304, 2007.

D. Karl, R. Letelier, L. Tupas, J. Dore, J. Christian, and D. Hebel. The role of nitrogen fixation in biogeochemical cycling in the subtropical North Pacific Ocean. *Nature*, 388(6642):533–538, August 1997.

D. Karl, A. Michaels, B. Bergman, D. Capone, E. Carpenter, R. Letelier, F. Lipschultz, H. Paerl, D. Sigman, and L. Stal. Dinitrogen fixation in the world's oceans. *Biogeochemistry*, 57-58:47–98, 2002.

D. M. Karl, R. Letelier, D. V. Hebel, D. F. Bird, and C. D. Winn. Trichodesmium blooms and new nitrogen in the North Pacific Gyre. In EJ. Carpenter, DG. Capone, and J. Rueter, editors, *Marine pelagic cyanobacteria: Trichodesmium and other diazotrophs*. Kluwer Academic Publishers, The Netherlands, 1992.

Sven A. Kranz, Orly Levitan, Klaus-Uwe Richter, Ondrej Prasil, Ilana Berman-Frank, and Bjorn Rost. Combined effects of CO_2 and light on the N_2-fixing cyanobacterium Trichodesmium IMS101: Physiological responses. *Plant Physiol.*, 154(1):334–345, 2010. doi: 10.1104/pp.110.159145.

I. Kriest. Different parameterizations of marine snow in a 1d-model and their influence on representation of marine snow, nitrogen budget and sedimentation. *Deep-Sea Research (Part I, Oceanographic Research Papers)*, 49(12):2133–2162, December 2002. doi: 10.1016/S0967-0637(02)00127-9.

I. Kudo and P.J. Harrison. Effect of iron nutrition on the marine cyanobacterium *Synechococcus* grown on different N sources and irradiances. *Journal of Phycology*, 33:232–240, 1997.

Adam Kustka, Edward J. Carpenter, and Sergio A. Sanũdo Wilhelmy. Iron and marine nitrogen fixation: progress and future directions. *Research in Microbiology*, 153(5):255–262, 2002. doi: 10.1016/S0923-2508(02)01325-6.

Rebecca J. Langlois, Diana Hummer, and Julie LaRoche. Abundances and distributions of the dominant *nifH* phylotypes in the Northern Atlantic Ocean. *Appl. Environ. Microbiol.*, 74(6):1922–1931, 2008. doi: 10.1128/AEM.01720-07.

Julie LaRoche and Eike Breitbarth. Importance of the diazotrophs as a source of new nitrogen in the ocean. *Journal of Sea Research*, 53(1-2):67–91, January 2005.

Ricardo M. Letelier and David M. Karl. Trichodesmium spp. physiology and nutrient fluxes in the North Pacific subtropical gyre. *Aquat Microb Ecol*, 15(3):265–276, 1998.

RM Letelier and DM Karl. Role of Trichodesmium spp. in the productivity of the subtropical North Pacific ocean. *Mar Ecol Prog Ser*, 133:263–273, 1996.

MD Mackey, DJ Mackey, HW Higgins, and SW Wright. CHEMTAX - a program for estimating class abundances from chemical markers: application to HPLC measurements of phytoplankton. *Mar Ecol Prog Ser*, 144:265–283, 1996.

Claire Mahaffey, Richard G. Williams, George A. Wolff, Natalie Mahowald, William Anderson, and Malcolm Woodward. Biogeochemical signatures of nitrogen fixation in the eastern North Atlantic. *Geophys. Res. Lett.*, 30(6):1300–, March 2003.

Claire Mahaffey, Anthony F. Michaels, and Douglas G. Capone. The conundrum of marine N_2 fixation. *Am. J. Sci.*, 305(6–8):546–595, 2005. doi: 10.2475/ajs.305.6-8.546.

Stẽphane Maritorena and David A. Siegel. Consistent merging of satellite ocean color data sets using a bio-optical model. *Remote Sensing of Environment*, 94(4):429 – 440, 2005. doi: 10.1016/j.rse.2004.08.014.

Stẽphane Maritorena, Odile Hembise, Fanton d'Andon, Antoine Mangin, and David A. Siegel. Merged satellite ocean color data products using a bio-optical model: Characteristics, benefits and issues. *Remote Sensing of Environment*, 114(8):1791–1804, 2010. doi: 10.1016/j.rse.2010.04.002.

C. Mark Moore, Matthew M. Mills, Eric P. Achterberg, Richard J. Geider, Julie LaRoche, Mike I. Lucas, Elaine L. McDonagh, Xi Pan, Alex J. Poulton, Micha J. A. Rijkenberg, David J. Suggett, Simon J. Ussher, and E. Malcolm S. Woodward. Large-scale distribution of Atlantic nitrogen fixation controlled by iron availability. *Nature Geosci*, 2(12):867–871, December 2009.

J. W. McClelland, C. M. Holl, and J. P. Montoya. Relating low δ^{15}N values of zooplankton to N_2-fixation in the tropical North Atlantic: insights provided by stable isotope ratios of amino acids. *Deep Sea Research Part I: Oceanographic Research Papers*, 50(7):849–861, 2003. doi: 10.1016/S0967-0637(03)00073-6.

M.M. Mills, C. Ridame, M. Davey, J. La Roche, and R. Geider. Iron and phosphorus co-limit nitrogen fixation in the eastern tropical North Atlantic. *Nature*, 429:292–294, 2004.

Joseph P. Montoya, Edward J. Carpenter, and Douglas G. Capone. Nitrogen fixation and nitrogen isotope abundances in zooplankton of the oligotrophic North Atlantic. *Limnology and Oceanography*, 47:1617–1628, 2002.

Joseph P. Montoya, Carolyn M. Holl, Jonathan P. Zehr, Andrew Hansen, Tracy A. Villareal, and Douglas G. Capone. High rates of N_2 fixation by unicellular diazotrophs in the oligotrophic Pacific Ocean. *Nature*, 430(7003):1027–1032, August 2004. ISSN 0028-0836.

J. Keith Moore, Scott C. Doney, Joanie A. Kleypas, David M. Glover, and Inez Y. Fung. An intermediate complexity marine ecosystem model for the global domain. *Deep Sea Research Part II: Topical Studies in Oceanography*, 49(1-3):403–462, 2001.

M. R. Mulholland and D. G. Capone. Nitrogen fixation, uptake and metabolism in natural and cultured populations of Trichodesmium spp. *Marine ecology Progress series*, 188:33–49, 1999.

Margaret R. Mulholland, Sheri Floge, Edward J. Carpenter, and Douglas G. Capone. Phosphorus dynamics in cultures and natural populations of Trichodesmium spp. *Mar Ecol Prog Ser*, 239: 45–55, 2002.

J. M. O'Neil and M. R. Roman. Ingestion of the cyanobacterium Trichodesmium spp. by pelagic harpacticoid copepods Macrosetella, Miracia and Oculosetella. *Hydrobiologia*, 292-293(1):235–240, January 1994.

Kazutoshi Onogi, Junichi Tsutsui, Hiroshi Koide, Masami Sakamoto, Shinya Kobayashi, Hiroaki Hatshushika, Takanori Matshumoto, Nobuo Yamazaki, Hirotaka Kamahort, Kiyotoshi Takahashi, Shinji Kadokura, Koji Wada, Koji Kato, Ryo Oyama, Tomoaki Ose, Nobutaka Mannoji, and Ryusuke Taira. The JRA-25 Reanalysis. *Journal of the Meteorological Society of Japan. Ser. II*, 85(3):369–432, 2007.

Elizabeth D. Orchard, James W. Ammerman, Michael W. Lomas, and Sonya T. Dyhrman. Dissolved inorganic and organic phosphorus uptake in Trichodesmium and the microbial community:

The importance of phosphorus ester in the Sargasso Sea. *Limnology and Oceanography*, 55:1390–1399, 2010.

Sarah E. Reynolds, Rhiannon L. Mather, George A. Wolff, Richard G. Williams, Angela Landolfi, Richard Sanders, and E. Malcolm S. Woodward. How widespread and important is N_2 fixation in the North Atlantic Ocean? *Global Biogeochem. Cycles*, 21(4):GB4015–, November 2007.

Sergio A. Sañudo Wilhelmy, Adam B. Kustka, Christopher J. Gobler, David A. Hutchins, Min Yang, Kamazima Lwiza, James Burns, Douglas G. Capone, John A. Raven, and Edward J. Carpenter. Phosphorus limitation of nitrogen fixation by Trichodesmium in the central Atlantic Ocean. *Nature*, 411(6833):66–69, May 2001.

M Schartau and A Oschlies. Simultaneous data-based optimization of a 1D-ecosystem model at three locations in the North Atlantic: Part I. Method and parameter estimates. *Journal of Marine Research*, 61(6):765–793, November 2003a.

M Schartau and A Oschlies. Simultaneous data-based optimization of a 1D-ecosystem model at three locations in the North Atlantic: Part II. Standing stocks and nitrogen fluxes. *Journal of Marine Research*, 61(6):795–821, November 2003b.

T.J. Smayda. The suspension and sinking of phytoplankton in the sea (RV). *Oceanography Marine Biology*, 8:353–414, 1970.

Jill A. Sohm and Douglas G. Capone. Phosphorus dynamics of the tropical and subtropical north Atlantic: Trichodesmium spp. versus bulk plankton. *Mar. Ecol. Prog. Ser.*, 317:21–28, 2006.

Jill A. Sohm, Claire Mahaffey, and Douglas G. Capone. Assessment of relative phosphorus limitation of *Trichodesmium* spp. in the North Pacific, North Atlantic, and the north coast of Australia. *Limnology and Oceanography*, 53:2495–2502, 2008.

Marc Staal, Sacco te Lintel Hekkert, Geert Jan Brummer, Marcel Veldhuis, Cor Sikkens, Stefan Persijn, and Lucas J. Stal. Nitrogen fixation along a north-south transect in the eastern Atlantic Ocean. *Limnology and Oceanography*, 52:1305–1316, 2007.

W.G. Sunda and S.A. Huntsman. Iron uptake and growth limitation in oceanic and coastal phytoplankton. *Marine Chemistry*, 50:189–206, 1995.

S. Torres-Valdès, V. M. Roussenov, R. Sanders, S. Reynolds, X. Pan, R. Mather, A. Landolfi, G. A. Wolff, E. P. Achterberg, and R. G. Williams. Distribution of dissolved organic nutrients and their effect on export production over the Atlantic Ocean. *Global Biogeochem. Cycles*, 23(4):GB4019, November 2009.

Toby Tyrrell, Emilio Maranon, Alex J. Poulton, Andrew R. Bowie, Derek S. Harbour, and E. Malcolm S. Woodward. Large-scale latitudinal distribution of Trichodesmium spp. in the Atlantic Ocean. *J. Plankton Res.*, 25(4):405–416, April 2003.

L. Umlauf and H. Burchard. Second-order turbulence closure models for geophysical boundary layers. A review of recent work. *Continental Shelf Research*, 25(7-8):795–827, 2005.

F Vallespinos. Nitrogen fixation by Trichodesmium thiebautii in the upwelling region off Northwest Africa. In C. Bas, R. Margalef, P. Rubies, and Inst. de Invest, editors, *Simposio Internacional sobre las Areas de Afloramiento Mas Important del Oeste Africano (Cabo Blanco Y Benguela)*, volume 1. Pesqueras Barcelona, Barcelona, 1985.

Marcel J. W. Veldhuis and Gijsbert W. Kraay. Phytoplankton in the subtropical Atlantic Ocean: towards a better assessment of biomass and composition. *Deep Sea Research Part I: Oceanographic Research Papers*, 51(4):507–530, 2004. doi: 10.1016/j.dsr.2003.12.002.

Tracy A. Villareal. Nitrogen-fixation by the cyanobacterial symbiont of the diatom genus Hemiaulus. *Mar. Ecol. Prog. Ser.*, 76:201–204, 1991.

Maren Voss, Peter Croot, Karin Lochte, Matthew Mills, and Ilka Peeken. Patterns of nitrogen fixation along 10°N in the tropical Atlantic. *Geophys. Res. Lett.*, 31(23):L23S09, 2004.

A. E. Walsby. The properties and buoyancy-providing role of gas vacuoles in Trichodesmium Ehrenberg. *British Phycological Journal*, 13(2):103–116, 1978.

S.W. Wilhelm and C.G. Trick. Iron-limited growth of cyanobacteria: Multiple siderophore production is a common response. *Limnology and Oceanography*, 39:1979–1984, 1994.

S.W. Wilhelm, D.P. Maxwell, and C.G. Trick. Growth, iron requirements, and siderophore production in iron-limited *Synechococcus* PCC 7002. *Limnology and Oceanography*, 41:89–97, 1996.

Jingfeng Wu, William Sunda, Edward A. Boyle, and David M. Karl. Phosphate depletion in the western North Atlantic Ocean. *Science*, 289(5480):759–762, 2000. doi: 10.1126/science.289.5480.759.

Y. Ye, C. Völker, and D. A. Wolf-Gladrow. A model of Fe speciation and biogeochemistry at the Tropical Eastern North Atlantic Time-Series Observatory site. *Biogeosciences*, 6(10):2041–2061, 2009. doi: 10.5194/bg-6-2041-2009.

Jonathan P. Zehr, Edward J. Carpenter, and Tracy A. Villareal. New perspectives on nitrogen-fixing microorganisms in tropical and subtropical oceans. *Trends in Microbiology*, 8(2):68–73, February 2000. ISSN 0966-842X.

Jonathan P. Zehr, John B. Waterbury, Patricia J. Turner, Joseph P. Montoya, Enoma Omoregie, Grieg F. Steward, Andrew Hansen, and David M. Karl. Unicellular cyanobacteria fix N_2 in the subtropical North Pacific Ocean. *Nature*, 412(6847):635–638, August 2001.

Table 2: Parameters in the ecosystem model. Parameters in the Fe model are described in (Ye et al., 2009), Tab. 4. Source of parameter values are shown as footnotes; other parameters are optimised for the North Atlantic by Schartau and Oschlies (2003a,b).

Parameters	Symbol	Unit	Value
maximum growth rate of Phy	$\mu_{\max}$	d^{-1}	0.27
maximum growth rate of Tri	$\mu_{\max_t}$	d^{-1}	0.75 [1]
Phy mortality	γ_p	d^{-1}	0.04
Tri mortality	γ_t	d^{-1}	0.04
initial slope P-I curve for Phy	α	$\mathrm{m}^2\,\mathrm{W}^{-1}\,\mathrm{d}^{-1}$	0.256
initial slope P-I curve for Tri	α_t	$\mathrm{m}^2\,\mathrm{W}^{-1}\,\mathrm{d}^{-1}$	9.2×10^{-3} [2]
nitrate half-saturation constant for Phy	K_{N}	$\mu\mathrm{mol}\,\mathrm{L}^{-1}$	0.7
nitrate half-saturation constant for Tri	$K_{\mathrm{N_t}}$	$\mu\mathrm{mol}\,\mathrm{L}^{-1}$	0.7
DIP half-saturation constant for Phy	K_{DIP}	$\mu\mathrm{mol}\,\mathrm{L}^{-1}$	0.015 [3]
DIP half-saturation constant for Tri	$K_{\mathrm{DIP_t}}$	$\mu\mathrm{mol}\,\mathrm{L}^{-1}$	0.4 [4]
DOP half-saturation constant for Tri	K_{DOP}	$\mu\mathrm{mol}\,\mathrm{L}^{-1}$	0.18 [5]
Fe half-saturation constant for Phy	K_{Fe}	$\mathrm{nmol}\,\mathrm{L}^{-1}$	0.2
Fe half-saturation constant for Tri	$K_{\mathrm{Fe_t}}$	$\mathrm{nmol}\,\mathrm{L}^{-1}$	0.75 [6]
maximum Fe:N ratio in Phy	$Q_{\mathrm{Fe}}^{\max}$	$\mathrm{nmol}\ \mathrm{L}^{-1}\ (\mu\mathrm{mol}\,\mathrm{L}^{-1})^{-1}$	0.033 [7]
minimum Fe:N ratio in Phy	$Q_{\mathrm{Fe}}^{\min}$	$\mathrm{nmol}\ \mathrm{L}^{-1}\ (\mu\mathrm{mol}\,\mathrm{L}^{-1})^{-1}$	6.6×10^{-3} [7]
maximum Fe:N ratio in Tri	$Q_{\mathrm{Fe_t}}^{\max}$	$\mathrm{nmol}\ \mathrm{L}^{-1}\ (\mu\mathrm{mol}\,\mathrm{L}^{-1})^{-1}$	0.3 [8]
minimum Fe:N ratio in Tri	$Q_{\mathrm{Fe_t}}^{\min}$	$\mathrm{nmol}\ \mathrm{L}^{-1}\ (\mu\mathrm{mol}\,\mathrm{L}^{-1})^{-1}$	0.033 [8]
Phy aggregation rate	γ_{p^2}	$(\mu\mathrm{mol}\,\mathrm{L}^{-1})^{-1}\,\mathrm{d}^{-1}$	0.025
Tri aggregation rate	γ_{t^2}	$(\mu\mathrm{mol}\,\mathrm{L}^{-1})^{-1}\,\mathrm{d}^{-1}$	0.025
maximum grazing rate	$g_{\max}$	d^{-1}	1.575
grazing preference for Tri	β	–	0.1 [9]
prey capture rate	ϵ	$(\mu\mathrm{mol}\,\mathrm{L}^{-1})^{-1}\,\mathrm{d}^{-1}$	1.6
assimilation efficiency	γ_{za}	–	0.925
excretion	γ_{zb}	d^{-1}	0.01
quadratic mortality of zooplankton	γ_{z^2}	$(\mu\mathrm{mol}\,\mathrm{L}^{-1})^{-1}\,\mathrm{d}^{-1}$	0.34

1 Resulted from tuning the modelled Tri abundance close to observations.
2 Breitbarth et al. (2008).
3 Sohm and Capone (2006).
4 Fu et al. (2005).
5 Sohm et al. (2008).
6 Kudo and Harrison (1997) measured this value for *Synechococcus*.
7 Sunda and Huntsman (1995).
8 Kustka et al. (2002).
9 Sensitivity study (Sect. 2.2).

(to be continued)

Table 3: Parameters in the ecosystem model (continued). Parameters in the Fe model are described in (Ye et al., 2009), Tab. 4. Source of parameter values are shown as footnotes; other parameters are optimised for the North Atlantic by Schartau and Oschlies (2003a,b).

Parameters	Symbol	Unit	Value
detritus remineralisation	γ_d	d^{-1}	0.048
DOP remineralisation	γ_{DOP}	d^{-1}	0.0048 [10]
sinking velocity of small particles	w_d	$\mathrm{m\,d}^{-1}$	1 [11]
sinking velocity of small particles	w_s	$\mathrm{m\,d}^{-1}$	5 [11]
sinking velocity of aggregates	w_l	$\mathrm{m\,d}^{-1}$	50 [12]
buoyancy of Tri	w_t	$\mathrm{m\,d}^{-1}$	5 [9]
coeff. for temp. func.	C_{ref}	–	1.066
PAR:short-wave irradiance ratio	f_{PAR}	–	0.43
attenuation due to chlorophyll	κ	$\mathrm{m}^2\,(\mathrm{mmol\ N})^{-1}$	0.03
mass:N ratio in organic matter	$r_{\mathrm{m:N}}$	$\mathrm{g\,mol}^{-1}$	159 [13]

10 Sensitivity study to tune DIP and DOP concentrations in surface waters to observations (Sect. 2.1.2).
11 Estimated from Stokes' Law, see Ye et al. (2009) Sect. 2.3.
12 Estimates by Smayda (1970); Asper et al. (1992); Asper and Smith (2003); Kriest (2002).
13 Calculated with Redfield C:N ratio and the assumption that 1 g C corresponds 2 g mass.

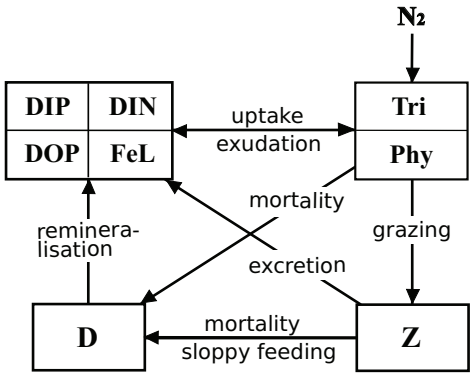

Figure 1: Schematic of the ecosystem model.

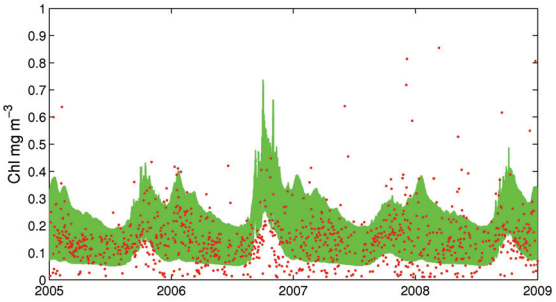

Figure 2: Modelled total surface chlorophyll concentration (green) and satellite-derived values (red). Modelled values are calculated from modelled total phytoplankton nitrogen, assuming the dependence of chlorophyll content on light, nutrient and temperature according to Cloern et al. (1995).

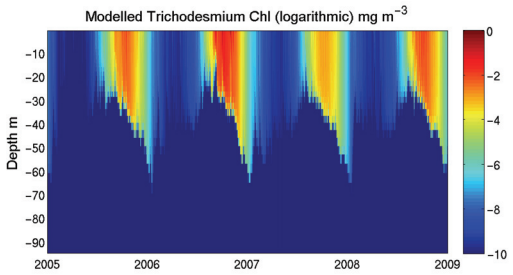

Figure 3: Seasonal variability of modelled *Trichodesmium* chlorophyll.

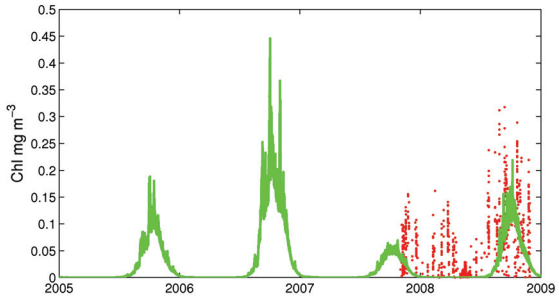

Figure 4: Modelled *Trichodesmium* surface chlorophyll (green) and satellite-derived phycobilin-containing cyanobacterial Chl a (red).

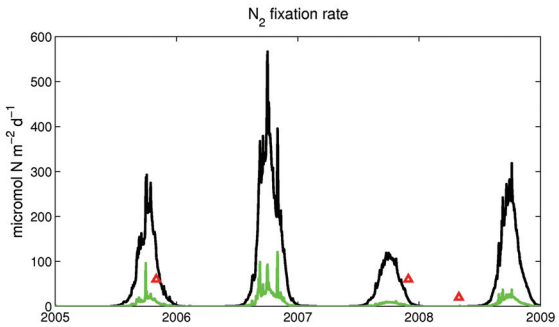

Figure 5: N_2 fixation rate integrated for the mixed layer: modelled — black curve, observed — red triangles. Modelled surface fixation rate is shown as green curve (mmol N m^{-3} d^{-1}).

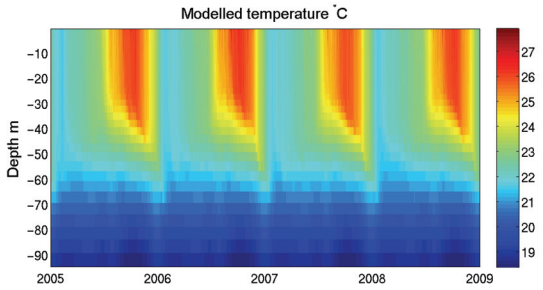

Figure 6: Modelled temperature in the upper 100 m.

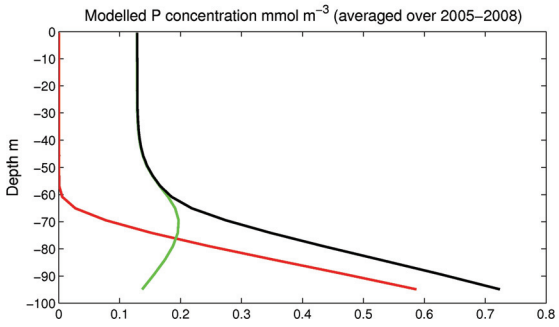

Figure 7: Annually averaged P profiles. Black: total P, red: DIP, green: DOP.

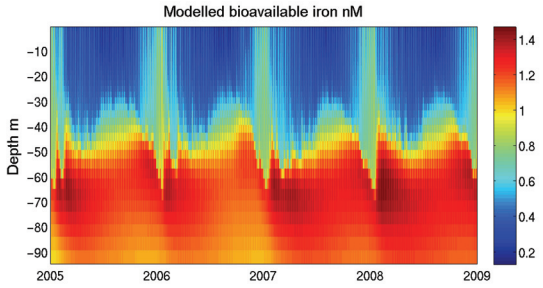

Figure 8: Modelled concentration of bioavailable iron.

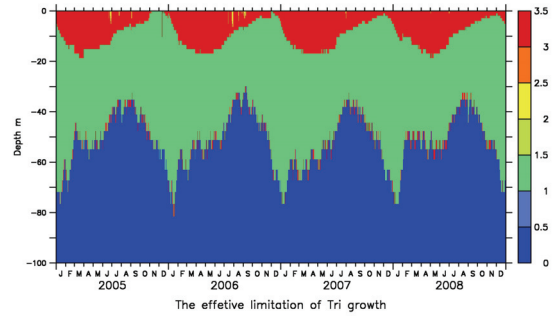

Figure 9: Modelled pattern of the effective limitation of N_2 fixation, comparing three limiting factors — light, Fe and P. Red: P-limitation dominates, yellow: Fe-limitation dominates, green: light-limitation dominates, blue: no Tri growth.

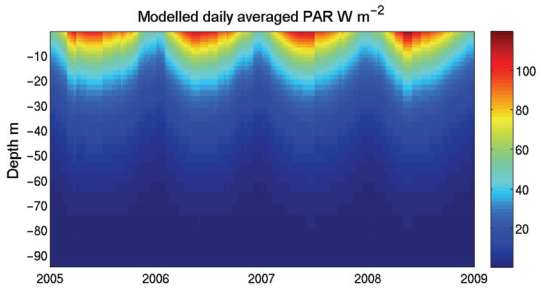

Figure 10: Modelled photosynthetically available radiation.

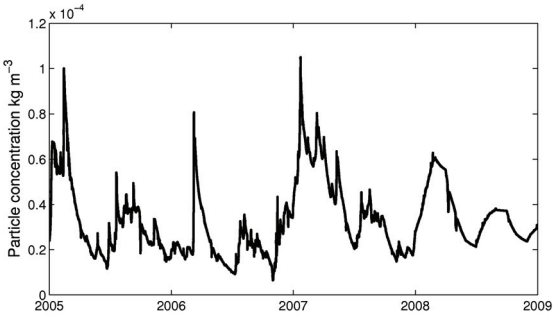

Figure 11: Concentration of dust particles in surface water.

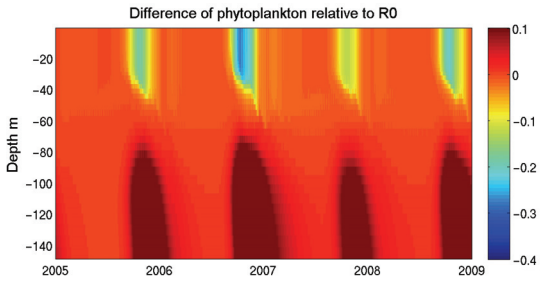

Figure 12: Relative difference of phytoplankton in the upper 150 m between the standard run and the run without N_2 fixation.

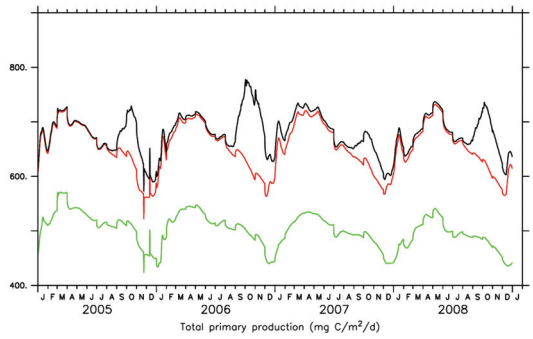

Figure 13: Modelled total primary production in the run R_0 (black), R_{nf} (red) and R_{nd} (green) (Sect. 3.4).

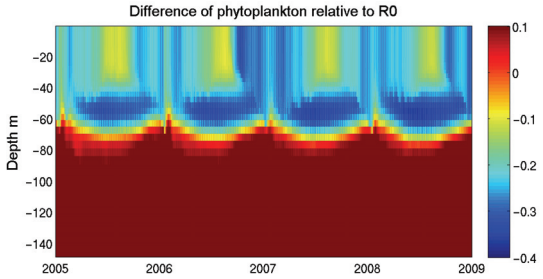

Figure 14: Relative difference of phytoplankton in the upper 150 m between the standard run and the run without dust deposition.

Chapter 3

Synthesis

3.1 Between dust and climate

A link between dust deposition and atmospheric CO_2 concentrations in the past was suggested based on the analysis of the Vostok ice core record (Martin, 1990). The impact of dust deposition on the biological carbon sequestration and thus on the climate becomes a vital issue in the marine research.

Dust can influence climate directly by changing the radiative properties of the atmosphere through scattering and absorption of solar and terrestrial radiation, or indirectly by changing cloud properties which in turn, affects the radiative and hydrological balances of the Earth (Maher et al., 2010, and citations therein). Less directly, dust deposition changes the nutrient availability in seawater, in particular Fe availability, and influences therefore the strength of the biological carbon fixation and thus the atmospheric CO_2 concentration.

Climate change also affects dust fluxes. A number of factors controlling dust flux are sensitive to climate change (Maher et al., 2010). For instance, source of dust and conditions of the source areas could be influenced by vegetative cover, sea level variation and erosion of exposed land area, while dust transport could be influenced by changes in wind speed and pattern. Variations in precipitation have an effect on wet deposition of dust along its transport path.

Among these multiple interactions between dust deposition and climate change, this thesis focuses on the understanding of the impact of dust deposition on Fe bioavailability and on the marine productivity, particularly in ocean regions with high dust fluxes. The findings from the individual chapters are summarised in Chap. 4. Here, only these that have a central bearing on the understanding of the connection between dust deposition, iron bioavailability and marine productivity are of interest.

3.2 Impact of dust deposition on Fe bioavailability

The impact of dust deposition on Fe availability in the euphotic zone depends on many factors, e.g. the solubility of iron in dust, iron speciation in seawater and the biological iron cycling.

The solubility of iron in dust primarily depends on properties of the atmosphere (Jickells and Spokes, 2001). Dust particles experience strongly varying pH and ionic strength, wetting and drying cycles during cloud formation and evaporation, before they are removed from the atmosphere by dry or wet deposition (Warneck, 1988). These processes increase the lability of metals in dust particles. Through these processes, the transport distance of dust particles influences Fe solubility (Baker and Jickells, 2006).

As dust particles come into surface waters, Fe dissolution and speciation, removal processes such as biological uptake and particle adsorption, mixing and ocean circulation regulate the regional and global Fe budget. These processes are affected by physico-chemical conditions such as stratification, solar radiation, temperature and pH of seawater. Biological activities on the one hand are controlled by Fe availability, and on the other hand they have an impact on Fe availability. For instance, faster biological regeneration of iron within the euphotic zone keeps iron bioavailable for longer and an excess of organic ligands over iron prevents iron from adsorptive removal.

The first two studies in this thesis focus on the chemical and biological processes controlling the fate of Fe dissolved from dust particles on regional scales. The biogeochemical cycles of iron in two ocean regions with relatively high dust fluxes were described in one-dimensional models: TENATSO in the tropical eastern North Atlantic and the DUNE experiment site in the Mediterranean Sea. The model study for TENATSO investigated Fe speciation, particularly the cycling of organic Fe-binding ligands (Sect. 3.2.1), while the focus of the model for the DUNE dust-enrichment experiment was the short-term impact of dust deposition on dissolved iron in surface waters (Sect. 3.2.2).

3.2.1 Cycle of organic ligands

Sources and fate of organic Fe-binding ligands have been intensively studied during the last decades (Boyd et al., 2007). The model for TENATSO considered the cycling of organic ligands, to improve the description of the iron cycling dynamics and the understanding of interactions between iron level and biological acquisition of iron.

3.2.1.1 Modelling the marine ligand cycle in a one-dimensional model

In existing models of Fe speciation and biogeochemical cycle involving organic Fe-binding ligands, ligand pools were not described dynamically and ligand concentration was fixed to locally observed mean values (Parekh et al., 2004; Tagliabue and Arrigo, 2006; Weber et al., 2007). In this study, the ligand cycle and its role in Fe speciation were studied with an explicit description of sources and decay of two ligand classes — strong and weak ligands. In surface waters, a steady state of the ligand cycle is stabilised rapidly by fast reactions including biological production of strong ligands and uptake of complexed iron, as well as the photoreduction of the complexes. Deeper in the water column, slow processes such as Fe release during remineralisation of organic matter and microbial degradation of ligands, mainly control the balance of the ligand cycle. A long degradation time is needed to reproduce the observed high concentrations of weak ligands in deeper waters with a small

depth gradient (Hunter and Boyd, 2007). This simulation of the ligand cycle in a one-dimensional (1D) model has revealed that weak ligands probably contain a fraction of more refractory material with decay times longer than 2600 days (approximately 7 years). This is consistent with hypotheses from other researchers (Hunter and Boyd, 2007; Kondo et al., 2008) and also supported by a recent finding of humic substances maintaining Fe in solution in deep waters (Laglera and van den Berg, 2009). In consequence, the model would have to be run for a longer integration period for reaching the steady state concentration of weak ligands. A 1D-model is however not a good tool to simulate changes over a long time period, since lateral transport processes are not taken into account. A reasonable description of the cycling of organic ligands can therefore only be attempted in a three-dimensional (3D) model.

3.2.1.2 Future steps

In a 3D-model including Fe speciation and the ligand cycling, hypotheses on the sources and sinks of organic ligands can be tested by integrating the model for hundreds or thousands of years. There are however disadvantages using a 3D-model. A 1D-model is able to resolve fast reactions of Fe speciation explicitly at a time step from seconds to minutes, whereas it is extremely time-consuming to calculate these reactions in a 3D-model. To overcome this problem in a 3D-model, Völker et al. (in prep.) suggests to assume an equilibrium of Fe species involved in fast reactions like photoredox species and organically complexed Fe. Their concentrations can then be calculated as diagnostic variables from other state variables, such as total dissolved Fe and total ligand, which change slowly with time.

Composition and degradation processes of weak ligands are still largely unknown (Hunter and Boyd, 2007). Some researchers suggested that concentrations of dissolved Fe (DFe) are not controlled by two classes of ligands as usually measured by CLE/CSV, but rather by a broad spectrum of dissolved organic matter (DOM) with a continuum of binding characteristics (Town and Filella, 2000; Hiemstra and van Riemsdijk, 2006; Wagener et al., 2008). Wagener et al. (2008) found a linear relationship between DFe and dissolved organic carbon (DOC) concentration in a Fe dissolution experiment, indicating that a fraction of DOC functions as Fe-binding ligand. Since DOC is a parameter widely determined in the ocean and often involved in global biogeochemical models (Hansell et al., 2009), this linear relationship to Fe solubility is suggested to be used to describe the concentration change of weak ligands (Tagliabue et al., in prep.).

In order to take the refractory fraction of organic ligands into account and keep a certain simplicity of models, a classification of DOC could be adapted in models of the ligand cycle. Hansell et al. (2009) divided DOC into three pools according to their stability to degradation: two pools of semi-labile DOC with lifetimes of about 3 and 10 years, and a pool representing refractory DOC with a lifetime of about 15,000 years. Since strong ligands are mainly produced and consumed in surface waters and have a much shorter lifetime than these classes of DOC, this classification is mostly applicable for weak ligands.

Chemical characteristics of DOM as well as those of refractory organic ligands are still relatively unknown. More laboratory studies on these ligands are necessary to unravel the mystery of this deepwater "ligand soup" (Boyd et al., 2007) and the fractionation of differ-

ently stable ligands also needs to be verified by field measurements. In modelling studies, an interesting issue in future work could be the comparison of model results based on different assumptions on the ligand cycle to observed ligand distributions.

3.2.2 Short-term impact of dust deposition on dissolved iron

The significant role of dust deposition in supplying Fe to the ocean has been recognised decades ago (Duce and Tindale, 1991; Jickells and Spokes, 2001). A number of bottle and mesoscale Fe-enrichment experiments have found evidence of the Fe control on marine productivity (e.g. Martin, 1990; Coale et al., 1996). However, there are only a few observations of a causative link between dust supply and biological response (Boyd et al., 2010). This indicates that processes transforming dust input into Fe input are not yet well understood.

Modelling the mesocosm dust-enrichment experiment near Corsica (Chap. 2.3) contributed to the understanding of the short-term impact of dust supply on DFe concentration under natural regional conditions. The model was able to describe the double role of dust particles as input and sink of DFe quantitatively, by taking into account the kinetics of iron dissolution and the role of particle surfaces as scavengers of DFe. The model result underlines the role of colloidal iron in removing iron from the dissolved pool. A concept of a critical DFe concentration in seawater, above which dust deposition acts as a net sink of DFe, rather than a source, has been developed from this study. This indicates that natural dust deposition could affect DFe surface concentration differently on a short time scale. Depending on properties of seawater and concentrations of excess organic ligands, the critical DFe concentration can be estimated for different ocean regions and this concept might help explaining biological responses immediately after dust events. In future work, more case studies are needed to prove and apply this concept on a broader spatial scale. Moreover, measurements of colloidal iron in dust-enrichment experiments could improve our understanding of the pathway — colloidal aggregation. Ultimately, this might also help in understanding the role of colloids in the long-term removal of dissolved iron in the deep ocean (Bergquist et al., 2007).

3.3 Impact of dust deposition on marine productivity

Iron may limit marine productivity on the one hand by limiting total primary production in the HNLC regions, and on the other hand by limiting N_2 fixation in regions with low nitrate concentrations (Falkowski, 1997). During glacial times, the global dust fluxes are estimated to have been 5 times greater than those in interglacial stages (Maher et al., 2010). Assuming that higher dust fluxes led to higher Fe availability in the ocean during the last glacial maximum, the increase in DFe could have different effects on primary production and CO_2 fixation in different ocean regions. In the N-limited regions like the tropical and subtropical oceans, the DFe increase might allow higher N_2 fixation and shift ecosystems from Fe- to P-limitation (Capone et al., 1997; Falkowski et al., 1998; Jickells and Spokes, 2001). There, the change of CO_2 fixation would depend on the availability of P. In the HNLC regions, e.g. the Southern Ocean, surface concentrations of DFe derived from atmospheric deposition

would be still too low to support a significant increase of CO_2 uptake (Jickells and Spokes, 2001). The increase of dust deposition globally could lead to a rise in deep water iron concentrations and thus a rise of iron concentrations in the euphotic zone by upwelling. This argues for a linkage between the elevated dust fluxes during glacial times and reduced CO_2 in the atmosphere.

However, are these mechanisms sufficient to explain the difference of atmospheric CO_2 between the glacial/interglacial times? And are we now able to predict the biological CO_2 sequestration in the future world based on the current knowledge on these mechanisms? These questions encourage more studies focusing on biological feedback mechanisms to changing dust fluxes. The third study in this thesis, the model study of N_2 fixation at TENATSO, made an effort to estimate the regional role of dust deposition in a dust–N_2 fixation–marine productivity linkage. The model results show temporal and vertical variations of the limitation of N_2 fixation by Fe, P, temperature and light. A complex pattern of competitive as well as mutually beneficial interactions between diazotrophs and non-diazotrophic phytoplankton is found in the model. Spring blooms of non-diazotrophic phytoplankton deplete dissolved inorganic phosphorus (DIP) in surface waters but enhance the concentration of dissolved organic phosphorus (DOP). This high DOP availability and the ability of *Trichodesmium* to take up DOP are crucial for their autumn blooms. The atmospheric iron input at the TENATSO site is required to enable the diazotrophic growth and to support the observed abundance of non-diazotrophic phytoplankton, however a simple relationship between dust fluxes and the amplitude of N_2 fixation is not found. Newly fixed nitrogen by diazotrophs increases the growth of non-diazotrophic phytoplankton significantly. The effect is mainly seasonal due to the periodically high abundance of *Trichodesmium* in autumn. These interactions within an ecosystem underline the importance of the community composition in controlling the biological responses to changing environmental factors. These aspects might complicate the search for the ultimate factor limiting N_2 fixation and appropriate tracers to determine the spatial extent of N_2 fixation. Yet, they are unavoidable for describing and predicting the interactions between dust deposition and climate change mediated by biological processes.

Bibliography

A. R. Baker and T. D. Jickells. Mineral particle size as a control on aerosol iron solubility. *Geophys. Res. Lett.*, 33:L17608, September 2006. doi: 10.1029/2006GL026557.

B.A. Bergquist, J. Wu, and E.A. Boyle. Variability in oceanic dissolved iron is dominated by the colloidal fraction. *Geochimica et Cosmochimica Acta*, 71(12):2960–2974, June 2007. doi: 10.1016/j.gca.2007.03.013.

P. W. Boyd, T. Jickells, C. S. Law, S. Blain, E. A. Boyle, K. O. Buesseler, K. H. Coale, J. J. Cullen, H. J. W. de Baar, M. Follows, M. Harvey, C. Lancelot, M. Levasseur, N. P. J. Owens, R. Pollard, R. B. Rivkin, J. Sarmiento, V. Schoemann, V. Smetacek, S. Takeda, A. Tsuda, S. Turner, and A. J. Watson. Mesoscale iron enrichment experiments 1993-2005: Synthesis and future directions. *Science*, 315(5812): 612–617, February 2007.

P.W. Boyd, D.S. Mackie, and K.A. Hunter. Aerosol iron deposition to the surface ocean—modes of iron supply and biological responses. *Marine Chemistry*, 120(1-4):128–143, 2010. doi: 10.1016/j.marchem.2009.01.008.

Douglas G. Capone, Jonathan P. Zehr, HansW. Paerl, Birgitta Bergman, and Edward J. Carpenter. Trichodesmium, a globally significant marine cyanobacterium. *Science*, 276(5316):1221–1229, 1997. doi: 10.1126/science.276.5316.1221.

Kenneth H. Coale, Kenneth S. Johnson, Steve E. Fitzwater, R. Michael Gordon, Sara Tanner, Francisco P. Chavez, Laurie Ferioli, Carole Sakamoto, Paul Rogers, Frank Millero, Paul Steinberg, Phil Nightingale, David Cooper, William P. Cochlan, Michael R. Landry, John Constantinou, Gretchen Rollwagen, Armando Trasvina, and Raphael Kudela. A massive phytoplankton bloom induced by an ecosystem-scale iron fertilization experiment in the equatorial Pacific Ocean. *Nature*, 383(6600):495–501, October 1996.

R.A. Duce and N.W. Tindale. Atmospheric transport of iron and its deposition in the ocean. *Limnology and Oceanography*, 36:1715–1726, 1991.

Paul G. Falkowski, Richard T. Barber, and Victor Smetacek. Biogeochemical controls and feedbacks on ocean primary production. *Science*, 281(5374):200–206, 1998. doi: 10.1126/science.281.5374.200.

P.G. Falkowski. Evolution of the nitrogen cycle and its influence on the biological sequestration of CO_2 in the ocean. *Nature*, 387:272–275, 1997.

Dennis A. Hansell, Craig A. Carlson, Daniel Repeta, and Reiner Schlitzer. Dissolved organic matter in the ocean–a controversy stimulates new insights. *Oceanography*, 22(4):202–211, 2009.

T. Hiemstra and W.H. van Riemsdijk. Biogeochemical speciation of Fe in ocean water. *Marine Chemistry*, 102(3-4):181–197, 2006.

K. A. Hunter and P. W. Boyd. Iron-binding ligands and their role in the ocean biogeochemistry of iron. *Environ. Chem.*, 4(4):221–232, August 2007.

T.D. Jickells and L.J. Spokes. Atmospheric iron inputs to the oceans. In D.R. Turner and K. Hunter, editors, *The Biogeochemistry of Iron in Seawater*, volume 7 of *IUPAC Book Series on Analytical and Physical Chemistry of Environmental Systems*, pages 85–121. J. Wiley, 2001.

Yoshiko Kondo, Shigenobu Takeda, Jun Nishioka, Hajime Obata, Ken Furuya, William Keith Johnson, and C. S. Wong. Organic iron (iii) complexing ligands during an iron enrichment experiment in the western subarctic north pacific. *Geophys. Res. Lett.*, 35:L12601, June 2008. doi: 10.1029/2008GL033354.

Luis M. Laglera and Constant M. G. van den Berg. Evidence for geochemical control of iron by humic substances in seawater. *Limnology and Oceanography*, 54(2):610–619, 2009.

B.A. Maher, J.M. Prospero, D. Mackie, D. Gaiero, P.P. Hesse, and Y. Balkanski. Global connections between aeolian dust, climate and ocean biogeochemistry at the present day and at the last glacial maximum. *Earth-Science Reviews*, 99(1-2):61 – 97, 2010. doi: 10.1016/j.earscirev.2009.12.001.

J.H. Martin. Glacial-interglacial CO_2 change: The iron hypothesis. *Paleoceanography*, 5:1–13, 1990.

P. Parekh, M.J. Follows, and E. Boyle. Modelling the global ocean iron cycle. *Global Biogeochemical Cycles*, 18:GB1002, 2004. doi: 1029/2003GB002061.

Alessandro Tagliabue and Kevin R. Arrigo. Processes governing the supply of iron to phytoplankton in stratified seas. *J. Geophys. Res.*, 111(C6):C06019–, June 2006.

Raewyn M. Town and Montserrat Filella. Dispelling the myths: Is the existence of L1 and L2 ligands necessary to explain metal ion speciation in natural waters? *Limnology and Oceanography*, 45(6):1341–1357, 2000.

Thibaut Wagener, Elvira Pulido-Villena, and Cécile Guieu. Dust iron dissolution in seawater: Results from a one-year time-series in the Mediterranean Sea. *Geophys. Res. Lett.*, 35(16):L16601, August 2008.

Peter Warneck. *Chemistry of the natural atmosphere*. San Diego, CA, Academic Press, Inc., 1988.

L. Weber, C. Völker, A. Oschlies, and H. Burchard. Iron profiles and speciation of the upper water column at the Bermuda Atlantic Time-series Study site: a model based sensitivity study. *Biogeosciences*, 4(4): 689–706, 2007.

Chapter 4

Summary

This thesis aims to provide a better understanding of some aspects of the impact of atmospheric iron input on the iron cycling and the biological productivity in the ocean. In seawater, the fate of iron supplied by dust deposition is influenced by various processes such as iron dissolution, speciation, particle surface adsorption and redissolution of particulate forms of iron. Two one-dimensional models of Fe speciation and biogeochemistry for different ocean regions focus on some of these processes in this thesis.

The iron cycle in the tropical eastern North Atlantic, a site with high episodic dust fluxes from the Saharan desert, is modelled in the first study. The role of dust particles in removing dissolved iron is studied by a complex description of particle aggregation and sinking. The vertical distribution of different particle classes shows a high sensitivity to changing aggregation rates. The model considers two classes of iron-binding organic ligands, strong and weak ligands, and describes their sources and fate explicitly. The long residence time of weak ligands that is required in the model to obtain realistic profiles indicates that a fraction of weak ligands is more refractory. Colloidal aggregation is present as the main iron removal process below the mixed layer in the model and organic colloids could play an important role in regulating the complexation and the removal of iron.

The other model for the Mediterranean Sea simulates a mesocosm dust addition experiment, in which a significant decrease of dissolved iron in seawater has been observed after dust addition. This model explains this decrease mainly based on the balance of abiotic iron sources and sinks such as dissolution and particle adsorption, considering sinking and aggregation of different-sized particles. A concept of a critical concentration of dissolved iron, above which dust deposition acts as a net sink of dissolved iron, rather than a source, has been developed from the study. Taking into account the role of excess iron-binding ligands, this concept might be applied to explain the short-term variability of dissolved iron after natural dust deposition events.

Iron can impact the marine productivity not only by directly limiting the growth of primary producers, in particular in the high-nutrient, low-chlorophyll regions, but also by limiting N_2 fixation which is characterised by a high Fe requirement, and thus limiting the availability of reactive nitrogen for other primary producers. To study the impact of iron supplied by dust deposition on marine productivity, an ecosystem model including diazotrophs is coupled with a complex Fe speciation model for the tropical eastern North Atlantic. The seasonality and the limitation pattern of N_2 fixation is investigated in this model study. Diazotrophs and other phytoplankton have been found in competitive as well as mutually beneficial interactions in regard to the availability of nitrogen, phosphorus, iron and light to grow. In this ocean region, dust deposition is necessary to support diazotrophy and also impacts the growth of other phytoplankton significantly. A simple relationship between dust fluxes and the magnitude of N_2 fixation is however not found.

Zusammenfassung

Ziel der Arbeit ist, einige Aspekte der Auswirkung von atmosphärischem Eiseneintrag auf den Eisenkreislauf und auf die Produktivität im Ozean besser zu verstehen. Verschiedene Prozesse beeinflussen das weitere Schicksal des Eisens nach dem Eintrag in den Ozean als Staubbestandteil, z.B. die Auflösung und seine Speziation, die Adsorption auf Partikeloberflächen sowie die Wiederauflösung von partikulärem Eisen. Zwei ein-dimensionale Modelle der Eisenspeziation und Biogeochemie beschäftigen sich näher mit einigen dieser Prozesse.

Der Eisenkreislauf im tropischen Nordostatlantik ist in der ersten Studie modelliert. Hohe und episodische Staubflüsse aus der Sahara-Wüste bestimmen dieses Gebiet. Das Modell beinhaltet eine komplexe Beschreibung von Partikelaggregation und -sinken, um die Rolle von Staubpartikeln in der Eisenentfernung aus dem gelösten Pool zu untersuchen. Annahmen über die Aggregationsraten kontrollieren die vertikale Partikelverteilung stark. Die Quellen und Senken von Eisen-bindenden organischen Liganden sind detailliert beschrieben. Eine lange Verweildauer der schwachen Liganden ergibt sich aus dem Modell. Das weist auf die Existenz eines refräktären Anteils an den schwachen Liganden im Tiefenwasser hin. Kolloidaggregation ist der Hauptverlustsweg des gelösten Eisens unterhalb der durchmischten Oberflächenschicht, wobei die organischen Eisenkolloide eine wichtige Rolle in der Eisenkomplexierung und Kolloidaggregation spielen können.

Ein anderes Modell für das Mittelmeer simuliert ein Staubadditionsexperiment in Mesokosmen, in dennen eine signifikante Abnahme vom gelösten Eisen beobachtet wurde. Das Modell berücksichtigt das Sinken und die Aggregation von Partikeln in unterschiedlichen Größen und erklärt die Eisenabnahme hauptsächlich mit der Bilanz von abiotischen Quellen und Senken, der Auflösung von Staubpartikeln und der Adsorption auf Partikeloberflächen. Daraus läßt sich ein Konzept der kritischen Konzentration vom gesamten gelösten Eisen entwickeln, oberhalb derer die Staubdeposition eher als eine Netto-Senke auf gelöstes Eisen wirkt. Dieses Konzept kann angewendet und verallgemeinert werden, unter Berücksichtigung von freien Eisen-bindenden organischen Liganden. Dieses könnte dabei helfen, die kurzzeitige Veränderung des gelösten Eisens nach natürlichen Staubdepositionen und die unmittelbaren biologischen Reaktionen besser zu erklären.

Eisen kann direkt das Wachstum der primären Produzenten limitieren und dadurch die marine Produktivität beeinflussen. Es kann aber auch ein Limitierungsfaktor für N_2-Fixierung sein, weil diese einen besonders hohen Eisenbedarf hat. Die Stickstoffbilanz im Ozean hängt von der N_2-Fixierung ab, so dass Eisenlimitierung darüber eine indirekte Kontrolle der marinen primären Produktion ausüben kann. Ein Ökosystemmodell inklusive N_2-Fixierern wurde mit einem komplizierten Modell für Eisenspeziation gekoppelt, um die Aus-

wirkung von Staub auf die marine Produktivität im tropischen Nordostatlantik zu untersuchen. Die Modellstudie befasste sich mit der Saisonalität der N_2-Fixierung und der Rolle der verschiedenen Limitierungsfaktoren. Die Koexistenz von N_2-Fixierern und anderem Phytoplankton im Modell ist abhängig davon, dass N_2-Fixierung letztlich zur Freisetzung von reaktivem Stickstoff führt, während andererseits die Frühjahrsblüte von nicht-diazotrophem Phytoplankton zur Akkumulation von organischen Phosphorverbindungen führt, die von N_2-Fixierern wie *Trichodesmium* teilweise genutzt werden können. Daneben konkurrieren jedoch N_2-Fixierer und anderes Phytoplankton um Licht und Eisen. Nach dem Modell deckt die Staubdeposition im tropischen Nordostatlantik den Eisenbedarf der beobachteten N_2-Fixierung und reguliert auch die Abundanz aller primären Produzenten stark.

Chapter 5

Appendix

Publication IV

Iron biogeochemistry across marine systems
—progress from the past decade

Biogeosciences, 7, 1075–1097, 2010
www.biogeosciences.net/7/1075/2010/

Biogeosciences

Iron biogeochemistry across marine systems – progress from the past decade

E. Breitbarth[1,2], **E. P. Achterberg**[3], **M. V. Ardelan**[4], **A. R. Baker**[5], **E. Bucciarelli**[6,7], **F. Chever**[6,7], **P. L. Croot**[8], **S. Duggen**[9], **M. Gledhill**[3], **M. Hassellöv**[2], **C. Hassler**[10], **L. J. Hoffmann**[1,11], **K. A. Hunter**[1], **D. A. Hutchins**[12], **J. Ingri**[13], **T. Jickells**[5], **M. C. Lohan**[14], **M. C. Nielsdóttir**[3], **G. Sarthou**[6,7], **V. Schoemann**[15], **J. M. Trapp**[16], **D. R. Turner**[2], **and Y. Ye**[17]

[1]Department of Chemistry, University of Otago, Dunedin, New Zealand
[2]Department of Chemistry, University of Gothenburg, Gothenburg, Sweden
[3]National Oceanography Center Southampton, University of Southampton, Southampton, UK
[4]Norwegian University of Science and Technology, Department of Chemistry, Trondheim, Norway
[5]School of Environmental Sciences, University of East Anglia, Norwich, UK
[6]Université Européenne de Bretagne, France
[7]Université de Brest, CNRS, IRD, UMR 6539 LEMAR, IUEM, Plouzané, France
[8]IFM-GEOMAR, Leibniz-Institute of Marine Sciences, Division Marine Biogeochemistry, Kiel Germany
[9]IFM-GEOMAR, Leibniz-Institute of Marine Sciences, Division Dynamics of the Ocean Floor, Kiel, Germany
[10]Centre for Australian Weather and Climate Research (CAWCR), Hobart, TAS, Australia
[11]Department of Plant and Environmental Sciences, University of Gothenburg, Gothenburg, Sweden
[12]Department of Biological Sciences, University of Southern California, Los Angeles, CA, USA
[13]Luleå University of Technology, Division of Applied Geology, Luleå, Sweden
[14]Marine Institute, University of Plymouth, Plymouth, UK
[15]Ecologie des Systèmes Aquatiques, Université Libre de Bruxelles, Bruxelles, Belgium
[16]University of Miami, Rosenstiel School of Marine and Atmospheric Science, Department of Marine and Atmospheric Chemistry, Miami, USA
[17]Alfred Wegener Institute for Polar and Marine Research, Bremerhaven, Germany

Received: 31 May 2009 – Published in Biogeosciences Discuss.: 7 July 2009
Revised: 20 January 2010 – Accepted: 31 January 2010 – Published: 19 March 2010

Abstract. Based on an international workshop (Gothenburg, 14–16 May 2008), this review article aims to combine interdisciplinary knowledge from coastal and open ocean research on iron biogeochemistry. The major scientific findings of the past decade are structured into sections on natural and artificial iron fertilization, iron inputs into coastal and estuarine systems, colloidal iron and organic matter, and biological processes. Potential effects of global climate change, particularly ocean acidification, on iron biogeochemistry are discussed. The findings are synthesized into recommendations for future research areas.

Correspondence to: E. Breitbarth
(ebreitbarth@chemistry.otago.ac.nz)

1 Preface

An international workshop addressing the biogeochemistry of iron in the context of global change across marine ecosystems was held in Gothenburg, Sweden (14–16 May 2008). Largely driven by geographic separation, iron biogeochemistry in the open ocean and in coastal seas are often addressed as two distinct fields and the workshops organized over the past two decades have normally either been system- or task-specific. This has led to the development of system-specific expertise and research approaches, with potential separation of know-how. The aim of this workshop was to conduct a broader cross-system review of marine iron biogeochemistry by bringing together scientists from a wide range of coastal, shelf and deep-ocean environments to merge their system-specific knowledge into a truly cross-disciplinary and cross-system synthesis. This lead article is an attempt to

Published by Copernicus Publications on behalf of the European Geosciences Union.

summarize the scientific milestones of the past 10 years discussed during the workshop.

The Gothenburg workshop was convened almost ten years after a workshop meeting in Amsterdam, sponsored by SCOR and IUPAC which formed the basis for the book "The Biogeochemistry of Iron in Seawater" (Turner and Hunter, 2001). The Gothenburg workshop revisited the topics listed in the "Summary and Recommendations" of this book and took up two further cross-cutting aspects: (A) What can we learn from comparing Fe biogeochemistry in coastal and open ocean systems? And (B), how are global change processes expected to affect Fe biogeochemistry?

This article aims to synthesize the cross-system and interdisciplinary knowledge from atmospheric, chemical, biological, and geological angles discussed during the Gothenburg workshop and ties the manuscripts of the special issue "Iron biogeochemistry across marine systems at changing times" into this overall context. Due to this wide range of topics, it is not intended to be a comprehensive, in-depth review on all aspects of marine iron biogeochemistry. We follow the structure of the workshop topics, which were: Natural Fe fertilization (Sect. 2, articles: Ardelan et al., 2010; Chever et al., 2010; Duggen et al., 2010; Ye et al., 2009); artificial Fe fertilization (3: Bucciarelli et al., 2010; Chever et al., 2010); Fe inputs into coastal and estuarine systems (4: Gelting et al., 2009; Breitbarth et al., 2009); Colloidal iron and organic matter (5); Linking biological processes to iron chemistry (6: Breitbarth et al., 2009; Bucciarelli et al., 2010; Hassler and Schoemann, 2009; Steigenberger et al., 2010); and Iron and Climate Change (7: Breitbarth et al., 2010; Rose et al., 2009). Each section concludes with recommendations for future research.

2 Natural iron fertilization

The past decade brought major advances in the understanding of natural iron fertilization processes to the open ocean. The field is generally subdivided into two major areas: atmospheric deposition with the main focus on dust deposition from the continents and more recently addressing volcanic ash and pumice depositions; and marine processes, where particular areas of interest have been ice melting, hydrothermal vents, continental margins, and the island mass effects.

2.1 Atmospheric deposition – dust

Over the last 10 years, the importance of dust transport and deposition within the Earth System has become clear (Jickells et al., 2005). This includes the role of dust in transporting iron to the oceans, but also the transport of nutrients to land and impacts on albedo. Dust supply is episodic and predominantly from desert regions, and satellite advances have allowed these sources to be better characterized (Prospero et al., 2002). These satellite advances also allow some improvement in understanding of dust transport and deposition, but this is still limited to high dust regions where the total aerosol is dominated by dust (Mahowald et al., 2005). In regions remote from the desert sources, aerosols may be dominated by sea and acid salts. Furthermore close to a source region, particularly over the ocean off North Africa, the dust is transported at altitude, so the satellite detection of a dust plume, does not necessarily imply deposition to the oceans at that location (Mahowald et al., 2005). Since dust transport is episodic, field data to validate models and provide direct estimates of dust loading should ideally cover periods of months to years. Obviously though, shorter campaign style measurements can be useful for studying processes, and if repeated can provide long term average concentrations. The number of long-term dust monitoring stations is still very limited and broadly the same as identified in Jickells and Spokes (2001). This data set is dominated by the Prospero network (e.g. Ginoux et al., 2004), and the lack of data in the low dust regions, where ocean euphotic zone iron limitation is evident, is notable. Recent campaigns in some of these regions (Baker et al., 2006; Planquette et al., 2007; Wagener et al., 2008) do provide some confidence in the dust transport models, but the uncertainties in parameterizations within the models are still considerable and hence the uncertainties in flux estimates are still substantial. The work of Measures and colleagues (e.g. Han et al., 2008) has demonstrated the validity of a novel indirect approach of using surface water Al as a tracer of atmospheric deposition which provides data averaged over long time scales (months to years) in remote regions. Again this approach has significant uncertainties, but the broad agreement between this, long term field data, campaign data and models provides reassurance that the estimates of total dust deposition to the oceans and the regional patterns are realistic.

A major continuing source of uncertainty in estimating dust deposition to the oceans is associated with the parameterisation of wet and dry deposition, except in the few cases where wet deposition has been measured directly. The congruence of data and models noted above does provide some confidence that, at the global scale, the average deposition parameterization is approximately correct. This does not mean that the resultant dust flux from these averages is estimated correctly at the regional scale, or in the low dust regions of water column iron limitation. Duce et al. (1991) estimated uncertainties of a factor of three in the deposition flux and this uncertainty largely remains. Jickells et al. (1998) demonstrated that the use of ocean sediment trap data can provide a valuable constraint on the uncertainties in deposition fluxes and Mahowald et al. (2005) considered this further. However, the use of this technique in low dust regions does require high quality measurements of a dust tracer such as Al in the sediment traps and this is not always available. If this became routine it would offer a mechanism to significantly reduce uncertainties in deposition parameterization. Such an improvement would allow dust and iron mass

balance in individual regions and comparison to productivity estimates.

The conversion of dust deposition to soluble iron fluxes requires the solubility of iron from dust to be known. This is required ideally over the timescale of the residence times of dust in the water column (tens of days, see Jickells et al., 2005) and at realistically low dust loadings, although this is very difficult in practice and more pragmatic short term simple aerosol leaching schemes are usually applied (Baker and Croot, 2009).

Considerable effort has been put into studies of aerosol dust solubility over the last 10 years and this has tended to confirm that on a global average Fe solubility is low (Jickells et al., 2005; Mahowald et al., 2005), but also demonstrated that the use of a single solubility estimate is probably inappropriate and there does appear to be a systematic increase in solubility from high to low dust regions (Baker and Croot, 2009; Baker and Jickells, 2006). There is still considerable debate surrounding the drivers of this variation in solubility with four main possibilities; (i) atmospheric chemical processing during dust transport (Fan et al., 2006; Jickells and Spokes, 2001), (ii) systematic changes in aerosol particle size leading to changes in surface area and solubility (Baker and Jickells, 2006), (iii) an additional source of iron beside crustal dust (Jickells et al., 2005; Schroth et al., 2009); (iv) active biological acquisition and uptake mechanisms such as siderophores and grazing that can circumvent abiotic dissolution limitations (Barbeau and Moffett, 2000; Yoshida et al., 2002; Frew et al., 2006).

There is good evidence that solubility of iron from anthropogenic aerosol is higher than from soil dust (Schroth et al., 2009; Journet et al., 2008) but the significance of this high solubility anthropogenic dust to the global iron cycle is uncertain, and in particular it seems unlikely to be responsible for high iron solubilities in aerosols in remote regions seen for instance by Baker and Jickells (2006). However, recent measurements of iron speciation from African dust collected in the Trade Winds at Barbados support the case for anthropogenic iron controls over iron solubility. Trapp et al. (2010) show that Fe^{3+} dominates the iron solubility over the entire range of particle sizes. However, at low mineral dust concentrations Fe^{2+}, believed to be largely derived from anthropogenic sources, becomes increasingly important. Airmass back trajectories indicate biomass burning in southern Africa and potentially also South America as the source of this anthropogenic iron and dust samples had an Fe^{2+}/Fe^{3+} ratio twice that measured in dust-laden aerosols from North Africa. (Trapp et al., 2010).

In their contribution to this special issue, Ye et al. (2009) aim to improve the understanding of the impact of dust deposition on Fe bioavailability and marine primary productivity in modeling iron speciation and biogeochemistry at TENATSO (Tropical Eastern North Atlantic Time-series Observatory). Based on recent studies on Fe speciation and the existing model for the Bermuda Atlantic Time-series Study (BATS) (Weber et al., 2007), this model aims at studying the role of dust particles in Fe removal and providing a better description of the sources and fate of organic Fe-binding ligands.

Dry deposition probably dominates dust and iron deposition over some regions of the ocean, particularly those where winds flow off the land including areas downwind of major deserts such as the Sahara. Wet deposition is probably particularly important for total deposition in remote regions of the ocean. The data set for dust and soluble iron in wet deposition in the marine atmosphere is very small, and this requires improvement. To date, this discussion has largely considered only dust and iron deposition. However, atmospheric deposition delivers significant amounts of iron (Jickells et al., 2005) and nitrogen (Duce et al., 2008) and relatively small amounts of phosphorus (Mahowald et al., 2008) relative to phytoplankton requirements. Assorted trace metals that may play a role in phytoplankton productivity, including some that are potentially inhibitory, will also be deposited (e.g. Paytan et al., 2009). It is important that we evaluate the impacts of atmospheric deposition holistically, and not artificially separate the contributions of individual nutrients.

2.2 Other atmospheric and marine processes of natural Fe fertilization

All short-term artificial Fe fertilization experiments unequivocally showed the importance of Fe on the carbon cycle, in particular on the food web structure and functioning (e.g. Boyd, 2004; Boyd et al., 2007, 2000; Coale et al., 1996, 2004; Gervais et al., 2002; Tsuda et al., 2003; de Baar et al., 2005, see Sect. 2). However, it is difficult to reliably assess the magnitude of carbon export to the ocean interior using such methods (Blain et al., 2007). Recent natural Fe fertilization experiments carried out in the Southern Ocean showed that the efficiency of fertilization was at least 10 to 20 times greater than that of a phytoplankton bloom induced artificially by adding iron, (KEOPS and CROZEX, Blain et al., 2007; Pollard et al., 2009). Large losses of purposefully added iron can explain the lower efficiency of the induced bloom, as well as the mode of iron addition and the requirement of concomitant supply with major nutrients (Pollard et al., 2009; Blain et al., 2007). In the open ocean, a large variety of naturally iron-fertilized sites exist, which could allow for improved forecasting of the oceanic response to Fe fertilization and a better knowledge of Fe sources to the open ocean. Chever et al. (2010) provide a Fe budget for the naturally fertilized area above the Kerguelen Plateau, using total dissolvable Fe as an additional tracer to better constrain the Fe cycle in this area. They show that horizontal advection of water from South of the Plateau seems to be the predominant source of apparent particulate and dissolved iron above the plateau, over atmospheric and vertical inputs. Further, Ardelan et al. (2010) illustrate natural Fe enrichment processes from the South Shetland Islands-Antarctic Peninsula region.

As discussed in Sect. 2.1, aeolian inputs may have different origins, such as (i) the arid and semi-arid regions (Jickells et al., 2005), (ii) combustion sources (fossil fuel burning, incinerator use, biomass burning; (Spokes and Jickells, 2002; Guieu et al., 2005; Sedwick et al., 2007; Luo et al., 2008), but also by (iii) meteoritic material and extraterrestrial dust (Johnson, 2001), and (iv) volcanic origin (Benitez-Nelson et al., 2003; Duggen et al., 2007; Boyd et al., 1998). All atmospheric input may have an effect on biological productivity in the ocean (Schroth et al., 2009), in particular on bacterial activity (Pulido-Villena et al., 2008), although the causative link is not always obvious as shown by (Boyd et al., 2009).

While the meteoritic contribution is difficult to assess due to the sporadic events, the amount of soluble (presumably bioavailable) iron input into the ocean from extraterrestrial dust is estimated to be $7 \times 109\,\mathrm{g\,year^{-1}}$ (Johnson, 2001) and is thus not insignificant. More so, volcanic eruptions can transport volcanic ash up to several tens of kilometres high into the atmosphere and fine ash may encircle the globe for years, thereby reaching even the remotest and most iron-starved oceanic areas (Schmincke, 2004). The implication of volcanism for the marine biogeochemical iron-cycle is poorly constrained so far. Recent studies demonstrate that volcanic ash from volcanoes worldwide quickly releases soluble and bio-available iron on contact with water (e.g. Jones and Gislason, 2008; Duggen et al., 2007; Frogner et al., 2001). Drill core data from scientific ocean drilling show that volcanic ash layers and dispersed ash particles are frequently found in marine sediments and that volcanic ash deposition and therefore iron-injection into the oceans took place throughout much of the Earths history (Straub and Schmincke, 1998). It may thus well be possible that the contribution of volcanic ash to the marine biogeochemical iron-cycle is generally underestimated. A review paper (Duggen et al., 2010) summarises the development and the knowledge in a fairly young research field covering a wide range of chemical and biological issues and gives recommendations for future directions. The approach by Duggen et al. (2010) contributes to understanding of the role of volcanic ash for the marine biogeochemical iron-cycle, marine primary productivity and the ocean-atmosphere exchange of CO_2 and other gases relevant for climate throughout the Earths' history.

Melting of sea ice, icebergs and glacial inputs may contribute as Fe sources in polar regions. Estimates of these sources' magnitudes are poorly constraint. Recent studies have highlighted the importance of these sources (Lannuzel et al., 2008; Lannuzel et al., 2007; Statham et al., 2008; Aguilar-Islas et al., 2008; Raiswell et al., 2008, 2006; Smith et al., 2007; Croot et al., 2004). Iron accumulates in sea ice with concentrations one to two orders of magnitude higher than the underlying seawater. Atmospheric iron can be one source but flux estimates by Lannuzel et al. (2008, 2007) seem to indicate that iron must come mostly from below. The exact mechanism remains unclear, but recent evidence suggests that organic matter could play an essential role in trapping Fe in the sea ice not only during sea ice formation but also during ice algae proliferation in the bottom ice after its formation (Schoemann et al., 2008). Its release into the seawater during ice melting can occur in short time spans such as weeks. For example, Lannuzel et al. (2008) showed that 70% of the accumulated Fe in the sea ice could be released due to brine drainage in a 10 days period, while the sea ice cover was still present. This represents a significant Fe flux to the surface ocean that may be instrumental in sustaining springtime ice edge blooms in the marginal ice zone and polynias. Dense phytoplankton blooms have been observed in combination with the receding ice edge or in coastal shelf areas (e.g. Smith and Nelson, 1985; Holm-Hansen et al., 1989). Moreover, both sea ice and icebergs may constitute vectors of Fe transport far away from its initial source (Smith et al., 2007; Lancelot et al., 2009). Further to this, Edwards and Sedwick (2001) addressed the contribution of snow bound aerosol iron in the Antarctic seasonal sea ice zone.

The continental margins may also play a key role as a Fe source (Elrod et al., 2004; Laës et al., 2003, 2007; Chase et al., 2005; Blain et al., 2008). As an example, Lam and Bishop (2008) clearly showed that the continental margin was a key source of Fe to the HNLC (high nutrient low chlorophyll) North Pacific Ocean, since the lateral source of Fe is shallow enough to be accessible to phytoplankton by winter mixing and Fe can be transported at distance over 900 km from the continental shelf.

Our current challenge in regions where natural iron fertilization occurs is to have a better knowledge and quantification of these various Fe sources. For example, the global atmospheric iron fluxes are reasonably well known, but the fluxes to remote low iron regions are rather uncertain. Moreover, the aerosol iron solubility varies systematically, but the underlying causes of this are uncertain. In the deep waters, Fe can be transported far away from the source, especially in waters with anoxic conditions (Blain et al., 2008). Local and remote sources of Fe may not have the same impact on carbon cycle. We also need to understand how (i) the different sources of Fe influence its speciation and bioavailability; (ii) they contribute to the global Fe budget; (iii) they will be affected by global change, and (iv) what are the physical mechanisms that allow long distance Fe transport: advection (strong currents, ACC, EUC, de Baar et al., 1995; Mackey et al., 2002; Lam and Bishop, 2008; Loscher et al., 1997), internal waves and slope circulation (Laës et al., 2003), and eddies (Johnson et al., 2005). Finally, the physical mechanisms that allow Fe to be accessible for the food web should also be better understood and quantified (upwelling, diapycnal mixing, winter mixing, Blain et al., 2007).

To asses these challenging issues, there is a crucial need for (i) multi-disciplinary studies (physics/biogeochemistry/biology), (ii) multi-proxy approaches, such as the one promoted by the international

GEOTRACES program, including oceanic sections and intercalibration experiments for seawater and aerosols; (iii) the development of biogeochemical models that correctly take into account the various Fe sources and their impact on Fe speciation and bioavailability, and (iv) the development of regional iron budgets.

3 Artificial iron fertilization

The largest source of iron for the HNLC surface waters comes from deep water supply (Watson, 2001). However, the Fe:N or Fe:P ratio of the upwelled deep waters is often not high enough for optimum phytoplankton growth (Moore et al., 2006). Consequently, an additional source of iron is required, which could be derived from suboxic or anoxic sediments (Las et al., 2007) or dust inputs (Jickells et al., 2005). Fertilization of the Southern Ocean with dust has been suggested as an explanation for past glacial periods (Martin, 1990). During these periods iron dust inputs to the oceans were strongly enhanced, with the Southern Ocean receiving up to 10 times more dust-derived iron (Wolff et al., 2006), and consequent stimulation of phytoplankton growth and the biological carbon pump. Nevertheless, it has been estimated that the increase in iron stimulated productivity could have contributed perhaps 15–25% of the 80–100 ppm drawdown in atmospheric CO_2 observed during glacial maxima by enhancing the biological carbon pump (Sigman and Boyle, 2000; Bopp et al., 2003).

When trace metal clean techniques became available in the late 1980s it was possible to directly test the effect of iron additions on phytoplankton growth in HNLC regions. Ship-board iron-addition bottle experiments clearly showed that these additions stimulated phytoplankton growth (e.g. de Baar et al., 1990). However, the potential for bottle-effects during these experiments led researchers to plan and undertake mesoscale Lagrangian-type oceanic experiments to study the influence of iron additions on primary productivity, and investigate the consequences for nutrient utilization, ecosystem dynamics and carbon export. More than a dozen of these large scale (typically 10×10 km grid) iron addition experiments have been conducted to date in HNLC regions and were reviewed by de Baar et al. (2005) and Boyd et al. (2007). Recent experiments involved conducting iron, carbon, nutrient, climatically active gasses, and ecosystem observations, the latest being Lohafex (January–March, 2009; Editorial Nature Geoscience, Editorial, 2009) following a 300 km^2 iron addition in a stable Southern Ocean mesoscale eddy for >7 weeks. The longer time scale allowed a thorough examination of biogeochemical and ecosystem changes and carbon export.

In summary, all artificial iron experiments have confirmed that iron supply limits primary production and has impact on phytoplankton species composition and bloom dynamics in tropical as well as in polar HNLC waters (Boyd et al., 2007; de Baar et al., 2005). Iron limitation also induces a decoupling in the use of macronutrients by phytoplankton, likely to influence the cycling of the major biogeochemical cycles (C, N, P, Si, S) over geological time scales (de Baar and La Roche, 2003). In addition to iron, light has been shown to play an important role in the regulation of phytoplankton production in HNLC regions (Moore et al., 2007a, b; Maldonado et al., 1999; Boyd et al., 2001; Hoffmann et al., 2008; de Baar et al., 2005; Bucciarelli et al., 2010). Overall, in situ iron fertilization experiments have greatly enhanced our knowledge about iron solubility, organic iron complexation, and the importance of iron redox states (e.g. Rue and Bruland, 1995; Croot et al., 2001; Rue and Bruland, 1997), which apply to Fe biogeochemistry in the ocean in general.

Large scale iron oceanic addition has been suggested as an option for mitigating the present day increasing atmospheric CO_2 concentrations (Kintisch, 2007). The Southern Ocean is the HNLC region where iron stimulation of CO_2 sequestration would be most efficient and yield long-term carbon storage in deeper waters (Sarmiento and Orr, 1991). Currently there are a number of uncertainties surrounding intentional, large-scale, ocean iron fertilization, which will require further research for clarification. These have already been critically assessed by Chisholm et al. (2001) as well as more recently by Buesseler et al. (2008). Potential side effects include that the mineralization of the enhanced sinking phytoplankton biomass could result in local anoxia and consequent negative effects to oceanic ecosystems and the production of the harmful greenhouse gases nitrous oxide and methane (Cullen and Boyd, 2008; Furman and Capone, 1991). Other climate active gases, like dimethylsufide (DMS) might increase following Fe fertilisation (Liss et al., 2005). Direct ecosystem shifts resulting in for example proliferation of jellyfish have also been suggested. Furthermore, purposeful iron fertilization may result in a reduced nutrient inventory and consequently reduced productivity and potentially fisheries in oceanic systems downstream of the fertilization areas (Gnanadesikan et al., 2003).

A further key unknown is the efficiency of carbon removal. The amount of carbon sequestered per unit addition of iron is crucial to the effectiveness of iron fertilization (de Baar et al., 2008). The artificial experiments have indicated an efficiency of biological carbon export into deeper water (100–250 m) ranging from 650 (SERIES, Boyd et al., 2004) to 3300 (mol C/mol Fe) (SOFEX – south, Buesseler et al., 2004). The seasonal sequestration efficiencies estimated for natural Fe fertilization are much higher, 8640 for CROZEX (Pollard et al., 2009) and 154 000 for KEOPS (Chever et al., 2010). The discrepancies in effectiveness between natural and purposeful fertilizations might be partly due to the $\sim$75% immediate loss of added Fe in artificial fertilisations (de Baar et al., 2008). These values will need to be much more tightly constrained to allow a thorough assessment of the potential success of iron fertilization as a means to reduce the increasing atmospheric CO_2 concentrations and cost

(Boyd, 2008). The success of the large scale oceanic additions of iron has furthermore been put into doubt by modeling studies. Recent work by Dutkiewicz et al. (2005) and Aumont and Bopp (2006) suggests that large scale iron additions would only reduce atmospheric CO_2 concentrations by ca. 10 ppm, as other limiting factors such as light and zooplankton grazing become more important. It appears that large uncertainties remain with respect to the efficiency of iron fertilization that require further investigations using observation and models. For a recent in depth assessment of the topic see Boyd et al. (2007), as well as Boyd (2008) and associated publications. From a marine trace-metal research perspective, the attendants of the workshop came to the conclusion, that priority should be given to small scale open ocean Fe biogeochemistry studies that are specifically designed to address clearly defined research questions of trace-metal chemistry.

4 Fe inputs into coastal and estuarine systems

The coastal area is a key environment in the global iron cycle, where the brackish water environment changes the physicochemical speciation, and thus mobility, of river-introduced iron via aggregation, sedimentation and redox processes. The coastal waters also are a highly dynamic transition zone, resulting in very diverse temporal and spatial chemical and biological changes. Total concentrations of iron in coastal waters though are generally several orders of magnitude higher than open ocean values and at a first glance, iron limitation of primary production in coastal areas seems not very likely. However, temporal growth limitation by iron can occur in some coastal upwelling regions (Bruland et al., 2001; Hutchins and Bruland, 1998) and fjord systems (Öztürk et al., 2002).

The world's largest estuary, the Baltic Sea, serves as an excellent large scale laboratory to study trace metal chemistry over a wide salinity gradient. Here the total iron concentration decreases by more than an order of magnitude from the low salinity north-east (Bothnian Bay), via the Bothnian Sea to its central part (Baltic Proper), thus forming a natural well defined iron concentration gradient for studying physicochemical speciation of iron and the role of iron for primary production at different total (unfiltered) iron concentrations (Gelting et al., 2009). The authors observed significant variations in the physicochemical speciation, including the iron isotopes, at high temporal resolution from the euphotic zone. Other large river systems such as the Columbia River and Mississippi also show large gradients in iron concentrations but also act as significant sources of Fe to coastal regions (Powell and Wilson-Finelli, 2003; Lohan and Bruland, 2006).

In addition to photochemical processes and organic complexation it is the cycling of iron between particles, colloids and the truly dissolved fraction (<1 kD), rather than the total concentration, that determines the bioavailability of iron in coastal surface water. The truly dissolved fraction can rapidly be consumed during bloom conditions if this fraction is small and exchange processes between particulate-colloidal matter and the truly dissolved fraction are slow. Hence, knowledge about distribution and cycling of iron between these phases in the coastal zone is fundamental for predictions about iron limitation for plankton growth, and is key to understanding iron export pathways to the open ocean. For the Baltic Sea, Gelting et al. (2009) show that iron in the <1 kDa fraction never reached critical low levels during summer phytoplankton bloom conditions. Further, Fe(II) is generally not considered as an abundant source of bioavailable iron due to its short residence time in oxygenated water. However, a relatively high standing concentration of Fe(II), large enough to cover the demand for iron by cyanobacteria in Baltic Sea waters, was observed by Breitbarth et al. (2009) in a study paralleling Gelting et al. (2009).

Measurements of the physicochemical speciation of iron in freshwater during the last five years suggest that iron transport in rivers is associated with two types of carrier phases (besides detrital particles), an oxyhydroxide phase with associated CDOM (chromophoric dissolved organic matter, mostly consisting of humic acids) and an organic carbon (fulvic) phase (e.g. Lyvén et al., 2003; Andersson et al., 2006). Much of this fulvic phase is present as small colloids and in the truly dissolved fraction (<1 kD). When these phases reach the saline coastal water substantial aggregation of the Fe-oxyhydroxide fraction with associated CDOM is observed, whereas iron associated to the fulvic fraction show little aggregation (Stolpe and Hassellöv, 2007) and survives the sequential sequestration from the water column during gradual mixing with seawater (Krachler et al., 2005). It is possible that this land-derived fraction can reach the open ocean, as indicated by recent data (Laglera and van den Berg, 2009). With fulvic acid as one important carrier mechanism for riverine Fe, the influence of this Fe source reaches further out to sea than previously expected. Tovar-Sanchez et al. (2006) for example, suggested based on metal composition, that riverine and not dust born material was the main source of trace metal accumulation in a diazotroph (*Trichodesmium* sp.) dwelling the surface waters of the subtropical and tropical North Atlantic Ocean.

Back at the river-seawater interface, Gerringa et al. (2007) argue that particularly the weak iron ligand groups (L_2) may impede the precipitation of Fe in the Scheldt Estuary upon mixing with seawater and that the strong ligand (L_1) generally observed in the open ocean, albeit also present, were insufficient in concentration. Powell and Wilson-Finelli (2003) though point out that the latter is of crucial importance for Fe transport in the Mississippi river plume. Likewise, Buck et al. (2007) demonstrated the predominant importance L_1 type ligands for Fe transport into the sea from the Columbia River and San Francisco Bay plumes. The stability constants of these strong L_1 ligands are very similar to those reported by

Laglera and van den Berg (2009) for Fe bound to fulvic acids, indicating the importance of these ligands in controlling the solubility of dissolved iron in riverine and coastal systems. Clearly, Fe speciation in estuarine and near-shore waters can not be addressed in a generalized manner and systems may differ depending on watershed characteristics (e.g., pristine versus anthropogenically impacted) as well as the level and type of riverine input (Öztürk and Bizsel, 2003; Krachler et al., 2005) (see Sect. 5 for colloidal matter).

Ingri et al. (2006) suggest that iron isotopes could be used to roughly identify the two major suspended fractions for iron in river water, the oxyhydroxides phase, which shows positive δ^{56} values, and the fulvic fraction that has a more negative signal. River water-seawater mixing experiments by Bergquist and Boyle (2006) showed that aggregated Fe was enriched in heavy isotopes. Hence, aggregation and sedimentation of the oxyhydroxide fraction during estuarine mixing should remove heavy isotopes from surface suspended matter, resulting in a more negative signal in the suspended phase, as indicated by field data from the River Lena freshwater plume (J. Ingri, personal communication, 2009). Cycling of iron in coastal areas appears to result in export of a negative iron isotope signal in the truly dissolved fraction, suggesting that open ocean water generally has a negative dissolved isotope iron signal thus explaining the negative δ^{56} value in ferromanganese crusts in the deep-sea. However, recent data indicate that bottom water in the open ocean has a positive δ^{56} value (Lacan et al., 2008), although it should be noted that the dataset is limited to one depth profile.

Iron isotope data from surface water in the Baltic Sea reveal systematic temporal variations in the Fe-isotope signal. For example, the δ^{56} value changed from -0.1 to $+0.25$‰ during a diatom spring-bloom resulting in subsequent sedimentation of iron with a negative isotope signal (Gelting et al., 2009). During the summer a relatively stable positive δ^{56} value was measured in suspended matter at different locations. This was likely due to a combination of river introduced aggregated oxyhydroxides and particulate iron formed from oxidation of dissolved Fe(II) in surface water. In this low salinity system, river introduced Fe-oxyhydroxides aggregate, but may not sediment in the river estuaries due to the lack of detrital sinking and flocculation processes and hence can spread far into the Baltic Sea (Gustafsson et al., 2000). This system is in sharp contrast to recently revised very rapid aggregation and sedimentation processes for direct river – seawater mixing (Nowostawska et al., 2008).

Recent advances suggest that iron isotope measurements have a large potential to provide new information on iron cycling and iron transport from coastal areas to the open ocean (de Jong et al., 2007). Fe/Ti or Fe/Al ratios close to average crust material do not necessarily indicate that the suspended phase mainly reflects detrital particles. Both positive and negative iron isotope values have been measured although the sample has a Fe/Ti or Fe/Al ratio close to average crust material. Furthermore, a δ^{56} value around zero does not necessarily mean that the sample consists of mainly detrital rock fragments, as it usually is a mixture of iron particles with positive and negative δ^{56} values (Gelting et al., 2009). Recommendations for future work thus consist of a focus on this field including continuing the characterization of the carrier phase for Fe across the salinity gradient and into the open ocean.

5 Colloidal iron and organic matter

Ten years ago the focus of Fe biogeochemistry was on dissolved (filterable) iron speciation and quite specific iron complexes. Once overlooked and neglected (Wells, 1998), progress has been made in understanding the nature and importance of organic colloidal material in seawater and coastal systems and challenged the simple discrimination into particulate and dissolved iron (0.45 or 0.2 µm filtered). Furthermore, dynamic exchange between larger iron particles, colloidal iron, and soluble iron (defined as passing either a 0.02 µm or a 1 kDa filter) also directs interest towards the particulate and soluble phase. The FeCycle study, a mesoscale SF6 tracer release experiment without iron perturbation in HNLC waters southeast of New Zealand (Boyd et al., 2005), showed that iron recycling rates due to biological iron uptake and regeneration exceeded input of new iron by 10-fold. Further, particulate Fe would undergo a transformation from lithogenic to biogenic iron during settling through the mixed layer. Rapid biological processing (bacterivory and herbivory, subsequent biological uptake) after dissolution of dust deposited iron hydroxides and presumably also photolysis of siderophore complexed Fe(III)-hydroxide (Borer et al., 2005) resulted in exchange from the lithogenic particulate phase via the soluble to the biogenic particulate phase (Frew et al., 2006; Strzepek et al., 2005; Maldonado et al., 2005). The rapid exchange with particulate iron phases provides new insight into iron cycling and export dynamics since the role of particulate iron in iron biogeochemistry appears more important than previously assumed. During the Gothenburg workshop however, the main center of attention was on colloidal iron and we therefore focus thereon hereafter.

Moran et al. (1996) measured iron, among other bioactive trace metals, in colloidal matter obtained by cross-flow filtration of seawater. The major proportion of the dissolved Fe in open ocean seawater (here defined as 0.4 µm filtered) was found to be in the colloidal form (here defined as >0.02 µm–0.4 µm) (Wu et al., 2001), with continuing debate about the bioavailability of this fraction. Chen and Wang (2001) showed that freshly precipitated colloids were available to phytoplankton but aging processes (15 days) reduced markedly their availability. Wang and Dei (2003) demonstrated that Fe availability from colloidal matter to cyanobacteria (*Synechococcus*, *Trichodesmium*) is largely dependent on the size and origin of the material, with the tendency of Fe bound to smaller colloids and biogenic colloidal

material derived from the same species being more available. The transfer from the soluble to the colloidal fraction appears rapid for iron in comparison to for example Zn, resulting in dynamic cycling including particle formation, and the drawdown of colloidal Fe indicated uptake by phytoplankton (Hurst and Bruland, 2007). Further, colloidal Fe is photoreactive and thus also contributes to the bioavailable pool of Fe(II) in surface waters (Barbeau, 2006; Fan, 2008).

Dissolved organic matter (DOM, which contains the colloidal fraction) in seawater has previously been considered to be old (∼6 KY) and refractory (Bauer et al., 1992). This refractory pool is also known to be rich in aromatic chromophoric material therefore often called chromophoric DOM (CDOM). However, in the last ten years the picture has changed somewhat and now it is believed that in addition to the refractory pool seawater DOM also consists of in situ biologically derived material, rich in proteic matter and sacharides and saccharide derivatives as building blocks (Aluwihare et al., 1997). In addition significant findings have been made to understand that fractions of marine DOM possess a gel forming character, including spontaneous assembling into microgels after filtration, where calcium bridging is shown to be important (Chin et al., 1998). In addition, new microscopy based techniques have shown that fibrillar type materials, hypothesized to consist of acid polysaccharides, are abundant in many open ocean regimes (Santschi et al., 1998). This marine gel phase can be an important transfer route from truly dissolved to particulate pool of matter (Verdugo et al., 2004). These findings in the dissolved fraction seem to link well to the marine snow formation of transparent exopolymeric particles (TEP), which are important for carbon export (Engel et al., 2004), although direct experimental evidence linking the fibrillar material to TEP and sedimentation has been lacking.

To what extent these processes and phase transfers in organic matter are controlling the physicochemical states and vertical distributions of iron and other trace elements has previously only been hypothesized. Stolpe and Hassellöv (2010) coupled Flow Field Flow Fractionation (FlFFF) with ICPMS, on-line "humic" fluorescence and UV-absorbance detectors, and subsamples for Atomic Force Microscopy (AFM) to fractionate and identify different colloidal size classes and associated trace metals during phytoplankton bloom events in a Fjord on the North Sea coast of Sweden. They found both seasonal and vertical variations in the colloidal size distributions for iron and other trace elements and could use these in order to explain the apparent iron solubility and vertical distribution to a large extent (Stolpe and Hassellöv, 2010). During the winter season colloidal size distribution for iron (and many other elements) were only appearing in the CDOM fraction (∼0.5–3 nm), while during the spring bloom and summer bloom in two consecutive seasons the colloidal size distributions for iron were shifting dramatically. In addition to the CDOM phase, iron partitioned into two larger size classes. With AFM these two colloidal populations were identified to be semispherical (3–7 nm) and fibrillar (∼0.5 nm thick and 30–200 nm long). From the partitioning of other elements and their size and shape it was hypothesized that the semispherical colloids were mainly thiol rich proteic biopolymers, while the fibrillar materials were polysaccharide rich exudates that could be the precursors of the microgels proposed by Chin et al. (1998). The conclusion that the seasonal variations of iron association with different colloidal phases to some extent control the apparent iron solubility in estuarine water is in line with the findings from Bergquist et al. (2007), implying that colloids in the open ocean control iron solubility. Likewise, Boehme and Wells (2006) and Floge and Wells (2007), using FlFFF coupled to excitation emission matrix spectroscopy and a UV-absorbance detector, observed a shift in colloidal size class distribution between protein-like and humic-like fluorescence of CDOM during phytoplankton blooms in an estuary.

Progress has been made in studying the behavior of iron oxide nanoparticles in different freshwater and salt matrixes and drawing conclusions for the inorganic phase within the filterable fraction (Hassellöv and von der Kammer, 2008, and references therein). Partly based on this work, the understanding of flocculation processes has improved and previous concepts (Sholkovitz, 1978; Sholkovitz et al., 1978) have been confirmed. Mylon et al. (2004) using natural organic matter (NOM) coated synthesized hematite colloids, show that the rate of colloid aggregation reaches a maximum at a salinity of 12, resulting in a removal of 80–90% of dissolved iron in a process occurring on a time scale of seconds (Nowostawska et al., 2008). The colloidal particles are stabilized by NOM due to electrostatic and repulsive forces (Mosley et al., 2003; Sander et al., 2004). Theoretically in seawater the conditions would favor attachment, but low particle concentrations result in a low collision frequency. Further, colloidal matter undergoes a transformation in size distribution and elemental composition upon introduction from fresh water into a seawater system (Stolpe and Hassellöv, 2007). The efficiency of transport through salinity gradients needs more investigation and isotope studies may be of significant importance to form a proper understanding of fluvial iron inputs into the sea (see Sect. 4).

As aforementioned, recent methodological advancements include the application of field flow fractionation (FFF), in conjunction with size fractionation by membrane and/or ultrafiltration techniques, to studies of the metal-colloidal phase (Boehme and Wells, 2006; Stolpe et al., 2005). FFF was generally applied to samples from coastal systems and detection limits necessitate the use of pre-concentration steps. While being a powerful tool to characterize size fractionated material, FFF can also help in developing robust filtering methods particularly at the lower end of the size range, as results reveal artefacts from membrane filtration can result in unintended removal of undersized material (Howell et al., 2006). The relevance of this for open ocean seawater

requires further testing. Further, cross-flow ultra-filters are defined as a molar cut-off, which may result in retention of undersized components and permeation of oversized components, as well as separation of size and chemical composition (Assemi et al., 2004). An intercalibration of cross-flow filtration techniques was carried out previously (Buesseler et al., 1996), but a new approach including classical membrane filtration and utilizing FlFFF coupled to ICPMS may yield valuable information about the robustness of different filter membranes with regard to fractionation of colloidal size classes and their elemental composition.

We conclude that future research directions should encompass further in depth characterizations of the different phases (particulate, colloidal, soluble), which may lead to a redefinition of the term dissolved iron. This will also lead to a better structural definition of bioavailable iron. We need to learn how iron is fractionated into specific size classes, what the exchange kinetics between these phases are, and what controls/catalyzes them. Specifically, the origin and nature of iron binding ligands needs to be further addressed to elucidate the role and characteristics of different ligand classes (L_1, L_2). In that, we may need to overcome measurement artifacts due to pre-concentration procedures that are necessitated due to the detection limits especially in open ocean applications (see also last two paragraphs of Sect. 6).

6 Linking biological processes to iron chemistry

Most areas of the open ocean have surface trace metal concentrations between picomolar and nanomolar levels, which are about one millionth of the concentration in phytoplankton cells (Morel and Price, 2003). Iron is required for many important cellular processes such as photosynthesis, respiration, nitrogen fixation and nitrate reduction. A recent laboratory study involving 15 neritic and oceanic phytoplankton species produced an elemental ratio of $C_{124}N_{16}P_1Fe_{0.0075}$ (Ho et al., 2003), similar to previous reviews of Fe:C ratios which have found a range of 2.3–370 µmol:mol (Sarthou et al., 2005; see also Twining et al., 2004). Research has linked the oxygenation of the oceans and the subsequent drop in iron solubility and thus iron availability to the evolution of more iron efficient phytoplankton (Quigg et al., 2003; Saito et al., 2003) that are able to cope with the low iron open ocean conditions. Phytoplankton species have evolved very effective acquisition mechanisms with high trace mtal affinities that involve interactions with organic iron binding ligands. Uncertainties remain on the nature of such ligands, which control Fe chemistry and bioavailability in marine systems (Hunter and Boyd, 2007).

Culture experiments have established that marine phyto- and bacterioplankton have different iron requirements that are linked to their biogeographical sources (Sunda and Huntsman, 1995; Brand et al., 1983). More recent work has shown that picophytoplankton, which dominate the oligotrophic regions of the oceans, are able to grow optimally in culture at extremely low inorganic iron concentrations of 10–15 pM inorganic Fe, (Timmermans et al., 2005). Our ability to relate these studies to the real environment is however limited by our understanding of the chemical speciation of iron in the ocean (Gledhill and van den Berg, 1994; Rue and Bruland, 1995). These studies indicated that dissolved iron is strongly complexed in the ocean, results which have been confirmed on many occasions since (as discussed in Hunter and Boyd, 2007). The composition of this organic fraction is still not well understood, although it appears likely that it will consist of autochthonous complexing ligands produced by marine phyto- and bacterioplankton (Mawji et al., 2008; Boye et al., 2005; Kondo et al., 2008; Vong et al., 2007) and complex organics such as humic/fulvic acids (Laglera and van den Berg, 2009). Calculations of the inorganic iron concentration based on measurements carried out by competitive equilibration cathodic stripping voltammetry show that inorganic iron concentrations in the ocean are of the order of 10^{-14}–10^{-11} M (Morel et al., 2008), although these calculations neglect the contribution of Fe(II), which may also be present at concentrations of the order of 10^{-11} M in surface waters (e.g. Hansard et al., 2009; Roy et al., 2008b; Croot et al., 2001). It is not clear how much of the organically complexed iron is available to marine phyto- and bacterioplankton, and parameters controlling Fe bioavailability to primary producers are still poorly understood.

Fe bioavailability is influenced by its chemical forms (speciation, redox state), biological cycling, and the different uptake strategies of the phyto- and bacterio-plankton communities (Barbeau et al., 1996; Hutchins et al., 1999a; Strzepek et al., 2005). Competition for available Fe is strongest when Fe is in short supply (e.g. Worms et al., 2006). Recent advances in our understanding and abilities to model iron uptake by marine phytoplankton (Morel et al., 2008; Shaked et al., 2005; Salmon et al., 2006) indicate that even at these low inorganic iron concentrations, open ocean phytoplankton will have sufficient iron to grow. Initially iron uptake was thought to be proportional to the concentration of inorganic Fe species (Fe') (Hudson and Morel, 1990). However, this model proved to be too simplistic to explain phytoplankton growth in natural systems where concentrations of inorganic iron species were extremely low due to organic complexation. Thus either the iron-ligand complex (FeL) is directly taken up, or the inorganic Fe availability is increased, e.g. by reduction to Fe(II). More recently two models have been published to describe the kinetics of Fe uptake. The Fe(II) model by Shaked et al. (2005) and the FeL model by Salmon et al. (2006). There are significant distinctions between these models which lead to differences in the predictions of phytoplankton iron limitation in culture experiments. While the Fe(II) model considers the surface Fe(II) concentration and explicitly includes unchelated Fe(III) as a source of Fe(II) for phytoplankton uptake, the FeL model considers the bulk concentration of Fe(II) in the

media as the controlling parameter and excludes unchelated Fe(III) as an irrelevant source (Morel et al., 2008). Morel et al. (2008) point out that the observed decrease in Fe uptake rates with increasing EDTA concentrations can only be explained by the Fe(II) model, which results in the conclusion that unchelated Fe(III) is indeed an important source of Fe(II) for phytoplankton uptake. However, phytoplankton species behave differently under Fe limitation and it is likely that future experiments under more natural conditions without the presence of EDTA will result in more realistic iterations of the iron uptake models. The role of other trace metals and organic material in the partly species specific adaptations of the iron acquisition system are not completely understood. As one example, Peers and Price (2006) have shown that copper is essential for electron transport in *T. oceanica* regardless of Fe status implying that selection pressure imposed by Fe limitation has resulted in the use of a Cu protein for photosynthesis in an oceanic diatom.

Adaptations to low iron environments have been found to include a reduction in cell size (Sarthou et al., 2005), changes in photosynthetic architecture (Strzepek and Harrison, 2004; Peers and Price, 2006) and substitution of iron containing proteins for non-iron containing proteins (Peers and Price, 2006; McKay et al., 1999). Further possible adaptations include the induction of high affinity uptake mechanisms such as the production of siderophores by marine prokaryotes (Vraspir and Butler, 2009) and uptake mechanisms that target specific iron containing compounds such as hemes (Hopkinson et al., 2008) or the production of iron storage proteins (Marchetti et al., 2009).

Microorganisms can exert a feedback effect on Fe chemistry, for example by releasing organic matter which is able to react with Fe (e.g. siderophores, exopolymeric substances (EPS), cell lysis material or fecal pellets), which can enhance iron bioavailability (e.g. Hutchins et al., 1999b). Heldal et al. (1996), for example, visualized and quantified metals bound to bacterial extracellular matrixes in applying X-ray transmission electron microscopy. The role of grazing as a source of organic, iron binding material via sloppy feeding and/or as a direct source of iron is often discussed. Several studies address this topic and a general consensus about the importance of grazing for iron recycling in surface seawater exists (Sato et al., 2007; Barbeau et al., 1996; Dalbec and Twining, 2009; Sarthou et al., 2008; Hutchins and Bruland, 1994; Hutchins et al., 1995; Tovar-Sanchez et al., 2007; Zhang and Wang, 2004). However, some results are inconsistent and the detailed mechanisms as well as the contribution of different grazer types such as protozoa, copepods, krill, and salps and their specific feeding mechanisms are poorly understood. Therefore, it is difficult today to estimate the overall function of grazing on the biogeochemical cycles of iron especially in HNLC regions.

Most marine microorganisms (bacterio- and phytoplankton) produce polysaccharides that are either stored as energy reserves or secreted as exopolymeric substances (EPS) (Schoemann et al., 2001; Decho, 1990; Hoagland et al., 1993). It has recently been shown that iron starvation is coupled to transparent expolymer particles (TEP) production in *Trichodesmium* (Berman-Frank et al., 2007). Recent studies also provide evidence that high concentrations of saccharides or carbon-rich organic matrices can enhance the growth of phytoplankton (Vasconcelos et al., 2002) and efficiently retain Fe (II) (Öztürk et al., 2004; Toner et al., 2009), a highly bioavailable form (Morel et al., 2008). Steigenberger et al. (2010) show that polysaccharides and cell exudates of *Phaeodactylum* sp. can also result in high hydrogen peroxide production, while the authors still observe a net stabilizing effect of Fe(II) potentially due to a combination of organic Fe(II) retention paralleled by superoxide production.

Hassler and Schoemann (2009) explore a Fe-related biogeochemical role for polysaccharides, by examining the influence of various organic ligands (siderophore, porphyrin, mono- and poly-saccharides) on iron solubility and its bioavailability to four keystone phytoplankton species of the Southern Ocean, representing different phytoplankton functional groups and size classes (*Phaeocystis* sp., *Chaetoceros* sp., *Fragilariopsis kerguelensis* and *Thalassiosira antarctica* Comber). Results show that saccharides can increase Fe uptake rates and Fe solubility above the level observed for inorganic Fe. Similar observations were made on natural plankton community from the Southern Ocean (Hassler et al., 2007). Given the ubiquitous presence of saccharides in the ocean, these compounds might represent an important factor to control the basal level of soluble and bioavailable Fe.

Over the past years, the Fe(II) pool has been recognized as an important source of bioavailable Fe and intermediate in Fe cycling. Albeit short-lived due to rapid re-oxidation to Fe(III), significant concentrations of Fe(II) were detected in different oceanic and coastal provinces (Breitbarth et al., 2009; Croot and Laan, 2002; Croot et al., 2008, 2005; Roy et al., 2008b; Hopkinson and Barbeau, 2007; Ussher et al., 2007). There has been emerging evidence that Fe(II) is retained in oxygenated water by organic ligands (Croot et al., 2001), which may be a product of marine biota (Roy et al., 2008b) or also of other origin and rain introduced (Willey et al., 2008). See Barbeau (2006) for a comprehensive review and also Sect. 7. The role of Fe(II) for phytoplankton nutrition and Fe(II) organic complexation provide interesting and relevant research topics for the near future.

Iron limitation also induces a decoupling in the use of macronutrients by phytoplankton, likely to influence the cycling of the major biogeochemical cycles (C, N, P, Si, S) over geological time scales (de Baar and La Roche, 2003). Further, light intensity can play an important role (Hoffmann et al., 2008; Maldonado et al., 1999; de Baar et al., 2005; Moore et al., 2007a and b). Moreover, Bucciarelli et al. (2010) examined the effect of Fe-light co-limitation on cellular silica, carbon and nitrogen in two marine diatom species, *Thalassiosira oceanica* and *Ditylum brightwellii*, observing a

1.4-fold increase in C:N ratio with a decrease in growth rate by 70% in both species and a decrease in biogenic silica per cell under severe Fe or Fe-light limitation. These results however are seemingly in contradiction with many previous lab and field studies showing increased diatom silicification under Fe limitation (Hutchins and Bruland, 1998; Takeda, 1998; Firme et al., 2003; Franck et al., 2003).

A significant contribution to the increasing knowledge on the interaction of biological processes with iron chemistry is made by the improvement of methods in this field. Intercalibrations of Fe detection methods were carried out and measurements of Fe are now possible in near real time in the field at picomolar level (Bowie et al., 2002, 2005, 2006; Johnson et al., 2007), including Fe(II) (Croot and Laan, 2002). More sophisticated shipboard incubation systems are available (Hare et al., 2007a; Hutchins et al., 2003; Pickell et al., 2009; Hare et al., 2005), allowing for more realistic experimental designs to assess Fe phytoplankton interactions. Methods were developed to detect cell surface Fe reduction and uptake (Shaked et al., 2004) and to measure cellular Fe (Hassler et al., 2004). New highly sensitive electrochemical methods have pushed our understanding of organic iron complexation in new directions (Croot and Johansson, 2000; Laglera and van den Berg, 2009). Utilization of laboratory based extensive instrumentation such as FlFFF, x-ray spectroscopy with TEM microscopy, as well as bioreporters, molecular techniques and genomic information allow for in depth studies and visualization of Fe limitation and Fe organic matter interactions (e.g. Heldal et al., 1996; Toner et al., 2009; Stolpe et al., 2005) and particularly also of iron bioavailability (Lam et al., 2006; Boyanapalli et al., 2007; Hassler et al., 2006).

Nevertheless, some methods still depend on high material/biomass concentrations and future development and work may lead towards more direct measurement techniques overcoming pre-concentration artifacts. The majority of phytoplankton iron interaction studies have been carried out invitro and with a limited range of species, and mostly did not include co-effects of other trace metals. Strong iron chelators such as EDTA and DFOB are commonly used to induce iron limitation in culture experiments and experiments are in part difficult to compare due to the variety and combination of factors (e.g. light intensity, temperature) applied. Thus, it is not clear how predominant the known low iron regime adaptations are in the oceanic environment. Albeit very challenging, future experiments should aim towards using more realistic media chemistries and natural biomass densities of cultures that were recently isolated. Methods and experiments need to be designed to link Fe chemistry to biological processes, including potential biological feedback mechanisms on Fe chemistry as also discussed with regard to climate change in Sect. 7. Further, our increasing ability to detect and characterize iron in seawater and in organisms (Mawji et al., 2008; Gledhill, 2007; Laglera and van den Berg, 2009; Vong et al., 2007) coupled to developments in techniques such as shotgun genomics (Rusch et al., 2007; Venter et al., 2004; Yooseph et al., 2007) and the potential of proteomics (Nunn and Timperman, 2007; Dupont et al., 2006) should lead to great advances over the coming years in our understanding of how organisms have adapted to low iron environments, and the implications of these adaptations to overall marine productivity and biodiversity. The development of in-situ measurement technology as for example suggested in the approach of Roy at al. (2008a), with the potential for deployment on moored sensor arrays, will greatly improve the spatial and temporal resolution of Fe measurements.

7 Iron and climate change

Global climate change will greatly influence atmospheric and hydrographic processes in the future. Most prominent features include changes in thermohaline circulation of the North Atlantic, warming of the polar regions, changing wind patterns resulting in reduced upwelling and wind driven mixing, as well as increased sea-surface temperatures and stratification (Boyd and Doney, 2003). Projected changes in relative humidity and land vegetation cover, affecting soil moisture and local dust availability, together with changed patterns in wind and precipitation, as well as riverine transport, will ultimately modify the iron supply to the open ocean (Boyd and Doney, 2003; Jickells et al., 2005). Further, rising atmospheric CO_2 acidifies the oceans, leading to changes in saturation state with respect to calcium carbonate and shifts the aragonite and calcite saturation depths (Feely et al., 2004) and potentially trace metal solubility. The abovementioned processes, albeit uncertainty over their magnitude and exact interrelations in the future exists, will affect marine biota, causing regime shifts, and modifications of biogeochemical cycling (Boyd and Doney, 2003). While climate change needs to be understood holistically, there is a need to evaluate regional and small scale physical, chemical, and biological processes in order to derive potential biogeochemical feedback mechanisms.

We here focus on direct local effects acting upon iron chemistry in seawater and primarily discuss the emerging field of trace metal biogeochemistry research encompassing two main areas, temperature shifts and changing seawater pH. Both temperature and pH are master variables for chemical and biological processes and effects on trace metal biogeochemistry may be multifaceted and complex. Ten years ago, this research field did not exist and data are scarce. Assessing the potential effects of sea-surface warming and ocean acidification on iron biogeochemistry is crucial and predictions to date are based on our understanding of the current ocean system. Despite the expanding knowledge and increasing awareness for trace metal chemistry in open ocean research during the past 20 years and the recently defined

field and intensifying work on ocean acidification research, there is yet little communication between these fields.

A decrease of the surface seawater pH from pre-industrial 8.25 to 7.85 within this century, and further by up to 0.7 units until 2300 is predicted (Caldeira and Wickett, 2003; Jacobson, 2005). In general, the H^+ ion concentration can directly affect metal uptake by phytoplankton via altered membrane transport activity or via direct competition of the H^+ ion with metal ions for membrane transporters or other metabolically active sites on the cell surface (Sunda and Huntsman, 1983; Vigenault and Campbell, 2005). Further main aspects are the inorganic solubility of iron, changes in organic complexation, phytoplankton – trace metal feedback mechanisms, and differences in redox chemistry.

$Fe(OH)_3$ solubility and Fe(III) inorganic speciation are expected to changed with ocean acidification (Liu and Millero, 2002, 1999). When seawater pH falls below 8, changes in the inorganic speciation result in an increase of the thermodynamic Fe(III) hydroxide solubility. Enhanced solubility above pH 7 in seawater of the warm or temperate ocean though is mainly due to organic ligands and suggests any change in solubility arising from acidification will be mainly related to the organic complexes (Liu and Millero, 2002). However, in cold water the solubility of Fe can exceed FeL concentrations (P. Croot, personal communication, 2009, calculated based on Liu and Millero, 2002), bringing inorganic speciation shifts due to pH and temperature back into the game. Interesting questions arise concerning whether ocean acidification could potentially also affect metal leaching from atmospheric deposits (see Sects. 2.1 and 2.2) and how the metastable colloidal Fe phase may be affected (see Sect. 5). The potential effect of pH acting directly on FeL complexes depends on the nature of Fe-binding functional groups. The H^+ stoichiometry of the Fe(III) binding sites defines the magnitude of acid dissociation constants (pK_a). Carboxyl groups have a $pK_a \sim 5$ and thus the conditional stability constant of the FeL complex ($\log K_{FeL}$) should remain unchanged above pH 6. In contrast, phenolic groups have a $pK_a \sim 9$ and $\log K_{FeL}$ will increase with pH (Sillen and Martell, 1971). Both groups can be found in siderophores. While to date no published experimental data on the pH effect for FeL can be found, Averyt et al. (2004) show a decrease of $\log K_{CuL}$ with lower pH in two lakes. Similar effects were observed for Cd ligands, but less so for Zn ligands (Sander et al., 2007). Further, iron chelates are more photolabile at lower pH (Sunda and Huntsman, 2003), which directly involves effects on Fe photochemistry (see below). Overall though, while FeL complexes may or may not be directly pH affected, alterations of organic iron complexation may still arise from biological ligand production processes, should those be affected by pH and/or temperature (see below). Several models of Fe uptake mechanisms for phytoplankton exist (Morel et al., 2008; Shaked et al., 2005; Salmon et al., 2006, see also Sect. 6) and their pH dependence may be largely connected on their reliance on Fe(II) as the actual species taken up and on the species capability to regulate pH at the cell surface.

It can be expected that pH driven changes in trace metal availability will trigger biological feedback mechanisms, which regulate trace metal availability to marine phytoplankton. These can be in form of exudates, cell lysates, or chlorophyll degradation products, and can serve as trace metal ligands to prevent toxic effects or to increase trace metal uptake rates. The capability of eukaryotic phytoplankton species to produce trace metal binding ligands either to prevent toxic effects or to increase uptake has been addressed (Ahner et al., 1997; Barbeau et al., 2001; Hutchins et al., 1999b). However, information on biological feedback mechanisms in response to climate change that affect trace metal chemistry is very limited. It should be noted that in contrast to the open ocean, estuaries and coastal areas might show a wide range in pH (5 to >9) (e.g. Chen and Durbin, 1994; Sunda and Huntsman, 1998) and obviously in temperature, to which phytoplankton species are adapted to. However, even considering that phytoplankton blooms may cause temporal increases in surface water pH due to CO_2 uptake, open ocean species are adapted to a very narrow range in pH. Further, some coastal areas such as the Oregon shelf temporarily experience subsurface input of low pH water and such systems could be valuable analogs for acidification and temperature effects in natural settings.

Several studies were carried out during the past years assessing changes in phytoplankton physiology using laboratory batch cultures and mesocosm pCO_2 perturbations. Changes in carbon and nitrogen fixation rates, calcification rates, and carbon export are reflective of pH effects on the biogeochemistry of the manipulated system (Riebesell et al., 2007; Orr et al., 2005, see also Biogeosciences Special Issue "The ocean in the high-CO_2 world II"), which unequivocally will also affect trace metal cycling. Further studies also reported combined effects of pCO_2 and temperature change (Hare et al., 2007b), and modeling studies also suggest potential interactions with irradiance effects due to changing stratification in the future ocean on phytoplankton physiology and species composition (Boyd and Doney, 2002). Seen in coherence with biological effects on organic Fe complexation, and in return again with Fe availability effects on phytoplankton, these studies indicate that phytoplankton physiology and species composition could exert biological feedback mechanisms on trace metal cycling as a function of pCO_2 and temperature in seawater.

Data from a coastal mesocosm CO_2 enrichment experiment (Breitbarth et al., 2010) suggest increasing dissolved iron concentrations with ocean acidification. The authors invoke a biological feedback mechanism at future seawater pCO_2 resulting in increased organic Fe(III) complexation, which requires further testing. More so, changes in Fe(II) chemistry were observed. In part, the underlying processes can theoretically be derived based on established relationships of Fe(II) oxidation rates and inorganic Fe(II)

speciation in presence of different oxidizers over environmentally relevant ranges in pH, temperature, and salinity (Santana-Casiano et al., 2006; Gonzalez-Davila et al., 2006; Santana-Casiano et al., 2005; Millero and Sotolongo, 1989; Millero et al., 1987; Croot and Laan, 2002). For example, over a seawater pH decrease of 0.5 units, a 10-fold increase in the half-life of Fe(II) can be expected and the effects of ocean acidification may thus override the influences from sea-surface temperature changes (Santana-Casiano et al., 2005). Fe(II) oxidation kinetics are seemingly affected by organic complexation (e.g. Croot et al., 2001; Rose, 2003; Roy et al., 2008b, see also Sect. 6). Fe(II) ligands may be biologically mediated and potential biological feedback mechanisms in the future could thus further complicate the picture, requiring focused research in this field. Moreover, changing light regimes are expected to affect photochemical cycling of Fe in sunlit surface waters (Boyd and Doney, 2002). Both, light intensity and the light spectrum penetrating the water will influence photochemical processes and this field requires further attention.

Similar to seawater pH, temperature effects have been rarely studied in coherence with trace metal biogeochemical measurements in open ocean systems. It has been standard to date to carry out measurements of organic iron complexation at room temperature, but temperature has profound effects on metal speciation and solubility. Further, Rose et al. (2009) demonstrate synergistic effects of temperature and iron additions on phytoplankton physiology and community dynamics in Ross Sea waters. Likewise, Fu et al. (2008) demonstrate that pCO_2 perturbations alone may not give the sole answer to potential physiological changes in phytoplankton, since these can be modified by interactions with Fe limitation. CO_2 and N_2 fixation rates in the future ocean may be controlled by a combination of Fe availability and pCO_2, further stressing the need to elucidate future changes in seawater iron chemistry.

Overall, climate change effects on iron speciation and biological limitation are likely not going to be driven by a single factor, and Rose et al. (2009) stress the importance of multivariate studies in order to understand ecosystem changes. It also remains to be shown how climate change may alter the interrelations of iron with other trace metals and macronutrients. For example, laboratory experiments showed that cadmium toxicity can be reduced under high iron availability, suggesting that cadmium is a competitive inhibitor of the iron uptake system or iron dependent cellular processes (Foster and Morel, 1982; Sunda and Huntsman, 2000). Similar observation are made for iron limited natural phytoplankton assemblages from the Southern Ocean by Cullen et al. (2003) who suggest that Fe limited phytoplankton take up more Cd resulting in lower Cd:PO_4 ratios in surface waters. Iron co-limitations and interactions with other nutrients and trace metals have been observed (e.g. Schulz et al., 2004; Mills et al., 2004; Wu et al., 2003; Wells et al., 2005) and apparently the composition of trace metals and macro nutrients greatly affect natural Fe fertilization efficiency (see Sect. 2.2). Moreover, Statham et al. (2008) recently addressed glacier meltwater input of iron and colloidal matter from the Greenland Ice Sheet. In the context of the expected changes for Fe biogeochemistry discussed here, their study illustrates how atmospheric warming can act on various levels, evidentially affecting iron biogeochemistry in the sea.

We conclude that ocean acidification may result in increased Fe(III) solubility, is likely to decrease stability of some FeL complexes, and is likely to increase Fe(II) stability. It may also change the mechanisms of Fe acquisition by cells, which though depends on the Fe status of the regime and the type of phytoplankton species present. Temperature effects may be smaller in comparison, with most pronounced changes though to be expected in polar waters. Recommendations for future research directions are systematic measurements of Fe(III) solubility in pH range 7–9 and effects of Fe-binding ligands along with the study of temperature effects thereon, and field experiments in upwelling regions with a focus on low pH regimes. Moreover, the role of organic ligands in enhancing Fe(II) stability needs to be investigated as well as effects of pH and temperature on the photoreactivity of Fe(III)L complexes. It is largely unknown what the pH controls in organisms are, and how they affect Fe acquisition. More emphasis is needed on measurements and control of the seawater carbonate system, including pH, in field studies and laboratory cultures. Protocols carried out to achieve pH control need to be reported and researchers are urged to report pH data on the total or seawater pH scale to ensure comparability of different studies. The comprehensive "Guide for Best Practices in Ocean Acidification Research and Data Reporting" was recently published and should be adapted for trace metal research (http://www.epoca-project.eu/index.php/Home/Guide-to-OA-Research/).

Acknowledgements. Funding for the workshop was provided by EUR-OCEANS and the Swedish Research Council (VR). E. B. and L. J. H. acknowledge current funding by the German Research Foundation (DFG, BR 3794 and HO 4217). S. D. is funded by the DFG and the multi-disciplinary research group NOVUM (Nutrients Originating in Volcanoes and their effect on the eUphotic zone of the Marine ecosystem) by the Leibniz Institute of Marine Sciences, IFM-GEOMAR. D. H. acknowledges funding by US NSF ANT 0741411 and OCE 0825319. The authors greatly appreciate the comments received from P. W. Boyd on the manuscript.

Edited by: U. Riebesell

References

Aguilar-Islas, A. M., Rember, R. D., Mordy, C. W., and Wu, J.: Sea ice-derived dissolved iron and its potential influence on the spring algal bloom in the Bering Sea, Geophys. Res. Lett., 35, $L_2$4601, doi:10.1029/2008gl035736, 2008.

Ahner, B. A., Morel, F. M. M., and Moffett, J. W.: Trace metal control of phytochelatin production in coastal waters, Limnol. Oceanogr., 42, 601–608, 1997.

Aluwihare, L. I., Repeta, D. J., and Chen, R. F.: A major biopolymeric component to dissolved organic carbon in surface sea water, Nature, 387, 166–169, 1997.

Andersson, K., Dahlqvist, R., Turner, D., Stolpe, B., Larsson, T., Ingri, J., and Andersson, P.: Colloidal rare earth elements in a boreal river: Changing sources and distributions during the spring flood, Geochim. Cosmochim. Acta, 70, 3261–3274, doi:10.1016/j.gca.2006.04.021, 2006.

Ardelan, M. V., Holm-Hansen, O., Hewes, C. D., Reiss, C. S., Silva, N. S., Dulaiova, H., Steinnes, E., and Sakshaug, E.: Natural iron enrichment around the Antarctic Peninsula in the Southern Ocean, Biogeosciences, 7, 11–25, 2010, http://www.biogeosciences.net/7/11/2010/.

Assemi, S., Newcombe, G., Hepplewhite, C., and Beckett, R.: Characterization of natural organic matter fractions separated by ultrafiltration using flow field-flow fractionation, Water Res., 38, 1467–1476, doi:10.1016/j.watres.2003.11.031, 2004.

Aumont, O. and Bopp, L.: Globalizing results from ocean in situ iron fertilization studies, Global Biogeochem. Cy., 20, GB2017, Gb2017, doi:10.1029/2005gb002591, 2006.

Averyt, K. B., Kim, J. P., and Hunter, K. A.: Effect of pH on measurement of strong copper binding ligands in lakes, Limnol. Oceanogr., 49, 20–27, 2004.

Baker, A. R. and Jickells, T. D.: Mineral particle size as a control on aerosol iron solubility, Geophys. Res. Lett., 33, $L_1$7608 doi:10.1029/12006GL026557 2006.

Baker, A. R., Jickells, T. D., Witt, M., and Linge, K. L.: Trends in the solubility of iron, aluminium, manganese and phosphorus in aerosol collected over the Atlantic Ocean, Mar. Chem., 98, 43–58, doi:10.1016/j.marchem.2005.06.004, 2006.

Baker, A. R., and Croot, P. L.: Atmospheric and marine controls on aerosol iron solubility in seawater, Mar. Chem., in press, 2009.

Barbeau, K., Moffett, J. W., Caron, D. A., Croot, P. L., and Erdner, D. L.: Role of protozoan grazing in relieving iron limitation of phytoplankton, Nature, 380, 61–64, 1996.

Barbeau, K. and Moffett, J. W.: Laboratory and field studies of colloidal iron oxide dissolution as mediated by phagotrophy and photolysis, Limnol. Oceanogr., 45, 827–835, 2000.

Barbeau, K., Rue, E. L., Bruland, K. W., and Butler, A.: Photochemical cycling of iron in the surface ocean mediated by microbial iron(III)-binding ligands, Nature, 413, 409–413, 2001.

Barbeau, K.: Photochemistry of organic iron(III) complexing ligands in oceanic systems, Photochem. Photobiol., 82, 1505–1516, doi:10.1562/2006-06-16-ir-935, 2006.

Bauer, J. E., Williams, P. M., and Druffel, E. R. M.: C-14 activity of dissolved organic-carbon fractions in the North-Central Pacific and Sargasso Sea, Nature, 357, 667–670, 1992.

Benitez-Nelson, C. R., Vink, S. M., Carrillo, J. H., and Huebert, B. J.: Volcanically influenced iron and aluminum cloud water deposition to Hawaii, Atmos. Environ., 37, 535–544, 2003.

Bergquist, B. A. and Boyle, E. A.: Iron isotopes in the Amazon River system: Weathering and transport signatures, Earth Planet. Sci. Lett., 248, 54–68, doi:10.1016/j.epsl.2006.05.004, 2006.

Bergquist, B. A., Wu, J., and Boyle, E. A.: Variability in oceanic dissolved iron is dominated by the colloidal fraction, Geochim. Cosmochim. Acta, 71, 2960–2974, doi:10.1016/j.gca.2007.03.013, 2007.

Berman-Frank, I., Rosenberg, G., Levitan, O., Haramaty, L., and Mari, X.: Coupling between autocatalytic cell death and transparent exopolymeric particle production in the marine cyanobacterium Trichodesmium, Environ. Microbiol., 9, 1415–1422, doi:10.1111/j.1462-2920.2007.01257.x, 2007.

Blain, S., Queguiner, B., Armand, L., Belviso, S., Bombled, B., Bopp, L., Bowie, A., Brunet, C., Brussaard, C., Carlotti, F., Christaki, U., Corbiere, A., Durand, I., Ebersbach, F., Fuda, J.-L., Garcia, N., Gerringa, L., Griffiths, B., Guigue, C., Guillerm, C., Jacquet, S., Jeandel, C., Laan, P., Lefevre, D., Lo Monaco, C., Malits, A., Mosseri, J., Obernosterer, I., Park, Y.-H., Picheral, M., Pondaven, P., Remenyi, T., Sandroni, V., Sarthou, G., Savoye, N., Scouarnec, L., Souhaut, M., Thuiller, D., Timmermans, K., Trull, T., Uitz, J., van Beek, P., Veldhuis, M., Vincent, D., Viollier, E., Vong, L., and Wagener, T.: Effect of natural iron fertilization on carbon sequestration in the Southern Ocean, Nature, 446, 1070–1074, 2007.

Blain, S., Bonnet, S., and Guieu, C.: Dissolved iron distribution in the tropical and sub tropical South Eastern Pacific, Biogeosciences, 5, 269–280, 2008, http://www.biogeosciences.net/5/269/2008/.

Boehme, J. and Wells, M.: Fluorescence variability of marine and terrestrial colloids: Examining size fractions of chromophoric dissolved organic matter in the Damariscotta River estuary, Mar. Chem., 101, 95–103, doi:10.1016//j.marchem.2006.02.001, 2006.

Bopp, L., Kohfeld, K. E., Le Quere, C., and Aumont, O.: Dust impact on marine biota and atmospheric CO_2 during glacial periods, Paleoceanography, 18, 1046, doi:10.1029/2002pa000810, 2003.

Borer, P. M., Sulzberger, B., Reichard, P., and Kraemer, S. M.: Effect of siderophores on the light-induced dissolution of colloidal iron(III) (hydr)oxides, Mar. Chem., 93, 179–193, 2005.

Bowie, A. R., Achterberg, E. P., Sedwick, P. N., Ussher, S., and Worsfold, P. J.: Real-time monitoring of picomolar concentrations of iron(II) in marine waters using automated flow injection-chemiluminescence instrumentation, Environ. Sci. Technol., 36, 4600–4607, 2002.

Bowie, A. R., Achterberg, E. P., Ussher, S., and Worsfold, P. J.: Design of an automated flow injection-chemiluminescence instrument incorporating a miniature photomultiplier tube for monitoring picomolar concentrations of iron in seawater, Journal of Automated Methods andManagement in Chemistry, 2005, 37–43, doi:10.1155/JAMMC.2005.1137, 2005.

Bowie, A. R., Achterberg, E. P., Croot, P. L., de Baar, H. J. W., Laan, P., Moffett, J. W., Ussher, S., and Worsfold, P. J.: A community-wide intercomparison exercise for the determination of dissolved iron in seawater, Mar. Chem., 98, 81–99, 2006.

Boyanapalli, R., Bullerjahn, G. S., Pohl, C., Croot, P. L., Boyd, P. W., and McKay, R. M. L.: Luminescent whole-cell cyanobacterial bioreporter for measuring Fe availability in diverse marine environments, Appl. Environ. Microbiol., 73, 1019–1024, doi:10.1128/aem.01670-06, 2007.

Boyd, P.: Ironing out algal issues in the southern ocean, Science, 304, 396–397, 2004.

Boyd, P. W., Wong, C. S., Merrill, J., Whitney, F., Snow, J., Harrison, P. J., and Gower, J.: Atmospheric iron supply and enhanced vertical carbon flux in the NE subarctic Pacific: Is there a connection?, Global Biogeochem. Cy., 12, 429–441, 1998.

Boyd, P. W., Watson, A. J., Law, C. S., and Abraham, E. R.: A mesoscale phytoplankton bloom in the polar Southern Ocean stimulated by iron fertilization, Nature, 407, 695–702, 2000.

Boyd, P. W., Crossley, A. C., DiTullio, G. R., Griffiths, F. B., Hutchins, D. A., Queguiner, B., Sedwick, P. N., and Trull, T. W.: Control of phytoplankton growth by iron supply and irradiance in the subantarctic Southern Ocean: Experimental results from the SAZ Project, J. Geophys. Res.-Oceans, 106, 31573–31583, 2001.

Boyd, P. W. and Doney, S. C.: Modeling regional responses by marine pelagic ecosystems to global climate change, Geophys. Res. Lett., 29, 5351–5354, 2002.

Boyd, P. W. and Doney, S. C.: The impact of climate change and feedback processes on the ocean carbon cycle, in: Ocean Biogeochemistry, Global Change – the IGBP Series, Springer-Verlag Berlin, Berlin, 157–193, 2003.

Boyd, P. W., Law, C. S., Wong, C. S., Nojiri, Y., Tsuda, A., Levasseur, M., Takeda, S., Rivkin, R., Harrison, P. J., Strzepek, R., Gower, J., McKay, R. M., Abraham, E., Arychuk, M., Barwell-Clarke, J., Crawford, W., Crawford, D., Hale, M., Harada, K., Johnson, K., Kiyosawa, H., Kudo, I., Marchetti, A., Miller, W., Needoba, J., Nishioka, J., Ogawa, H., Page, J., Robert, M., Saito, H., Sastri, A., Sherry, N., Soutar, T., Sutherland, N., Taira, Y., Whitney, F., Wong, S. K. E., and Yoshimura, T.: The decline and fate of an iron-induced subarctic phytoplankton bloom, Nature, 428, 549–553, 2004.

Boyd, P. W., Law, C. S., Hutchins, D. A., Abraham, E. R., Croot, P. L., Ellwood, M., Frew, R. D., Hadfield, M., Hall, J., Handy, S., Hare, C., Higgins, J., Hill, P., Hunter, K. A., LeBlanc, K., Maldonado, M. T., McKay, R. M., Mioni, C., Oliver, M., Pickmere, S., Pinkerton, M., Safi, K., Sander, S., Sanudo-Wilhelmy, S. A., Smith, M., Strzepek, R., Tovar-Sanchez, A., and Wilhelm, S. W.: FeCycle: Attempting an iron biogeochemical budget from a mesoscale SF6 tracer experiment in unperturbed low iron waters, Global Biogeochem. Cy., 19, GB4S20, doi:10.1029/2005GB002494, 2005.

Boyd, P. W., Jickells, T., Law, C. S., Blain, S., Boyle, E. A., Buesseler, K. O., Coale, K. H., Cullen, J. J., de Baar, H. J. W., Follows, M., Harvey, M., Lancelot, C., Levasseur, M., Owens, N. P. J., Pollard, R., Rivkin, R. B., Sarmiento, J., Schoemann, V., Smetacek, V., Takeda, S., Tsuda, A., Turner, S., and Watson, A. J.: Mesoscale Iron Enrichment Experiments 1993–2005: Synthesis and Future Directions, Science, 315, 612–617, doi:10.1126/science.1131669, 2007.

Boyd, P. W.: Implications of large-scale iron fertilization of the oceans – Introduction and synthesis, Mar. Ecol.-Prog. Ser., 364, 213–218, 2008.

Boyd, P. W., Mackie, D. S., and Hunter, K. A.: Aerosol iron deposition to the surface ocean – Modes of iron supply and biological responses, Mar. Chem., in press, doi:10.1016/j.marchem.2009.01.008, 2009.

Boye, M., Nishioka, J., Croot, P. L., Laan, P., Timmermans, K. R., and de Baar, H. J. W.: Major deviations of iron complexation during 22 days of a mesoscale iron enrichment in the open Southern Ocean, Mar. Chem., 96, 257–271, 2005.

Brand, L. E., Sunda, W. G., and Guillard, R. R. L.: Limitation of marine-phytoplankton reproductive rates by zinc, manganese, and iron Limnol. Oceanogr., 28, 1182–1198, 1983.

Breitbarth, E., Gelting, J., Walve, J., Hoffmann, L. J., Turner, D. R., Hassellöv, M., and Ingri, J.: Dissolved iron (II) in the Baltic Sea surface water and implications for cyanobacterial bloom development, Biogeosciences, 6, 2397–2420, 2009, http://www.biogeosciences.net/6/2397/2009/.

Breitbarth, E., Bellerby, R. J., Neill, C. C., Ardelan, M. V., Meyerhöfer, M., Zöllner, E., Croot, P. L., and Riebesell, U.: Ocean acidification affects iron speciation during a coastal seawater mesocosm experiment, Biogeosciences, 7, 1065–1073, 2010, http://www.biogeosciences.net/7/1065/2010/.

Bruland, K. W., Rue, E. L., and Smith, G. J.: Iron and macronutrients in California coastal upwelling regimes: Implications for diatom blooms, Limnol. Oceanogr., 46, 1661–1674, 2001.

Bucciarelli, E., Pondaven, P., and Sarthou, G.: Effects of an iron-light co-limitation on the elemental composition (Si, C, N) of the marine diatoms *Thalassiosira oceanica* and *Ditylum brightwellii*, Biogeosciences, 7, 657–669, 2010, http://www.biogeosciences.net/7/657/2010/.

Buck, K. N., Lohan, M. C., Berger, C. J. M., and Bruland, K. W.: Dissolved iron speciation in two distinct river plumes and an estuary: Implications for riverine iron supply, Limnol. Oceanogr., 52, 843–855, 2007.

Buesseler, K. O., Bauer, J. E., Chen, R. F., Eglinton, T. I., Gustafsson, O., Landing, W., Mopper, K., Moran, S. B., Santschi, P. H., VernonClark, R., and Wells, M. L.: An intercomparison of cross-flow filtration techniques used for sampling marine colloids: Overview and organic carbon results, Mar. Chem., 55, 1–31, 1996.

Buesseler, K. O., Andrews, J. E., Pike, S. M., and Charette, M. A.: The Effects of Iron Fertilization on Carbon Sequestration in the Southern Ocean, Science, 304, 414–417, 2004.

Buesseler, K. O., Doney, S. C., Karl, D. M., Boyd, P. W., Caldeira, K., Chai, F., Coale, K. H., de Baar, H. J. W., Falkowski, P. G., Johnson, K. S., Lampitt, R. S., Michaels, A. F., Naqvi, S. W. A., Smetacek, V., Takeda, S., and Watson, A. J.: Ocean Iron Fertilization – Moving Forward in a Sea of Uncertainty, Science, 319, 162, doi:10.1126/science.1154305, 2008.

Caldeira, K. and Wickett, M. E.: Anthropogenic carbon and ocean pH, Nature, 425, 365–365, 2003.

Chase, Z., Johnson, K. S., Elrod, V. A., Plant, J. N., Fitzwater, S. E., Pickell, L., and Sakamoto, C. M.: Manganese and iron distributions off central California influenced by upwelling and shelf width, Mar. Chem., 95, 235–254, doi:10.1016/j.marchem.2004.09.006, 2005.

Chen, C. Y., and Durbin, E. G.: Effects on pH on the growth and carbon uptake of marine phytoplankton, Marine Ecology Progress Series, 109, 83-94, 1994.

Chen, M. and Wang, W. X.: Bioavailability of natural colloid-bound iron to marine plankton: Influences of colloidal size and aging, Limnol. Oceanogr., 46, 1956–1967, 2001.

Chever, F., Sarthou, G., Bucciarelli, E., Blain, S., and Bowie, A. R.: An iron budget during the natural iron fertilisation experiment KEOPS (Kerguelen Islands, Southern Ocean), Biogeosciences, 7, 455–468, 2010,

http://www.biogeosciences.net/7/455/2010/.

Chin, W.-C., Orellana, M. V., and Verdugo, P.: Spontaneous assembly of marine dissolved organic matter into polymer gels, Nature, 391, 568–572, 1998.

Chisholm, S. W., Falkowski, P. G., and Cullen, J. J.: Oceans – Discrediting ocean fertilization, Science, 294, 309–310, 2001.

Coale, K., Johnson, K., Fitzwater, S., Gordon, R., Tanner, S., Chavez, F., Ferioli, L., Sakamoto, C., Rogers, P., Millero, F., Steinberg, P., Nightingale, P., Cooper, D., Cochlan, W., Landry, M., Constantinou, J., Rollwagen, G., Trasvina, A., and Kudela, R.: A massive phytoplankton bloom induced by an ecosystem-scale iron fertilization experiment in the equatorial Pacific Ocean, Nature, 383, 495–501, 1996.

Coale, K. H., Johnson, K. S., Chavez, F. P., Buesseler, K. O., Barber, R. T., Brzezinski, M. A., Cochlan, W. P., Millero, F. J., Falkowski, P. G., Bauer, J. E., Wanninkhof, R. H., Kudela, R. M., Altabet, M. A., Hales, B. E., Takahashi, T., Landry, M. R., Bidigare, R. R., Wang, X., Chase, Z., Strutton, P. G., Friederich, G. E., Gorbunov, M. Y., Lance, V. P., Hilting, A. K., Hiscock, M. R., Demarest, M., Hiscock, W. T., Sullivan, K. F., Tanner, S. J., Gordon, R. M., Hunter, C. N., Elrod, V. A., Fitzwater, S. E., Jones, J. L., Tozzi, S., Koblizek, M., Roberts, A. E., Herndon, J., Brewster, J., Ladizinsky, N., Smith, G., Cooper, D., Timothy, D., Brown, S. L., Selph, K. E., Sheridan, C. C., Twining, B. S., and Johnson, Z. I.: Southern Ocean Iron Enrichment Experiment: Carbon Cycling in High- and Low-Si Waters, Science, 304, 408–414, 2004.

Croot, P. L., and Johansson, M.: Determination of iron speciation by cathodic stripping voltammetry in seawater using the competing ligand 2-(2-thiazolylazo)-p-cresol (TAC), Electroanalysis, 12, 565–576, 2000.

Croot, P. L., Bowie, A. R., Frew, R. D., Maldonado, M. T., Hall, J. A., Safi, K. A., La Roche, J., Boyd, P. W., and Law, C. S.: Retention of dissolved iron and Fe-II in an iron induced Southern Ocean phytoplankton bloom, Geophys. Res. Lett., 28, 3425–3428, 2001.

Croot, P. L. and Laan, P.: Continuous shipboard determination of Fe(II) in polar waters using flow injection analysis with chemiluminescence detection, Analytica Chimica Acta, 466, 261–273, 2002.

Croot, P. L., Andersson, K., Öztürk, M., and Turner, D. R.: The distribution and speciation of iron along 6° E in the Southern Ocean, Deep Sea Res., 51, 2857–2879, 2004.

Croot, P. L., Laan, P., Nishioka, J., Strass, V., Cisewski, B., Boye, M., Timmermans, K. R., Bellerby, R. G., Goldson, L., Nightingale, P., and de Baar, H. J. W.: Spatial and temporal distribution of Fe(II) and H_2O_2 during EisenEx, an open ocean mescoscale iron enrichment, Mar. Chem., 95, 65–88, 2005.

Croot, P. L., Bluhm, K., Schlosser, C., Streu, P., Breitbarth, E., Frew, R. D., and Ardelan, M. V.: Cycling of Fe(II) in Southern Ocean Iron Mesoscale Enrichment Experiments: EIFEX and SOFEX, Geophys. Res. Lett., 35, $L_1$9606. doi:19610.11029/12008GL035063, 2008.

Cullen, J. J. and Boyd, P. W.: Predicting and verifying the intended and unintended consequences of large-scale ocean iron fertilization, Mar. Ecol. Progress Ser., 364, 295–301, doi:10.3354/meps07551, 2008.

Cullen, J. T., Chase, Z., Coale, K. H., Fitzwater, S. E., and Sherrell, R. M.: Effect of iron limitation on the cadmium to phosphorus ratio of natural phytoplankton assemblages from the Southern Ocean, Limnol. Oceanogr., 48, 1079–1087, 2003.

Dalbec, A. A. and Twining, B. S.: Remineralization of bioavailable iron by a heterotrophic dinoflagellate, Aquatic Microbial Ecol., 54, 279–290, doi:10.3354/ame01270, 2009.

de Baar, H. J. W., Buma, A. G. J., Nolting, R. F., Cadée, G. C., Jacques, G., and Tréguer, P. J.: On iron limitation of the Southern Ocean: experimental observations in the Weddell and Scotia Seas, Mar. Ecol. Progr. Series, 65, 105–122, 1990.

de Baar, H. J. W., Dejong, J. T. M., Bakker, D. C. E., Loscher, B. M., Veth, C., Bathmann, U., and Smetacek, V.: Importance of iron for plankton blooms and carbondioxide drawdown in the Southern Ocean, Nature, 373, 412–415, 1995.

de Baar, H. J. W., and La Roche, J.: Trace Metals in the Oceans: Evolution, Biology and Global Change, in: Marine Science Frontiers for Europe, edited by: Wefer, G., Lamy, F., and Mantoura, F., Springer Verlag, Berlin, 79–105, 2003.

de Baar, H. J. W., Boyd, P. W., Coale, K. H., Landry, M. R., Tsuda, A., Assmy, P., Bakker, D. C. E., Bozec, Y., Barber, R. T., Brzezinski, M. A., Buesseler, K. O., Boye, M., Croot, P. L., Gervais, F., Gorbunov, M. Y., Harrison, P. J., Hiscock, W. T., Laan, P., Lancelot, C., Law, C. S., Levasseur, M., Marchetti, A., Millero, F. J., Nishioka, J., Nojiri, Y., van Oijen, T., Riebesell, U., Rijkenberg, M. J. A., Saito, H., Takeda, S., Timmermans, K. R., Veldhuis, M. J. W., Waite, A. M., and Wong, C. S.: Synthesis of iron fertilization experiments: From the Iron Age in the Age of Enlightenment, J. Geophys. Res., 110, C09S16, doi:10.1029/2004JC002601, 2005.

de Baar, H. J. W., Gerringa, L. J. A., Laan, P., and Timmermans, K. R.: Efficiency of carbon removal per added iron in ocean iron fertilization, Mar. Ecol. Progr. Series, 364, 269–282, doi:10.3354/meps07548, 2008.

de Jong, J., Schoemann, V., Tison, J. L., Becquevort, S., Masson, F., Lannuzel, D., Petit, J., Chou, L., Weis, D., and Mattielli, N.: Precise measurement of Fe isotopes in marine samples by multi-collector inductively coupled plasma mass spectrometry (MC-ICP-MS), Analytica Chimica Acta, 589, 105–119, doi:10.1016/j.aca.2007.02.055, 2007.

Decho, A. W.: Microbial exopolymer secretions in ocean environments – their role(s) in food webs and marine processes, Oceanogr. Mar. Biol., 28, 73–153, 1990.

Duce, R. A., Liss, P. S., Merrill, J. T., Atlas, E. L., Buat-Menard, P., Hicks, B. B., Miller, J. M., Prospero, J. M., Arimoto, R., Church, T. M., Ellis, W., Galloway, J. N., Hansen, L., Jickells, T. D., Knap, A. H., Reinhardt, K. H., Schneider, B., Soudine, A., Tokos, J. J., Tsunogai, S., Wollast, R., and Zhou, M.: The atmospheric input of trace species to the world ocean, Global Biogeochem. Cy., 5, 193–259, 1991.

Duce, R. A., LaRoche, J., Altieri, K., Arrigo, K. R., Baker, A. R., Capone, D. G., Cornell, S., Dentener, F., Galloway, J., Ganeshram, R. S., Geider, R. J., Jickells, T., Kuypers, M. M., Langlois, R., Liss, P. S., Liu, S. M., Middelburg, J. J., Moore, C. M., Nickovic, S., Oschlies, A., Pedersen, T., Prospero, J., Schlitzer, R., Seitzinger, S., Sorensen, L. L., Uematsu, M., Ulloa, O., Voss, M., Ward, B., and Zamora, L.: Impacts of atmospheric anthropogenic nitrogen on the open ocean, Science, 320, 893–897, doi:10.1126/science.1150369, 2008.

Duggen, S., Croot, P., Schacht, U., and Hoffmann, L.: Subduction zone volcanic ash can fertilize the surface ocean and stim-

ulate phytoplankton growth: Evidence from biogeochemical experiments and satellite data, Geophys. Res. Lett., 34, L01612, doi:10.01029/02006GL027522 2007.

Duggen, S., Olgun, N., Croot, P., Hoffmann, L., Dietze, H., Delmelle, P., and Teschner, C.: The role of airborne volcanic ash for the surface ocean biogeochemical iron-cycle: a review, Biogeosciences, 7, 827–844, 2010, http://www.biogeosciences.net/7/827/2010/.

Dupont, C. L., Yang, S., Palenik, B., and Bourne, P. E.: Modern proteomes contain putative imprints of ancient shifts in trace metal geochemistry, Proc. Natl. Acad. Sci. USA, 103, 17822–17827, doi:10.1073/pnas.0605798103, 2006.

Dutkiewicz, S., Follows, M. J., and Parekh, P.: Interactions of the iron and phosphorus cycles: A three-dimensional model study, Global Biogeochem. Cy., 19, GB1021, doi:10.1029/2004gb002342, 2005.

Editorial: The Law of the Sea, Nature Geosci., 2, 153–153, doi:10.1038/ngeo464, 2009.

Edwards, R. and Sedwick, P.: Iron in East Antarctic snow: Implications for atmospheric iron deposition and algal production in Antarctic waters, Geophys. Res. Lett., 28, 3907–3910, 2001.

Elrod, V. A., Berelson, W. M., Coale, K. H., and Johnson, K. S.: The flux of iron from continental shelf sediments: A missing source for global budgets, Geophys. Res. Lett., 31(4), $L_1$2307, doi:10.1029/2004gl020216, 2004.

Engel, A., Thoms, S., Riebesell, U., Rochelle-Newall, E., and Zondervan, I.: Polysaccharide aggregation as a potential sink of marine dissolved organic carbon, Nature, 428, 929–932, 2004.

Fan, S.-M.: Photochemical and biochemical controls on reactive oxygen and iron speciation in the pelagic surface ocean, Mar. Chem., 109, 152–164, 2008.

Fan, S. M., Moxim, W. J., and Levy, H.: Aeolian input of bioavailable iron to the ocean, Geophys. Res. Lett., 33, L07602, doi:10.1029/2005gl024852, 2006.

Feely, R. A., Sabine, C. L., Lee, K., Berelson, W., Kleypas, J., Fabry, V. J., and Millero, F. J.: Impact of Anthropogenic CO_2 on the $CaCO_3$ System in the Oceans, Science, 305, 362–366, doi:10.1126/science.1097329, 2004.

Firme, G. F., Rue, E. L., Weeks, D. A., Bruland, K. W., and Hutchins, D. A.: Spatial and temporal variability in phytoplankton iron limitation along the California coast and consequences for Si, N, and C biogeochemistry, Global Biogeochem. Cy., 17(13), 1016, doi:10.1029/2001gb001824, 2003.

Floge, S. A. and Wells, M. L.: Variation in colloidal chromophoric dissolved organic matter in the Damariscotta Estuary, Maine, Limnol. Oceanogr., 52, 32–45, 2007.

Foster, P. L. and Morel, F. M. M.: Reversal of cadmium toxicity in a diatom: An interaction between cadmium activity and iron, Limnol. Oceanogr., 27, 745–752, 1982.

Franck, V. M., Bruland, K. W., Hutchins, D. A., and Brzezinski, M. A.: Iron and zinc effects on silicic acid and nitrate uptake kinetics in three high-nutrient, low-chlorophyll (HNLC) regions, Mar. Ecol.-Prog. Ser., 252, 15–33, 2003.

Frew, R. D., Hutchins, D. A., Nodder, S., Sanudo-Wilhelmy, S., Tovar-Sanchez, A., Leblanc, K., Hare, C. E., and Boyd, P. W.: Particulate iron dynamics during FeCycle in subantarctic waters southeast of New Zealand, Global Biogeochemical Cycles, 20, GB1S93, doi:10.1029/2005GB002558, 2006.

Frogner, P., Gislason, S. R., and Oskarsson, N.: Fertilizing potential of volcanic ash in ocean surface water, Geology, 29, 487–490, 2001.

Fu, F.-X., Mulholland, M. R., Garcia, N. S., Beck, A., Bernhardt, P. W., Warner, M. E., Sañudo-Wilhelmy, S. A., and Hutchins, D. A.: Interactions between changing pCO_2, N_2 fixation, and Fe limitation in the marine unicellular cyanobacterium *Crocosphaera*, Limnol. Oceanogr., 53, 2472–2484, 2008.

Furman, J. A. and Capone, D. G.: Possible biogeochemical consequences of ocean fertilization, Limnol. Oceanogr., 36, 1951–1959, 1991.

Gelting, J., Breitbarth, E., Stolpe, B., Hassellöv, M., and Ingri, J.: Fractionation of iron species and iron isotopes in the Baltic Sea euphotic zone, Biogeosciences Discuss., 6, 6491–6537, 2009, http://www.biogeosciences-discuss.net/6/6491/2009/.

Gerringa, L. J. A., Rijkenberg, M. J. A., Wolterbeek, H. T., Verburg, T. G., Boye, M., and de Baar, H. J. W.: Kinetic study reveals weak Fe-binding ligand, which affects the solubility of Fe in the Scheldt estuary, Mar. Chem., 103, 30–45, 2007.

Gervais, F., Riebesell, U., and Gorbunov, M. Y.: Changes in primary productivity and chlorophyll a in response to iron fertilization in the Southern Polar Frontal Zone, Limnol. Oceanogr., 47, 1324–1335, 2002.

Ginoux, P., Prospero, J. M., Torres, O., and Chin, M.: Long-term simulation of global dust distribution with the GOCART model: correlation with North Atlantic Oscillation, Environmental Modelling & Software, 19, 113–128, doi:10.1016/s1364-8152(03)00114-2, 2004.

Gledhill, M. and van den Berg, C. M. G.: Determination of compeaxtion of Fe(III) with natural organic complexing ligands in seawater using cathodic stripping voltammetry, Mar. Chem., 47, 41–54, 1994.

Gledhill, M.: The determination of heme b in marine phyto- and bacterioplankton, Mar. Chem., 103, 393–403, doi:10.1016/j.marchem.2006.10.008, 2007.

Gnanadesikan, A., Sarmiento, J. L., and Slater, R. D.: Effects of patchy ocean fertilization on atmospheric carbon dioxide and biological production, Global Biogeochem.l Cy., 17(17), 1050, doi:10.1029/2002gb001940, 2003.

Gonzalez-Davila, M., Santana-Casiano, J. M., and Millero, F. J.: Competition between O-2 and H_2O_2 in the oxidation of Fe(II) in natural waters, J. Solut. Chem., 35, 95–111, 2006.

Guieu, C., Bonnet, S., Wagener, T., and Loye-Pilot, M. D.: Biomass burning as a source of dissolved iron to the open ocean?, Geophys. Res. Lett., 32, $L_1$9608, doi:10.11029/12005GL022962, 2005.

Gustafsson, O., Widerlund, A., Andersson, P. S., Ingri, J., Roos, P., and Ledin, A.: Colloid dynamics and transport of major elements through a boreal river – brackish bay mixing zone, Mar. Chem., 71, 1–21, 2000.

Han, Q., Moore, J. K., Zender, C., Measures, C., and Hydes, D.: Constraining oceanic dust deposition using surface ocean dissolved Al, Global Biogeochem. Cy., 22, GB2003, doi:10.1029/2007gb002975, 2008.

Hansard, S. P., Landing, W. M., Measures, C. I., and Voelkar, B. M.: Dissolved iron(II) in the Pacific Ocean: Measurements from PO_2 and P16N Clivar/CO_2 repeat hydrography expeditions, Deep Sea Res. I, 56(7), 1117–1129, 2009.

Hare, C. E., DiTullio, G. R., Trick, C. G., Wilhelm, S. W., Bruland, K. W., Rue, E. L., and Hutchins, D. A.: Phytoplankton commu-

nity structure changes following simulated upwelled iron inputs in the Peru upwelling region, Aquatic Microbial Ecology, 38, 269–282, 2005.

Hare, C. E., DiTullio, G. R., Riseman, S. F., Crossley, A. C., Popels, L. C., Sedwick, P. N., and Hutchins, D. A.: Effects of changing continuous iron input rates on a Southern Ocean algal assemblage, Deep-Sea Research Part I-Oceanographic Research Papers, 54, 732–746, doi:10.1016/j.dsr.2007.02.001, 2007a.

Hare, C. E., Leblanc, K., DiTullio, G. R., Kudela, R. M., Zhang, Y., Lee, P. A., Riseman, S., and Hutchins, D. A.: Consequences of increased temperature and CO_2 for phytoplankton community structure in the Bering Sea, Marine Ecology Progress Series, 352, 9–16, doi:10.3354/meps07182, 2007b.

Hassellöv, M. and von der Kammer, F.: Iron Oxides as Geochemical Nanovectors for Metal Transport in Soil-River Systems, Elements, 4, 401–406, doi:10.2113/gselements.4.6.401, 2008.

Hassler, C. S., Slaveykova, V. I., and Wilkinson, K. J.: Discriminating between intra- and extracellular metals using chemical extractions, Limnol. Oceanogr. Methods, 2, 237–247, 2004.

Hassler, C. S., Twiss, M. R., McKay, R. M. L., and Bullerjahn, G. S.: Optimization of iron-dependent cyanobacterial (Synechococcus, cyanophyceae) bioreporters to measure iron bioavailability, J. Phycol., 42, 324–335, 2006.

Hassler, C. S., Chafin, R. D., Klinger, M. B., and Twiss, M. R.: Application of the biotic ligand model to explain potassium interaction with thallium uptake and toxicity to plankton, Environ. Toxicol. Chem., 26, 1139–1145, 2007.

Hassler, C. S. and Schoemann, V.: Bioavailability of organically bound Fe to model phytoplankton of the Southern Ocean, Biogeosciences, 6, 2281–2296, 2009, http://www.biogeosciences.net/6/2281/2009/.

Heldal, M., Fagerbakke, K. M., Tuomi, P., and Bratbak, G.: Abundant populations of iron and manganese sequestering bacteria in coastal water, Aquatic Microbial Ecology, 11, 127–133, 1996.

Ho, T. Y., Quigg, A., Finkel, Z. V., Milligan, A. J., Wyman, K., Falkowski, P. G., and Morel, F. M. M.: The elemental composition of some marine phytoplankton, J. Phycol., 39, 1145–1159, 2003.

Hoagland, K. D., Rosowski, J. R., Gretz, M. R., and Roemer, S. C.: Diatom extracellular polymetric substances – function, fine-structure, chemistry, and physiology, J. Phycol., 29, 537–566, 1993.

Hoffmann, L. J., Peeken, I., and Lochte, K.: Iron, silicate, and light co-limitation of three Southern Ocean diatom species, Polar Biol., 31, 1067–1080, doi:10.1007/s00300-008-0448-6, 2008.

Holm-Hansen, O., Mitchell, B. G., Hewes, C. D., and Karl, D. M.: Phytoplankton blooms in the vicinity of Palmer Station, Antarctica, Polar Biology, 10, 49–57, 1989.

Hopkinson, B. M. and Barbeau, K. A.: Organic and redox speciation of iron in the eastern tropical North Pacific suboxic zone, Mar. Chem., 106, 2–17, 2007.

Hopkinson, B. M., Roe, K. L., and Barbeau, K. A.: Heme uptake by *Microscilla marina* and evidence for heme uptake systems in the genomes of diverse marine bacteria, Appl. Environ. Microbiol., 74, 6263–6270, doi:10.1128/aem.00964-08, 2008.

Howell, K. A., Achterberg, E. P., Tappin, A. D., and Worsfold, P. J.: Colloidal metals in the tamar estuary and their influence on metal fractionation by membrane filtration, Environ. Chem., 3, 199–207, doi:10.1071/en06004, 2006.

Hudson, R. J. M. and Morel, F. M. M.: Iron transport in marine phytoplankton – kinetics of cellular and medium coordination reactions, Limnol. Oceanogr., 35, 1002–1020, 1990.

Hunter, K. A., and Boyd, P. W.: Iron-binding ligands and their role in the ocean biogeochemistry of iron, Environ. Chem., 4, 221–232, doi:10.1071/en07012, 2007.

Hurst, M. P. and Bruland, K. W.: An investigation into the exchange of iron and zinc between soluble, colloidal, and particulate size-fractions in shelf waters using low-abundance isotopes as tracers in shipboard incubation experiments, Mar. Chem., 103, 211–226, doi:10.1016/j.marchem.2006.07.001, 2007.

Hutchins, D. A. and Bruland, K. W.: Grazer-mediated regeneration and assimilation of Fe, Zn and Mn from planktonic prey, Mar. Ecol. Progr. Series, 110, 259–269, 1994.

Hutchins, D. A., Wang, W. X., and Fisher, N. S.: Copepod grazing and the biogeochemical fate of diatom iron, Limnol. Oceanogr., 40, 989–994, 1995.

Hutchins, D. A. and Bruland, K. W.: Iron-limited diatom growth and Si:N uptake ratios in a coastal upwelling regime, Nature, 393, 561–564, 1998.

Hutchins, D. A., Franck, V. M., Brzezinski, M. A., and Bruland, K. W.: Inducing phytoplankton iron limitation in iron-replete coastal waters with a strong chelating ligand, Limnol. Oceanogr., 44, 1009–1018, 1999a.

Hutchins, D. A., Witter, A. E., Butler, A., and Luther III, G. W.: Competition among marine phytoplankton for different chelated iron species, Nature, 400, 858–861, 1999b.

Hutchins, D. A., Pustizzi, F., Hare, C. E., and DiTullio, G. R.: A shipboard natural community continuous culture system for ecologically relevant low-level nutrient enrichment experiments, Limnol. Oceanogr.-Methods, 1, 82–91, 2003.

Ingri, J., Malinovsky, D., Rodushkin, I., Baxter, D. C., Widerlund, A., Andersson, P., Gustafsson, O., Forsling, W., and Ohlander, B.: Iron isotope fractionation in river colloidal matter, Earth Planet. Sci. Lett., 245, 792–798, 2006.

Jacobson, M. Z.: Studying ocean acidification with conservative, stable numerical schemes for nonequilibrium air-ocean exchange and ocean equilibrium chemistry, J. Geophys. Res.-Atmos., 110, D07302, doi:10.01029/02004JD005220 2005.

Jickells, T. and Spokes, L. J.: Atmospheric iron inputs into the oceans, in: The Biogeochemistry of Iron in Seawater, edited by: Turner, D. R., and Hunter, K. A., John Wiley and Sons Ltd., West Sussex, England, 85–121, 2001.

Jickells, T. D., Dorling, S., Deuser, W. G., Church, T. M., Arimoto, R., and Prospero, J. M.: Air-borne dust fluxes to a deep water sediment trap in the Sargasso Sea, Global Biogeochem. Cy., 12, 311–320, 1998.

Jickells, T. D., An, Z. S., Andersen, K. K., Baker, A. R., Bergametti, G., Brooks, N., Cao, J. J., Boyd, P. W., Duce, R. A., Hunter, K. A., Kawahata, H., Kubilay, N., laRoche, J., Liss, P. S., Mahowald, N., Prospero, J. M., Ridgwell, A. J., Tegen, I., and Torres, R.: Global Iron Connections Between Desert Dust, Ocean Biogeochemistry, and Climate, Science, 308, 67–71, 2005.

Johnson, K. S.: Iron supply and demand in the upper ocean: Is extraterrestrial dust a significant source of bioavailable iron?, Glob. Biogeochem. Cy., 15, 61–63, 2001.

Johnson, K. S., Boyle, E., Bruland, K. W., Coale, K., Measures, C., Moffett, J., Aguilar-Islas, A., Barbeau, K., Bergquist, B., Bowie, A., Buck, K., Cai, Y., Chase, Z., Cullen, J., Doi, T., Elrod, V.,

Fitzwater, S., Gordon, M., King, A., Laan, P., Laglera-Baquer, L., Landing, W., Lohan, M., Mendez, J., Milne, A., Obata, H., Ossiander, L., Plant, J., Sarthou, G., Sedwick, P., Smith, G. J., Sohst, B., Tanner, S., van den Berg, S., and Wu, J.: The SAFe Iron Intercomparison Cruise: An International Collaboration to Develop Dissolved Iron in Seawater Standards, EOS, Transactions of the American Geophysical Union, 88, 131–132, 2007.

Johnson, W. K., Miller, L. A., Sutherland, N. E., and Wong, C. S.: Iron transport by mesoscale Haida eddies in the Gulf of Alaska, Deep-Sea Res., 52, 933–953, doi:10.1016/j.dsr2.2004.08.017, 2005.

Jones, M. T. and Gislason, S. R.: Rapid releases of metal salts and nutrients following the deposition of volcanic ash into aqueous environments, Geochim. Cosmochim. Acta, 72, 3661–3680, 2008.

Journet, E., Desboeufs, K. V., Caquineau, S., and Colin, J. L.: Mineralogy as a critical factor of dust iron solubility, Geophys. Res. Lett., 35, L07805, doi:10.1029/2007gl031589, 2008.

Kintisch, E.: Carbon sequestration: Should oceanographers pump iron?, Science, 318, 1368–1370, 2007.

Kondo, Y., Takeda, S., Nishioka, J., Obata, H., Furuya, K., Johnson, W. K., and Wong, C. S.: Organic iron(III) complexing ligands during an iron enrichment experiment in the western subarctic North Pacific, Geophys. Res. Lett., 35, L_12601, doi:10.1029/2008gl033354, 2008.

Krachler, R., Jirsa, F., and Ayromlou, S.: Factors influencing the dissolved iron input by river water to the open ocean, Biogeosciences, 2, 311–315, 2005, http://www.biogeosciences.net/2/311/2005/.

Lacan, F., Radic, A., Jeandel, C., Poitrasson, F., Sarthou, G., Pradoux, C., and Freydier, R.: Measurement of the isotopic composition of dissolved iron in the open ocean, Geophys. Res. Lett., 35, L_24610, doi:10.1029/2008gl035841, 2008.

Laës, A., Blain, S., Laan, P., Achterberg, E. P., Sarthou, G., and de Baar, H. J. W.: Deep dissolved iron profiles in the eastern North Atlantic in relation to water masses, Geophys. Res. Lett., 30(4), 1902, doi:10.1029/2003gl017902, 2003.

Laës, A., Blain, S., Laan, P., Ussher, S. J., Achterberg, E. P., Trguer, P., and de Baar, H. J. W.: Sources and transport of dissolved iron and manganese along the continental margin of the Bay of Biscay, Biogeosciences, 4, 181–194, 2007, http://www.biogeosciences.net/4/181/2007/.

Laglera, L. M. and van den Berg, C. M. G.: Evidence for geochemical control of iron by humic substances in seawater, Limnol. Oceanogr., 54, 610–619, 2009.

Lam, C. K. S. C. C., Jickells, T. D., Richardson, D. J., and Russell, D. A.: Fluorescence-Based Siderophore Biosensor for the Determination of Bioavailable Iron in Oceanic Waters, Anal. Chem., 78, 5040–5045, doi:10.1021/ac060223t, 2006.

Lam, P. J. and Bishop, J. K. B.: The continental margin is a key source of iron to the HNLC North Pacific Ocean, Geophys. Res. Lett., 35(5), L07608, doi:10.1029/2008gl033294, 2008.

Lancelot, C., de Montety, A., Goosse, H., Becquevort, S., Schoemann, V., Pasquer, B., and Vancoppenolle, M.: Spatial distribution of the iron supply to phytoplankton in the Southern Ocean: a model study, Biogeosciences, 6, 2861–2878, 2009, http://www.biogeosciences.net/6/2861/2009/.

Lannuzel, D., Schoemann, V., de Jong, J., Tison, J. L., and Chou, L.: Distribution and biogeochemical behaviour of iron in the East Antarctic sea ice, Mar. Chem., 106, 18–32, doi:10.1016/j.marchem.2006.06.010, 2007.

Lannuzel, D., Schoemann, V., de Jong, J., Chou, L., Delille, B., Becquevort, S., and Tison, J.-L.: Iron study during a time series in the western Weddell pack ice, Mar. Chem., 108, 85–95, 2008.

Liss, P., Chuck, A., Bakker, D., and Turner, S.: Ocean fertilization with iron: effects on climate and air quality, Tellus Ser. B-Chem. Phys. Meteorol., 57, 269–271, 2005.

Liu, X. W. and Millero, F. J.: The solubility of iron hydroxide in sodium chloride solutions, Geochim. Cosmochim. Acta, 63, 3487–3497, 1999.

Liu, X. W. and Millero, F. J.: The solubility of iron in seawater, Mar. Chem., 77, 43–54, 2002.

Lohan, M. C. and Bruland, K. W.: Importance of vertical mixing for additional sources of nitrate and iron to surface waters of the Columbia River plume: Implications for biology, Mar. Chem., 98, 260–273, doi:10.1016/j.marchem.2005.10.003, 2006.

Loscher, B. M., DeBaar, H. J. W., DeJong, J. T. M., Veth, C., and Dehairs, F.: The distribution of Fe in the Antarctic Circumpolar Current, Deep-Sea Res., 44, 143–187, 1997.

Luo, C., Mahowald, N., Bond, T., Chuang, P. Y., Artaxo, P., Siefert, R., Chen, Y., and Schauer, J.: Combustion iron distribution and deposition, Global Biogeochem. Cy., 22(17), GB1012, doi:10.1029/2007gb002964, 2008.

Lyvén, B., Hassellov, M., Turner, D. R., Haraldsson, C., and Andersson, K.: Competition between iron- and carbon-based colloidal carriers for trace metals in a freshwater assessed using flow field-flow fractionation coupled to ICPMS, Geochim. Cosmochim. Acta, 67, 3791–3802, 2003.

Mackey, D. J., O'Sullivan, J. E., and Watson, R. J.: Iron in the western Pacific: a riverine or hydrothermal source for iron in the Equatorial Undercurrent?, Deep-Sea Res., 49, 877–893, 2002.

Mahowald, N., Jickells, T. D., Baker, A. R., Artaxo, P., Benitez-Nelson, C. R., Bergametti, G., Bond, T. C., Chen, Y., Cohen, D. D., Herut, B., Kubilay, N., Losno, R., Luo, C., Maenhaut, W., McGee, K. A., Okin, G. S., Siefert, R. L., and Tsukuda, S.: Global distribution of atmospheric phosphorus sources, concentrations and deposition rates, and anthropogenic impacts, Global Biogeochem. Cy., 22, GB4026, doi:10.1029/2008gb003240, 2008.

Mahowald, N. M., Baker, A. R., Bergametti, G., Brooks, N., Duce, R. A., Jickells, T. D., Kubilay, N., Prospero, J. M., and Tegen, I.: Atmospheric global dust cycle and iron inputs to the ocean, Global Biogeochem. Cy., 19, GB4025, doi:10.1029/2004gb002402, 2005.

Maldonado, M. T., Boyd, P. W., Harrison, P. J., and Price, N. M.: Co-limitation of phytoplankton growth by light and Fe during winter in the NE subarctic Pacific Ocean, Deep-Sea Res., 46, 2475–2485, 1999.

Maldonado, M. T., Strzepek, R. F., Sander, S., and Boyd, P. W.: Acquisition of iron bound to strong organic complexes, with different Fe binding groups and photochemical reactivities, by plankton communities in Fe-limited subantarctic waters, Global Biogeochem., 19, GB4S23, doi:10.1029/2005GB002481, 2005.

Marchetti, A., Parker, M. S., Moccia, L. P., Lin, E. O., Arrieta, A. L., Ribalet, F., Murphy, M. E. P., Maldonado, M. T., and Armbrust, E. V.: Ferritin is used for iron storage in bloom-forming marine pennate diatoms, Nature, 457, 467–470, doi:10.1038/nature07539, 2009.

Martin, J. H.: Glacial-interglacial CO_2 change: the iron hypothesis, Paleoceanography, 5, 1–13, 1990.

Mawji, E., Gledhill, M., Milton, J. A., Tarran, G. A., Ussher, S., Thompson, A., Wolff, G. A., Worsfold, P. J., and Achterberg, E. P.: Hydroxamate Siderophores: Occurrence and Importance in the Atlantic Ocean, Environ. Sci. Technol., 42, 8675–8680, doi:10.1021/es801884r, 2008.

McKay, R., Michael, L, la Roche, J., Yakunin, A., F, Durnford, D. G., and Geider, R. J.: Accumulation of Ferredoxin and Flavodoxin in a Marine Diatom in response to Fe, J. Phycology, 35, 510–519, 1999.

Millero, F. J., Sotolongo, S., and Izaguirre, M.: The oxidation kinetics of Fe(II) in seawater, Geochim. Cosmochim. Acta, 51, 793–801, 1987.

Millero, F. J. and Sotolongo, S.: The oxidation of Fe(II) with H_2O_2 in seawater, Geochim. Cosmochim. Acta, 53, 1867–1873, 1989.

Mills, M. M., Ridame, C., Davey, M., La Roche, J., and Geider, R. J.: Iron and phosphorus co-limits nitrogen fixation in the eastern tropical North Atlantic, Nature, 429, 292–294, 2004.

Moore, C. M., Mills, M. M., Milne, A., Langlois, R., Achterberg, E. P., Lochte, K., Geider, R. J., and La Roche, J.: Iron limits primary productivity during spring bloom development in the central North Atlantic, Global Change Biol., 12, 626–634 doi:610.1111/j.1365-2486.2006.01122.x, 2006.

Moore, C. M., Hickman, A. E., Poulton, A. J., Seeyave, S., and Lucas, M. I.: Iron-light interactions during the CROZet natural iron bloom and EXport experiment (CROZEX): II – Taxonomic responses and elemental stoichiometry, Deep-Sea Res., 54, 2066–2084, doi:10.1016/j.dsr2.2007.06.015, 2007a.

Moore, C. M., Seeyave, S., Hickman, A. E., Allen, J. T., Lucas, M. I., Planquette, H., Pollard, R. T., and Poulton, A. J.: Iron-light interactions during the CROZet natural iron bloom and EXport experiment (CROZEX) I: Phytoplankton growth and photophysiology, Deep-Sea Res., 54, 2045–2065, doi:10.1016/j.dsr2.2007.06.011, 2007b.

Moran, S. B., Yeats, P. A., and Balls, P. W.: On the role of colloids in trace metal solid-solution partitioning in continental shelf waters: A comparison of model results and field data, Cont. Shelf Res., 16, 397–408, 1996.

Morel, F. M. M. and Price, N. M.: The biogeochemical cycles of trace metals in the oceans, Science, 300, 944–947, 2003.

Morel, F. M. M., Kustka, A. B., and Shaked, Y.: The role of unchelated Fe in the iron nutrition of phytoplankton, Limnol. Oceanogr., 53, 400–404, 2008.

Mosley, L. M., Hunter, K. A., and Ducker, W. A.: Forces between colloid particles in natural waters, Environ. Sci. Technol., 37, 3303–3308, doi:10.1021/es026216d, 2003.

Mylon, S. E., Chen, K. L., and Elimelech, M.: Influence of natural organic matter and ionic composition on the kinetics and structure of hematite colloid aggregation: Implications to iron depletion in estuaries, Langmuir, 20, 9000–9006, doi:10.1021/la049153g, 2004.

Nowostawska, U., Kim, J. P., and Hunter, K. A.: Aggregation of riverine colloidal iron in estuaries: A new kinetic study using stopped-flow mixing, Mar. Chem., 110, 205–210, 2008.

Nunn, B. L. and Timperman, A. T.: Marine Proteomics, Mar. Ecol. Progr. Series, 332, 281–289, 2007.

Orr, J. C., Fabry, V. J., Aumont, O., Bopp, L., Doney, S. C., Feely, R. A., Gnanadesikan, A., Gruber, N., Ishida, A., Joos, F., Key, R. M., Lindsay, K., Maier-Reimer, E., Matear, R., Monfray, P., Mouchet, A., Najjar, R. G., Plattner, G. K., Rodgers, K. B., Sabine, C. L., Sarmiento, J. L., Schlitzer, R., Slater, R. D., Totterdell, I. J., Weirig, M. F., Yamanaka, Y., and Yool, A.: Anthropogenic ocean acidification over the twenty-first century and its impact on calcifying organisms, Nature, 437, 681–686, 2005.

Öztürk, M., Steinnes, E., and Sakshaug, E.: Iron Speciation in the Trondheim Fjord from the Perspective of Iron Limitation for Phytoplankton, Estuarine, Coastal Shelf Sci.e, 55, 197–212, 2002.

Öztürk, M. and Bizsel, N.: Iron speciation and biogeochemistry in different nearshore waters, Mar. Chem., 83, 145–156, 2003.

Öztürk, M., Croot, P. L., Bertilsson, S., Abrahamsson, K., Karlson, B., David, R., Fransson, A., and Sakshaug, E.: Iron enrichment and photoreduction of iron under UV and PAR in the presence of hydroxycarboxylic acid: implications for phytoplankton growth in the Southern Ocean, Deep Sea Res., 51, 2841–2856, 2004.

Paytan, A., Mackey, K. R. M., Chen, Y., Lima, I. D., Doney, S. C., Mahowald, N., Labiosa, R., and Postf, A. F.: Toxicity of atmospheric aerosols on marine phytoplankton, Proc. Natl. Acad. Sci. USA, 106, 4601–4605, di:10.1073/pnas.0811486106, 2009.

Peers, G. and Price, N. M.: Copper-containing plastocyanin used for electron transport by an oceanic diatom, Nature, 441, 341–344, 2006.

Pickell, L. D., Wells, M. L., Trick, C. G., and Cochlan, W. P.: A sea-going continuous culture system for investigating phytoplankton community response to macro- and micro-nutrient manipulations, Limnol. Oceanogr.-Methods, 7, 21–32, 2009.

Planquette, H., Statham, P. J., Fones, G. R., Charette, M. A., Moore, C. M., Salter, I., Nedelec, F. H., Taylor, S. L., French, M., Baker, A. R., Mahowald, N., and Jickells, T. D.: Dissolved iron in the vicinity of the Crozet Islands, Southern Ocean, Deep-Sea Res., 54, 1999–2019, doi:10.1016/j.dsr2.2007.06.019, 2007.

Pollard, R. T., Salter, I., Sanders, R. J., Lucas, M. I., Moore, C. M., Mills, R. A., Statham, P. J., Allen, J. T., Baker, A. R., Bakker, D. C. E., Charette, M. A., Fielding, S., Fones, G. R., French, M., Hickman, A. E., Holland, R. J., Hughes, J. A., Jickells, T. D., Lampitt, R. S., Morris, P. J., Nedelec, F. H., Nielsdottir, M., Planquette, H., Popova, E. E., Poulton, A. J., Read, J. F., Seeyave, S., Smith, T., Stinchcombe, M., Taylor, S., Thomalla, S., Venables, H. J., Williamson, R., and Zubkov, M. V.: Southern Ocean deep-water carbon export enhanced by natural iron fertilization, Nature, 457, 577–580, 2009.

Powell, R. T. and Wilson-Finelli, A.: Importance of organic Fe complexing ligands in the Mississippi River plume, Estuarine, Coastal Shelf Sci., 58, 757–763, 2003.

Prospero, J. M., Ginoux, P., Torres, O., Nicholson, S. E., and Gill, T. E.: Environmental characterization of global sources of atmospheric soil dust identified with the Nimbus 7 Total Ozone Mapping Spectrometer (TOMS) absorbing aerosol product, Rev. Geophys., 40, 1002, doi:1010.1029/2000RG000095, 2002.

Pulido-Villena, E., Wagener, T., and Guieu, C.: Bacterial response to dust pulses in the western Mediterranean: Implications for carbon cycling in the oligotrophic ocean, Global Biogeochem. Cy., 22(12), GB1020, doi:10.1029/2007GB003091, 2008.

Quigg, A., Finkel, Z. V., Irwin, A. J., Rosenthal, Y., Ho, T. Y., Reinfelder, J. R., Schofield, O., Morel, F. M. M., and Falkowski, P. G.: The evolutionary inheritance of elemental stoichiometry in marine phytoplankton, Nature, 425, 291–294, 2003.

Raiswell, R., Tranter, M., Benning, L. G., Siegert, M., De'ath, R., Huybrechts, P., and Payne, T.: Contributions from glacially derived sediment to the global iron (oxyhydr)oxide cycle: Implications for iron delivery to the oceans, Geochim. Cosmochim. Acta, 70, 2765–2780, doi:10.1016/j.gca.2005.12.027, 2006.

Raiswell, R., Benning, L. G., Tranter, M., and Tulaczyk, S.: Bioavailable iron in the Southern Ocean: the significance of the iceberg conveyor belt, Geochem. Trans., 9(7), doi:10.1186/1467-4866-9-7, 2008.

Riebesell, U., Schulz, K. G., Bellerby, R. G. J., Botros, M., Fritsche, P., Meyerhofer, M., Neill, C., Nondal, G., Oschlies, A., Wohlers, J., and Zollner, E.: Enhanced biological carbon consumption in a high CO_2 ocean, Nature, 450, 545–510, doi:10.1038/nature06267, 2007.

Rose, A. L.: Effect of Dissolved Natural Organic Matter on the Kinetics of Ferrous Iron Oxygenation in Seawater, Environ. Sci. Technol., 37, 4877–4886, doi:10.1021/es034152g, 2003.

Rose, J. M., Feng, Y., DiTullio, G. R., Dunbar, R. B., Hare, C. E., Lee, P. A., Lohan, M., Long, M., W. O. Smith Jr., Sohst, B., Tozzi, S., Zhang, Y., and Hutchins, D. A.: Synergistic effects of iron and temperature on Antarctic phytoplankton and microzooplankton assemblages, Biogeosciences, 6, 3131–3147, 2009, http://www.biogeosciences.net/6/3131/2009/.

Roy, E. G., Jiang, C. H., Wells, M. L., and Tripp, C.: Determining subnanomolar iron concentrations in oceanic seawater using a siderophore-modified film analyzed by infrared spectroscopy, Anal. Chem., 80, 4689–4695, doi:10.1021/ac800356p, 2008a.

Roy, E. G., Wells, M. L., and King, D. W.: Persistence of iron(II) in surface waters of the western subarctic Pacific, Limnol. Oceanogr., 53, 89–98, 2008b.

Rue, E. L. and Bruland, K. W.: Complexation of iron(III) by natural organic ligands in the Central North Pacific as determined by a new competitive ligand equilibration/adsorptive cathodic stripping voltammetric method, Mar. Chem., 50, 117–138, 1995.

Rue, E. L. and Bruland, K. W.: The role of organic complexation on ambient iron chemistry in the equatorial Pacific Ocean and the response of a mesoscale iron addition experiment, Limnol. Oceanogr., 42, 901–910, 1997.

Rusch, D. B., Halpern, A. L., Sutton, G., Heidelberg, K. B., Williamson, S., Yooseph, S., Wu, D., Eisen, J. A., Hoffman, J. M., Remington, K., Beeson, K., Tran, B., Smith, H., Baden-Tillson, H., Stewart, C., Thorpe, J., Freeman, J., Andrews-Pfannkoch, C., Venter, J. E., Li, K., Kravitz, S., Heidelberg, J. F., Utterback, T., Rogers, Y. H., Falcón, L. I., Souza, V., Bonilla-Rosso, G., Eguiarte, L. E., Karl, D. M., Sathyendranath, S., Platt, T., Bermingham, E., Gallardo, V., Tamayo-Castillo, G., Ferrari, M. R., Strausberg, R. L., Nealson, K., Friedman, R., Frazier, M., and Venter, J. C.: The Sorcerer II Global Ocean Sampling expedition: northwest Atlantic through eastern tropical Pacific, PLoS biology, 5(e77), 398–431, 2007.

Saito, M. A., Sigman, D. M., and Morel, F. M. M.: The bioinorganic chemistry of the ancient ocean: the co- evolution of cyanobacterial metal requirements and biogeochemical cycles at the Archean-Proterozoic boundary?, Inorganic Chimica Acta, 356, 308–318, 2003.

Salmon, T. P., Rose, A. L., Neilan, B. A., and Waite, T. D.: The FeL model of iron acquisition: Nondissociative reduction of ferric complexes in the marine environment, Limnol. Oceanogr., 51, 1744–1754, 2006.

Sander, S., Mosley, L. M., and Hunter, K. A.: Investigation of interparticle forces in natural waters: Effects of adsorbed humic acids on iron oxide and alumina surface properties, Environ. Sci. Technol., 38, 4791–4796, doi:10.1021/es049602z, 2004.

Sander, S., Ginon, L., Anderson, B., and Hunter, K. A.: Comparative study of organic Cd and Zn complexation in lake waters – seasonality, depth and pH dependence, Environ. Chem., 4, 410–423, 2007.

Santana-Casiano, J. M., Gonzalez-Davila, M., and Millero, F. J.: Oxidation of Nanomolar Levels of Fe(II) with Oxygen in Natural Waters, Environ. Sci. Technol., 39, 2073–2079, 2005.

Santana-Casiano, J. M., Gonzalez-Davila, M., and Millero, F. J.: The role of Fe(II) species on the oxidation of Fe(II) in natural waters in the presence of O_2 and H_2O_2, Mar. Chem., 99, 70–82, 2006.

Santschi, P. H., Balnois, E., Wilkinson, K. J., Zhang, J. W., Buffle, J., and Guo, L. D.: Fibrillar polysaccharides in marine macromolecular organic matter as imaged by atomic force microscopy and transmission electron microscopy, Limnol. Oceanogr., 43, 896–908, 1998.

Sarmiento, J. L. and Orr, J. C.: 3-dimensional simulations of the impact of Southern-Ocean nutrient depletion on atmospheric CO_2 and ocean chemistry, Symp on What Controls Phytoplankton Production in Nutrient-Rich Areas of the Open Sea, San Marcos, Ca, 1991, ISI:A1991HR98100032, 1928–1950,

Sarthou, G., Timmermans, K. R., Blain, S., and Treguer, P.: Growth physiology and fate of diatoms in the ocean: a review, J. Sea Res., 53, 25–42, 2005.

Sarthou, G., Vincent, D., Christaki, U., Obernosterer, I., Timmermans, K. R., and Brussaard, C. P. D.: The fate of biogenic iron during a phytoplankton bloom induced by natural fertilisation: Impact of copepod grazing, Deep-Sea Res., 55, 734–751, doi:10.1016/j.dsr2.2007.12.033, 2008.

Sato, M., Takeda, S., and Furuya, K.: Iron regeneration and organic iron(III)-binding ligand production during in situ zooplankton grazing experiment, Mar. Chem., 106, 471–488, 2007.

Schmincke, H.-U.: Volcanism, Springer-Verlag, Berlin Heidelberg New York, 324 pp., 2004.

Schoemann, V., Wollast, R., Chou, L., and Lancelot, C.: Effects of photosynthesis on the accumulation of Mn and Fe by Phaeocystis colonies, Limnol. Oceanogr., 46, 1065–1076, 2001.

Schoemann, V., De Jong, J. T. M., Lannuzel, D., Tison, J. L., Dellile, B., Chou, L., Lancelot, C., and Becquevort, S.: Microbiological control on the cycling Fe and its isotopes in Antarctic sea ice, 8th Annual V M Goldschmidt Conference, Vancouver, CANADA, ISI:000257301602198, A837–A837, 2008.

Schroth, A. W., Crusius, J., Sholkovitz, E. R., and Bostick, B. C.: Iron solubility driven by speciation in dust sources to the ocean, Nature Geosci., 2, 337–340, 2009.

Schulz, K. G., Zondervan, I., Gerringa, L. J. A., Timmermans, K. R., Veldhuis, M. J. W., and Riebesell, U.: Effect of trace metal availability on coccolithophorid calcification, Nature, 430, 673–676, 2004.

Sedwick, P. N., Sholkovitz, E. R., and Church, T. M.: Impact of anthropogenic combustion emissions on the fractional solubility of aerosol iron: Evidence from the Sargasso Sea, Geochem. Geophys. Geosyst., 8, 21, Q10q06, doi:10.1029/2007gc001586, 2007.

Shaked, Y., Kustka, A. B., Morel, F. M. M., and Erel, Y.: Simulta-

neous determination of iron reduction and uptake by phytoplankton, Limnol. Oceanogr.-Methods, 2, 137–145, 2004.

Shaked, Y., Kustka, A. B., and Morel, F. M. M.: A general kinetic model for iron acquisition by eukaryotic phytoplankton, Limnol. Oceanogr., 50, 872–882, 2005.

Sholkovitz, E. R.: Flocculation of dissolved Fe, Mn, Al, Cu, Ni,Co, and Cd during estuarine mixing, Earth Planet. Sci. Lett., 41, 77–86, 1978.

Sholkovitz, E. R., Boyle, E. A., and Price, N. B.: Removal of dissolved humic acids and iron during estuarine mixing, Earth Planet. Sci. Lett., 40, 130–136, 1978.

Sigman, D. M. and Boyle, E. A.: Glacial/interglacial variations in atmospheric carbon dioxide, Nature, 407, 859–869, 2000.

Sillen, L. G. and Martell, A. E.: Stability Constants, Chemical Society, London, 1971.

Smith, K. L., Robison, B. H., Helly, J. J., Kaufmann, R. S., Ruhl, H. A., Shaw, T. J., Twining, B. S., and Vernet, M.: Free-drifting icebergs: Hot spots of chemical and biological enrichment in the Weddell Sea, Science, 317, 478–482, doi:10.1126/science.1142834, 2007.

Smith, W. O. and Nelson, D. M.: Phytoplankton bloom produced by a receeding ice edge in the Ross Sea – spacial coherence with the density field, Science, 227, 163–166, 1985.

Spokes, L. and Jickells, T. D.: Speciation of metals in the atmosphere, in: Chemical Speciation in the Environment, edited by: Ure, A. and Davidson, C., Blackwell, Malden, 159–187, 2002.

Statham, P. J., Skidmore, M., and Tranter, M.: Inputs of glacially derived dissolved and colloidal iron to the coastal ocean and implications for primary productivity, Global Biogeochem. Cy., 22, GB3013, doi:10.1029/2007gb003106, 2008.

Steigenberger, S., Statham, P. J., Völker, C., and Passow, U.: The role of polysaccharides and diatom exudates in the redox cycling of Fe and the photoproduction of hydrogen peroxide in coastal seawaters, Biogeosciences, 7, 109–119, 2010, http://www.biogeosciences.net/7/109/2010/.

Stolpe, B., Hassellöv, M., Andersson, K., and Turner, D. R.: High resolution ICPMS as an on-line detector for flow field-flow fractionation; multi-element determination of colloidal size distributions in a natural water sample, Analytica Chimica Acta, 535, 109–121, 2005.

Stolpe, B. and Hassellöv, M.: Changes in size distribution of fresh water nanoscale colloidal matter and associated elements on mixing with seawater, Geochim. Cosmochim. Acta, 71, 3292–3301, 2007.

Stolpe, B., and Hassellöv, M.: Colloidal biopolymers binding iron, copper, silver, lanthanum and lead in coastal seawater – significance for the seasonal and spatial variations in element size distributions, Limnol. Oceanogr., 55(1), 187–202, 2010.

Straub, S. M. and Schmincke, H. U.: Evaluating the tephra input into Pacific Ocean sediments: distribution in space and time, Geologische Rundschau, 87, 461–476, 1998.

Strzepek, R. F. and Harrison, P. J.: Photosynthetic architecture differs in coastal and oceanic diatoms, Nature, 431, 689–692, 2004.

Strzepek, R. F., Maldonado, M. T., Higgins, J. L., Hall, J., Safi, K., Wilhelm, S. W., and Boyd, P. W.: Spinning the "Ferrous Wheel": The importance of the microbial community in an iron budget during the FeCycle experiment, Global Biogeochem. Cy., 19, GB4S26, doi:10.1029/2005GB002490, 2005.

Sunda, W. and Huntsman, S.: Effect of pH, light, and temperature on Fe-EDTA chelation and Fe hydrolysis in seawater, Mar. Chem., 84, 35–47, 2003.

Sunda, W. G. and Huntsman, S. A.: Effect of competitive interactions between manganese and copper on cellular manganese and growth in estuarine and oceanic species of the diatom Thalassiosira, Limnol. Oceanogr., 28, 924–934, 1983.

Sunda, W. G. and Huntsman, S. A.: Iron uptake and growth limitation in oceanic and coastal phytoplankton, Mar. Chem., 50, 189–206, 1995.

Sunda, W. G. and Huntsman, S. A.: Processes regulating cellular metal accumulation and physiological effects: Phytoplankton as a model system, The Sciences of the Total Environment, 219, 165–181, 1998.

Sunda, W. G. and Huntsman, S. A.: Effect of Zn, Mn, and Fe on Cd accumulation in phytoplankton: Implications for oceanic Cd cycling, Limnol. Oceanogr., 45, 1501–1516, 2000.

Takeda, S.: Influence of iron availability on nutrient consumption ratio of diatoms in oceanic waters, Nature, 393, 774–777, 1998.

Timmermans, K. R., van der Wagt, B., Veldhuis, M. J. W., Maatman, A., and de Baar, H. J. W.: Physiological responses of three species of marine pico-phytoplankton to ammonium, phosphate, iron and light limitation, J. Sea Res., 53, 109–120, 2005.

Toner, B. M., Fakra, S. C., Manganini, S. J., Santelli, C. M., Marcus, M. A., Moffett, J., Rouxel, O., German, C. R., and Edwards, K. J.: Preservation of iron(II) by carbon-rich matrices in a hydrothermal plume, Nature Geosci., 2, 197–201, doi:10.1038/ngeo433, 2009.

Tovar-Sanchez, A., Sanudo-Wilhelmy, S. A., Kustka, A. B., Agusti, S., Dachs, J., Hutchins, D. A., Capone, D. G., and Duarte, C. M.: Effects of dust deposition and river discharges on trace metal composition of Trichodesmium spp. in the tropical and subtropical North Atlantic Ocean, Limnol. Oceanogr., 51, 1755–1761, 2006.

Tovar-Sanchez, A., Duarte, C. M., Hernández-León, S., and Sañudo-Wilhelmy, S. A.: Krill as a central node for iron cycling in the Southern Ocean, Geophys. Res. Lett., 34, $L_1$1601, doi:10.1029/12006GL029096, 022007, 2007.

Trapp, J. M., Millero, F. J., and Prospero, J. M.: Trends in the solubility of iron in dust-dominated aerosols in the Equatorial Atlantic Trade Winds: The importance of iron speciation and sources, Geochem. Geophys. Geosyst., 11(1), in press, 2010.

Tsuda, A., Takeda, S., Saito, H., Nishioka, J., Nojiri, Y., Kudo, I., Kiyosawa, H., Shiomoto, A., Imai, K., Ono, T., Shimamoto, A., Tsumune, D., Yoshimura, T., Aono, T., Hinuma, A., Kinugasa, M., Suzuki, K., Sohrin, Y., Noiri, Y., Tani, H., Deguchi, Y., Tsurushima, N., Ogawa, H., Fukami, K., Kuma, K., and Saino, T.: A mesoscale iron enrichment in the western Subarctic Pacific induces a large centric diatom bloom, Science, 300, 958–961, 2003.

Turner, D. R. and Hunter, K. A.: The Biogeochemistry of Iron in Seawater, IUPAC Series on Analytical and Physical Chemistry of Environmental Systems, John Wiley and Sons Ltd., West Sussex, England, 396 pp., 2001.

Twining, B. S., Baines, S. B., Fisher, N. S., and Landry, M. R.: Cellular iron contents of plankton during the Southern Ocean Iron Experiment (SOFeX), Deep-Sea Res., 51, 1827–1850, doi:10.1016/j.dsr.2004.08.007, 2004.

Ussher, S. J., Worsfold, P. J., Achterberg, E. P., Laes, A., Blain, S., Laan, P., and de Baar, H. J. W.: Distribution and redox speciation

of dissolved iron on the European continental margin, Limnol. Oceanogr., 52, 2530–2539, 2007.

Vasconcelos, M., Leal, M. F. C., and van den Berg, C. M. G.: Influence of the nature of the exudates released by different marine algae on the growth, trace metal uptake, and exudation of Emiliania huxleyi in natural seawater, Mar. Chem., 77, 187–210, 2002.

Venter, J. C., Remington, K., Heidelberg, J. F., Halpern, A. L., Rusch, D., Eisen, J. A., Wu, D. Y., Paulsen, I., Nelson, K. E., Nelson, W., Fouts, D. E., Levy, S., Knap, A. H., Lomas, M. W., Nealson, K., White, O., Peterson, J., Hoffman, J., Parsons, R., Baden-Tillson, H., Pfannkoch, C., Rogers, Y. H., and Smith, H. O.: Environmental genome shotgun sequencing of the Sargasso Sea, Science, 304, 66–74, doi:10.1126/science.1093857, 2004.

Verdugo, P., Alldredge, A. L., Azam, F., Kirchman, D. L., Passow, U., and Santschi, P. H.: The oceanic gel phase: a bridge in the DOM-POM continuum, Mar. Chem., 92, 67–85, 2004.

Vigenault, B. and Campbell, P. G. C.: Uptake of cadmium by freshwater green algae: Effects of pH and aquatic humic substances, J. Phycol., 41, 55–61, 2005.

Vong, L., Laës, A., and Blain, S.: Determination of iron-porphyrin-like complexes at nanomolar levels in seawater, Analytica Chimica Acta, 588, 237–244, doi:10.1016/j.aca.2007.1002.1007 2007.

Vraspir, J. and Butler, A.: Chemistry of marine ligands and siderophores, Ann. Rev. Mar. Sci., 1, 43–63, 2009.

Wagener, T., Guieu, C., Losno, R., Bonnet, S., and Mahowald, N.: Revisiting atmospheric dust export to the Southern Hemisphere ocean: Biogeochemical implications, Global Biogeochem. Cy., 22, GB2006, doi:10.1029/2007gb002984, 2008.

Wang, W. X. and Dei, R. C. H.: Bioavailability of iron complexed with organic colloids to the cyanobacteria *Synechococcus* and *Trichodesmium*, Aquatic Microbial Ecology, 33, 247–259, 2003.

Watson, A. J.: Iron limitation in the oceans, in: The biogeochemistry of iron in seawater, edited by: Turner, D. R., and Hunter, K. A., John Wiley & Sons Ltd., Chicester, 9–33, 2001.

Weber, L., Völker, C., Oschlies, A., and Burchard, H.: Iron profiles and speciation of the upper water column at the Bermuda Atlantic Time-series Study site: a model based sensitivity study, Biogeosciences, 4, 689–706, 2007, http://www.biogeosciences.net/4/689/2007/.

Wells, M. L.: A neglected dimension, Nature, 391, 530–531, 1998.

Wells, M. L., Trick, C. G., Cochlan, W. P., Hughes, M. P., and Trainer, V. L.: Domoic acid: The synergy of iron, copper, and the toxicity of diatoms, Limnol. Oceanogr., 50, 1908–1917, 2005.

Willey, J. D., Kieber, R. J., Seaton, P. J., and Miller, C.: Rainwater as a source of Fe(II)-stabilizing ligands to seawater, Limnol. Oceanogr., 53, 1678–1684, 2008.

Wolff, E. W., Fischer, H., Fundel, F., Ruth, U., Twarloh, B., Littot, G. C., Mulvaney, R., Rothlisberger, R., de Angelis, M., Boutron, C. F., Hansson, M., Jonsell, U., Hutterli, M. A., Lambert, F., Kaufmann, P., Stauffer, B., Stocker, T. F., Steffensen, J. P., Bigler, M., Siggaard-Andersen, M. L., Udisti, R., Becagli, S., Castellano, E., Severi, M., Wagenbach, D., Barbante, C., Gabrielli, P., and Gaspari, V.: Southern Ocean sea-ice extent, productivity and iron flux over the past eight glacial cycles, Nature, 440, 491–496, doi:10.1038/nature04614, 2006.

Worms, I., Simon, D. F., Hassler, C. S., and Wilkinson, K. J.: Bioavailability of trace metals to aquatic microorganisms: importance of chemical, biological and physical processes on biouptake, Biochimie, 88, 1721–1731, doi:10.1016/j.biochi.2006.09.008, 2006.

Wu, J. F., Boyle, E., Sunda, W., and Wen, L. S.: Soluble and colloidal iron in the olgotrophic North Atlantic and North Pacific, Science, 293, 847–849, 2001.

Wu, J. F., Chung, S. W., Wen, L. S., Liu, K. K., Chen, Y. L. L., Chen, H. Y., and Karl, D. M.: Dissolved inorganic phosphorus, dissolved iron, and Trichodesmium in the oligotrophic South China Sea, Global Biogeochem. Cy., 17, doi:10.1029/2002GB001924, 2003.

Ye, Y., Völker, C., and Wolf-Gladrow, D. A.: A model of Fe speciation and biogeochemistry at the Tropical Eastern North Atlantic Time-Series Observatory site, Biogeosciences, 6, 2041–2061, 2009, http://www.biogeosciences.net/6/2041/2009/.

Yooseph, S., Sutton, G., Rusch, D. B., Halpern, A. L., Williamson, S. J., Remington, K., Eisen, J. A., Heidelberg, K. B., Manning, G., Li, W. Z., Jaroszewski, L., Cieplak, P., Miller, C. S., Li, H. Y., Mashiyama, S. T., Joachimiak, M. P., van Belle, C., Chandonia, J. M., Soergel, D. A., Zhai, Y. F., Natarajan, K., Lee, S., Raphael, B. J., Bafna, V., Friedman, R., Brenner, S. E., Godzik, A., Eisenberg, D., Dixon, J. E., Taylor, S. S., Strausberg, R. L., Frazier, M., and Venter, J. C.: The Sorcerer II Global Ocean Sampling expedition: Expanding the universe of protein families, PLoS. Biol., 5, 432–466, doi:10.1371/journal.pbio.0050016, 2007.

Yoshida, T., Hayashi, K., and Ohmoto, H.: Dissolution of iron hydroxides by marine bacterial siderophore, Chem. Geol., 184, 1–9, 2002.

Zhang, W. and Wang, W.-X.: Colloidal organic carbon and trace metal (Cd, Fe, and Zn) releases by diatom exudation and copepod grazing, Journal of Experimental Marine Biology and Ecology, 307, 17–34, 2004.